

**3*d*-Transition Metal Complexes of C_3 Symmetric
Tritopic Ligands: Directed Syntheses of Trinuclear
Compounds and Higher Nuclearity Aggregates**

Dissertation

zur Erlangung des akademischen Grades doctor rerum naturalium
(Dr. rer. nat.)

vorgelegt dem Rat der Chemisch-Geowissenschaftlichen Fakultät der
Friedrich-Schiller-Universität Jena

von Diplom-Chemiker Daniel Plaul
geboren am 21. Oktober 1980 in Schmöln

Gutachter:

1. Prof. Dr. Winfried Plass, Institut für Anorganische und Analytische Chemie, Friedrich-Schiller-Universität Jena
2. Prof. Dr. Matthias Westerhausen, Institut für Anorganische und Analytische Chemie, Friedrich-Schiller-Universität Jena
3. Prof. Dr. Jiří Pinkas, Institut für Chemie, Masaryk-Universität Brunn, Tschechische Republik

Tag der öffentlichen Verteidigung: 30. September 2009

*"Die Neugier steht immer an erster Stelle eines Problems,
das gelöst werden will."*

Galileo Galilei (1564–1642)

Danksagung

An erster Stelle möchte ich mich bei Prof. Dr. Winfried Plass für die Möglichkeit bedanken, die Arbeiten zu dieser Dissertation in seiner Arbeitsgruppe durchzuführen. Des Weiteren bedanke ich mich für die mir gewährte wissenschaftliche Freiheit, die eine individuelle Forschung und vielfältige Einblicke in verschiedenste Themenbereiche gestattete. Außerdem bedanke ich mich für das entgegengebrachte Vertrauen und nicht zuletzt für die Möglichkeit an zahlreichen nationalen und internationalen Tagungen teilzunehmen und meine Forschungsergebnisse zu präsentieren.

Prof. Dr. Matthias Westerhausen danke ich für die Anfertigung des Zweitgutachtens und Prof. Dr. Jiří Pinkas für die Anfertigung des Drittgutachtens

Dem Freistaat Thüringen danke ich für die finanzielle Unterstützung im Rahmen eines Graduiertenstipendiums.

Für die Durchführung verschiedenster Analysen danke ich dem gesamten wissenschaftlichen Personal des Instituts für Anorganische und Analytische Chemie und des Instituts für Organische und Makromolekulare Chemie.

Besonders danke ich Dr. Helmar Görls für die Durchführung der Kristallstrukturanalysen und natürlich für die immer wieder spektakulären und hochdramatischen Präsentationen der Ergebnisse. Außerdem danke ich Christa Felbel für die Magnetisierungsmessungen von unzähligen Komplexen.

Ich danke meinen KollegInnen der AG Plass für die angenehme und freundschaftliche Atmosphäre, nicht nur während der Arbeitszeit sondern auch im Hinblick auf die zahlreichen gemeinsamen Unternehmungen.

Speziell möchte ich mich bei Juliane Bauer und Dirk Schuch für die entspannte, lockere Arbeitsatmosphäre im Büro und Labor bedanken. Ganz besonders danke ich Eike T. Spielberg und Robert Debel sowie den ehemaligen Mitgliedern Dr. Anja Burkhardt und

Dr. Arne Roth für die zahlreichen Diskussionen, teils bis spät in die Nacht, sowohl über synthetische Probleme als auch nichtfachliche Themen und die freundschaftliche Unterstützung. Darüber hinaus danke ich Eike für die Hilfe bei dem ein oder anderem Problem der Magnetochemie. Außerdem danke ich Dr. Axel Buchholz für die Hilfestellung bei der Lösung der Kristallstrukturen und die geduldige Einführung in das weite Feld der Kristallstrukturanalyse.

Der größte Dank gebührt meiner Schwester Diana für die moralische Unterstützung, insbesondere für die aufmunternden Worte in den weniger erfolgreichen Phasen. Tausend Dank auch für das Korrekturlesen der Arbeit.

Nicht zuletzt möchte ich mich bei meinen Eltern und Freunden für einfach Alles bedanken. Das hat mir den nötigen Rückhalt gegeben.

List of Publications

Scientific Articles

- ***meta*-Phenylene-bridged double Schiff-base copper(II) complexes as building blocks for 1D coordination polymers: Synthesis, crystal structure and magnetic properties.** Daniel Plaul, Axel Buchholz, Helmar Görls, Winfried Plass, *Polyhedron* **2007**, *26*, 4581–4590.
- **Mono- and dinuclear copper(II) complexes with *meta*-phenylene-bridging ligands: Synthesis, structure and magnetic properties.** Daniel Plaul, Daniel Geibig, Helmar Görls, Winfried Plass, *Polyhedron* **2009**, *28*, 1982–1990.

Poster Presentations

- **Transition Metal Complexes as Precursors for Dendritic Molecular Magnets.** Daniel Plaul, Adrian E. Ion, Aksana Zharkouskaya, Winfried Plass, *1st European Chemistry Congress*, August 27 – 31, **2006**, Budapest, Hungary.
- **Complexes with Triaminoguanidine Ligands as Building Blocks for Magnetic Molecules and Coordination Polymers.** Daniel Plaul, Eike T. Spielberg, Juliane Bauer, Aksana Zharkouskaya, Adrian E. Ion, Axel Buchholz, Winfried Plass, *European Material Research Congress*, May 28 – June 1, **2007**, Strasbourg, France.
- **Directed Synthesis and Magnetic Properties of Triaminoguanidine Bridged Polynuclear Complexes.** Daniel Plaul, Eike T. Spielberg, Adrian E. Ion, Winfried Plass, *11th International Conference on Molecule-based Magnets*, September 21 – 24, **2008**, Florence, Italy.
- **Synthesis and Magnetic Properties of Transition Metal Complexes with C₃ symmetric Ligands.** Daniel Plaul, Eike T. Spielberg, Dirk Schuch, Winfried Plass, *Colloquy of the DFG-Priority Program 1137 "Molecular Magnetism"*, February 8 – 10, **2009**, Bad Dürkheim, Germany.

- **Synthesis and Magnetic Properties of Transition Metal Complexes with C_3 symmetric Ligands.** Daniel Plaul, Eike T. Spielberg, Dirk Schuch, Winfried Plass, *Deutsches Koordinationschemie-Treffen*, February 22 – 24, **2009**, Erlangen, Germany.

Further Posters

- **Transition Metal and Lanthanide Complexes with Triaminoguanidine Ligands as Building Blocks for Magnetic Molecules and Coordination Polymers.** Aksana Zharkouskaya, Daniel Plaul, Adrian E. Ion, Eike T. Spielberg, Juliane Bauer, Axel Buchholz, Arne Roth, Winfried Plass, *233rd ACS National Meeting*, March **2007**, Chicago, IL, USA.
- **Magnetic Interactions in Copper Complexes with Triaminoguanidine Ligands.** Eike T. Spielberg, Daniel Plaul, Adrian E. Ion, Aksana Zharkouskaya, Winfried Plass, *Colloquy of the DFG-Priority Program 1137 "Molecular Magnetism"*, May **2007**, Bad Dürkheim, Germany.
- **Polynuclear Heterometallic Complexes Based on Triaminoguanidine Ligands: Synthesis, Structure and Magnetic Characterization.** Eike T. Spielberg, Daniel Plaul, Lorenzo Sorace, Dante Gatteschi, Winfried Plass, *38th International Conference on Coordination Chemistry*, July **2008**, Jerusalem, Israel.
- **Three-dimensional Coordination Polymers Based on Triaminoguanidine Ligands.** Juliane Bauer, Daniel Plaul, Eike T. Spielberg, Aksana Zharkouskaya, Axel Buchholz, Winfried Plass, *1st International Conference on Metal Organic Frameworks and Open Framework Compounds*, October **2008**, Augsburg, Germany.

Contents

Danksagung	v
List of Publications	vii
1 Introduction	1
RESULTS	11
2 Phloroglucinol-Bridged Complexes	13
2.1 Ligand and Complex Design	13
2.2 Synthesis and Characterization	15
2.3 Crystal Structures	18
2.4 Magnetic Properties	38
3 Triaminobenzene-Bridged Complexes	45
3.1 Ligand and Complex Design	45
3.2 Metallamacrocyclic Complexes with the Amide-Based Ligand $\text{H}_3\text{L}2^{pic}$. .	47
3.2.1 Synthesis and Characterization	47
3.2.2 Crystal Structures	49
3.2.3 Magnetic Properties	56
3.3 Metallamacrocyclic Complexes with the Schiff-Base Ligand $\text{H}_3\text{L}2^{tBusal}$. .	61
3.3.1 Synthesis and Characterization	61
3.3.2 Crystal Structures	64
3.3.3 Magnetic Properties	72
4 Triaminoguanidine-Bridged Complexes	79
4.1 Ligand and Complex Design	79
4.2 Iron(III) Complexes with the Ligand $\text{H}_5\text{L}3^{Brsal}$	80
4.2.1 Synthesis and Characterization	80

4.2.2	Crystal Structures	83
4.2.3	Magnetic Properties	90
4.3	Pentanuclear Heterometallic Complexes with the Ligands $\text{H}_5\text{L3}^{Brsal}$ and $\text{H}_5\text{L3}^{Hsal}$	96
4.3.1	Synthesis and Characterization	96
4.3.2	Crystal Structure	103
4.3.3	Magnetic Properties	107
4.4	Trinuclear Transition Metal Complexes with the Ligand $\text{H}_2\text{L3}^{py}$	110
4.4.1	Synthesis and Characterization	110
4.4.2	Crystal Structures	114
4.4.3	Magnetic Properties	126
4.5	Coordination Polymers Based on Trinuclear Complex Units with the Ligand $\text{H}_2\text{L3}^{py}$	137
4.5.1	Synthesis and Characterization	137
4.5.2	Crystal Structures	140
4.5.3	Magnetic Properties	147
5	Conclusion	151
6	Zusammenfassung	159
7	Future Perspective	169
	EXPERIMENTAL	173
8	General	175
9	Physical Measurements	177
10	Crystal Structure Determinations	179
11	Syntheses	181
11.1	Materials	181
11.2	Syntheses of the Ligands	181
11.2.1	Phloroglucinol-Based Ligands	181
11.2.2	Triaminobenzene-Based Ligands	183

11.2.3 Triaminoguanidine-Based Ligands	184
11.3 Syntheses of the Complexes	185
11.3.1 Phloroglucinol-Bridged Complexes	185
11.3.2 Triaminobenzene-Bridged Complexes	188
11.3.3 Triaminoguanidine-Bridged Complexes	191
APPENDIX	199
A.1 Ligand-Overview	201
A.2 Complex-Overview	203
A.3 Crystallographic Details	204
Bibliography	227
Declaration of Originality	243
Curriculum Vitae	245

1 Introduction

Magnetic materials are important in our daily routines. The evolution is closely associated with the scientific as well as social progress of the society. Magnets are used in various different areas, starting with acoustic components such as loud speakers and microphones, in electronic data processing as data storages right up to medical diagnostic as magnet resonance tomography. Moreover these are essential for modern analytic methodologies, like NMR and ESR, not only for chemists.^[1]

Today predominantly conventional magnetic materials are utilized consisting of inorganic solids such as metals, metal oxides or alloys. These classical magnets are two- or three-dimensional arrays of transition metal or lanthanide ions as well as a combination between both in the modern alloys. The synthesis is very energy-intensive which results in high costs and the properties of the materials can be modified only in a narrow range. Consequently the development of new magnetic materials has become of growing interest.

The aim of this new interdisciplinary field of research is the synthesis of molecular based magnets including the combination of interesting material properties with magnetic properties. Herein the spin carriers are organic radicals or transition metal ions as well as lanthanide ions. Examples for the former one are nitronyl-nitroxide^[2-6] and dithiadiazolyl radicals^[7,8], which have been extensively studied. The nitroxide derivatives are a group of molecules containing a NO-functionality with an unpaired electron in the π^* orbital, which is stabilized in presence of sterically demanding (bulky) groups preventing the dimerization reaction. Furthermore various phenylene derivatives have been synthesized and magnetically investigated. These behave as weak bulk ferromagnets at very low temperatures close to zero.^[9,10] The sulfur based dithiadiazolyl radicals show weak ferromagnetism at higher Curie temperatures, T_C , up to 36 K.^[9,11,12] An extremely interesting feature of the organic radicals arises from the reaction with hexafluoroacetate salts of anisotropic transition metal as well as lanthanide ions, for example

cobalt(II) and dysprosium(III), affording single-chain magnets (SCMs).^[13–19] SCMs exhibit bulk ferromagnetic interaction in one-dimensional coordination polymers.

Another class of molecular magnetic materials is based on the syntheses of charge-transfer-complexes. The most famous examples are the $[\text{Fe}(\text{C}_5\text{Me}_5)_2]^+[\text{TCNE}]^-$ (TCNE= tetracyanoethylene)^[20] with a spontaneous long-range ferromagnetic ordering below a T_C of 4.8 K and the vanadium complex $[\text{V}(\text{TCNE})_x] \cdot y\text{CH}_2\text{Cl}_2$ with a very high T_C value above room temperature approximated of about 400 K.^[21–23]

A milestone in the field of molecule-based magnets was the observation that the complex $[\text{Mn}_{12}\text{O}_{12}(\text{O}_2\text{CCH}_3)_{16}(\text{OH}_2)_4]$ (Mn_{12}Ac) exhibits a hysteresis in the magnetization, which arises from pure molecular origin termed as single-molecule magnet (SMM).^[24–26] The molecular structure contains oxo-bridged manganese(III) and manganese(IV) centers coordinated by additional acetate ligands. Beside a high-spin ground state a large magnetic anisotropy is necessary for SMM behavior. Since the SMMs are bistable in the sense that they can be magnetized in two directions, applications in data storage devices was proposed for Mn_{12}Ac .^[27] This would drastically increase the storage capacity of computer hard disks as one example. Various other SMMs have been reported up to now, utilizing predominantly manganese^[28–39] and more recently dysprosium^[40–42] due to the high anisotropy of both metal ions. Furthermore other polynuclear homometallic complexes containing for example iron, cobalt or nickel ions as well as heterometallic complexes have been published.^[43–56] The polynuclear complexes exhibit ferri- or ferromagnetic exchange interactions between the metal centers mediated through the bridging ligands resulting in a high-spin ground state. More recently also mononuclear lanthanide-based so-called *double-decker* complexes have been reported to show SMM behavior.^[57–60]

The polynuclear SMMs are commonly synthesized through self assembly process of metal ions and small organic ligands. Similarly most polynuclear metal complexes as well as coordination polymers are prepared following this synthesis approach. Unfortunately the topology of the metal centers within the final complex molecules or polymer architectures can not be controlled directly. An important issue related to the rational design of molecular-based magnetic materials is to utilize synthesis strategies in order to generate new systems exhibiting desired physical and chemical properties. In this context especially complexes of small organic ligands as well as linear symmetric bridging

ligands are extensively studied. In contrast the use of C_3 symmetric bridging ligands has been less exploited.

From the magnetochemistry point of view tritopic C_3 symmetric ligands can provide several promising features. The probably most employed concept in this context is spin polarization, which for tritopic aromatic ligands with a bridging benzene core unit should give rise to ferromagnetic exchange between the transition metal ions, allowing the generation of high-spin molecules.^[61,62] The bridging coordination of the metal ions is realized by additional *meta*-positioned functional groups at the aromatic ring.^[61–63] The concept is well established for purely organic systems, leading to ferromagnetic interactions in the case of *meta*-phenylene-bridged organic spin carriers and antiferromagnetic interactions in *ortho*- and *para*-phenylene-bridged analogues as shown in figure 1.1.^[64–66] In contrast to the purely organic systems, the transition metal complexes do not strictly exhibit ferromagnetic interactions, instead depending on the relative orientation of the metal moieties also antiferromagnetic interactions are observed. This can be attributed to the fact, that both spin polarization and superexchange effects contribute to the overall coupling behavior in these systems.^[67–70] More complexes with new ligands have to be synthesized to get further insights into the exchange interactions through the bridging π -system. This might provide an access to the directed synthesis of metal complexes with predictable magnetic properties.

The alternative approach aims at the contrary, i.e. the specific generation of antiferromagnetically coupled systems. Transition metal ions with half-integer spin are of particular interest, as they afford trinuclear metal complexes with a resulting non-zero spin ground state. In an equilateral triangular arrangement, it is impossible to obtain an antiparallel alignment of all three spins. This has been termed as spin frustration meaning that two spins are antiferromagnetically coupled and the third spin cannot be simultaneously antiferromagnetically coupled with both of the spins.^[71] In this context predominantly copper complexes are reported which have been synthesized through serendipitous self-assembly of three monomer complex units.^[72–82] Besides the fundamental interest in the properties of spin-frustrated system,^[83] such a situation is proposed to enable new perspectives in fields like quantum computing with magnetic molecules exhibiting relevant electronic properties.^[84–86]

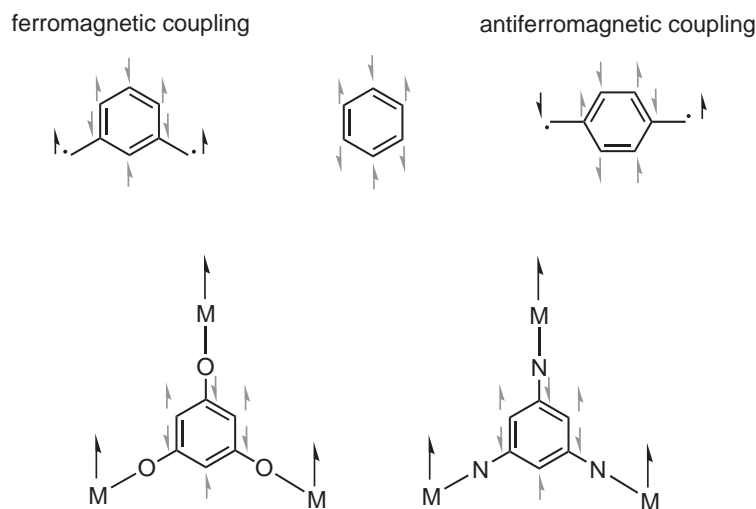


Figure 1.1: Schematic representation of the spin polarization concept. The arrows represent the unpaired electrons. Top: Exchange interactions in organic radicals. Bottom: Extension of this concept to trinuclear transition metal complexes leading to ferromagnetic exchange interactions, wherein M represent the 3d-transition metal ions.

Only a scarce number of ligands bridging three metal ions in a highly symmetric matter and transmitting magnetic exchange interactions between them have been published, e.g. derivatives of trihydroxybenzene,^[87–89] triaminobenzene,^[90] triaminoguanidine^[91,92], hexaazatriphenylene^[93] and benzenetricarboxylic acid^[94]. Among these, the two latter did not predominantly afford trinuclear complexes. These ligand systems are very flexible towards the number of coordinated metal centers leading to various complex topologies, predominantly to coordination polymers.^[95–97]^[98–110] Furthermore only very weak exchange interactions are mediated through the bridging π -system of hexaazatriphenylene.^[93] The coupling through the benzenetricarboxylic acid depends on the relative position of the carboxylate groups in relation to the benzene ring, which is determined by serendipity in the complexes. Nevertheless the mediated exchange interactions are also rather weak.^[61,94,103] Therefore only ligands based on the other three bridging units have been synthesized and utilized for the coordination of transition metal ions within this thesis. The trihydroxybenzene and triaminobenzene-bridged complexes are generated as new high-spin compounds utilizing the concept of spin polarization, whereas the triaminoguanidine one aims toward the generation of antiferromagnetically coupled complexes related to the spin frustration phenomenon.

Phloroglucinol-bridged Complexes

Phloroglucinol-bridged trinuclear $3d$ -transition metal complexes can not be prepared by simple reaction of phloroglucinol with three equivalents of a metal salt together with appropriate co-ligands.^[111] Only the isolation of a trinuclear Molybdenum(V) complex was successful using chromatographic separation of the mono-, di-, and trinuclear phloroglucinol complexes.^[112] Additional chelating side chains in the 2,4,6-position of the phloroglucinol are necessary, enhancing the stability of the complexes by the use of the chelate effect. The resulting binding pockets prevent the polymerization during complexation reaction and control the connectivity leading to discrete trinuclear complexes.

A C_3 symmetric Schiff-base ligand of 1,3,5-trisacetyl-2,4,6-phloroglucinol in combination with appropriate co-ligands has been used for the syntheses of trinuclear copper(II) complexes as shown in figure 1.2.^[89] The three copper centers are bridged in a *meta*-phenylene arrangement by a phloroglucinol backbone exhibiting ferromagnetic exchange interactions, due to the spin polarization mechanism. Depending on the utilized co-ligand significant differences are observed in the magnitude of the coupling. The use of 2,2'-bipyridine (bipy) results in $J = +4.0 \text{ cm}^{-1}$, whereas salicylic aldehyde (Hsal) affords a stronger exchange interaction with $J = +6.6 \text{ cm}^{-1}$. (All coupling constants J in this thesis are related to the Heisenberg-Dirac-van Vleck-Hamiltonian in the form of $\hat{H} = -J\hat{S}_i\hat{S}_j$.) In a series of phloroglucinol-bridged salen-like coordinated trinuclear copper(II) complexes these interactions are clearly weaker,^[62,113] whereas in the corresponding trinuclear manganese(III) complex the exchange interaction is even antiferro-

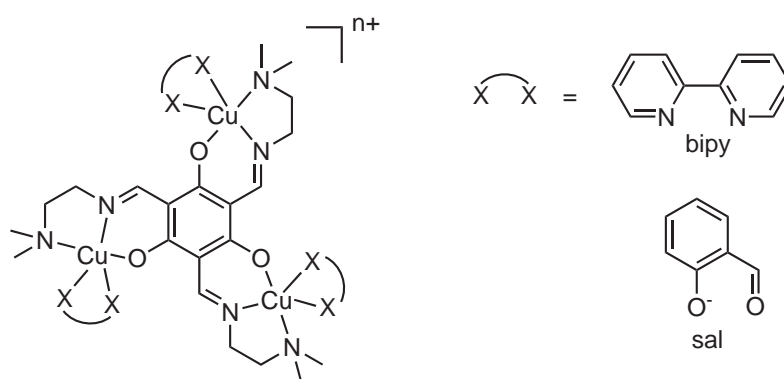


Figure 1.2: Schematic representation of the trinuclear phloroglucinol-bridged copper(II) complexes.^[89]

magnetic.^[114] Competing superexchange and spin polarization mechanisms caused by the orientation of the magnetic orbitals relative to the bridging ligand plane have been accounted for these differences in the exchange interactions. In the vanadium(IV) complex very weak ferromagnetic exchange interactions were observed with $J = +0.88 \text{ cm}^{-1}$.^[115] In addition to them the corresponding trinuclear nickel(II) complexes have been synthesized, wherein the nickel(II) ions exhibit a square planar coordination environment and hence a non-magnetic $S = 0$ ground state.^[87,88]

The rational linkage of two trinuclear manganese complexes utilizing $[\text{M}(\text{CN})_6]^{n-}$ ($\text{M}=\text{Fe}^{\text{III}}, \text{Cr}^{\text{III}}$) was also reported which leads to heptanuclear heterometallic complexes with interesting magnetic properties.^[116,117] In the case of chromium the complex exhibit single-molecule magnet behavior.^[117]

Until now only these two ligand systems have been investigated. Hence complexes with new ligands have to be synthesized to get further insights into the exchange interactions. Complexes with other transition metal ions promise interesting magnetic properties, for example high-spin nickel(II) and cobalt(II) complexes.

Triaminobenzene-bridged Complexes

Another class of bridging ligands mediating magnetic exchange interactions between the metal ions are substituted *meta*-aminobenzenes.^[118] Additional donors have been introduced by Schiff-base condensation^[119,120] or amide formation reactions^[121] of the amino groups. Predominantly metallamacrocyclic dinuclear transition metal complexes composed of two ligand molecules together with two metal ions have been published.

The magnetic exchange interactions within the copper complexes range between ferromagnetic^[121-123] and weak antiferromagnetic^[119,120,124,125], again ascribed to the above mentioned competing superexchange and spin polarization mechanism. The strongest ferromagnetic exchange interaction is observed in a dinuclear copper complex with an amide ligand shown in figure 1.3.^[121] The coupling of $J = +16.8 \text{ cm}^{-1}$ is significantly stronger compared to the previously discussed hydroxybenzene-bridged complexes. This results from a more efficient exchange interaction through spin polarization over the central *meta*-phenylene bridges. The corresponding dinuclear nickel(II) and cobalt(II) complexes possess antiferromagnetic exchange interactions.^[125] Furthermore the only reported dinuclear iron(III) complex shows ferromagnetic interactions.^[126]

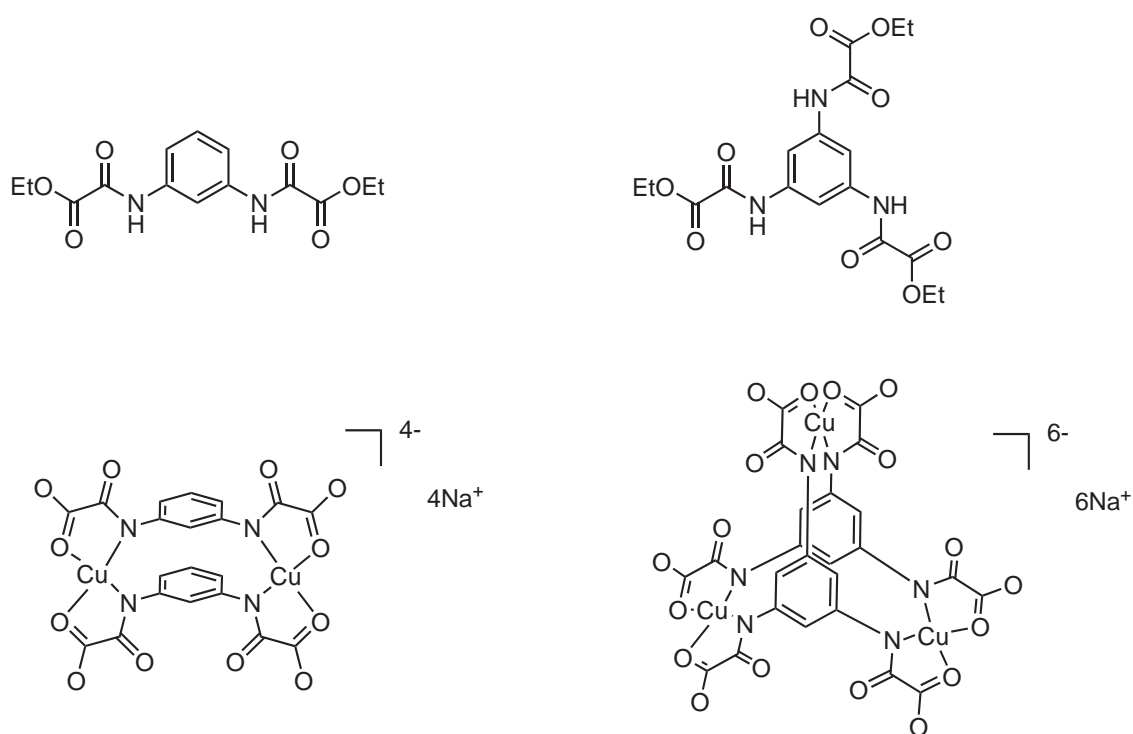


Figure 1.3: Left: Schematic representation of the C_2 symmetric aminobenzene-based ligand and the corresponding dinuclear metallamacrocyclic copper(II) complex.^[121] Right: The analogous C_3 symmetric ligand and the trinuclear metallamacrocyclic copper(II) complex with a 1,3,5-metallacyclophane core structure.^[63]

Although different dinuclear complexes bridged in a *meta*-phenylene arrangement have been studied, the trinuclear analogues are still rare. There is only one trinuclear transition metal complex reported in literature.^[63,90] The tritopic ligand, depicted in figure 1.3, provide *meta*-positioned oxamate side chains on a central benzene ring. Three copper ions are chelated and bridged by two ligand molecules under formation of a C_3 symmetric metallacyclophane structure. The complex shows rather strong ferromagnetic exchange interactions ascribed to the spin polarization mechanism with $J = +11.6 \text{ cm}^{-1}$. Furthermore a theoretical approach towards the exchange interactions in dinuclear *meta*-phenylenediamine copper(II) complexes predict extremely strong ferromagnetic couplings with J up to $+325 \text{ cm}^{-1}$ depending on the ligand side chain.^[123] Therefore new ligands have to be designed aiming at stronger magnetic couplings in the resulting transition metal complexes.

Triaminoguanidine-bridged Complexes

Guanidin derivatives can act as a ligand for different metal ions, for instance transition, main group as well as lanthanide metal ions.^[127–131] However the complexation of three metal ions in a threefold symmetry has not been reported. A potential way to prepare trinuclear complexes is the utilization of the stabilizing chelate effect as in the case of the triaminoguanidinium cation. C_3 symmetric ligands have been synthesized by Müller *et al.* through Schiff-base reaction of triaminoguanidine and salicylaldehyde derivatives which are illustrated in figure 1.4.^[91,92] These ligands possess a planar structure with three equivalent cavities capable of chelating transition metal ions leading to rather short metal–metal distances. The preferred coordination geometry of the metal ions determines the number and possible coordination sites for co-ligands. Beside a few trinuclear transition metal complexes,^[91,92,132] several discrete cage molecules with interesting topologies have been synthesized utilizing predominantly diamagnetic metal ions, as zinc(II), cadmium(II), palladium(II) and platinum(II).^[92,132–137]

This concept was extended towards paramagnetic transition metal ions by our group.^[138] A series of C_3 symmetric trinuclear copper(II) and nickel(II) complexes have been synthesized by the addition of capping co-ligands, like 2,2'-bipyridine (bipy) as well as 2,4,6-tris(2-pyridyl)-1,3,5-triazine (tptz).^[139–141] If copper(II) ions are coordinated

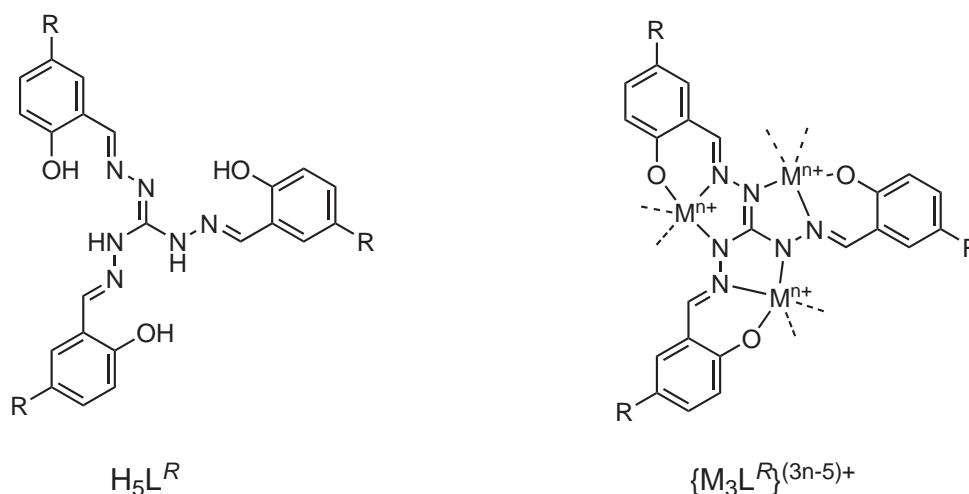


Figure 1.4: Schematic representation of the C_3 symmetric Schiff-base ligands based on triaminoguanidine and the bridging coordination of transition metal ions.^[91,92]

in the absence of potentially capping co-ligands, inorganic coordination polymers are obtained through aggregation via μ -phenoxy bridges formed between metal centers.^[142] Moreover substituents at the salicylidene side chains results in the formation of a porous chiral 3D networks.^[143]

Temperature dependent magnetic susceptibility measurements reveal efficient antiferromagnetic exchange couplings in all complexes. The interaction is caused by superexchange between the metal ions through the N-N diazine bridges of the ligand. Due to the close proximity of the three metal ions the coupling is much stronger, compared to the rather weak exchange in phloroglucinol as well as triaminobenzene-bridged complexes mediated by spin polarization through the central benzene bridges.

Although the exchange interactions are antiferromagnetic the trinuclear complexes are very interesting. The triangular antiferromagnetically ordered magnetic spins play a key-role in molecular magnetism owing to their potential to show magnetic frustration.^[71,83] In this context a promising candidate for quantum bits (qubits) are systems with an odd number of antiferromagnetically coupled odd spins. The simplest molecule exhibiting this characteristic is an equilateral triangle of three $S = 1/2$. The resulting doubly degenerated doublet ground state is said to be a good candidate for quantum bit storing due to suppression of pathways of decoherence.^[144] The stronger the coupling, the greater is the distance to the excited quartet state, leading to a better thermal isolation of the computational active doublet states.^[145] Hence especially the trinuclear copper(II) and iron(III) complexes are potentially interesting in the interdisciplinary field of molecular spintronics.^[84,146,147]

Based on these researches, the objective of this thesis is the directed synthesis of C_3 symmetric trinuclear transition metal complexes with tritopic ligands mediating magnetic exchange interactions between the three metal centers. Novel ligands need to be synthesized to enlarge the scarce number of published examples, as the prediction of the magnetic properties is not straight forward. The coordination chemistry of various transition metal ions as well as the magnetic properties will be studied. Moreover the linkage of the trinuclear units utilizing *step-by-step* synthetic approaches into higher aggregates and coordination polymers will be investigated.

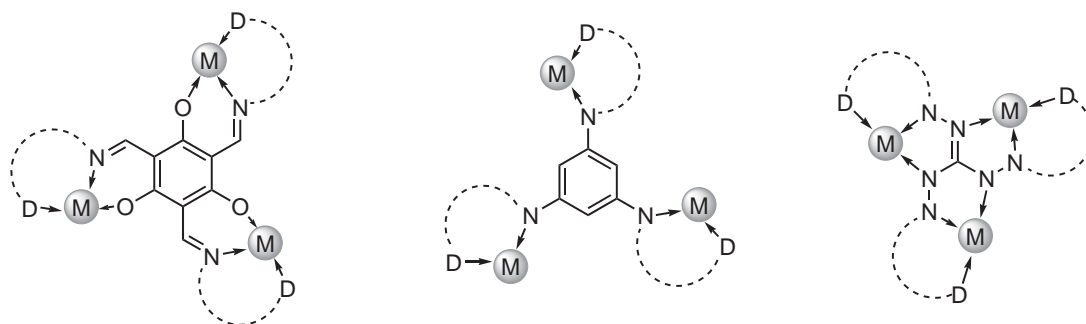


Figure 1.5: Schematic representation of the C_3 symmetric bridging units in trinuclear transition metal complexes. The dotted lines represent the modification of the binding pockets of the ligands with additional donor atoms D.

Three different bridging units as shown in figure 1.5 will be used. Additional chelating side arms in combination with capping co-ligands allow for the directed synthesis of trinuclear metal complexes. Utilizing bridging co-ligands provides access to the assembly of higher aggregates.

– Results –

2 Phloroglucinol-Bridged Complexes

2.1 Ligand and Complex Design

The four different ligands based on phloroglucinol as shown in figure 2.1 were synthesized. Schiff-base ligands were utilized due to their easy accessibility. Furthermore the binding pockets together with the potential donor atoms within the ligand side chains can be varied very easily.

Each ligand provides three equal binding pockets, allowing the bridging coordination of three metal ions in a *meta*-phenylene arrangement. The coordination of the metal ions will be realized through the heteroatoms under formation of thermodynamically favorable five- and six-membered chelate rings. Except the ligand $\text{H}_3\text{L1}^{unspenp}$ with five donor atoms within each binding pocket, all other ligands provide tris-chelating binding pockets. The ligands can not coordinate to a single metal center including two or three side chains, due to the rigid planar phloroglucinol core. Hence additional co-ligands or solvent molecules are inevitable for the formation of stable trinuclear complexes. Depending on the preferred coordination geometry of the metal ion monodentate as well as chelating co-ligands are utilized shown in figure 2.2. Moreover the co-ligands are different concerning their ionic nature, whereas imidazole (Him) and bis(pyridin-2-ylethyl)-amine (Hbpea) act as neutral co-ligands, bis(pyridin-2-ylcarbonyl)-amine (Hbpca) coordinates in its monoanionic form. The focus lies on the syntheses of magnetically relevant trinuclear nickel complexes with an octahedral coordination geometry, which has not been described in literature. Only trinuclear phloroglucinol-bridged nickel(II) complexes with triplesalen ligands are known wherein the nickel(II) ions are coordinated in a square planar coordination environment resulting in diamagnetic complexes.^[87,88] In addition the coordination of copper(II) and cobalt(II) ions is studied. The determination of the exact complex structure is essential for the interpretation of the temperature dependent magnetic susceptibility measurements. Thus only complex syntheses affording single crystals suitable for X-ray crystallography measurements are presented within this chapter.

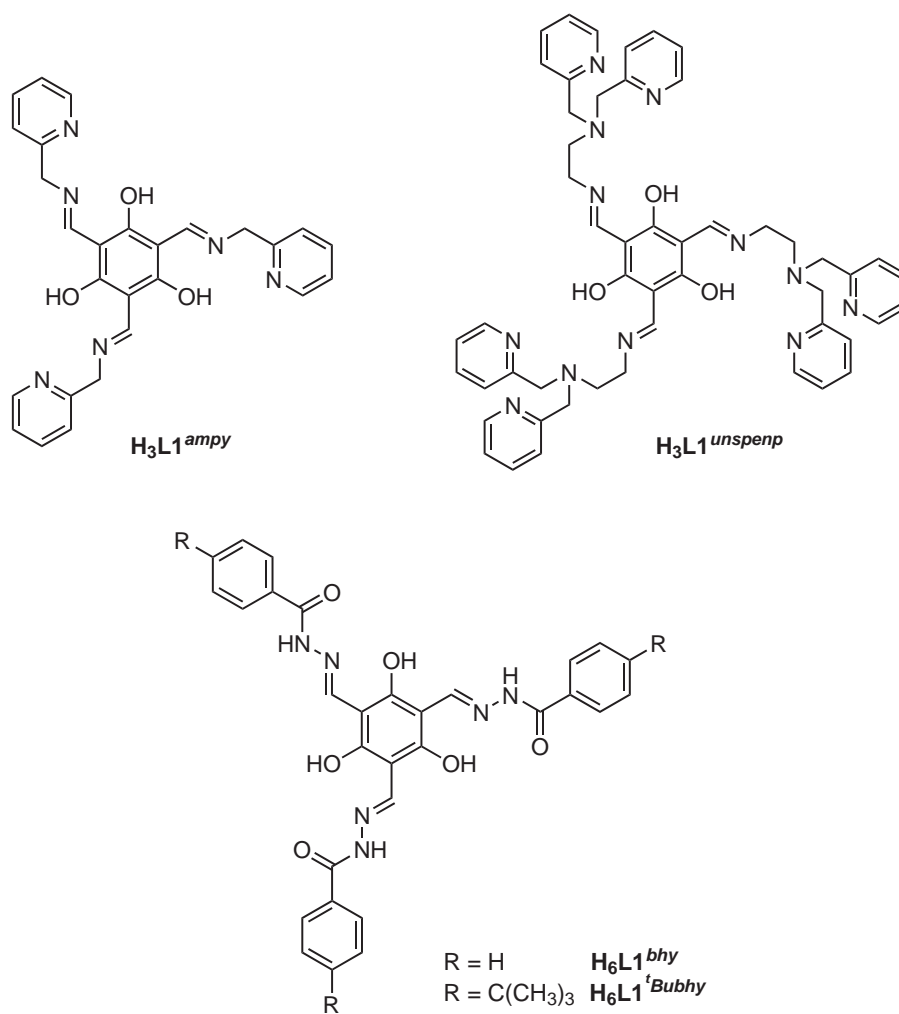


Figure 2.1: The synthesized ligands based on phloroglucinol.

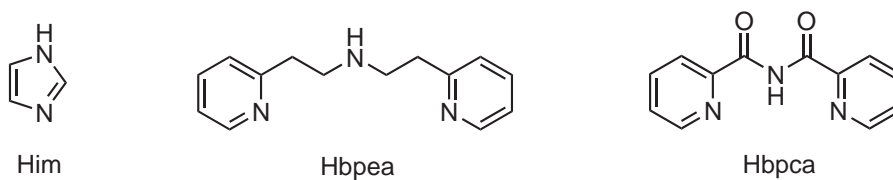


Figure 2.2: The utilized capping co-ligands for the trinuclear complex syntheses.

2.2 Synthesis and Characterization

The phloroglucinol-based ligands, shown in figure 2.1, were prepared by Schiff-base condensation of 2,4,6-triformylphloroglucinol with three equivalents of the corresponding amine. 2,4,6-Triformylphloroglucinol is accessible in a one step synthesis through Duff formylation of phloroglucinol.^[148] Although the yield is not very high with about 14 %, the reaction is simple, takes only two hours, and afforded an analytically pure product. The subsequent reaction with different primary amines in alcohol at ambient temperature enabled high yields of ligands ranging from 58 % up to 100 %.

The ligands can be divided into two groups, on the one hand the imine-based ligands $\text{H}_3\text{L1}^{ampy}$ and $\text{H}_3\text{L1}^{unspenp}$ and on the other hand the hydrazide-based ligands $\text{H}_6\text{L1}^{bhy}$ and $\text{H}_6\text{L1}^{tBubhy}$. The latter exhibit the expected threefold symmetry (C_3) in solution with five and six resonances in the ^1H NMR spectra for $\text{H}_6\text{L1}^{bhy}$ and $\text{H}_6\text{L1}^{tBubhy}$, respectively. Both hydrazide-based ligands are present in the commonly encountered enol-imine(OH) form, confirmed by a singlet of the imine proton at 8.9 ppm and the phenol proton at 13.9 ppm. The large downfield shift of the latter signal indicates strong intramolecular hydrogen bonding interaction within the molecules. This is due to interactions with the imine nitrogen atoms, as also observed in *N*-salicylidenehydrazide ligands.^[149–153]

The ^1H NMR spectra of both imine-based ligands were surprisingly complicated. Whereas singlets were expected for the imine and phenol protons, the spectra showed multiple peaks between 8.2 – 8.3 and 11.1 – 11.6 ppm for $\text{H}_3\text{L1}^{ampy}$ as well as 8.1 – 8.2 and 10.9 – 11.4 ppm for $\text{H}_3\text{L1}^{unspenp}$. The $^1\text{H}\{^1\text{H}\}$ COSY spectra revealed coupling between the signals in these two regions. Both ^1H NMR spectra show that exclusively the all-keto-enamine(NH) form of the ligands is present in a mixture of two geometric isomers shown in figure 2.3.^[154–160] Moreover the ^{13}C NMR spectra corroborate this showing the carbonyl resonances of the central ring in the region between 182 and 188 ppm, characteristic of the keto isomer.^[161]

The ligand $\text{H}_3\text{L1}^{ampy}$ provides three tridentate $[\text{N}_2\text{O}]$ binding pockets with the carbonyl oxygen atom, the amine nitrogen atom and the pyridine nitrogen atom as potential donors acting as a trianionic ligand after deprotonation. The reaction with three equivalents of copper(II) perchlorate hexahydrate in methanol in the presence of three equivalents of aqueous ammonia causes the precipitation of a green solid, which immediately redis-

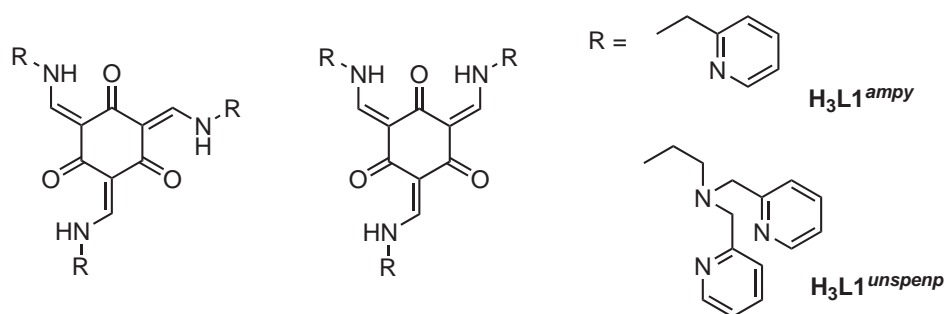


Figure 2.3: The two isomers of the imine-based ligands $\text{H}_3\text{L1}^{\text{ampy}}$ and $\text{H}_3\text{L1}^{\text{unspenp}}$.

solve after complete addition. The subsequent addition of acetonitrile followed by slow evaporation of the dark green solution afforded green prism of the trinuclear copper(II) complex $[\text{Cu}_3(\text{L1}^{\text{ampy}})(\text{MeCN})(\text{H}_2\text{O})_2](\text{ClO}_4)_3$ ($\text{Cu}_3\text{L1}^{\text{ampy}}$) (1).

The analogous reaction with three equivalents of nickel(II) perchlorate hexahydrate followed by the addition of three equivalents of Hbpea leads to the formation of red-brown prism of the trinuclear nickel(II) complex $[\text{Ni}_3(\text{L1}^{\text{ampy}})(\text{Hbpea})_3](\text{ClO}_4)_3$ ($\text{Ni}_3\text{L1}^{\text{ampy}}$) (2).

The ligand $\text{H}_3\text{L1}^{\text{unspenp}}$ provides three pentadentate $[\text{N}_4\text{O}]$ binding pockets with the carbonyl oxygen atoms, two amine nitrogen atoms and two pyridine nitrogen atoms as potential donors. Due to the large donor set within the binding pockets no co-ligand have to be added. Again, the ligand coordinates in its trianionic form to three metal ions. The reaction with three equivalents of nickel(II) perchlorate hexahydrate in methanol in the presence of three equivalents of aqueous ammonia afforded rose needles. These were redissolved in acetonitrile resulting in dark red block prism of $[\text{Ni}_3(\text{L1}^{\text{unspenp}})(\text{H}_2\text{O})_3](\text{ClO}_4)_3$ ($\text{Ni}_3\text{L1}^{\text{unspenp}}$) (3).

The hydrazide ligands $\text{H}_6\text{L1}^{\text{bhy}}$ and $\text{H}_6\text{L1}^{\text{tBubhy}}$ possess three tridentate $[\text{N}_2\text{O}]$ binding pockets with the phenolate oxygen atom, the imine nitrogen atom and the carbonyl oxygen atom as potential donors. Both ligands can adopt a variable protonation state depending on the pH-value of the solution in contrast to the imine-based ligands. Beside the three phenol groups, the amide groups within the ligand side chains can also be deprotonated. This has been reported in copper(II)^[162] as well as vanadium(V) complexes^[163–165] with different *N*-salicylidenehydrazide ligands. After coordination of the

transition metal ion at the carbonyl oxygen atom, the amide proton is removed by comparable moderate bases like aqueous ammonia. Hence the ligand can act as a tri- or hexaanionic ligand.

Both ligands are only sparingly soluble in most common solvents, like methanol, acetonitrile and chloroform. Therefore the complexation of the 3d-transition metal ions was performed with suspensions of the ligands in methanol. After addition of the corresponding metal salt the ligands dissolved, accompanied by a color change of the reaction mixture.

The reaction of $\text{H}_6\text{L1}^{bhy}$ with three equivalents of copper(II) perchlorate hexahydrate in methanol in the presence of aqueous ammonia afforded a dark green solution. The subsequent addition of three equivalents of imidazole results in the formation of the trinuclear copper(II) complex $[\text{Cu}_3(\text{H}_2\text{L1}^{bhy})(\text{Him})_3](\text{ClO}_4)_2$ ($\text{Cu}_3\text{L1}^{bhy}$) (4). Upon drying in air, the crystals lose the co-crystallized solvent molecules. The ligand coordinates in its tetraanionic form. Beside the three phenolate groups, one amide group is deprotonated, whereas both other remain protonated which results in a rather unexpected coordination mode of the ligand within this complex.

The reaction with three equivalents of nickel(II) perchlorate hexahydrate in methanol in the presence of aqueous ammonia results in a yellow solution. Subsequent addition of three equivalents of Hbpea leads to the formation of red needles. Vapor diffusion of diethylether into a saturated solution in a mixture of acetonitrile and methanol yielded the trinuclear nickel(II) complex $[\text{Ni}_3(\text{H}_3\text{L1}^{bhy})(\text{Hbpea})_3](\text{ClO}_4)_3$ ($\text{Ni}_3\text{L1}^{bhy}$) (5).

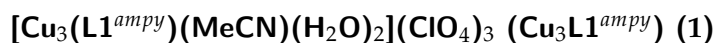
The reaction of the *tert*-butyl substituted hydrazide ligand $\text{H}_6\text{L1}^{tBubhy}$ with cobalt(II) chloride hexahydrate leads to a red colored solution. This solution turned immediately deep brown when aqueous ammonia was added ascribed to the aerial oxidation of the cobalt(II) ions. After addition of three equivalents of Hbpca the neutral trinuclear cobalt(III) complex $[\text{Co}_3(\text{L1}^{tBubhy})(\text{bpca})_3]$ ($\text{Co}_3\text{L1}^{tBubhy}$) (6). Herein the ligand is fully deprotonated coordinating in its hexaanionic form. Moreover the three co-ligands are deprotonated counterbalancing the positive charge of the cobalt centers.

All complexes were characterized by X-ray structural analysis, elemental analysis, mass spectrometry and IR spectroscopy. The crystals of the trinuclear copper complex $\text{Cu}_3\text{L1}^{ampy}$ (1) stay intact and is in agreement with the elemental analysis data. All the other complexes mainly lose the co-crystallized solvent molecules upon drying in air.

The IR spectra of the copper complexes $\text{Cu}_3\text{L1}^{ampy}$ (1) and $\text{Cu}_3\text{L1}^{bhy}$ (4) as well as the nickel complexes $\text{Ni}_3\text{L1}^{ampy}$ (2), $\text{Ni}_3\text{L1}^{unspenp}$ (3), and $\text{Ni}_3\text{L1}^{bhy}$ (5) exhibit a characteristic strong broad band centered at around 1100 cm^{-1} which can be attributed to the stretching vibrations of the perchlorate counterions.^[166] The $\tilde{\nu}_{\text{C}=\text{N}}$ and $\tilde{\nu}_{\text{C}=\text{C}}$ bands partly overlap resulting in a broad band centered at about 1600 cm^{-1} in complexes $\text{Cu}_3\text{L1}^{ampy}$ (1), $\text{Ni}_3\text{L1}^{ampy}$ (2), and $\text{Ni}_3\text{L1}^{unspenp}$ (3). Furthermore for the copper complex $\text{Cu}_3\text{L1}^{bhy}$ (4) and the nickel complex $\text{Ni}_3\text{L1}^{bhy}$ (5) additional bands are observed in this region due to stretching vibrations within the amide moieties of the hydrazide ligand side chains. Therefore the bands can not be unambiguously assigned to an individual stretching vibration. The nickel complexes $\text{Ni}_3\text{L1}^{ampy}$ (2) and $\text{Ni}_3\text{L1}^{bhy}$ (5) as well as the copper complex $\text{Cu}_3\text{L1}^{bhy}$ (4) exhibit a characteristic band at about 3250 cm^{-1} , which can be attributed to the NH stretching vibration of the amine of the Hbpea co-ligands together with the amide groups of the hydrazide ligand side chains. In the IR spectrum of the cobalt complex $\text{Co}_3\text{L1}^{tBubhy}$ (6) this band is absent in accordance to the complete deprotonation of the ligand amide groups. Moreover the IR spectrum is dominated by characteristic bands of the coordinated anionic bpca co-ligands with the carbonyl oxygen stretching vibration observed at 1719 cm^{-1} .

2.3 Crystal Structures

2.3.1 Copper Complexes



The trinuclear copper complex $\text{Cu}_3\text{L1}^{ampy}$ (1) crystallizes in the triclinic space group $P\bar{1}$. Three copper centers are chelated by the triple deprotonated ligand $(\text{L1}^{ampy})^{3-}$ and connected in a *meta*-phenylene arrangement through a central phloroglucinol bridge. The molecular structure and the heteroatom labeling scheme of the trinuclear complex cation $[\text{Cu}_3(\text{L1}^{ampy})(\text{MeCN})(\text{H}_2\text{O})_2]^{3+}$ of $\text{Cu}_3\text{L1}^{ampy}$ (1) is depicted in figure 2.4. Selected bond lengths and angles are listed in table 2.1.

All copper ions are placed in a tetragonal coordination plane assembled by the phenolate oxygen atom, the imine nitrogen atom and the pyridine nitrogen atom of the bridging ligand and an additional coordinated solvent molecule. The copper center Cu1 is coordinated by an acetonitrile molecule, whereas Cu2 and Cu3 are bound to water

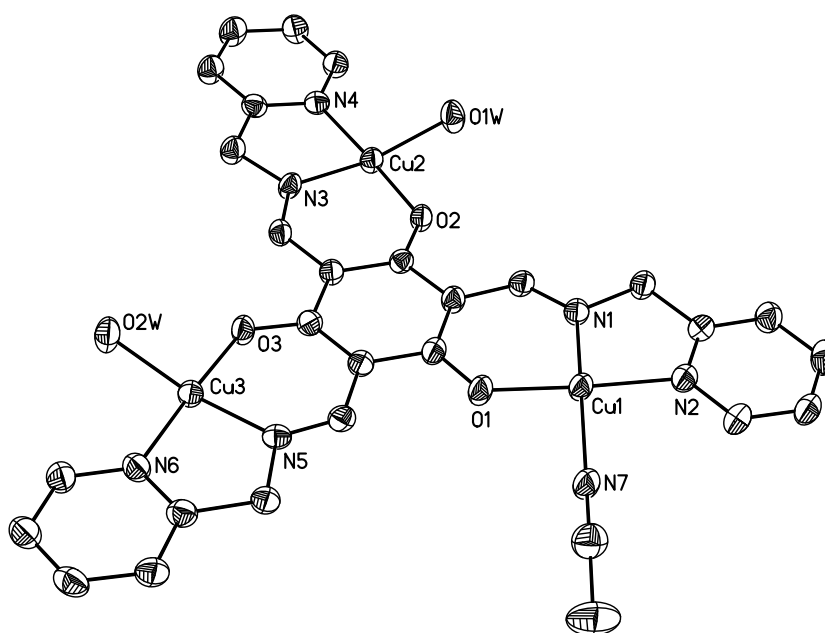


Figure 2.4: Molecular structure of the complex cation $[\text{Cu}_3(\text{L1}^{\text{ampy}})(\text{MeCN})(\text{H}_2\text{O})_2]^{3+}$ of **Cu₃L1^{ampy}** (**1**). Thermal ellipsoids are drawn at the 50% probability level. The hydrogen atoms are omitted for clarity.

molecules. Although the coordinated solvent molecules are different, all donor-copper distances are rather similar for each copper center ranging between 190 and 199 pm. The distances can be divided into two groups situated at the lower and upper end of this range. The short distance group consists of the phenolate oxygen atoms and the imine nitrogen atoms, whereas longer bonds are formed to the pyridine nitrogen atoms as well as the solvent molecules. Furthermore the angles differ only slightly for each copper ion, mainly caused by crystal packing effects. The *trans* angles range between 163° and 177° indicating a slight distortion of the square planar geometry.

The ligand is nearly planar with a mean deviation of only 9 pm from the best least square plane including the ligand atoms. Therefore the copper centers are almost perfectly aligned within the plane of the central phloroglucinol bridge deviating from approximately 3 pm for Cu3 and 8 pm for Cu1 and Cu2. The distortion of the tetragonal planes at each copper center is mainly caused by the coordinated solvent molecules slightly displaced from the ligand plane. Due to the planarity, the complex cations assemble coplanar with a rather short distance of about 316 pm.

Table 2.1: Selected bond lengths [pm] and angles [°] for complex **Cu₃L1^{ampy}** (**1**).

Cu1–O1	189.8(3)	Cu2–O2	190.0(3)	Cu3–O3	189.2(3)
Cu1–N1	191.3(4)	Cu2–N3	191.1(4)	Cu3–N5	191.7(4)
Cu1–N2	198.1(4)	Cu2–N4	199.5(4)	Cu3–N6	198.8(4)
Cu1–N7	198.8(4)	Cu2–O1W	196.8(4)	Cu3–O2W	198.0(4)
O1–Cu1–N1	93.05(14)	O2–Cu2–O1W	86.72(15)	O3–Cu3–O2W	84.61(15)
O1–Cu1–N2	176.78(14)	O2–Cu2–N3	92.92(14)	O3–Cu3–N5	93.18(14)
O1–Cu1–N7	88.32(15)	O2–Cu2–N4	176.16(14)	O3–Cu3–N6	177.16(14)
N1–Cu1–N2	83.81(15)	N3–Cu2–O1W	163.34(18)	N5–Cu3–O2W	168.42(18)
N1–Cu1–N7	165.90(19)	N3–Cu2–N4	83.43(15)	N5–Cu3–N6	83.99(15)
N2–Cu1–N7	94.90(16)	N4–Cu2–O1W	96.44(16)	N6–Cu3–O2W	98.22(17)

The complex cation crystallizes together with three perchlorate ions and water solvent molecules. In the crystal structure, two perchlorate ions function as weakly bound apical ligands in distances of 245 up to 262 pm. As compared to the bond lengths of the relevant equatorial donor atoms, these distances are significantly elongated due to the typical Jahn-Teller distortion of the copper(II) ions. Two coplanar assembled trinuclear complex cations are linked through coordination of the perchlorate ion Cl1 in the apical positions of copper Cu2 and Cu3 in distances of 245 pm (Cu2–O11) and 262 pm (Cu3–O12). This leads to the cationic dimer structure shown in figure 2.5. Moreover the perchlorate ion Cl2 coordinate to the Cu1 in a distance of 256 pm (Cu1–O21) at the opposite site of the above defined ligand plane. Therefore the coordination geometry of the three copper ions can be best described as distorted (4+1) square pyramidal.

The cationic dimers further assemble to 1D chains through hydrogen bonding interactions between the perchlorate ion Cl2 and the coordinated water molecule O2W along the *b*-axis of the unit cell (see figure 2.6). Additional weak apical interactions are formed between the copper center Cu1 and the imine nitrogen atom N1A within these chains in a rather large distance of 347 pm. The same interaction has been observed in a similar dinuclear resorcinol-bridged copper complex.^[167] Furthermore these chains are cross-linked through hydrogen bonding interactions between the perchlorate ion Cl2 and the coordinated water molecule O2W of a parallel aligned chain. In addition the co-crystallized water molecules and the perchlorate ion Cl3 are involved in this hydrogen bonding in-

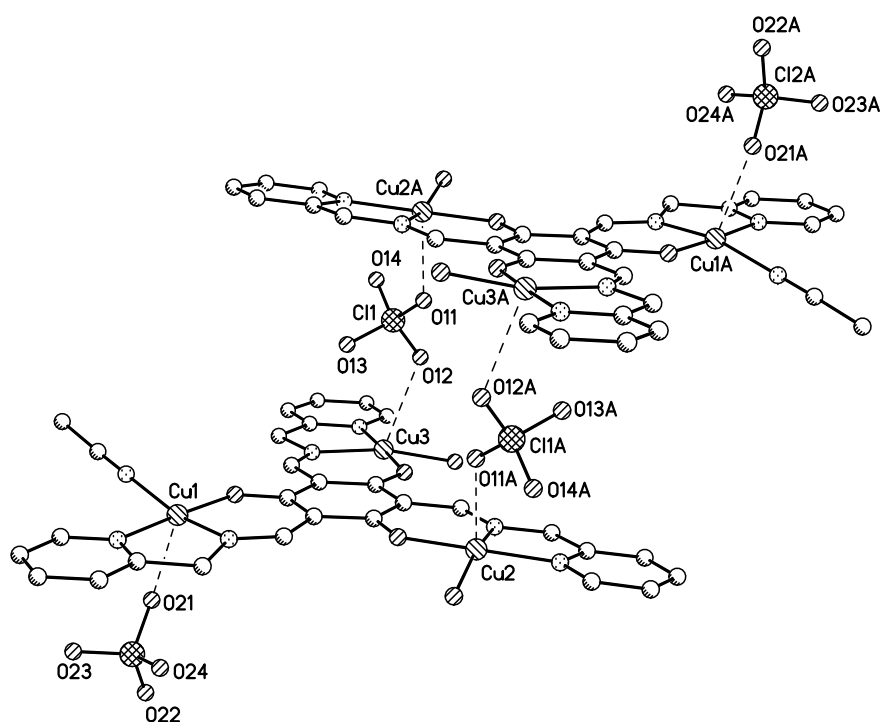


Figure 2.5: Representation of the cationic dimers of complex $\text{Cu}_3\text{L1}^{\text{ampy}}$ (1). Hydrogen atoms are omitted for clarity. Symmetry equivalent atoms are labeled with the suffix A. Dashed lines indicate weak apical coordinations of the copper centers in distances (pm) of Cu1...O21 256.3, Cu2...O11A 245.1, and Cu3...O12 261.8.

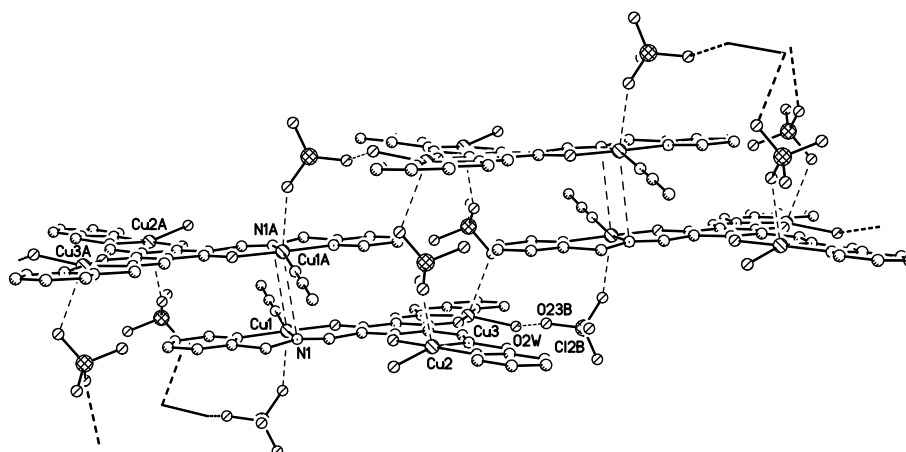


Figure 2.6: Representation of the 1D supramolecular chains of complex $\text{Cu}_3\text{L1}^{ampy}$ (1). Hydrogen atoms are omitted for clarity. The non-coordinating perchlorate ion Cl3 and the co-crystallized water molecules are also not shown. Symmetry equivalent atoms are labeled with the suffix A and B. Dashed lines indicate either weak apical contacts at the copper centers or hydrogen bonding interactions. Pertinent distances (pm): $\text{Cu1} \cdots \text{N1A}$ 347.2 and $\text{O2W} \cdots \text{O23B}$ 288.1.

teractions leading to the formation of a compact 3D network. It should be noted that all perchlorate counterions within this complex do not show any disorder, presumably due to the bridging connectivity within the 3D network. The compact supramolecular network results in short separations between the copper centers of adjacent trinuclear complex molecules at distances of 423 pm for $\text{Cu1} \cdots \text{Cu1A}$, 451 pm for $\text{Cu1} \cdots \text{Cu1B}$ and 689 pm for $\text{Cu2} \cdots \text{Cu3C}$, compared to the large interatomic $\text{Cu} \cdots \text{Cu}$ separation of about 730 pm within the trinuclear complex cations.

$[\text{Cu}_3(\text{H}_2\text{L1}^{bhy})(\text{Him})_3](\text{ClO}_4)_2$ ($\text{Cu}_3\text{L1}^{bhy}$) (4)

The copper complex $[\text{Cu}_3(\text{H}_2\text{L1}^{bhy})(\text{Him})_3](\text{ClO}_4)_2$ crystallizes in the monoclinic space group $P\bar{1}$ as two independent trinuclear complex molecules within the asymmetric unit. It crystallizes together with methanol molecules which are partially disordered over different crystallographic positions. Both cationic complex molecules are very similar. Three copper centers are coordinated by the tetra-anionic ligand $(\text{H}_2\text{L1}^{bhy})^{4-}$ and linked through a central phloroglucinol bridge. The molecular structures of one independent complex cation of $\text{Cu}_3\text{L1}^{bhy}$ (4) is depicted in figure 2.7.

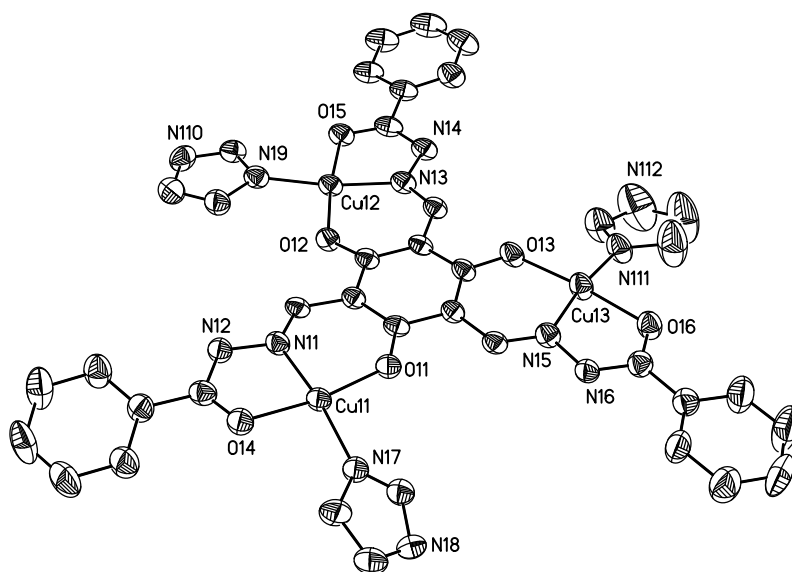


Figure 2.7: Molecular structure of one independent complex cation $[\text{Cu}_3(\text{H}_2\text{L1}^{bhy})(\text{Him})_3]^{2+}$ of $\text{Cu}_3\text{L1}^{bhy}$ (**4**). Thermal ellipsoids are drawn at the 50% probability level. Hydrogen atoms are omitted for clarity.

Each copper ion is coordinated in a square planar coordination environment by an N_2O_2 donor set. Three coordination sites at the copper center are occupied by the phenolate oxygen atom, the imine nitrogen atom and the carbonyl oxygen atom of the deprotonated ligand forming one six- and one five-membered chelate ring. The fourth equatorial position is occupied by the nitrogen atom of an imidazole molecule. As a result of the rigid and planar coordination mode of the ligand, the structural parameters of the tetragonal coordination planes within both molecules are very similar for all copper centers. The bond lengths, summarized in table 2.2, range from 190 to 199 ($j = 1$) as well as from 188 to 199 pm ($j = 2$) ($j = 1, 2$; running number assigned to the independent ligand moieties). The *trans* angles vary from 171 to 174° ($j = 1$) and 167 to 172° ($j = 2$) indicating only slight distortions of the corresponding square planes.

The ligand molecules are nearly planar with a mean deviation of 9 pm ($j = 1$) and 5 pm ($j = 2$) from the corresponding best least square plane including all ligand atoms, except the three phenylene rings of the side chains. These are slightly twisted due to the crystal packing. The two independent complex molecules assemble nearly coplanar in close proximity with a interplanar distance of approximately 330 pm and an angle of about 2° between their normal vectors. This is caused by weak interactions of the

Table 2.2: Selected bond lengths [pm] and angles [°] for both independent complex molecules of **Cu₃L1^{bhy}** (4)

Cu11–O11	188.3(4)	Cu21–O21	190.8(4)
Cu11–O14	196.9(4)	Cu21–O24	195.6(4)
Cu11–N11	190.2(4)	Cu21–N21	190.8(5)
Cu11–N17	191.9(5)	Cu21–N27	193.8(5)
Cu12–O12	193.7(3)	Cu22–O22	192.0(4)
Cu12–O15	195.4(3)	Cu22–O25	196.6(4)
Cu12–N13	190.3(5)	Cu22–N23	189.8(4)
Cu12–N19	194.7(5)	Cu22–N29	194.3(4)
Cu13–O13	193.1(4)	Cu23–O23	191.9(4)
Cu13–O16	199.4(4)	Cu23–O26	199.3(4)
Cu13–N15	190.9(4)	Cu23–N25	189.9(5)
Cu13–N111	193.7(5)	Cu23–N211	194.7(5)
O11–Cu11–O14	170.36(16)	O21–Cu21–O24	172.38(17)
O11–Cu11–N11	92.02(16)	O21–Cu21–N21	91.44(17)
O11–Cu11–N17	92.38(17)	O21–Cu21–N27	95.14(18)
O14–Cu11–N11	81.99(16)	O24–Cu21–N21	81.52(17)
O14–Cu11–N17	95.13(17)	O24–Cu21–N27	92.14(19)
N11–Cu11–N17	166.74(19)	N21–Cu21–N27	171.68(19)
O12–Cu12–O15	173.25(16)	O22–Cu22–O25	173.50(14)
O12–Cu12–N13	92.15(16)	O22–Cu22–N23	92.30(17)
O12–Cu12–N19	94.44(17)	O22–Cu22–N29	94.13(19)
O15–Cu12–N13	81.23(16)	O25–Cu22–N23	81.25(17)
O15–Cu12–N19	92.28(17)	O25–Cu22–N29	92.38(19)
N13–Cu12–N19	171.50(18)	N23–Cu22–N29	170.70(20)
O13–Cu13–O16	172.11(14)	O23–Cu23–O26	171.27(16)
O13–Cu13–N15	90.66(17)	O23–Cu23–N25	91.17(17)
O13–Cu13–N111	95.69(19)	O23–Cu23–N211	94.45(18)
O16–Cu13–N15	81.52(17)	O26–Cu23–N25	81.06(18)
O16–Cu13–N111	92.19(19)	O26–Cu23–N211	92.84(18)
N15–Cu13–N111	171.43(21)	N25–Cu23–N211	171.43(22)

copper centers with the imine and imidazole nitrogen as well as the phenolate and carbonyl oxygen atoms of the other independent trinuclear complex molecule in distances ranging from 276 pm up to 332 pm. The resulting supramolecular arrangement is depicted in figure 2.8. Moreover a perchlorate and a methanol molecule function as weakly bound axial co-ligands at the copper centers Cu_j3 in distances of 250 pm ($Cu13-O61$) and 279 pm ($Cu23-O2M$). These dimers further assemble to 1D chains along the b -axis of the unit cell through additional axial interactions between the copper centers Cu_j2 and the phenolate oxygen atoms O_j2 of adjacent complex molecules in distances of 339 pm ($j = 1$) and 299 pm ($j = 2$). Therefore the short non-covalent distances between the copper centers within the coordination chains are found between 346 and 419 pm, whereas the distances within each trinuclear complex cation across the phloroglucinol bridge are clearly longer with about 733 pm. The parallel chains are further cross-linked into a 3D network through hydrogen bonding interactions involving the perchlorate counterions and co-crystallized methanol molecules.

In the complex, each trinuclear cation crystallizes together with two perchlorate ions. To counterbalance the positive charge of three copper centers, the ligand has to be four times deprotonated. Consequently, beside the three phenolic oxygen atoms, one amide nitrogen atom of each ligand has to be deprotonated caused by the coordination of the copper centers in combination with basic reaction conditions. This is confirmed by a comparison of the bond lengths within the amide moieties in both independent complex molecules. The relevant distances are summarized in table 2.3. Obviously the carbonyl C_j16-O_j5 distance of 130 pm is significantly longer while the C_j16-N_j4 bond length of 131 pm is shorter compared to the corresponding averaged distances of the other amide moieties of 126 pm and 133 pm. These are nearly equal within both complex molecules. Hence the $O_j5-C_j16-N_j4$ angle of 124° is enlarged compared to 119° and in addition significantly different even within the 3σ range. This is caused by the deprotonation of the amide nitrogen atoms N_j4 . The negative charge is localized at the amide oxygen atom O_j5 resulting in a stronger polarization and an elongation of the C_j16-O_j5 bond. This is in excellent agreement with the amide bond lengths found in neutral vanadium(V) complexes of *N*-salicylidenehydrazide ligands compared to the corresponding mono-anionic vanadium(V) complexes, confirming the tetra-anionic nature of the ligand molecule within this complex.^[163–165,168]

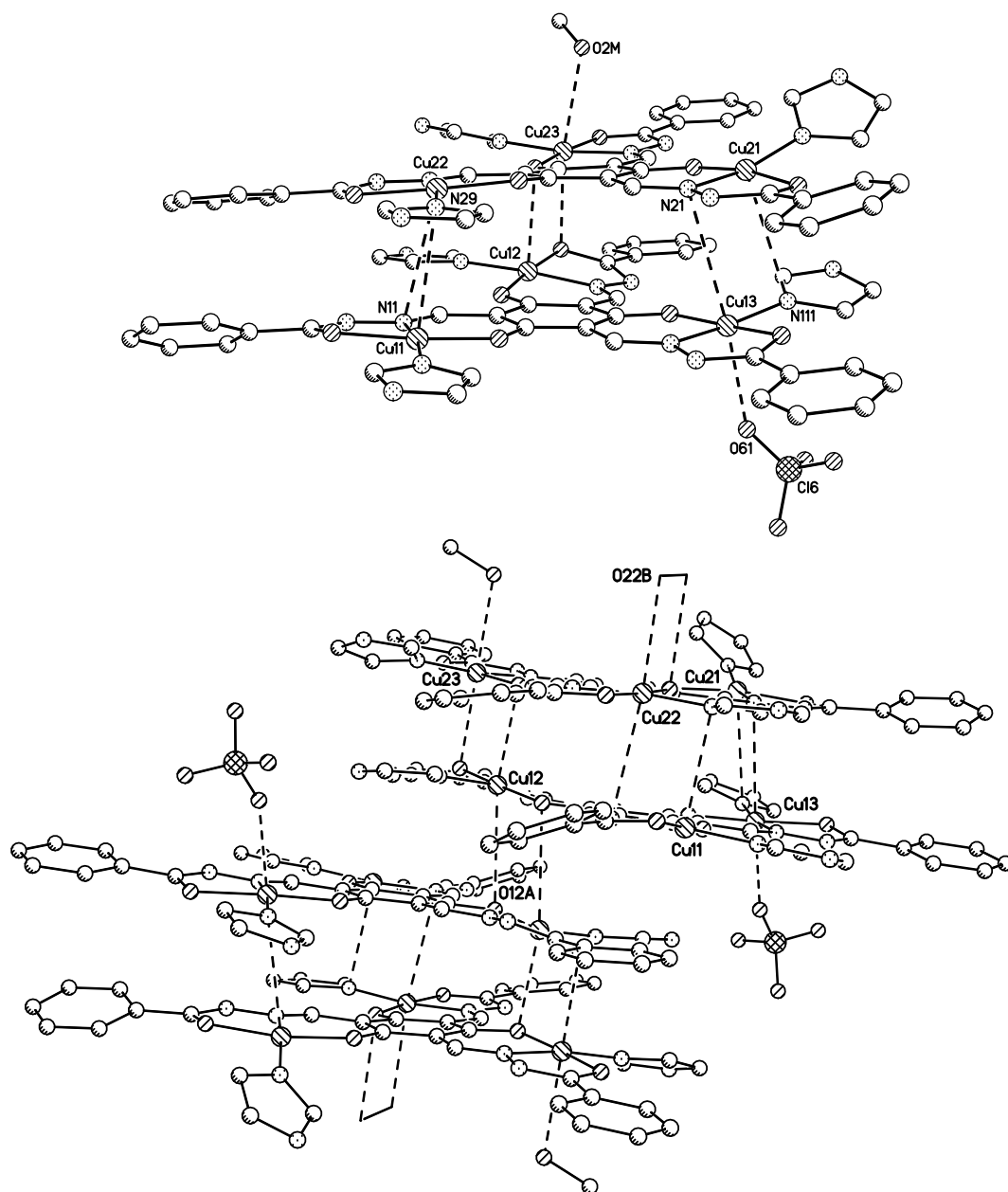


Figure 2.8: Supramolecular arrangement of both independent complex cations of $\text{Cu}_3\text{L1}^{bhy}$ (**4**). Axial copper donor contacts are drawn as dashed lines. Hydrogen atoms are omitted for clarity. Top: Repeating unit of the two independent complex cations. Pertinent axial copper donor distances (pm): Cu11 \cdots N29 310.4, Cu12 \cdots O23 276.1, Cu13 \cdots N21 338.4, Cu13 \cdots O61 250.0, Cu21 \cdots N111 331.9, Cu22 \cdots N11 331.5, Cu23 \cdots O15 267.4, Cu23 \cdots O2M 279.1. Bottom: Arrangement of the repeating units into 1D supramolecular chains along the [010] direction. Pertinent axial copper donor distances (pm): Cu12 \cdots O12A 338.8 and Cu22 \cdots O22B 299.1.

Table 2.3: Selected bond lengths [pm] and angles [°] for both independent complex molecules ($j = 1, 2$) of $\text{Cu}_3\text{L1}^{bhy}$ (**4**).

	$j = 1$	$j = 2$
Cj8–Oj4	125.7(7)	126.8(7)
Cj8–Nj2	133.1(7)	134.3(6)
Cj16–Oj5	130.1(6)	129.5(7)
Cj16–Nj4	130.5(7)	130.6(7)
Cj24–Oj6	127.5(7)	125.7(6)
Cj24–Nj6	131.1(7)	134.1(7)
Oj4–Cj8–Nj2	119.6(5)	119.6(5)
Oj5–Cj16–Nj4	123.6(5)	124.2(4)
Oj6–Cj24–Nj6	118.0(5)	118.9(5)

2.3.2 Nickel Complexes

$[\text{Ni}_3(\text{L1}^{ampy})(\text{Hbpea})_3](\text{ClO}_4)_3$ ($\text{Ni}_3\text{L1}^{ampy}$) (**2**)

The trinuclear complex $\text{Ni}_3\text{L1}^{ampy}$ (**2**) is obtained as crystals together with co-crystallized acetonitrile, methanol and water molecules, which are predominantly located at partially occupied positions. The complex crystallizes as a two independent complex molecules in the monoclinic space group $P2_1/n$. The molecular structure and labeling scheme of one complex cation of $\text{Ni}_3\text{L1}^{ampy}$ (**2**) is depicted in figure 2.9. Three nickel centers are connected in a *meta*-phenylene arrangement through a central phloroglucinol bridge. The coordination geometries of all nickel centers within both independent complex molecules are almost equal. Furthermore the bond lengths and angles are very similar summarized in table 2.4.

Each nickel ion is coordinated in a slightly distorted octahedral geometry with a N_5O donor set as indicated by the *trans* angles varying from 167° to 174° . One tridentate binding pocket of the *meta*-phenylene bridging ligand and the co-ligand Hbpea are coordinated in a meridional fashion forming one five- and three six-membered chelate rings at each nickel center. The coordinative bond lengths including all nickel(II) ions range between 198 to 218 pm. Comparatively short distances are present within the six-membered chelate ring formed with the phenolate oxygen atom and the imine nitrogen

Table 2.4: Selected bond lengths [pm] and angles [°] for both independent complex molecules of complex **Ni₃L1^{ampy}** (**2**).

Ni11–O11	202.1(3)	Ni21–O21	201.7(3)
Ni11–N11	198.5(4)	Ni21–N21	198.9(4)
Ni11–N12	210.9(4)	Ni21–N22	207.9(4)
Ni11–N17	217.8(4)	Ni21–N27	214.6(4)
Ni11–N18	210.3(4)	Ni21–N28	212.5(4)
Ni11–N19	214.8(4)	Ni21–N29	213.4(4)
Ni12–O12	202.3(3)	Ni22–O22	202.9(3)
Ni12–N13	200.0(3)	Ni22–N23	198.5(4)
Ni12–N14	211.6(4)	Ni22–N24	212.6(4)
Ni12–N110	215.7(4)	Ni22–N210	214.3(5)
Ni12–N111	212.8(4)	Ni22–N211	210.5(4)
Ni12–N112	212.8(4)	Ni22–N212	217.1(5)
Ni13–O13	202.5(3)	Ni23–O23	202.7(3)
Ni13–N15	197.9(4)	Ni23–N25	199.1(4)
Ni13–N16	210.3(4)	Ni23–N26	211.3(4)
Ni13–N113	216.4(4)	Ni23–N213	218.1(4)
Ni13–N114	211.4(4)	Ni23–N214	212.5(4)
Ni13–N115	213.4(4)	Ni23–N215	214.4(4)
O11–Ni11–N12	167.06(13)	O21–Ni21–N22	168.83(13)
N11–Ni11–N18	172.77(16)	N21–Ni21–N28	173.36(15)
N17–Ni11–N19	173.06(15)	N27–Ni21–N29	174.25(14)
O12–Ni12–N14	166.03(13)	O22–Ni22–N24	166.78(14)
N13–Ni12–N111	171.81(15)	N23–Ni22–N211	172.92(18)
N110–Ni12–N112	173.89(14)	N210–Ni22–N212	173.80(17)
O13–Ni13–N16	168.91(13)	O23–Ni23–N26	166.06(14)
N15–Ni13–N114	172.86(15)	N25–Ni23–N214	172.49(17)
N113–Ni13–N115	173.05(13)	N213–Ni23–N215	172.96(16)

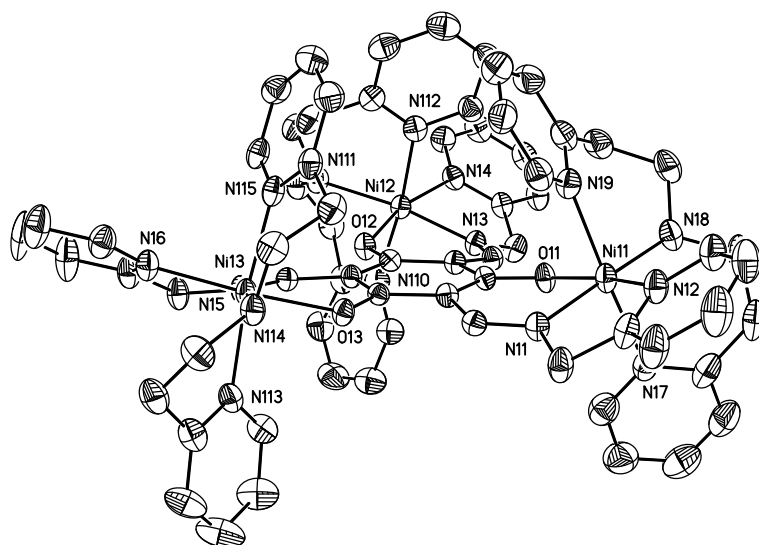


Figure 2.9: Molecular structure of one of the two independent complex cations of $\text{Ni}_3\text{L1}^{ampy}$ (**2**). Thermal ellipsoids are drawn at the 50% probability level. Hydrogen atoms are omitted for clarity.

atom, whereas the bond lengths to the amine nitrogen atom and all three pyridine nitrogen atoms are elongated situated at the upper end of range.

In contrast to the trinuclear copper complex $\text{Cu}_3\text{L1}^{ampy}$ (**1**) the overall geometry of the ligand molecule is not planar but bowl-shaped. Therefore the nickel ions are displaced out of the plane defined by the central bridging phloroglucinol with about 47 pm for Ni11, 42 pm for Ni12, and 49 pm for Ni13. Although the complex exhibits no crystallographically imposed symmetry, it possess nearly C_3 symmetry confirmed by the nickel centers all located at the same site towards the phloroglucinol moiety. Furthermore the Hbpea co-ligand molecules are also assembled corresponding to the symmetry, without any disorder of the pyridin-2-ylethyl groups. The second independent complex cation shows an overall higher distortion concerning the C_3 symmetry as an effect of the crystal packing. The nickel ions show a displacement from the phloroglucinol plane of about 61 pm for Ni21, 44 pm for Ni22 and 37 pm for Ni23.

The trinuclear cations are arranged coplanar concerning the planes defined by the phloroglucinol bridge perpendicular to the [001] direction of the unit cell. The positive charge is counterbalanced by three perchlorate ions situated, analogous to the observed symmetry, each nearby the protonated amine atom of the corresponding Hbpea co-ligand under formation of hydrogen bonding interactions. These establish further $\text{CH}\cdots\text{O}$ in-

teractions with the pyridine rings of the Hbpea co-ligands and the ligand side chains of adjacent complex molecules leading to an extended 3D network. The co-crystallized methanol and water molecules contribute also to this 3D network.



In complex $\text{Ni}_3\text{L1}^{\text{unspenp}}$ (3) three nickel ions are chelated and linked in a *meta*-phenylene arrangement by the triple deprotonated ligand. The positive charge of the trinuclear complex molecules is counterbalanced by three perchlorate ions in the crystal lattice. The molecular structure and heteroatom labeling scheme of the complex cation of $\text{Ni}_3\text{L1}^{\text{unspenp}}$ (3) is depicted in figure 2.10. Selected bond lengths and angles are summarized in table 2.5.

The complex crystallizes in the rhombohedral space group $R\bar{3}$ and therefore possess a crystallographic C_3 symmetry perpendicular to the phloroglucinol plane. Three crystallographically equivalent nickel ions are connected in a *meta*-phenylene arrangement through a central phloroglucinol bridge. The asymmetric unit contains only one nickel ion coordinated in an almost ideal octahedral environment. The coordination sites at the nickel ion are occupied by the N_4O donor set of the deprotonated ligand with distances ranging from 198 to 212 pm. The octahedral geometry is completed by a water molecule which binds in a distance of 215 pm. The distances to the phenolate oxygen atom O1 and the imine nitrogen atom N1 are with 198 pm and 199 pm rather short compared to the amine nitrogen atom N2 as well as both pyridine nitrogen atoms N3 and N4 all situated on the upper end of the respective range.

The *trans* angles are 174° (O1–Ni–N2), 176° (N1–Ni–O1W) and 160° (N3–Ni–N4) indicating only slight distortions from the octahedral geometry. Mainly this is caused by the ligand strain forming one six-membered and three five-membered chelate rings with the coordinated nickel ion. Both pyridine nitrogen atoms N3 and N4 and the amine nitrogen atom N2 are coordinated in a meridional fashion to the nickel center under formation of two five-membered chelate rings. This leads to a rather small N3–Ni–N4 *trans* angle of 160° compared to the trinuclear complex $\text{Ni}_3\text{L1}^{\text{ampy}}$ (2). Herein the meridional coordinated Hbpea co-ligand forms two six-membered chelate rings with the nickel ion resulting in a larger averaged *trans* angle of about 173° . Within the plane of the phloroglucinol bridge, the nickel center is coordinated by the phenolate oxygen atom O1, the imine

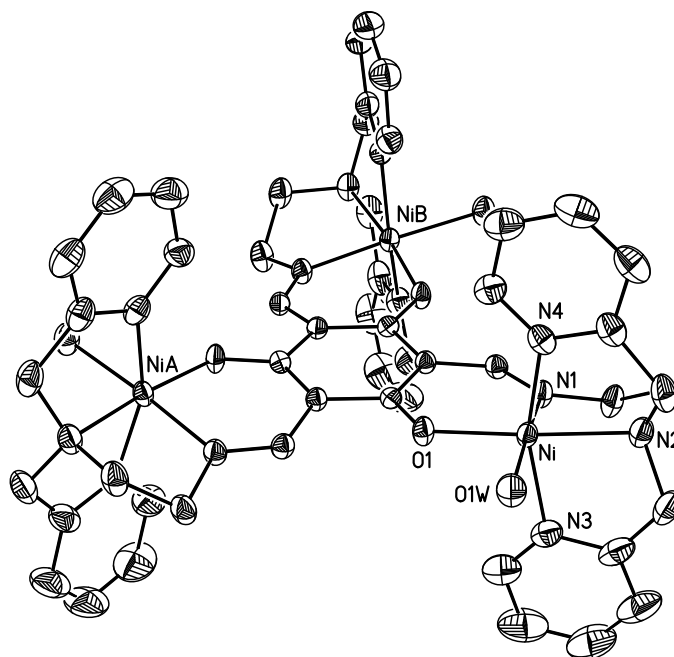


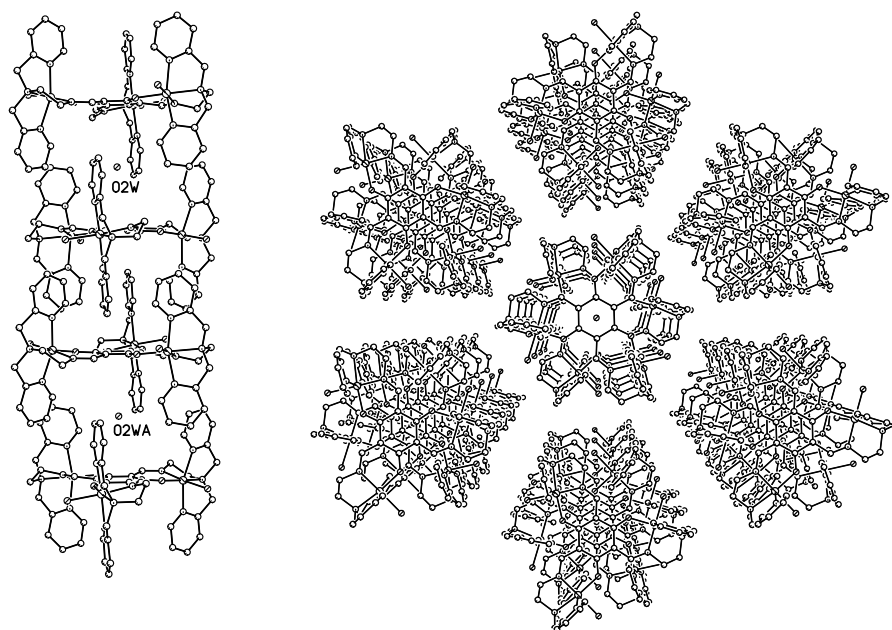
Figure 2.10: Molecular structure of the trinuclear complex cation of $\text{Ni}_3\text{L1}^{\text{unspenp}}$ (**3**). Thermal ellipsoids are drawn at the 50% probability level. Hydrogen atoms are omitted for clarity. Symmetry equivalent atoms are labeled with the suffixes A and B.

nitrogen atom N1, the amine nitrogen atom N3 and the water molecule O1W. The corresponding idealized tetragonal plane is nearly coplanar with a dihedral angle of about 12° . Therefore the nickel ion is situated quite nicely within the phloroglucinol plane with a displacement of only 24 pm. This leads to an interatomic Ni \cdots Ni separation of 740 pm.

In the crystal packing the cationic molecules assemble coplanar concerning the phloroglucinol bridge under formation of pillared arrangement along the c -axis of the unit cell including the co-crystallized water molecules shown in figure 2.11. Herein the water molecules are located on the crystallographic C_3 axis each encapsulated by two staggered trinuclear complex molecules in a distance of about 406 pm from the phloroglucinol planes. The perchlorate counterions are located between these pillars and establish hydrogen bonding interactions with the coordinated water O1W in a distance of 289 pm (O1W \cdots O14). In addition the perchlorate ions do not show any disorder, due to additional CH \cdots O interactions formed with carbon bound hydrogen atoms of parallel pillars.

Table 2.5: Selected bond lengths [pm] and angles [°] for complex **Ni₃L1**^{unspenp} (3).

Ni–O1	197.6(2)	Ni–N1	199.2(2)
Ni–N2	211.5(2)	Ni–N3	206.5(2)
Ni–N4	207.3(2)	Ni–O1W	215.3(2)
O1–Ni–O1W	90.69(9)	O1–Ni–N1	89.89(8)
O1–Ni–N2	173.68(8)	O1–Ni–N3	98.67(9)
O1–Ni–N4	100.13(8)	N1–Ni–O1W	176.04(11)
N1–Ni–N2	83.85(9)	N1–Ni–N3	89.31(9)
N1–Ni–N4	97.70(9)	N2–Ni–O1W	95.61(9)
N2–Ni–N3	82.14(10)	N2–Ni–N4	79.95(9)
N3–Ni–O1W	86.74(11)	N3–Ni–N4	159.92(10)
N4–Ni–O1W	86.05(11)		

**Figure 2.11:** Supramolecular pillared arrangement of the trinuclear complex cations of **Ni₃L1**^{unspenp} (3). Hydrogen atoms are omitted for clarity. Symmetry equivalent atoms are labeled with the suffix A. Left: Sideview parallel to the *c*-axis, Right: Topview along the *c*-axis of the unit cell.

$$[\text{Ni}_3(\text{H}_3\text{L1}^{bhy})(\text{Hbpea})_3](\text{ClO}_4)_3 \quad (\text{Ni}_3\text{L1}^{bhy}) \quad (5)$$

The trinuclear complex $\text{Ni}_3\text{L1}^{bhy}$ (5) is obtained as crystals together with co-crystallized acetonitrile and methanol molecules. The ligand coordinate three nickel ions in its three-anionic form after deprotonation of the phenolic oxygen atoms. The molecular structure of the complex cation of $\text{Ni}_3\text{L1}^{bhy}$ together with the labeling scheme is depicted in figure 2.12. Selected bond lengths and angles are listed in table 2.6.

Analogous to the nickel complex $\text{Ni}_3\text{L1}^{unspenp}$ (3), this complex has a crystallographically imposed C_3 symmetry crystallizing in the rhombohedral space group $R\bar{3}$ with a C_3 axis perpendicular to the phloroglucinol plane. The asymmetric unit contains only one nickel ion with a slightly distorted octahedral coordination environment which is similar to them in the nickel complex $\text{Ni}_3\text{L1}^{ampy}$ (2).

Three coordination sites at the nickel center are occupied by the NO_2 donor set of the central phloroglucinol ligand coordinating in a meridional fashion with bite angles of about 87° and 78° for O1-Ni-N1 and O2-Ni-N1 . The octahedral geometry is completed by the tris-chelating Hbpea co-ligand with bite angles of about 92° and 84° for N3-Ni-N4 and N4-Ni-N5 . The coordinative bond lengths at the nickel(II) ion range between 200 to 214 pm. The distances to the phenolate oxygen atom O1 and the imine nitrogen atom N1 are with approximately 201 pm rather short compared to the carbonyl oxygen atom

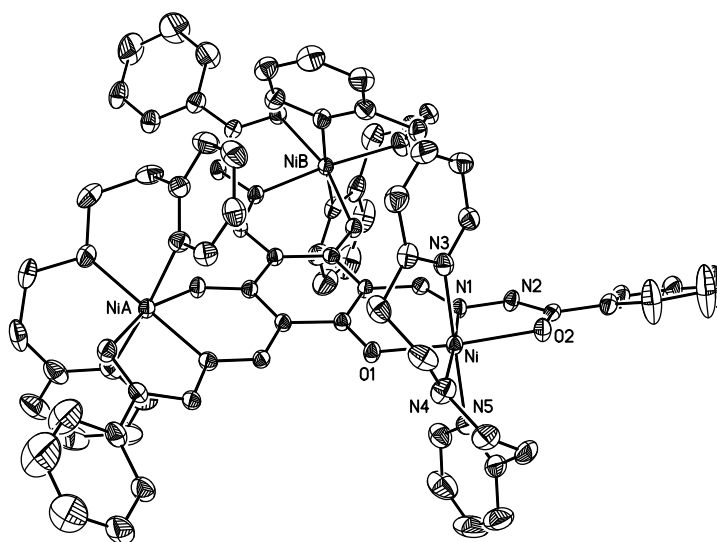


Figure 2.12: Molecular structure of the trinuclear complex cation of complex $\text{Ni}_3\text{L1}^{bhy}$ (5). Thermal ellipsoids are drawn at the 50% probability level. Hydrogen atoms are omitted for clarity.

Table 2.6: Selected bond lengths [pm] and angles [°] for complex **Ni₃L1^{bhy}** (5).

Ni–O1	201.2(2)	Ni–O2	214.0(2)
Ni–N1	199.8(2)	Ni–N3	213.2(3)
Ni–N4	209.5(3)	Ni–N5	212.4(3)
O1–Ni–O2	164.09(8)	O1–Ni–N1	86.72(8)
O1–Ni–N3	92.14(9)	O1–Ni–N4	88.94(10)
O1–Ni–N5	88.94(9)	O2–Ni–N1	77.59(8)
O2–Ni–N3	90.78(9)	O2–Ni–N4	106.59(10)
O2–Ni–N5	89.19(9)	N1–Ni–N3	91.09(10)
N1–Ni–N4	174.75(11)	N1–Ni–N5	92.70(10)
N3–Ni–N4	92.14(9)	N3–Ni–N5	176.11(10)
N4–Ni–N5	84.26(11)		

O2, the amine nitrogen atom N4 as well as both pyridine nitrogen atoms N4 and N5, all situated on the upper end of the respective range.

A tetragonal plane can be defined for the three donor atoms of the tridentate ligand (O1, O2 and, N1) and the amine nitrogen atom N4 of the Hbpea co-ligand whereas the nickel ion is situated nearly perfect within having a minimal displacement of 6 pm. The apical positions are occupied by the pyridine nitrogen atoms N3 and N5 of the co-ligand. The three *trans* angles range between 164° and 174° indicating only a slight distortion from the octahedral geometry. The dihedral angle between the defined tetragonal plane and the mean plane of the central phloroglucinol bridge, defined by the six carbon and three oxygen atoms, is about 20° due to the bowl-shaped ligand molecule within the trinuclear complex. Therefore the nickel centers are displaced by 61 pm out of the phloroglucinol plane. This leads to an interatomic Ni···Ni separation of 738 pm.

The complex cation of **Ni₃L1^{bhy}** (5) crystallizes together with three perchlorate counterions. Each perchlorate ion forms intramolecular hydrogen bonding interactions with the protonated nitrogen atoms N2 of the ligand and N4b of the Hbpea co-ligand in distances of 316 pm (N2···O13), 304 pm (N2···O14) and 322 pm (N4B···O12). Further strong CH···anion hydrogen bonding is formed with the pyridine ring of the Hbpea co-ligands of adjacent molecules in a distance of 335 pm (C14···O11), situated at the lower end of the usually observed range.^[169] This leads to a 2D hydrogen bonding network oriented

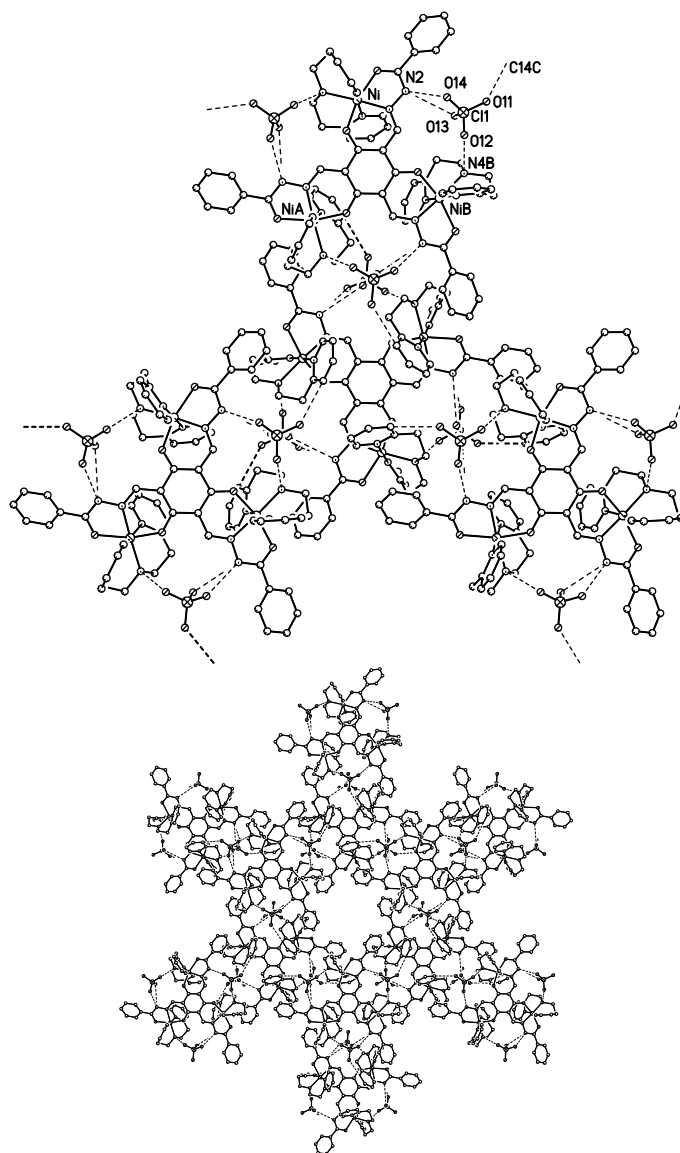


Figure 2.13: Representation of the 2D hydrogen bonding network in the crystal structure of $\text{Ni}_3\text{L1}^{bhy}$ (5), view along the [001] direction of the unit cell. Dashed lines indicate hydrogen bonding interactions. Symmetry-related atoms are labeled with the suffix A to C. Pertinent distances (pm): O11 \cdots C14C 334.9, O12 \cdots N4B 321.8, O13 \cdots N2 316.0, O14 \cdots N2 304.0.

perpendicular to the crystallographic c -axis of the unit cell which is shown in figure 2.13. Therefore the perchlorate counterions do not show any disorder. These layers further assemble into a 3D network through π - π interactions between the pyridine rings of the Hbpea co-ligands with a interplanar distance of about 350 pm.

2.3.3 Cobalt Complex

 $[\text{Co}_3(\text{L}^{\text{tBubhy}})(\text{bpca})_3] (\text{Co}_3\text{L}^{\text{tBubhy}}) \text{ (6)}$

The molecular structure as well as the labeling scheme of the trinuclear cobalt(III) complex $\text{Co}_3\text{L}^{\text{tBubhy}}$ (6) is depicted in figure 2.14. The complex crystallizes in the triclinic space group $P\bar{1}$ with three cobalt centers within the asymmetric unit. Each cobalt is coordinated within one binding pocket of the ligand linked through the phloroglucinol bridge. In contrast to previously discussed transition metal complexes $\text{Cu}_3\text{L}^{\text{bhy}}$ (4) and $\text{Ni}_3\text{L}^{\text{bhy}}$ (5) of the unsubstituted ligand, the ligand is fully deprotonated coordinating in the hexaanionic form to three cobalt ions. The single deprotonated bpca co-ligand completes the coordination sphere of each cobalt(III) center resulting in a neutral trinuclear cobalt complex. Analogous to $\text{Cu}_3\text{L}^{\text{bhy}}$ (4), the cobalt complex exhibits a pseudo C_3 symmetry with only slight variations within the bond lengths and angles summarized in table 2.7.

Each cobalt ion is embedded in a slightly distorted octahedral coordination environment with an N_4O_2 donor set as indicated by the *trans* angles varying from 166° to 180° .

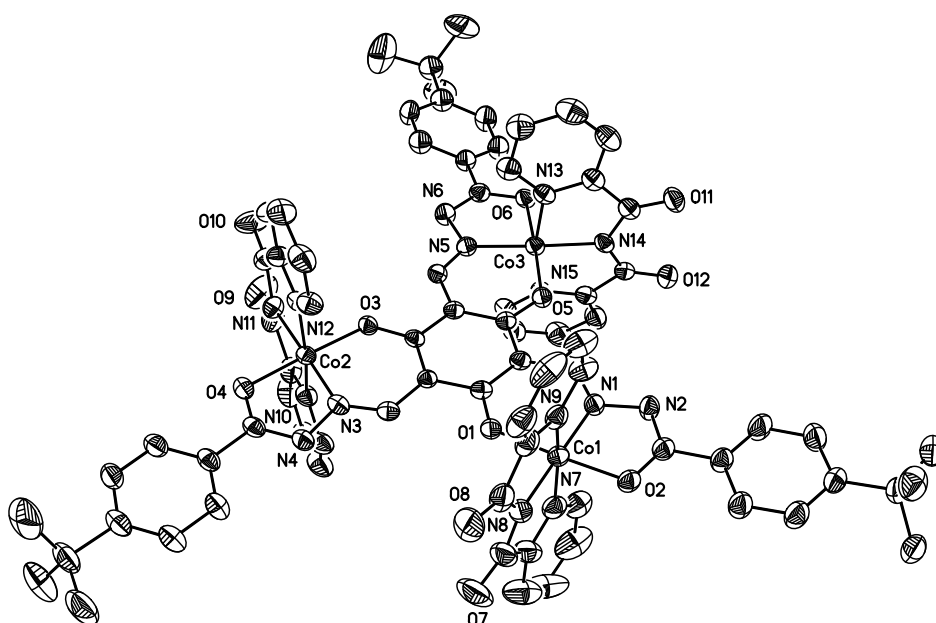


Figure 2.14: Molecular structure of the trinuclear complex $\text{Co}_3\text{L}^{\text{tBubhy}}$ (6). Thermal ellipsoids are drawn at the 50% probability level. Solvent molecules and hydrogen atoms are omitted for clarity.

Table 2.7: Selected bond lengths [pm] and angles [°] for complex **Co₃L1^{tBubhy}** (6).

Co1–O1	188.6(4)	Co2–O3	187.8(4)	Co3–O5	190.7(4)
Co1–O2	190.0(4)	Co2–O4	189.3(4)	Co3–O6	189.1(4)
Co1–N1	186.9(5)	Co2–N3	186.7(5)	Co3–N5	186.0(5)
Co1–N7	193.8(6)	Co2–N10	193.1(5)	Co3–N13	193.0(5)
Co1–N8	190.7(5)	Co2–N11	189.7(5)	Co3–N14	189.3(5)
Co1–N9	193.1(5)	Co2–N12	193.4(5)	Co3–N15	193.3(5)
O1–Co1–O2	176.97(17)	O3–Co2–O4	177.65(17)	O5–Co3–O6	177.31(17)
N1–Co1–N8	179.6(2)	N3–Co2–N11	179.1(2)	N5–Co3–N14	177.0(2)
N7–Co1–N9	166.1(2)	N10–Co2–N12	167.1(2)	N13–Co3–N15	166.3(2)

A tetragonal plane can be defined by the phenolate oxygen atom, the imine nitrogen atom and the carbonyl oxygen atom of the ligand binding pocket together with the amide nitrogen atom of the bpca co-ligand with only small variations of the averaged bond lengths ranging from 187 to 190 pm. Both apical positions are occupied by the pyridine nitrogen atoms of the bpca co-ligand in slightly larger distances of about 193 pm. All bond lengths are shorter compared to them in the nickel complex **Ni₃L1^{bhy}** (5) due to the closed-shell electronic structure of the diamagnetic cobalt(III) ion. Moreover all distances are in the observed range typical for octahedral low-spin cobalt(III) complexes.^[170–173] In addition the low-spin character is confirmed by magnetic measurements affording a diamagnetic signal at 300 K.

The averaged *trans* angles within the tetragonal planes are with about 177° for O–Co–O and 179° for N–Co–N very close to 180° of an ideal octahedron. Hence the cobalt centers are located exactly within the corresponding plane. Furthermore all planes are coplanar with the phloroglucinol bridge having a maximal dihedral angle of about 3° confirming the planarity of the ligand molecule. Only the phenylene rings with the essentially not planar *tert*-butyl substituents are slightly twisted, due to packing effects. This leads to an interatomic Co···Co separation of about 725 pm.

In the crystal packing the trinuclear complex molecules assemble coplanar concerning the phloroglucinol plane analogous to all other described phloroglucinol-bridged complexes. The trinuclear complex molecules assemble into 1D chains through π - π interactions with an interplanar separation of 344 pm between adjacent pyridine rings of the

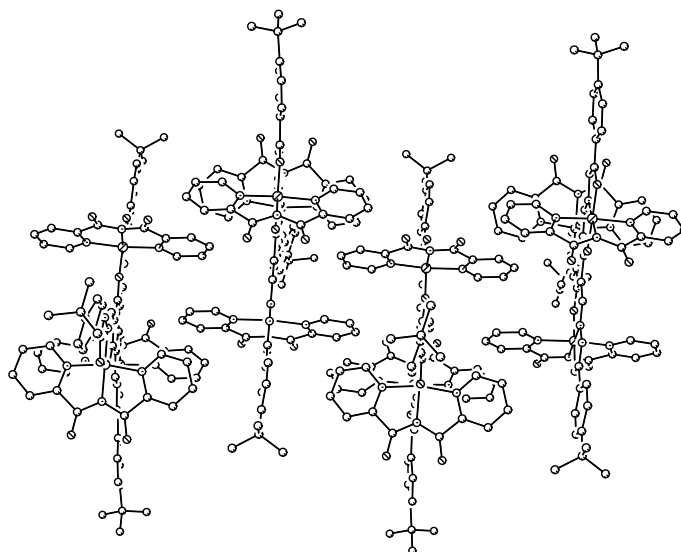


Figure 2.15: Representation of the π - π stacking of the trinuclear complex molecules of $\text{Co}_3\text{L1}^{t\text{Bubhy}}$ (6). Hydrogen atoms as well co-crystallized solvent molecules are omitted for clarity.

bpca co-ligand coordinated at the Co2 center. This is shown in figure 2.15. The 1D chains are aligned parallel and cross-linked through hydrogen bonding interactions with the co-crystallized methanol and water molecules resulting in a 3D network.

2.4 Magnetic Properties

The magnetization of polycrystalline samples of both copper(II) complexes $\text{Cu}_3\text{L1}^{ampy}$ (1) and $\text{Cu}_3\text{L1}^{bhy}$ (4) as well as the three nickel(II) compounds $\text{Ni}_3\text{L1}^{ampy}$ (2), $\text{Ni}_3\text{L1}^{unspenp}$ (3), and $\text{Ni}_3\text{L1}^{bhy}$ (5) are measured in a temperature range between 2 and 300 K. The magnetic susceptibility data of the trinuclear cobalt(III) complex $\text{Co}_3\text{L1}^{t\text{Bubhy}}$ (6) at 300 K reveals a diamagnetic $S = 0$ ground state, which is in agreement with the crystallographic data indicating all cobalt centers to be in the low-spin state.

Trinuclear Copper Complexes

Variable temperature (2–300 K) magnetic susceptibility data for the trinuclear copper complexes $\text{Cu}_3\text{L1}^{ampy}$ (1) and $\text{Cu}_3\text{L1}^{bhy}$ (4) are depicted in figure 2.16 as $\chi_M = f(T)$ and $\chi_M T = f(T)$ plots. The experimental $\chi_M T$ value of both complexes at 300 K is $1.34 \text{ cm}^3 \text{ K mol}^{-1}$, which is close to the theoretical spin-only value expected for three in-

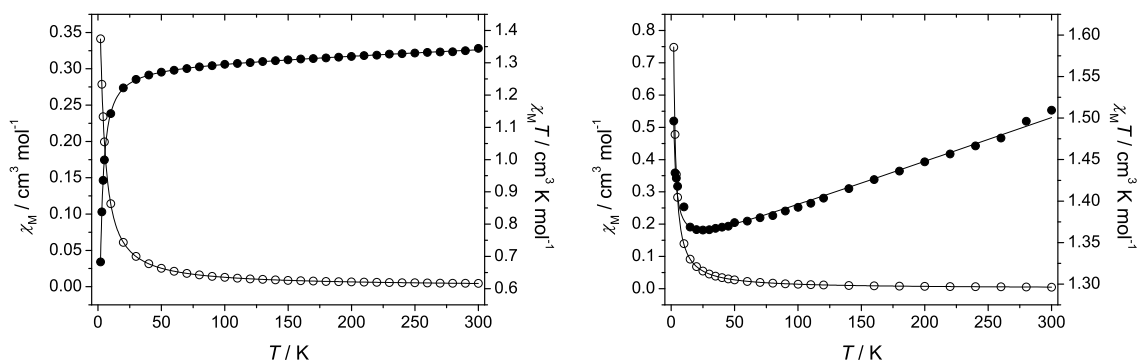


Figure 2.16: Plot of the thermal dependence of χ_M (empty circles, \circ) and $\chi_M T$ (black filled circles, \bullet) for the complexes **Cu₃L1^{ampy} (1)** (left) and **Cu₃L1^{bhy} (4)** (right) measured with an applied magnetic field of 2000 Oe. The corresponding fit functions according to equation 2.2 are drawn as solid lines (for parameters see text).

dependent copper(II) ions. For both complexes a different temperature dependency of the magnetic susceptibility is observed. Upon lowering the temperature the $\chi_M T$ value slightly decreases down to $1.17 \text{ cm}^3 \text{ K mol}^{-1}$ at 50 K and then rapidly decreases down to $0.68 \text{ cm}^3 \text{ K mol}^{-1}$ at 2 K for complex **Cu₃L1^{ampy} (1)**. This behavior indicates an antiferromagnetic coupling between the three copper ions mediated through the phloroglucinol bridge. In complex **Cu₃L1^{bhy} (4)** the $\chi_M T$ value slightly decreases upon lowering the temperature reaching a minimum value of $1.21 \text{ cm}^3 \text{ K mol}^{-1}$ at 25 K. Further lowering the temperature leads to a rapid increase of the $\chi_M T$ value. This behavior is characteristic for ferromagnetic exchange interactions between the three copper ions. The slight decrease of the $\chi_M T$ values of both complexes in the high temperature region can be ascribed to a temperature independent paramagnetism.

The three copper ions in both complexes are coordinated by the ligands in an almost C_3 symmetric triangular arrangement. Hence for symmetry reasons the three copper centers can be treated as an equilateral triangle with three equal pairwise magnetic interactions. The corresponding isotropic spin Hamiltonian is given as:

$$\hat{H} = -J(\hat{S}_1\hat{S}_2 + \hat{S}_1\hat{S}_3 + \hat{S}_2\hat{S}_3) \quad (2.1)$$

For $S_1 = S_2 = S_3 = 1/2$ this leads to the expression given in equation 2.2 with the abbreviation $A = -3J/2kT$.

$$\chi_M = \frac{N_A \beta^2 g^2}{4kT} \frac{5 + \exp A}{1 + \exp A} + \chi_{TIP} \quad (2.2)$$

Herein χ_{TIP} represents the contribution due to the temperature independent paramagnetism. The best fit of the experimental data according to equation 2.2 results in $J = -1.636(2) \text{ cm}^{-1}$, $g = 2.143(1)$, and $\chi_{TIP} = 1.8(2) \cdot 10^{-4} \text{ cm}^3 \text{ mol}^{-1}$ for complex **Cu₃L1^{ampy}** (**1**) with $r^2 = 0.99994$. For complex **Cu₃L1^{bhy}** (**4**) this leads to $J = +0.330(11) \text{ cm}^{-1}$, $g = 2.055(1)$, and $\chi_{TIP} = 4.7(1) \cdot 10^{-4} \text{ cm}^3 \text{ mol}^{-1}$ with $r^2 = 0.98499$.

For both complexes **Cu₃L1^{ampy}** (**1**) and **Cu₃L1^{bhy}** (**4**) very weak exchange interactions are obtained. Within the trinuclear complex **Cu₃L1^{bhy}** (**4**) the interaction is ferromagnetic as expected from the spin polarization mechanism. The ferromagnetic coupling is significantly weaker compared to published trinuclear phloroglucinol-bridged copper(II) complexes with J ranging from $+2.04$ up to $+6.61 \text{ cm}^{-1}$.^[62,89,113] Within the trinuclear complex **Cu₃L1^{ampy}** (**1**) the interaction is even antiferromagnetic.

Although the simple picture of a spin polarization mechanism would predict a ferromagnetic ground state for a *meta*-phenylene-bridged system, it has been shown by *Bencini et al.* that both spin polarization and superexchange effects contribute to the overall coupling behavior in such systems.^[70] Within both complexes the copper centers are coordinated in a square planar arrangement with negligible semi-coordinated axial contacts. Hence the magnetic orbital at each copper ion has basically $d_{x^2-y^2}$ character, which is almost orthogonal to the π -system of the phloroglucinol bridge. Therefore only an indirect spin polarization is possible, which is less effective. This is corroborated by a series of phloroglucinol-bridged square planar copper complexes differing in the ligand folding. Herein flat geometries weaken the ferromagnetic coupling, while ligand folding strengthens the ferromagnetic coupling.^[113] Density functional calculations indicate that this effect cannot be ascribed only to spin polarization but spin-delocalization is also effective. This is also in agreement with results of DFT calculations on similar dinuclear *meta*-phenylene-bridged copper(II) complexes.^[174] In complex **Cu₃L1^{bhy}** (**4**) the ligand exhibits an overall stronger distortion compared to the nearly planar copper complex

$\text{Cu}_3\text{L1}^{ampy}$ (**1**), which is in agreement with the stronger ferromagnetic exchange interaction through spin polarization mechanism. Consequently, the more effective superexchange pathway through the *meta*-phenylene-bridging unit dominates in the complex $\text{Cu}_3\text{L1}^{ampy}$ (**1**) and leads to the overall antiferromagnetic exchange coupling between the copper centers.

Trinuclear Nickel Complexes

Variable temperature (2–300 K) magnetic susceptibility data for the trinuclear nickel complexes $\text{Ni}_3\text{L1}^{ampy}$ (**2**), $\text{Ni}_3\text{L1}^{unspenp}$ (**3**), and $\text{Ni}_3\text{L1}^{bhy}$ (**5**) are depicted in figures 2.17, 2.18, and 2.19 as $\chi_M = f(T)$ and $\chi_M T = f(T)$ plots. The experimental $\chi_M T$ values at 300 K of $3.61 \text{ cm}^3 \text{ K mol}^{-1}$ for $\text{Ni}_3\text{L1}^{ampy}$ (**2**), $3.86 \text{ cm}^3 \text{ K mol}^{-1}$ for $\text{Ni}_3\text{L1}^{unspenp}$ (**3**), and $3.67 \text{ cm}^3 \text{ K mol}^{-1}$ for $\text{Ni}_3\text{L1}^{bhy}$ (**5**) are very similar and furthermore characteristic for the spin-only value of three independent nickel(II) centers with $S = 1$. The magnetic behavior of the three complexes is nearly identical. Upon lowering the temperature the $\chi_M T$ value slightly decreases up to a temperature of about 50 K and then drops to a value of $2.17 \text{ cm}^3 \text{ K mol}^{-1}$ for $\text{Ni}_3\text{L1}^{ampy}$ (**2**), $2.47 \text{ cm}^3 \text{ K mol}^{-1}$ for $\text{Ni}_3\text{L1}^{unspenp}$ (**3**), and $1.89 \text{ cm}^3 \text{ K mol}^{-1}$ for $\text{Ni}_3\text{L1}^{bhy}$ (**3**). This indicate either antiferromagnetic exchange in-

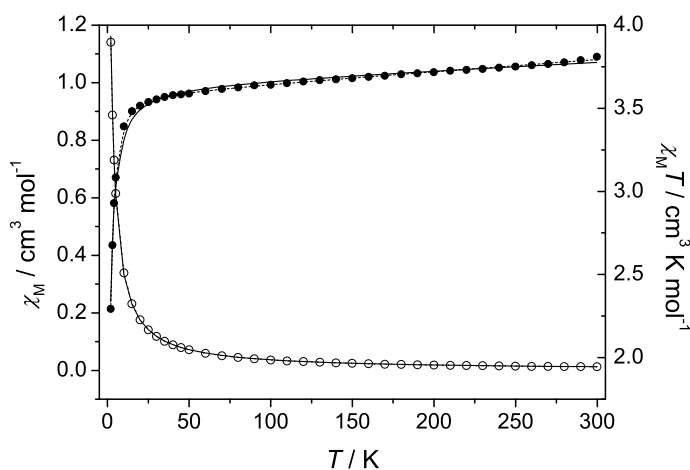


Figure 2.17: Plot of the thermal dependence of χ_M (empty circles, \circ) and $\chi_M T$ (black filled circles, \bullet) for complex $\text{Ni}_3\text{L1}^{ampy}$ (**2**) measured with an applied magnetic field of 2000 Oe. The solid lines represent the theoretical curves derived from equation 2.4 assuming exclusively isotropic exchange interactions. The dashed lines represent the best fit according to equation 2.5 taken additional ZFS into account (for parameters see text).

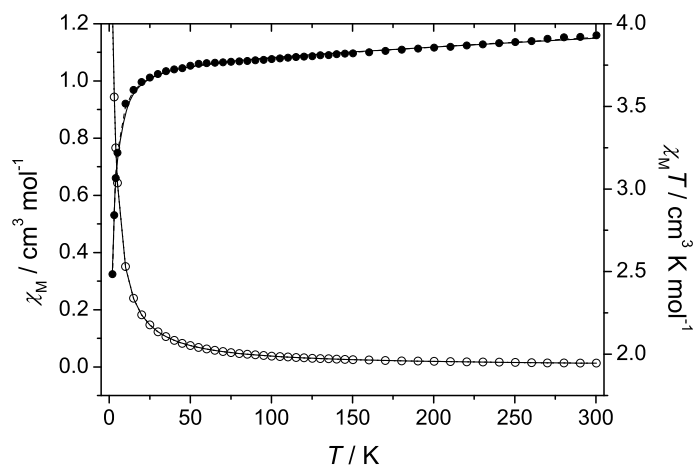


Figure 2.18: Plot of the thermal dependence of χ_M (empty circles, \circ) and $\chi_M T$ (black filled circles, \bullet) for complex $\text{Ni}_3\text{L1}^{\text{unspenp}}$ (**3**) measured with an applied magnetic field of 2000 Oe. The solid lines represent the theoretical curves derived from equation 2.4 assuming exclusively isotropic exchange interactions. The dashed lines represent the best fit according to equation 2.5 taken additional ZFS into account (for parameters see text).

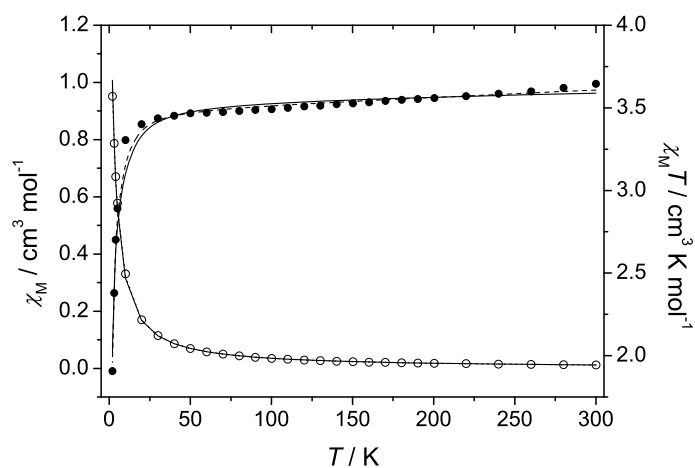


Figure 2.19: Plot of the thermal dependence of χ_M (empty circles, \circ) and $\chi_M T$ (black filled circles, \bullet) for complex $\text{Ni}_3\text{L1}^{\text{bhy}}$ (**5**) measured with an applied magnetic field of 2000 Oe. The solid lines represent the theoretical curves derived from equation 2.4 assuming exclusively isotropic exchange interactions. The dashed lines represent the best fit according to equation 2.5 taken additional ZFS into account (for parameters see text).

interactions or zero-field splittings (ZFS) in the trinuclear nickel(II) complexes with local spins of $S = 1$. However, a combination between these two effects might also be possible. Therefore the experimental data has been analyzed first taking into account the isotropic exchange interactions between the three nickel centers regardless to the ZFS.

Analogous to the copper complexes the Ni_3 core units within the three nickel complexes can be treated as an equilateral triangle with three equal pairwise magnetic interactions. The corresponding isotropic spin Hamiltonian is given as:

$$\hat{H} = -J(\hat{S}_1\hat{S}_2 + \hat{S}_1\hat{S}_3 + \hat{S}_2\hat{S}_3) \quad (2.3)$$

For $S_1 = S_2 = S_3 = 1$ the van Vleck equation leads to the expression given in the equation 2.2 with the following abbreviations: $A = J/kT$, $B = 3J/kT$, and $C = 6J/kT$.

$$\chi_M = \frac{2N_A\beta^2g^2}{kT} \frac{3\exp A + 10\exp B + 14\exp C}{1 + 9\exp A + 10\exp B + 7\exp C} + \chi_{TIP} \quad (2.4)$$

The temperature independent paramagnetism (χ_{TIP}) was also taken into account, as a result of the course of the experimental magnetic data in the temperature region above 50 K. The best fit according to equation 2.4 is obtained with the parameters $J = -0.462(7) \text{ cm}^{-1}$, $g = 2.203(2)$, and $\chi_{TIP} = 4.8(4) \cdot 10^{-4} \text{ cm}^3 \text{ mol}^{-1}$ for $\text{Ni}_3\text{L1}^{ampy}$ (**2**) with $r^2 = 0.99602$. Similar values could be obtained for complex $\text{Ni}_3\text{L1}^{unspenp}$ (**3**) with $J = -0.420(3) \text{ cm}^{-1}$, $g = 2.225(1)$, and $\chi_{TIP} = 4.7(2) \cdot 10^{-4} \text{ cm}^3 \text{ mol}^{-1}$ as well as for complex $\text{Ni}_3\text{L1}^{bhy}$ (**5**) with $J = -0.58(1) \text{ cm}^{-1}$, $g = 2.171(3)$, and $\chi_{TIP} = 2.5(7) \cdot 10^{-4} \text{ cm}^3 \text{ mol}^{-1}$ with $r^2 = 0.99838$ and $r^2 = 0.99122$, respectively.

The negative coupling constants of all complexes confirm the presence of weak antiferromagnetic interactions between the three nickel centers through the phloroglucinol bridge. Moreover the exchange couplings in the nickel complexes are nearly equal, in line with what is expected considering the highly related structural arrangements. The isotropic exchange interactions are rather strong compared to the antiferromagnetically coupled copper complex $\text{Cu}_3\text{L1}^{ampy}$ (**1**) with $J = -1.63 \text{ cm}^{-1}$. Moreover especially in the cases of weak exchange interactions, as in the current nickel complexes, the ZFS should be taken into account in order to reliably determine the exchange parameter J .^[175,176] Hence the

decrease of $\chi_M T = f(T)$ at lower temperatures might be attributed to additional ZFS, typical for hexa-coordinated nickel(II) complexes. Therefore the experimental data is analyzed with the program package DAVE using the appropriate spin hamiltonian given in equation 2.5.^[177] These include the isotropic exchange Hamiltonian, the single-ion zero-field splitting, and the single-ion Zeeman interaction. Due to C_3 symmetry of the complexes and to avoid overparametrization only one axial ZFS parameter D equal for the three nickel centers is assumed.

$$\hat{H} = -J(\hat{S}_1\hat{S}_2 + \hat{S}_1\hat{S}_3 + \hat{S}_2\hat{S}_3) + \sum_{i=1}^3 D_i[\hat{S}_{z,i}^2 - \frac{1}{3}(S_i(S_i + 1))] + \sum_{i=1}^3 g_i\beta\hat{S}_i\vec{H} \quad (2.5)$$

Considering χ_{TIP} , the best fit for complex $\text{Ni}_3\text{L1}^{ampy}$ (2) is obtained with parameters $J = -0.14 \text{ cm}^{-1}$, $D = -5.5 \text{ cm}^{-1}$, $g = 2.18$, and $\chi_{TIP} = 7.2 \cdot 10^{-4} \text{ cm}^3 \text{ mol}^{-1}$. A similarly good agreement with the experimental data could be obtained for complex $\text{Ni}_3\text{L1}^{unspenp}$ (3) with the best fit parameters $J = -0.37 \text{ cm}^{-1}$, $D = -1.8 \text{ cm}^{-1}$, $g = 2.23$, and $\chi_{TIP} = 5.4 \cdot 10^{-4} \text{ cm}^3 \text{ mol}^{-1}$. For complex $\text{Ni}_3\text{L1}^{bhy}$ (5) the best fit results in $J = -0.28 \text{ cm}^{-1}$, $D = -5.3 \text{ cm}^{-1}$, $g = 2.16$, and $\chi_{TIP} = 4.1 \cdot 10^{-4} \text{ cm}^3 \text{ mol}^{-1}$. It should be noted here, that it is difficult to unambiguously determine the sign of D from magnetic susceptibility data derived from powder measurements, because the variations of $\chi_M T$ are in general not very sensitive to the sign of D .^[178] The fits carried out with reversal sign for the D parameter led to only marginal worse fittings of the experimental magnetic data. Nevertheless the large D values of the complexes $\text{Ni}_3\text{L1}^{ampy}$ (2) and $\text{Ni}_3\text{L1}^{bhy}$ (5) are consistent with the observed distorted octahedral coordination geometry of the nickel(II) ions. The D value of complex $\text{Ni}_3\text{L1}^{unspenp}$ (3) is smaller, which is in excellent agreement with the almost ideal octahedral coordination geometry of the nickel centers in comparison to both other complexes. The magnetic anisotropy of the three nickel complexes is consistent with the fact, that no signal could be detected in the X-band EPR spectra. Moreover the D values are within the generally observed broad range from -22 to $+12 \text{ cm}^{-1}$.^[179-182] All complexes exhibit very weak antiferromagnetic exchange interactions between the three nickel ions. In complex $\text{Ni}_3\text{L1}^{unspenp}$ (3) the coupling is somewhat stronger, attributed to minor displacements of about 20 pm of the nickel ions relating to the bridging phloroglucinol plane compared to averaged 47 pm for complex $\text{Ni}_3\text{L1}^{ampy}$ (2) as well as 61 pm for complex $\text{Ni}_3\text{L1}^{bhy}$ (5). This is consistent with results obtained for the trinuclear copper complexes in the last section.

3 Triaminobenzene-Bridged Complexes

3.1 Ligand and Complex Design

In the previous chapter C_3 symmetric ligands based on phloroglucinol and the trinuclear transition metal complexes have been synthesized and characterized. In this chapter the tritopic arrangement of three metal ions with *meta*-phenylene linkage is based on 1,3,5-triaminobenzene. This approach has been only scarcely utilized in literature.^[63] In contrast the *meta*-phenylene linkage of two metal ions based on 1,3-diaminobenzene ligands has been more intensively studied.^[90,118–126,183–186] Some Schiff-base ligands as well as one amide ligand have been synthesized. Besides a few iron(III), cobalt(II) and nickel(II) complexes predominantly copper(II) complexes have been structurally characterized. The reaction with copper(II) ions leads to the formation of metallamacrocyclic dinuclear complexes, wherein two copper centers are coordinated by two ligand molecules. Two different complex structures have been reported and schematically shown in figure 3.1.

In the *anti*-orientation the *meta*-phenylene rings are parallel to each other but mutually shifted,^[119,120,122–124] whereas in the *syn*-orientation these rings are stacked.^[121] A closer analysis of the complex structures reveals, that the *anti*-arrangement is obtained with binding pockets forming six-membered chelate rings with the metal ion, whereas five-membered chelate rings favor the *syn*-arrangement.

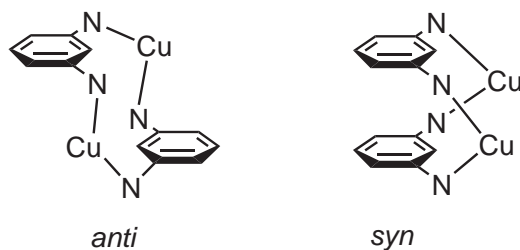


Figure 3.1: The central core structures in dinuclear 1,3-diaminobenzene-bridged copper(II) complexes.

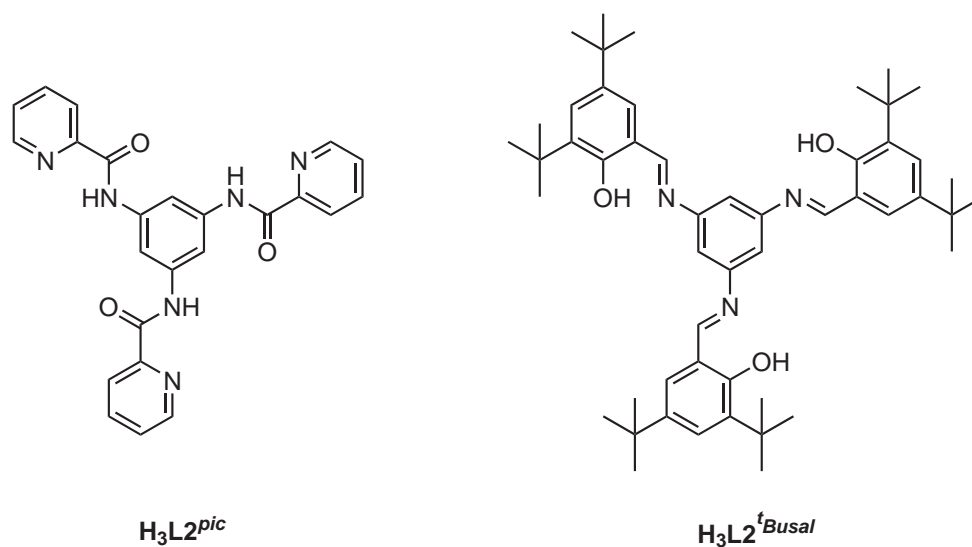


Figure 3.2: The new tritopic ligands based on 1,3,5-triaminobenzene.

Up to now only a single C_3 symmetric ligand based on 1,3,5-triaminobenzene has been reported.^[90] The reaction with copper(II) ions forms a trinuclear complex wherein three copper ions are coordinated by two ligand molecules under formation of 1,3,5-metallacyclophane shown in figure 1.3. The copper ions are coordinated by the ligand under formation of five-membered chelate rings leading to the *syn*-orientation of the benzene rings. This is in agreement with the results obtained from the analogue dinuclear complex.^[121] Hence C_3 symmetric ligands forming six-membered chelate rings with the coordinated copper(II) ion should lead to metallamacrocyclic complexes with *anti*-oriented phenylene rings. Therefore the directed synthesis of novel metallamacrocyclic complexes through molecular-programmed self-assembly of the ligands should be possible depending on the design of the ligand binding pockets. In this context the two ligands depicted in figure 3.2 were synthesized. Beside a new amide ligand **H₃L₂^{pic}**, a novel Schiff-base ligand **H₃L₂^{tBusal}** was synthesized. Upon coordination the ligand **H₃L₂^{pic}** forms five-membered chelate rings with the coordinated metal ions, whereas the latter forms six-membered rings. This results in two different types of metallamacrocyclic complex structures, which will be discussed separately in the following sections.

3.2 Metallamacrocyclic Complexes with the Amide-Based Ligand $\text{H}_3\text{L2}^{\text{pic}}$

3.2.1 Synthesis and Characterization

The new ligand $\text{H}_3\text{L2}^{\text{pic}}$ was synthesized starting from 1,3,5-triaminobenzene. This was prepared in a two step synthesis starting from 1,3,5-trihydroxybenzene shown in figure 3.3. The reaction with hydroxylamine followed by the hydrogenolysis using Raney-nickel yielded 1,3,5-triaminobenzene as colorless crystals in high quantity.^[187,188] The subsequent reaction with 2-pyridinecarboxylic acid in dry pyridine under addition of triphenyl phosphite yielded the amide ligand $\text{H}_3\text{L2}^{\text{pic}}$ in excellent yield of 91%. This synthetic route is well known from literature.^[189,190]

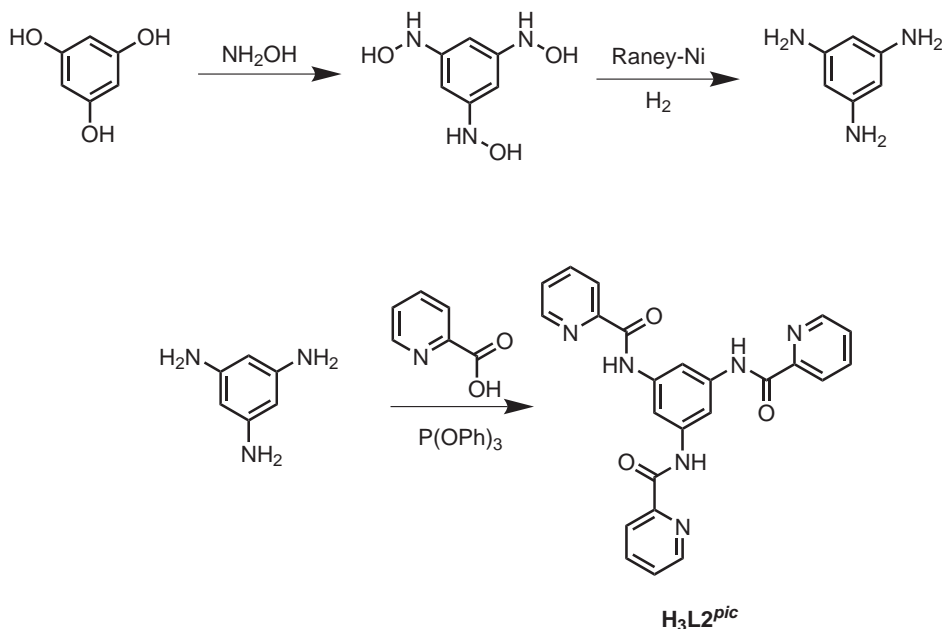


Figure 3.3: Synthesis of the ligand $\text{H}_3\text{L2}^{\text{pic}}$ starting from 1,3,5-trihydroxybenzene.

The ligand $\text{H}_3\text{L2}^{\text{pic}}$ provides three equal bidentate [N_2] binding pockets, with the pyridine nitrogen and the amide nitrogen atoms, accessible after deprotonation, as potential donors. The ligand coordinates to three metal ions in its trianionic form. Moreover the coordination of transition metal ions results in six-membered chelate rings formed with the metal centers. This favors the *syn*-arrangement of the phenylene bridges leading to trinuclear complexes. The ligand is only slightly soluble in dimethylformamide and

dimethylsulfoxide, because of the planar structure and formation of hydrogen bonding as well as π - π stacking interactions, limiting the reaction conditions for complexation.

The reaction with copper(II) perchlorate hexahydrate in dimethylsulfoxide in the molar ratio of 2 : 3 under addition of triethylamine results in the formation of a trinuclear copper complex $\text{Cu}_3\text{L}_2^{\text{pic}}$. Two ligand molecules coordinate three copper ions resulting in the neutral metallamacrocycle $[\text{Cu}_3(\text{L}_2^{\text{pic}})_2(\text{DMSO})_3]$ (7). This complex is one of only three examples of a structural characterized 1,3,5-metallacyclophane.^[63,191]

The reaction of the ligand $\text{H}_3\text{L}_2^{\text{pic}}$ with copper(II) perchlorate hexahydrate in the molar ratio of 1 : 3 under addition of triethylamine and sodium azide leads to the formation of the tetranuclear copper complex $[\text{Cu}_4(\text{L}_2^{\text{pic}})_2(\mu_{1,3}\text{-N}_3)(\mu\text{-OH})(\text{H}_2\text{O})(\text{DMF})]$ ($\text{Cu}_4\text{L}_2^{\text{pic}}$) (8). This complex exhibits a novel structural core motif. The complexation affords a neutral metallamacrocycle composed of two trisbidentate ligands, four copper(II) ions and one bridging hydroxide as well as azide ion. Three copper ions are chelated by each ligand. Two of them are coordinated by both ligand molecules, whereas the other copper centers are bound in both remaining binding pockets and further linked through a di- μ -hydroxo- $\mu_{1,3}$ -azido bridge. This complex cannot be prepared by stoichiometric reaction of the ligand and copper(II) perchlorate in the molar ratio of 1 : 2 as present in the compound. In this case the trinuclear metallacyclophane complex $\text{Cu}_3\text{L}_2^{\text{pic}}$ (7) crystallizes from the reaction solution within a few hours.

Both complexes were characterized by X-ray structural analysis, elemental analysis, thermogravimetric analysis (TGA) measurements and IR spectroscopy. The trinuclear complex $\text{Cu}_3\text{L}_2^{\text{pic}}$ (7) crystallizes together with dimethylsulfoxide and water molecules. During washing process the crystals crumble into powder. All dimethylsulfoxide molecules including both coordinated and co-crystallized ones are eliminated resulting in the complex constitution of $[\text{Cu}_3(\text{L}_2^{\text{pic}})_2] \cdot 7\text{H}_2\text{O}$ obtained after drying in air. This is confirmed by elemental analysis, and TGA measurements. The latter reveals a weight loss of 10.5% in a temperature range up to 100 °C, which can be assigned to the loss of seven water molecules. This indicates seven water molecules per trinuclear complex molecule, which is in excellent agreement with the elemental analysis data.

The tetranuclear complex $\text{Cu}_4\text{L}_2^{\text{pic}}$ (8) crystallizes together with dimethylformamide and water solvent molecules. Upon drying in air the crystals loose the dimethylformamide molecules and crumble into powder. Elemental analysis reveals a higher

water content leading to the final complex composition of $[\text{Cu}_4(\text{L}_2^{\text{pic}})_2(\mu_{1,3}\text{-N}_3)(\mu\text{-OH})(\text{H}_2\text{O})(\text{DMF})] \cdot 14\text{H}_2\text{O}$. This is also confirmed by TGA measurements. Heating up to 250°C reveals a weight loss of 25.1%, meanwhile the complex starts to decompose. This weight loss can be attributed to the removal of 15 water, one dimethylformamide and one azide molecule, which is in excellent agreement to the elemental analysis data.

In the IR spectra of both complexes the $\tilde{\nu}_{\text{N-H}}$ stretching vibration of the ligand at 3335 cm^{-1} is absent due to the deprotonation of the amide protons. Furthermore the amide $\tilde{\nu}_{\text{O=C-N}}$ vibration at 1686 cm^{-1} is shifted to frequencies lower than 1620 cm^{-1} , as a result of the coordination of the amide nitrogen atoms to the copper ions. In the tetranuclear complex $\text{Cu}_4\text{L}_2^{\text{pic}}$ (8) an additional characteristic band is observed at 2037 cm^{-1} , which can be attributed to the $\tilde{\nu}_{\text{N}\equiv\text{N}}$ stretching vibration of the azide bridge.

3.2.2 Crystal Structures

$[\text{Cu}_3(\text{L}_2^{\text{pic}})_2(\text{DMSO})_3] (\text{Cu}_3\text{L}_2^{\text{pic}})$ (7)

The trinuclear copper complex $\text{Cu}_3\text{L}_2^{\text{pic}}$ (7) co-crystallizes with dimethylsulfoxide and water molecules in crystals of $[\text{Cu}_3(\text{L}_2^{\text{pic}})_2(\text{DMSO})_3] \cdot 3\text{DMSO} \cdot 6\text{H}_2\text{O}$. Three copper ions are chelated and bridged by two triply deprotonated *meta*-phenylene ligands under formation of a neutral 1,3,5-metallacyclophane. The complex crystallizes in the centrosymmetric cubic space group $Pa\bar{3}$ as a racemic mixture of two independent trinuclear molecules within the unit cell ($j = 1, 2$ running number assigned to the two independent chiral complex molecules). The chirality is caused by a helical twist within the individual complex molecules.

The molecular structure and labeling scheme of one of the two independent molecules of $\text{Cu}_3\text{L}_2^{\text{pic}}$ is depicted in figure 3.4. Selected bond lengths and angles are summarized in table 3.1. Both neutral trinuclear complex molecules are highly symmetric with a C_3 axis perpendicular through the planes of the stacked *meta*-phenylene bridges. Thus, the three copper centers within each molecule are crystallographically identical.

The copper ions Cu^j1 are tetra-coordinated with a N_4 donor set through the deprotonated amide nitrogen atoms N^j1 and N^j3 and the pyridine nitrogen atoms N^j2 and N^j4 of both ligand molecules with averaged bite angles of 82° . The bond lengths range from 195 to 203 pm ($j = 1$) and from 196 to 206 pm ($j = 2$). Furthermore dimethylsulfoxide molecules are weakly bound through the oxygen atoms $\text{O}1\text{D}^j$ at larger distances of

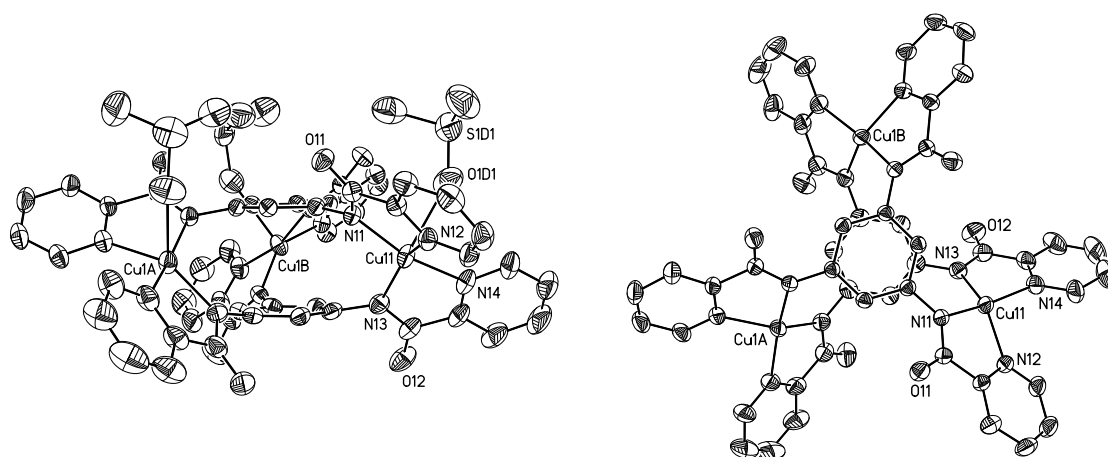


Figure 3.4: Molecular structure of the complex molecule of $\text{Cu}_3\text{L}_2^{\text{pic}}$ (7) (one of two crystallographically independent molecules is shown). Thermal ellipsoids are drawn at the 50% probability level. Solvent molecules and hydrogen atoms are omitted for clarity. Symmetry equivalent atoms are labeled with the suffix A and B. Left: Side view of the molecular structure. Right: Top view of the molecular structure. Herein the coordinated dimethylsulfoxide molecule at each copper center is omitted for clarity.

264 pm ($j = 1$) and 228 pm ($j = 2$). This leads to a (4+1) coordination geometry for each copper center. The $\text{N}j_2\text{-Cu}j_1\text{-N}j_3$ angles of 146° ($j = 1$) and 137° ($j = 2$) are rather small compared to the $\text{N}j_1\text{-Cu}j_1\text{-N}j_4$ angles of 165° ($j = 1$) and 173° ($j = 2$) within the tetragonal coordination indicating a strong distortion. The differences between both independent molecules are due to the weakly bound dimethylsulfoxide molecules. The distortion of the tetragonal coordination can be best described by the dihedral angle between both planes formed by the copper center and the corresponding nitrogen donor atoms of the five-membered chelate rings. Herein 0° is equal to an ideal square planar and 90° is equal to an ideal tetrahedral environment.^[192] The dihedral angles within both complex molecules are half in between with 40° ($j = 1$) and 45° ($j = 2$). Such an intermediate geometry has been previously observed in dinuclear metallamacrocyclic complexes,^[120,122,193,194] caused by the geometric ligand strain.^[195] The distortion within this complex may be ascribed to steric effects between the pyridine rings. The *ortho*-positioned hydrogen atoms on the pyridine rings prevent the square planar coordination geometry at the copper centers. The additional coordination of the dimethylsulfoxide molecules leads to a rather unusual highly distorted (4+1) penta-coordination of the copper ions.

Table 3.1: Selected bond lengths [pm] and angles [$^\circ$] for both independent complex molecules ($j = 1, 2$) in complex $Cu_3L_2^{pic}$ (7).

	$j = 1$	$j = 2$
Cuj1–Nj1	194.5(3)	196.1(3)
Cuj1–Nj2	203.0(3)	205.6(3)
Cuj1–Nj3	198.8(3)	200.3(3)
Cuj1–Nj4	199.4(3)	200.1(3)
Cuj1–O1Dj	263.8(4)	228.1(3)
Nj1–Cuj1–Nj2	82.57(12)	81.36(12)
Nj1–Cuj1–Nj3	104.66(13)	104.19(12)
Nj1–Cuj1–Nj4	164.60(14)	173.12(14)
Nj2–Cuj1–Nj3	146.12(13)	137.27(13)
Nj2–Cuj1–Nj4	99.71(14)	98.22(13)
Nj3–Cuj1–Nj4	82.02(14)	80.83(13)
O1Dj–Cuj1–Nj1	87.15(12)	89.65(12)
O1Dj–Cuj1–Nj2	89.87(13)	98.90(12)
O1Dj–Cuj1–Nj3	123.11(13)	123.15(12)
O1Dj–Cuj1–Nj4	77.66(14)	83.65(12)

The interatomic Cu···Cu separation in both independent molecules of the trinuclear complex is 670 pm. The bridging phenylene rings of the ligand molecules are twisted to accommodate a staggered arrangement with distances of about 312 pm between the averaged planes. These are equal to a reported trinuclear platinum(II) cyclophane complex with 1,3,5-tris(diphenylphosphino)benzene.^[191] However, in an enneanuclear copper(II) complex containing a 1,3,5-metallacyclophane core unit the distance is larger with 323 pm due to the square planar coordination geometry of the copper ions with an almost perpendicular arrangement concerning the double *meta*-phenylene bridge.^[90]

In the crystal packing no significant intermolecular contacts occur between the trinuclear complex molecules due to the co-crystallized dimethylsulfoxide and water molecules. Consequently the complex molecules are well separated with the shortest intermolecular Cu···Cu separation of 1080 pm.

[Cu₄(L^{pic})₂(μ_{1,3}-N₃)(μ-OH)(H₂O)(DMF)] (Cu₄L₂^{pic}) (8)

The tetranuclear complex **Cu₄L₂^{pic}** (**8**) co-crystallizes with dimethylformamide and water solvent molecules in crystals of [Cu₄L₂(μ_{1,3}-N₃)(μ-OH)(H₂O)(DMF)] · 2DMF · 3H₂O in the monoclinic space group *P*2₁/*n*. The coordination results in a novel neutral metallamacrocycle composed of two tris-bidentate ligands, four copper(II) ions, one bridging hydroxide and azide ion. Herein two of the copper ions are coordinated by two ligand molecules whereas the other two copper ions are coordinated by one ligand binding pocket and further linked through a di-μ-hydroxide-μ_{1,3}-azide bridge. The molecular structure of the tetranuclear complex is shown in figure 3.5. Selected bond lengths and angles are listed in table 3.2.

The coordination environments of the copper centers Cu1 and Cu3 are nearly identical and similar to the tetragonal coordination in the symmetric trinuclear complex **Cu₃L₂^{pic}** (**7**). Each copper ion is coordinated by a N₄ donor set of two ligand molecules through the deprotonated amide and the pyridine nitrogen atoms with similar averaged bite angles

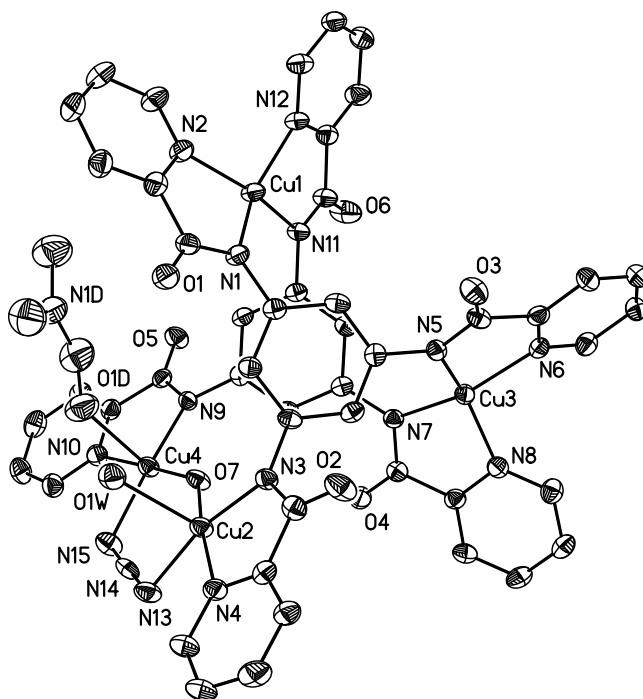


Figure 3.5: Molecular structure of the tetranuclear complex molecule **Cu₄L₂^{pic}** (**8**). Thermal ellipsoids are drawn at the 50% probability level. Solvent molecules and hydrogen atoms are omitted for clarity.

Table 3.2: Selected bond lengths, interatomic distances [pm] and angles [$^\circ$] for complex $Cu_4L_2^{pic}$ (**8**).

Cu1–N1	196.8(3)	Cu3–N5	194.7(3)
Cu1–N2	198.6(3)	Cu3–N6	199.7(3)
Cu1–N11	194.5(3)	Cu3–N7	195.9(3)
Cu1–N12	201.9(3)	Cu3–N8	199.8(3)
Cu2–O7	194.5(3)	Cu4–O7	192.1(3)
Cu2–N3	195.8(3)	Cu4–N9	195.9(3)
Cu2–N4	200.2(3)	Cu4–N10	200.4(3)
Cu2–N13	205.3(3)	Cu4–N15	200.4(3)
Cu2–O1W	230.3(3)	Cu4–O1D	248.5(3)
Cu1···Cu2	754.91(7)	Cu2···Cu3	687.35(7)
Cu1···Cu3	662.19(6)	Cu2···Cu4	364.18(6)
Cu1···Cu4	691.00(7)	Cu3···Cu4	748.13(6)
N1–Cu1–N2	83.18(13)	N5–Cu3–N6	82.50(13)
N1–Cu1–N11	105.84(13)	N5–Cu3–N7	104.50(12)
N1–Cu1–N12	152.10(14)	N5–Cu3–N8	148.54(13)
N2–Cu1–N11	157.77(14)	N6–Cu3–N7	158.33(13)
N2–Cu1–N12	99.83(13)	N6–Cu3–N8	100.78(13)
N11–Cu1–N12	81.78(13)	N7–Cu3–N8	84.01(12)
O7–Cu2–N3	98.71(12)	O7–Cu4–N9	99.77(12)
O7–Cu2–N4	170.19(12)	O7–Cu4–N10	177.56(13)
O7–Cu2–N13	88.92(12)	O7–Cu4–N15	88.82(12)
O7–Cu2–O1W	88.56(11)	O7–Cu4–O1D	87.07(12)
N3–Cu2–N4	82.60(13)	N9–Cu4–N10	82.23(13)
N3–Cu2–N13	167.37(13)	N9–Cu4–N15	166.76(13)
N3–Cu2–O1W	100.66(12)	N9–Cu4–O1D	95.37(12)
N4–Cu2–N13	88.21(13)	N10–Cu4–N15	89.46(13)
N4–Cu2–O1W	100.79(12)	N10–Cu4–O1D	91.36(12)
N13–Cu2–O1W	89.52(12)	N15–Cu4–O1D	95.12(13)

of about 83° . The other angles within both coordination polyhedra range from 100° to 158° indicating a strong distortion of the tetragonal planes. The coordination geometry is between square planar and tetrahedral with dihedral angles of 38° for Cu1 and 41° for Cu3 between both N–Cu–N planes of the five-membered chelate rings.

The copper centers Cu2 and Cu4 are coordinated by one ligand in a bidentate manner through the amide and pyridine nitrogen atoms, respectively. The bridging hydroxide and end-to-end azide ion complete the square planar coordination with *trans* angles ranging between 167° and 178° . Additionally the Cu2 is coordinated by the water molecule O1W and the Cu4 by the oxygen atom O1D of a dimethylformamide molecule in the apical position. Both distances are rather large with about 230 pm (Cu2–O1W) and 249 pm (Cu4–O1D) compared to the equatorial bond lengths of the two copper centers ranging from 195 to 205 pm. Therefore the coordination geometries of both copper centers can be best described as (4+1) square-pyramidal as a result of Jahn-Teller distortion typical for copper(II) complexes. The Cu2 is displaced by 16 pm and the Cu4 by 7 pm out of the corresponding tetragonal plane towards the apical position. These planes are nearly coplanar with a dihedral angle of about 13° . The copper ions are in close proximity with a separation of 364 pm and a rather large hydroxide bridging angle of 141° . In contrast all other Cu···Cu separations within the tetranuclear metallamacrocycle are rather large with distances ranging from 662 to 755 pm (see table 3.2).

The μ -hydroxide- μ -azide-bridged dinuclear copper unit supports the formation of an intramolecular hydrogen bonding interaction between the apical coordinated dimethylformamide and the water molecule with a distance of 291 pm (O1D···O1W). Further hydrogen bonding is established involving the co-crystallized water molecules and the carbonyl oxygen atoms of the complex molecule leading to the formation of 1D chains along the [101] direction of the unit cell shown in figure 3.6. The co-crystallized dimethylformamide molecules are located between these chains without any hydrogen bonding interactions.

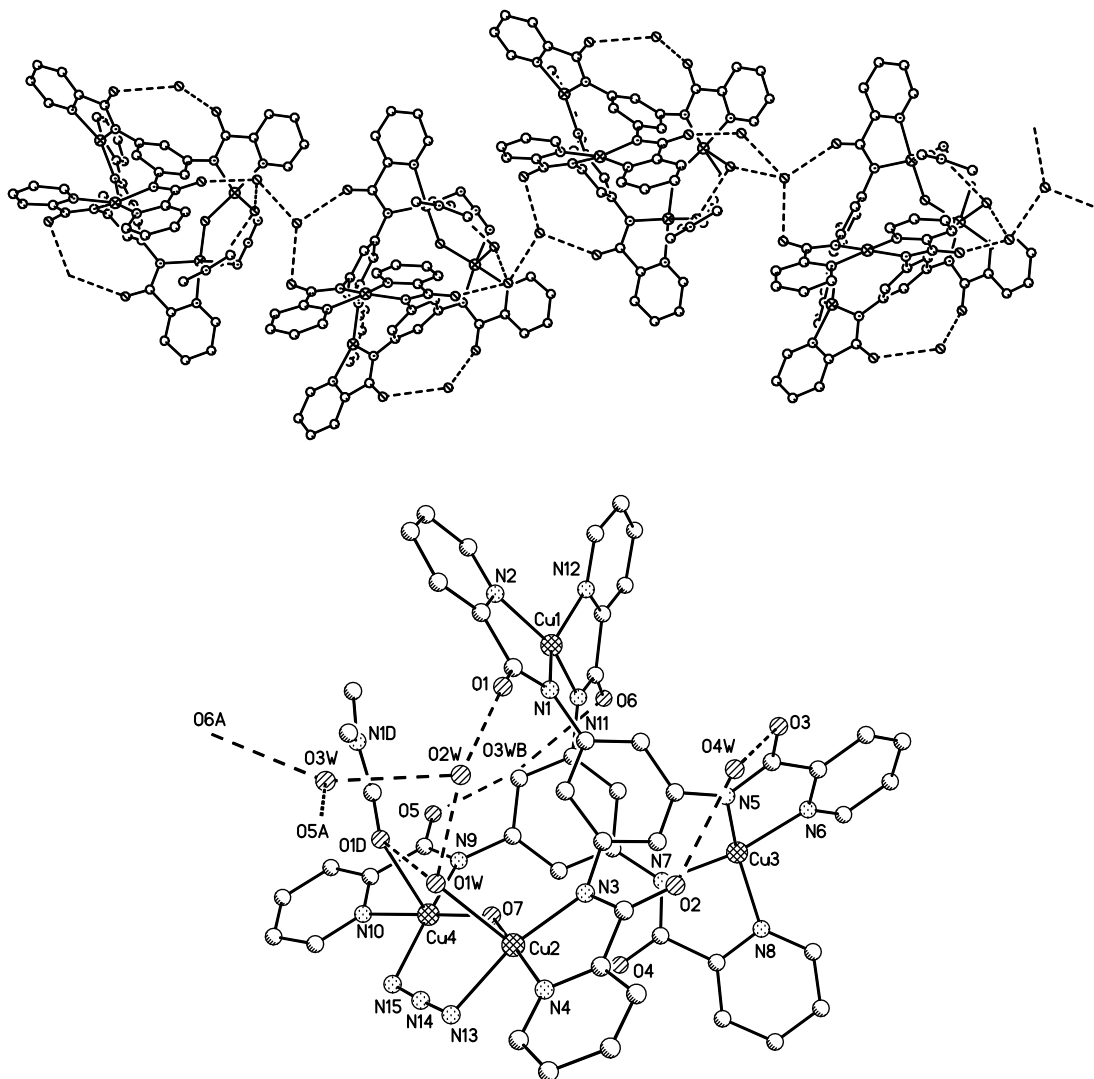


Figure 3.6: Representation of the supramolecular structure of complex $Cu_4L_2^{pic}$ (**8**). The 1D chain run along the [101] direction of the unit cell. Dashed lines indicate hydrogen bonding interactions. Symmetry equivalent atoms are labeled with the suffixes A and B. Pertinent distances (pm): O1W \cdots O1D 291.4, O1W \cdots O2W 282.3, O2W \cdots O1 277.0, O2W \cdots O3W 281.1, O3W \cdots O5A 279.7, O3W \cdots O6A 303.9, O4W \cdots O2 279.1, O4W \cdots O3 304.4.

3.2.3 Magnetic Properties

Trinuclear Metallamacrocyclic Complex

Variable temperature (2-300 K) magnetic susceptibility data for complex $\text{Cu}_3\text{L2}_2^{\text{pic}}$ (7) is depicted in figure 3.7 as $\chi_M = f(T)$ and $\chi_M T = f(T)$. The experimental $\chi_M T$ value at 300 K is $1.42 \text{ cm}^3 \text{ K mol}^{-1}$, which is slightly higher than the theoretical spin-only value expected for three independent copper(II) ions. Upon lowering the temperature $\chi_M T$ slightly decreases to $1.41 \text{ cm}^3 \text{ K mol}^{-1}$ at 240 K and then continuously increases up to $2.03 \text{ cm}^3 \text{ K mol}^{-1}$ at 10 K. Below 10 K, $\chi_M T$ decreases again reaching a value of $1.91 \text{ cm}^3 \text{ K mol}^{-1}$ at 2 K.

The gradual increase of the $\chi_M T$ values observed upon cooling in the temperature range between 240 and 10 K indicate a ferromagnetic coupling between the three copper centers mediated through the *meta*-phenylene bridges. Moreover magnetization measurements at 2 K confirm the $S = 3/2$ triplet ground state which are shown in figure 3.8. The high temperature course can be attributed to a temperature-independent paramagnetism present in this complex. Furthermore this is consistent with the higher experimental room temperature value. The decrease below 10 K is due to additional weak intermolecular antiferromagnetic exchange interactions.

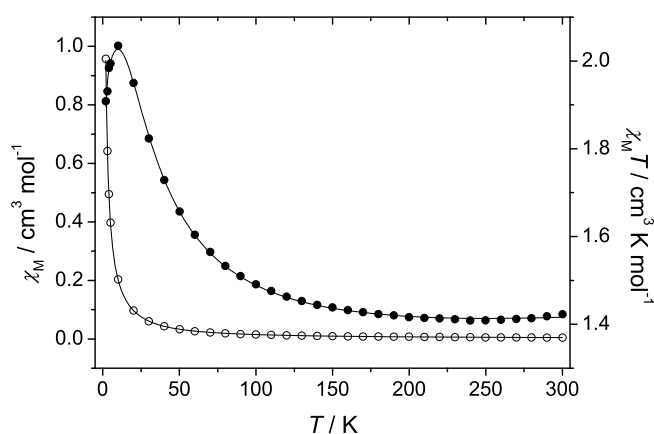


Figure 3.7: Plot of the thermal dependence of χ_M (empty circles, \circ) and $\chi_M T$ (black filled circles, \bullet) for complex $\text{Cu}_3\text{L2}_2^{\text{pic}}$ (7) measured with an applied magnetic field of 2000 Oe. The corresponding fit functions according to equation 3.2 are drawn as solid lines (for parameters see text).

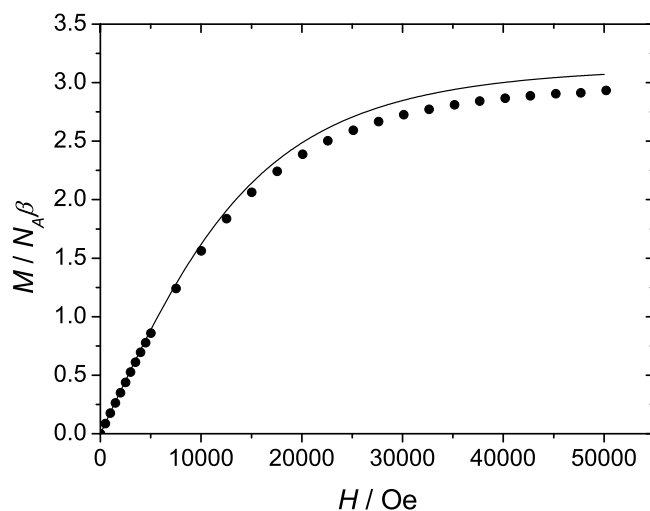


Figure 3.8: Field dependence of the magnetization for complex $\mathbf{Cu}_3\mathbf{L}_2^{pic}$ (7) at 2 K (•). The Brillouin function for $S = 1.5$ and $g = 2.10$ is plotted as solid line.

Due to the C_3 symmetry the triangular Cu_3 unit was treated as an equilateral triangle with three equal pairwise magnetic interactions. The experimental $\chi_M T$ data was analyzed using the corresponding isotropic spin hamiltonian given as:

$$\hat{H} = -J(\hat{S}_1\hat{S}_2 + \hat{S}_1\hat{S}_3 + \hat{S}_2\hat{S}_3) \quad (3.1)$$

For $S_1 = S_2 = S_3 = 1/2$ this leads to the expression for the molar susceptibility given in equation 3.2 with the abbreviation $A = -3J/2kT$.^[178]

$$\chi_M = \frac{N_A\beta^2 g^2}{4k(T - \theta)} \frac{5 + \exp A}{1 + \exp A} + \chi_{TIP} \quad (3.2)$$

In equation 3.2 χ_{TIP} represents the contribution of the temperature independent paramagnetism and θ reflects the intermolecular exchange interaction. The best fit of the experimental data set for the theoretical expression given in equation 3.2 results in $J = +24.8(4) \text{ cm}^{-1}$, $g = 2.099(3)$, $\theta = -0.18(1) \text{ K}$, and $\chi_{TIP} = 3.4(1) \cdot 10^{-4} \text{ cm}^3 \text{ mol}^{-1}$ with $r^2 = 0.9994$.

The ferromagnetic coupling J is exceptionally strong compared to the large separation of the copper ions in the complex of about 670 pm. This is due to interactions through spin

polarization of the double *meta*-phenylenetriamine linkage.^[196] The coupling is stronger compared to a series of trinuclear copper containing 1,3,5-metallacyclophane with J ranging from $+7.3$ to $+16.5$ cm^{-1} .^[63,90] This might be attributed to a variation in the coordination geometry of the copper centers. Compared to the intermediate coordination geometry between square planar and tetrahedral in complex $\text{Cu}_3\text{L}_2^{\text{pic}}$ (7), these copper ions exhibit a square planar coordination environment. The three reported hexaanionic trinuclear complexes differ only in the counteranions together with a somewhat different content of co-crystallized water. Unfortunately only one complex is structurally characterized wherein the basal planes of the copper centers are nearly perpendicular to the bridging benzene rings. Nevertheless slight variations within the crystal packing have a large influence on the coupling constant.^[63]

In addition, the exchange interaction is much stronger compared to phloroglucinol-bridged trinuclear copper complexes with $J < +6.6$ cm^{-1} wherein the basal planes of the square pyramidal copper centers are nearly coplanar with the bridging benzene.^[89] In the phloroglucinol-bridged copper complexes with square planar coordination geometries the coupling is weaker with J in the range of $+2.0$ up to $+3.1$ cm^{-1} .^[62,113] Moreover the coupling within both trinuclear copper complexes, discussed in the last chapter, is also weaker with $J = +0.3$ cm^{-1} in $\text{Cu}_3\text{L}_1^{\text{ampy}}$ (1) and even antiferromagnetic with $J = -1.6$ cm^{-1} in $\text{Cu}_3\text{L}_1^{\text{bhy}}$ (4). Up to now, $J = +24.8$ cm^{-1} is the strongest ferromagnetic coupling which was reported for metal complexes resulting from the spin polarization.

Tetranuclear Metallamacrocyclic Complex

The magnetic data of the tetranuclear complex $\text{Cu}_4\text{L}_2^{\text{pic}}$ (8) is depicted in figure 3.9 as $\chi_M = f(T)$ and $\chi_M T = f(T)$. The experimental $\chi_M T$ value at room temperature is 0.95 $\text{cm}^3 \text{K mol}^{-1}$, which is far from the theoretical spin-only value expected for four independent copper(II) ions. Upon lowering the temperature $\chi_M T$ decreases to a minimum of 0.88 $\text{cm}^3 \text{K mol}^{-1}$ at 100 K and then rapidly increases to 1.01 $\text{cm}^3 \text{K mol}^{-1}$ at 15 K. Below 15 K the $\chi_M T$ value decreases again. The overall course of the $\chi_M T$ values indicates different magnetic exchange interactions within the tetranuclear complex molecule. The decrease of the $\chi_M T$ value observed upon cooling indicates a strong antiferromagnetic exchange coupling, which is in agreement with the rather low room

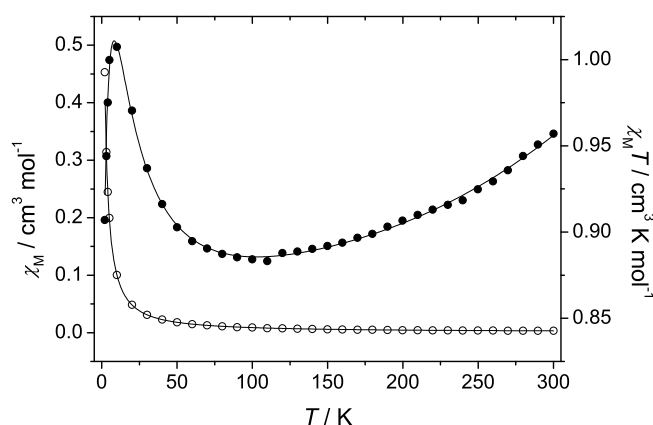


Figure 3.9: Plot of the thermal dependence of χ_M (empty circles, \circ) and $\chi_M T$ (black filled circles, \bullet) for complex $Cu_4L_2^{pic}$ (**8**) measured with an applied magnetic field of 2000 Oe. The corresponding fit functions according to equation 3.4 are drawn as solid lines (for parameters see text).

temperature value. The subsequent increase indicates an additional ferromagnetic exchange interaction. The minimum $\chi_M T$ value of $0.88 \text{ cm}^3 \text{ K mol}^{-1}$ at 100 K is very close to the spin-only value of two independent copper(II) ions indicating a rather strong antiferromagnetic coupling between two copper centers within the tetranuclear complex. Thus the subsequent increase with decreasing temperature is the result of a ferromagnetic exchange interaction between the two remaining copper centers. Moreover the decrease of the $\chi_M T$ value below 15 K can be attributed to an additional weak intermolecular antiferromagnetic exchange interaction.

Beside the linkage through both ligand molecules, the copper centers Cu2 and Cu4 are μ -hydroxide- μ -azide-bridged within the tetranuclear complex. This results in a close proximity with a separation of 364 pm compared to all other rather large Cu...Cu distances ranging from 662 to 755 pm. A lot of effort has been spent on the interpretation of the magneto-structural correlations in symmetrical di- μ -hydroxo,^[197-199] di- μ -alkoxo,^[200] and di- μ -phenoxo-bridged copper(II) complexes,^[201,202] whereas for other cases with single oxygen atom bridges or mixed-bridged complexes such correlations are still lacking. In general, the dependency between the Cu–O–Cu bridging angle α and the magnetic coupling constant is found to be linear. In case of the di- μ -hydroxo complexes, the relationship $J = 7270 - 74.53\alpha$ was derived. Applied to the dinuclear moiety within

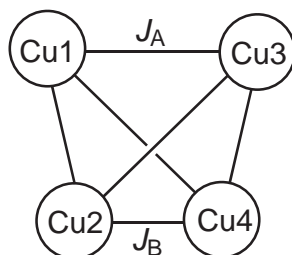


Figure 3.10: The spin topology of the employed two- J model for the tetranuclear copper complex $\text{Cu}_4\text{L}_2\text{L}'_2$ (8).

the tetranuclear complex $\text{Cu}_4\text{L}_2\text{L}'_2$ (8) with a large Cu–O–Cu bridging angle of 141° between Cu2 and Cu4 this correlation predicts a very strong antiferromagnetic interaction. Mono- μ -hydroxo-bridged copper(II) dimers exhibiting similarly large Cu–O–Cu angles (132 – 144°) show very strong antiferromagnetic superexchange interactions with a singlet state stabilized by more than 500 cm^{-1} with respect to the triplet state.^[203,204] Moreover an additional azide bridge in an end-to-end fashion enforces the antiferromagnetic interaction.^[178] A reported similar $\mu\text{-OR}-\mu_{1,3}\text{-N}_3$ dinuclear copper complex is still diamagnetic even at room temperature.^[205] This is in excellent agreement with the general course of the experimental data in the high temperature region.

Because of the very strong antiferromagnetic interaction between these two copper ions even at room temperature and to avoid overparametrization the tetranuclear complex was simplified and treated as two non-interacting copper dimers. The spin topology is depicted in figure 3.10. Herein J_A accounts for the exchange interaction within the *meta*-phenylene-bridged Cu1Cu3 pair and J_B within the $\mu\text{-OH}-\mu_{1,3}\text{-N}_3$ -bridged Cu2Cu4 pair. The corresponding spin hamiltonian is given as:

$$\hat{H} = -J_A \hat{S}_1 \hat{S}_3 - J_B \hat{S}_2 \hat{S}_4 \quad (3.3)$$

For $S_1 = S_2 = S_3 = S_4 = 1/2$ this leads to the expression for the molar magnetic susceptibility given in equation 3.4 under consideration of the temperature independent paramagnetism (χ_{TIP}) as well as an additional intermolecular exchange interaction (θ).^[178] Herein the abbreviations are equivalent to $A = -J_A/kT$ and $B = -J_B/kT$.

$$\chi_M = \frac{2N_A\beta^2g^2}{k(T-\theta)} \frac{1}{3+\exp A} + \frac{2N_A\beta^2g^2}{kT} \frac{1}{3+\exp B} + \chi_{TIP} \quad (3.4)$$

The best fit of the experimental data is obtained through the analytical expression given in equation 3.4 and results in $J_A = +17.8(7) \text{ cm}^{-1}$, $J_B = -1045(30) \text{ cm}^{-1}$, $g = 2.066(5)$, $\chi_{TIP} = 3.9(2) \cdot 10^{-4} \text{ cm}^3 \text{ mol}^{-1}$ and $\theta = -0.36(2) \text{ K}$ with $r^2 = 0.9975$.

The large calculated coupling constant J_B within the $\mu\text{-OH}-\mu_{1,3}\text{-N}_3$ copper dimer is in excellent agreement to the above mentioned literature values as a result of the superexchange interaction. Compared to the trinuclear complex $\text{Cu}_3\text{L}_2^{\text{pic}}$ (7) the ferromagnetic exchange interaction J_A through the *meta*-phenylenetriamine linkage is somewhat smaller. This can be attributed to distortions within the structure resulting in a less efficient interaction through the spin polarization mechanism. Moreover, reported dinuclear *meta*-phenylenediamine-bridged copper complexes exhibit exchange interactions ranging from weak antiferromagnetic^[120,124] up to strong ferromagnetic.^[121–123,206] The calculated J_A is close to the strongest reported coupling with $J = +16.8 \text{ cm}^{-1}$ within a dinuclear metallacyclophane.^[121]

3.3 Metallamacrocyclic Complexes with the Schiff-Base Ligand $\text{H}_3\text{L}_2^{\dagger\text{Busal}}$

3.3.1 Synthesis and Characterization

The novel ligand $\text{H}_3\text{L}_2^{\dagger\text{Busal}}$, shown in figure 3.2, is accessible through Schiff-base condensation of 3,5-di-*tert*-butylsalicylaldehyde with 1,3,5-triaminobenzene. The reaction in methanol afforded an excellent ligand yield of 90 %.

The ligand provides three equal bidentate [NO] binding pockets, with the imine nitrogen and the phenolate oxygen atom, accessible after deprotonation. In contrast to the amide ligand $\text{H}_3\text{L}_2^{\text{pic}}$ forming five-membered chelate rings upon complexation, six-membered chelate rings are formed with the metal centers in the complexes. Therefore the *anti*-arrangement of the phenylene bridges will be favored leading to novel complex assemblies.

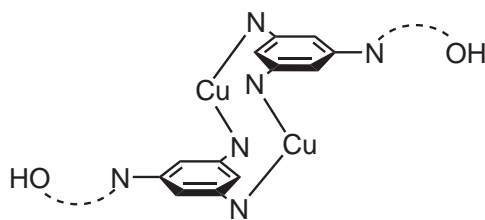


Figure 3.11: Schematic representation of the dinuclear copper complex $\text{Cu}_2\text{L}_2^{\text{tBusal}}$ (**9**).

The reaction of the ligands with one equivalent of copper(II) perchlorate hexahydrate in a chloroform-methanol-mixture under addition of triethylamine afforded a neutral dinuclear complex illustrated in figure 3.11. As expected the phenylene bridges are *anti*-oriented. Two binding pockets of each ligand are occupied by two copper ions under formation of the metallamacrocyclic complex $[\text{Cu}_2(\text{HL}_2^{\text{tBusal}})_2]$ ($\text{Cu}_2\text{L}_2^{\text{tBusal}}$) (**9**). The third binding pocket of each ligand is not occupied.

The complex was characterized by X-ray structural analysis, IR spectroscopy, mass spectrometry and elemental analysis. The crystals of complex $\text{Cu}_2\text{L}_2^{\text{tBusal}}$ (**9**) crumble into powder upon drying in air due to the loss of the co-crystallized chloroform molecules. This is confirmed by elemental analysis. The ESI mass spectrum shows predominantly one signal at $m/z = 1689$ which can be attributed to the complex cation $[\text{Cu}_2(\text{HL}_2^{\text{tBusal}})_2 + \text{Na}]^+$ confirming the high stability of the dinuclear complex in solution. The IR spectrum of the ligand exhibits two characteristic bands at 1619 and 1571 cm^{-1} , which can be attributed to the stretching vibrations of the imine moieties ($\tilde{\nu}_{\text{C}=\text{N}}$) and the phenylene rings ($\tilde{\nu}_{\text{C}=\text{C}}$). Upon coordination of the copper(II) ions these bands are slightly shifted to 1617 and 1576 cm^{-1} in complex (**9**). An additional band is observed at 1526 cm^{-1} , which can be attributed to another stretching vibration of the phenylene rings ($\tilde{\nu}_{\text{C}=\text{C}}$).

The analogous dinuclear cobalt(II) complex is also accessible through reaction of the ligand $\text{H}_3\text{L}_2^{\text{tBusal}}$ with cobalt(II) acetate dihydrate in the molar ratio of 1 : 1. The reaction yielded red prism of complex $[\text{Co}_2(\text{HL}_2^{\text{tBusal}})_2]$ ($\text{Co}_2\text{L}_2^{\text{tBusal}}$) (**10**) suitable for X-ray crystallography. As in complex $\text{Cu}_2\text{L}_2^{\text{tBusal}}$ (**9**) the two cobalt centers are coordinated by two ligand molecules, arranged in *anti*-orientation, under formation of a metallamacrocycle. The third binding pocket of each ligand molecule is unoccupied.

The complex was also characterized by IR spectroscopy, mass spectrometry and elemental analysis. All data confirms the structure derived from the X-ray structural analysis. The ESI mass spectrum shows the signal of the complex cation $[\text{Co}_2(\text{HL}_2^{\dagger\text{Busal}})_2]^+$ at $m/z = 1657$ and an additional intense signal at $m/z = 772$ due to the free ligand. Moreover the IR spectrum is almost identical to the one observed for the dinuclear copper(II) complex $\text{Cu}_2\text{L}_2^{\dagger\text{Busal}}$ (**9**), which is in agreement with the similar structure. Only slight shifting of the relevant bands are observed.

Both dinuclear complexes $\text{Cu}_2\text{L}_2^{\dagger\text{Busal}}$ (**9**) and $\text{Co}_2\text{L}_2^{\dagger\text{Busal}}$ (**10**) provide two free binding pockets, which should be accessible for coordination of transition metal ions. This might lead to homometallic as well as heterometallic tetranuclear complexes under addition of co-ligands. 1,1,1,5,5,5-Hexafluoroacetylacetone (Hhfac) was utilized as it is known to form stable complexes with various transition metal ions. All trials starting from the dinuclear cobalt complex $\text{Co}_2\text{L}_2^{\dagger\text{Busal}}$ (**10**) were unfortunately not successful. The addition of copper(II) salts results in the formation of the dinuclear copper(II) complex $\text{Cu}_2\text{L}_2^{\dagger\text{Busal}}$ (**9**), which was confirmed by IR spectroscopy in combination with ESI mass spectrometry. In contrast the reaction of the dinuclear complex $\text{Cu}_2\text{L}_2^{\dagger\text{Busal}}$ (**9**) with copper(II) chloride dihydrate and Hhfac under addition of triethylamine yielded the novel tetranuclear copper complex, wherein two copper centers occupy the free binding pockets of the dinuclear precursor complex. Only small quantities of the complex could be prepared by this synthetic route. Nevertheless the tetranuclear complex can also be directly prepared starting from the ligand $\mathbf{H}_3\mathbf{L}_2^{\dagger\text{Busal}}$. A solution of the deprotonated ligand in chloroform was reacted with two equivalents of copper(II) chloride dihydrate dissolved in methanol. The subsequent addition of one equivalent of Hhfac dissolved in chloroform afforded brown crystals of $[\text{Cu}_4(\text{L}_2^{\dagger\text{Busal}})_2(\text{hfac})_2(\text{MeOH})_2]$ ($\text{Cu}_4\text{L}_2^{\dagger\text{Busal}}$) (**11**) suitable for X-ray crystallography. This tetranuclear complex exhibits a novel structural core motif. Two triangular *meta*-phenylene-bridged Cu_3 subunits are connected by two common copper centers accommodated in two bidentate binding pockets of both ligands. The synthesis is very sensitive towards the solvent mixture, which means lowering the methanol content afforded the dinuclear complex $\text{Cu}_2\text{L}_2^{\dagger\text{Busal}}$ (**9**).

The tetranuclear complex $\text{Cu}_4\text{L}_2^{\dagger\text{Busal}}$ was further characterized by IR spectroscopy, mass spectrometry and elemental analysis. The complex loses all solvent molecules including both the co-crystallized chloroform and methanol molecules as well as the

coordinated methanol molecules. This is confirmed by elemental analysis and furthermore by thermogravimetric measurements, which revealed no weight loss up to 250 °C. In the ESI mass spectrum a fragmentation of the complex is observed leading to fragments of different nuclearity as well as a small signal of the tetranuclear complex cation $[\text{Cu}_4(\text{L}_2^{\text{tBusal}})_2(\text{hfac})_2+\text{Na}]^+$ at $m/z = 2228$. The most intense signal was detected at $m/z = 1690$ unambiguously assigned to the dinuclear complex $\text{Cu}_2\text{L}_2^{\text{tBusal}}$ (**9**). The IR spectrum shows all relevant bands of the dinuclear complex $\text{Cu}_2\text{L}_2^{\text{tBusal}}$ (**9**). Moreover an additional band is observed at 1645 cm^{-1} characteristic for the carbonyl stretching vibration of the hfac co-ligands ($\tilde{\nu}_{\text{C=O}}$).

3.3.2 Crystal Structures

$[\text{Cu}_2(\text{HL}_2^{\text{tBusal}})_2] (\text{Cu}_2\text{L}_2^{\text{tBusal}})$ (**9**)

The molecular structure as well as the heteroatom labeling scheme of the dinuclear complex $\text{Cu}_2\text{L}_2^{\text{tBusal}}$ is depicted in figure 3.12. Selected bond lengths and angles are listed in table 3.3. Two copper ions are chelated and bridged by two deprotonated ligands in a neutral centrosymmetric complex molecule. The third binding pocket of each ligand molecule remains unoccupied. The structure can be viewed as a metallamacrocycle of two phenylene rings connected by two N–Cu–N fragments.

The copper ions are tetra-coordinated by a N_2O_2 donor set of both ligand molecules. The coordination sites are occupied by two phenolate oxygen atoms and two imine nitrogen atoms in distances of 189 pm and 198 pm, respectively. The dihedral angle between the planes formed by the copper center and both donor atoms of the six-membered chelate rings is 36° . This leads to coordination polyhedra, which are highly distorted

Table 3.3: Selected bond lengths [pm] and angles [$^\circ$] for complex $\text{Cu}_2\text{L}_2^{\text{tBusal}}$ (**9**).

Cu–O1	188.8(3)	Cu–O2A	189.3(3)
Cu–N1	197.5(4)	Cu–N2A	197.6(4)
O1–Cu–O2A	87.90(15)	O1–Cu–N1	92.07(16)
O1–Cu–N2A	154.18(18)	O2A–Cu–N2A	92.51(15)
N1–Cu–O2A	152.60(18)	N1–Cu–N2A	99.11(16)

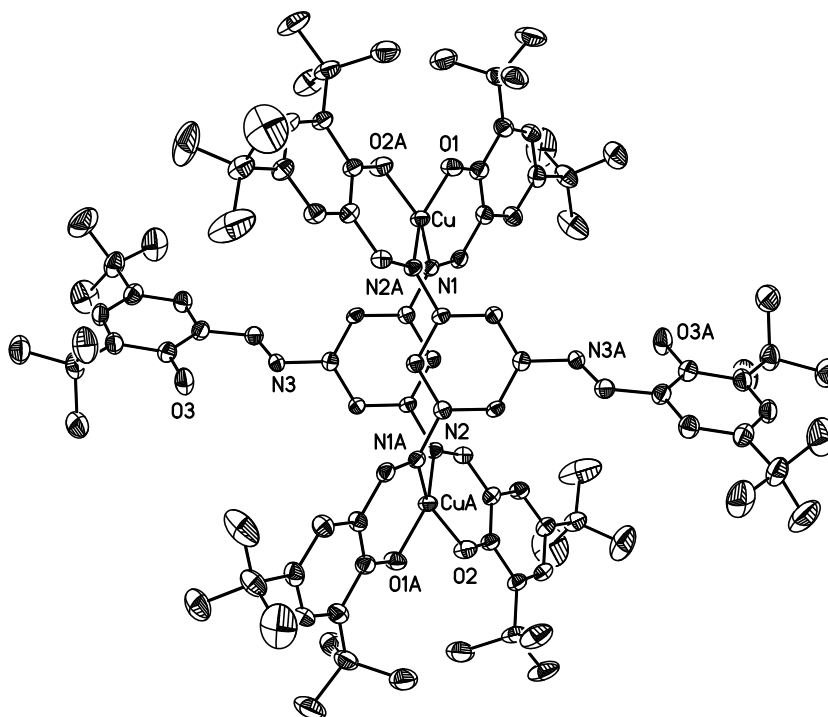


Figure 3.12: Molecular structure of the centrosymmetric dinuclear complex $Cu_2L_2^{Busal}$ (**9**). Thermal ellipsoids are drawn at the 50% probability level. Solvent molecules and hydrogen atoms are omitted for clarity. Symmetry equivalent atoms are labeled with the suffix A.

nearly half in between square-planar and tetrahedral. Furthermore the O1–Cu–N2A and N1–Cu–O2A angles are rather small with 154° and 153° confirming the high distortion of the tetragonal plane. The intramolecular Cu···Cu separation is 748 pm. The phenylene rings of the ligand side chains are twisted towards the same site of the central benzene ring with dihedral angles of about 47° for both coordinating and 54° for the non-coordinating side chains. The bridging *meta*-phenylene rings of the ligands are parallel to each other but mutually shifted with a interplanar distance of 304 pm. This *anti*-orientation leads to an offset π - π interaction with a centroid–centroid distance of 346 pm shown in figure 3.13. Each ligand molecule possesses a free binding pocket stabilized by an intramolecular hydrogen bonding interaction between the imine nitrogen atom and the phenolic hydrogen atom.

In the crystal packing no significant intermolecular contacts occur between the dinuclear complex molecules due to the bulky *tert*-butyl substituents in the ligand side chains. Consequently the complex molecules are well separated with the shortest intermolecular

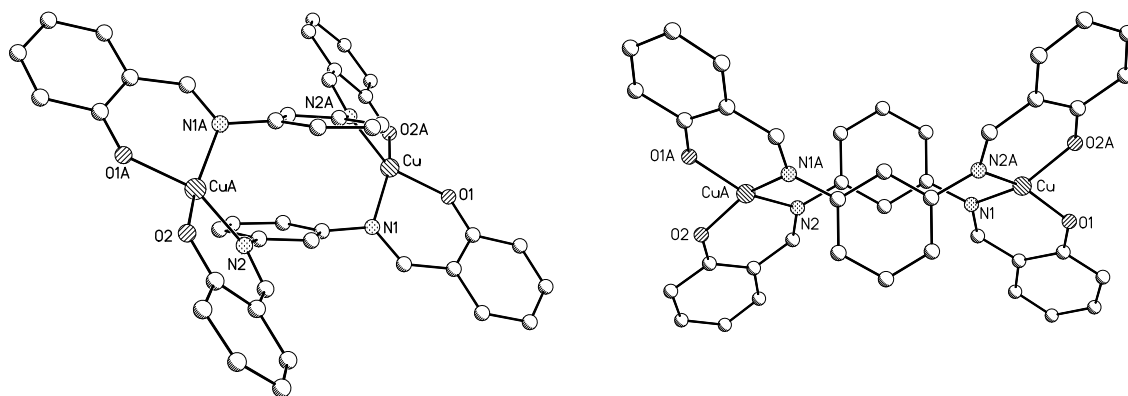


Figure 3.13: Perspective view of the molecular structure of complex $\text{Cu}_2\text{L}_2^{\text{tBusal}}$ (**9**) showing the *anti*-orientation of the *meta*-phenylene bridges. The *tert*-butyl substituents in the ligand side chains as well as the third binding pocket of each ligand molecule are omitted for clarity. Solvent molecules and hydrogen atoms are also not shown. Symmetry equivalent atoms are labeled with the suffix A.

$\text{Cu} \cdots \text{Cu}$ separation of 1004 pm. These are packed under formation of pillars parallel to the *c*-axis of the unit cell. Co-crystallized chloroform molecules are situated in between and partially high disordered. This is typical for non-interacting chloroform molecules and is responsible for the high ωR_2 value. Nevertheless this does not have a significant influence on the bond lengths and angles within the dinuclear complex molecule.

$[\text{Co}_2(\text{HL}_2^{\text{tBusal}})_2] (\text{Co}_2\text{L}_2^{\text{tBusal}})$ (**10**)

The molecular structure of the cobalt complex $\text{Co}_2\text{L}_2^{\text{tBusal}}$ is very similar to the dinuclear copper complex $\text{Cu}_2\text{L}_2^{\text{tBusal}}$ (**9**). Again two cobalt(II) ions are chelated by two binding pockets of two doubly deprotonated ligands in a centrosymmetric complex molecule depicted in figure 3.14. The complex crystallizes in the orthorhombic space group *Pbca*. Selected bond lengths and angles are listed in table 3.4.

The cobalt ions are tetra-coordinated by a N_2O_2 donor set of both ligand molecules. The coordination sites are occupied by two phenolate oxygen and two imine nitrogen atoms of both ligands. Therein Co–O bond lengths are nearly equal with 190 pm. The Co–N distances are slightly longer with 198 pm. All distances are in the generally observed range typical for tetra-coordinated cobalt(II) complexes.^[170,207,208]

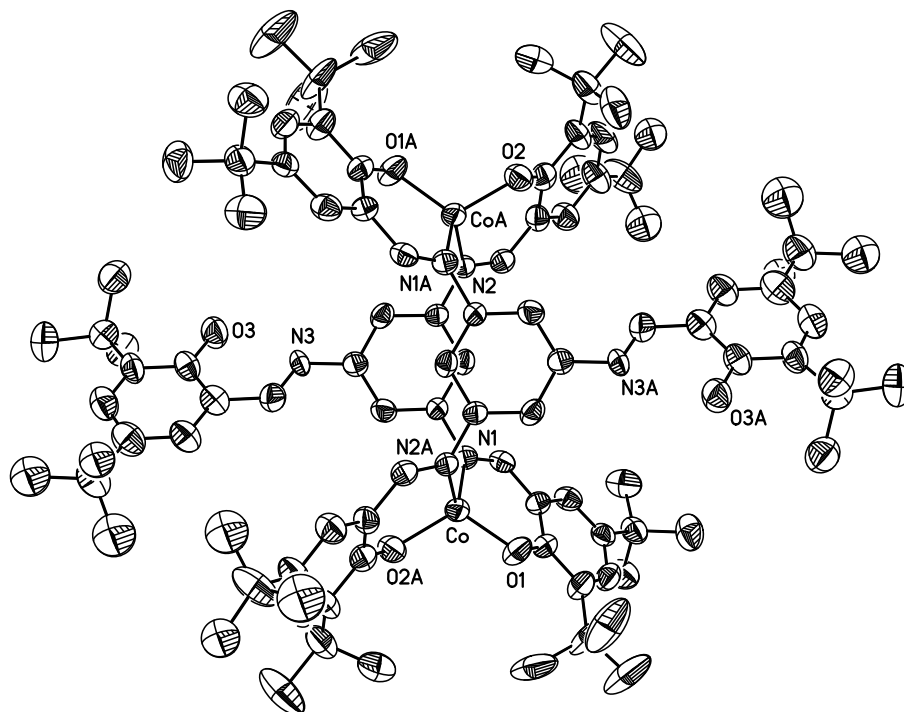


Figure 3.14: Molecular structure of the centrosymmetric dinuclear complex $Co_2L_2^{tBusal}$ (**10**). Thermal ellipsoids are drawn at the 50% probability level. Solvent molecules as well as hydrogen atoms are omitted for clarity. Symmetry equivalent atoms are labeled with the suffix A.

Table 3.4: Selected bond lengths [pm] and angles [°] for complex $Co_2L_2^{tBusal}$ (**10**).

Co–O1	189.5(5)	Co–O2A	189.4(5)
Co–N1	197.7(6)	Co–N2A	198.5(6)
O1–Co–O2A	115.5(2)	O1–Co–N1	94.7(2)
O1–Co–N2A	129.2(2)	O2A–Co–N2A	95.0(2)
N1–Co–O2A	120.7(2)	N1–Co–N2A	103.8(2)

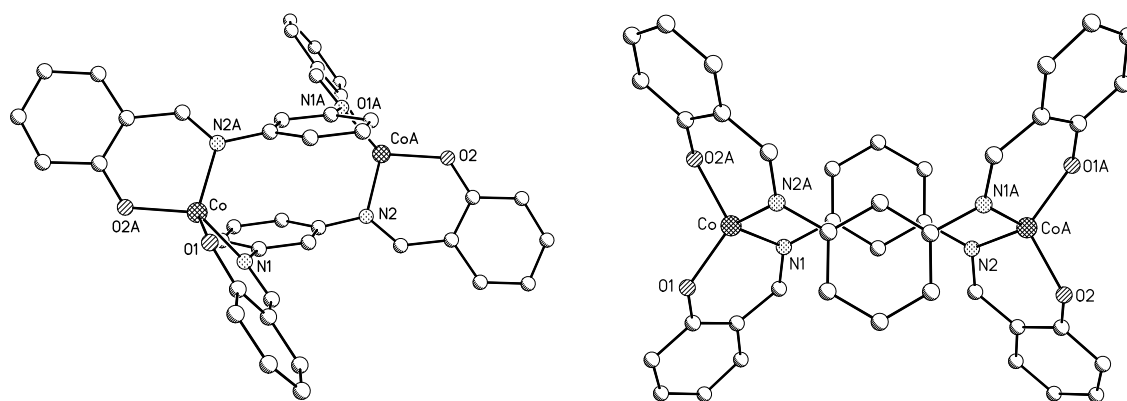


Figure 3.15: Perspective view of the molecular structure of complex $\text{Co}_2\text{L}_2^{\text{tBusal}}$ (**10**) showing the *anti*-orientation of the *meta*-phenylene bridges. The *tert*-butyl substituents in the ligand side chains as well as the third binding pocket of each ligand molecule are omitted for clarity. Solvent molecules and hydrogen atoms are also not shown. Symmetry equivalent atoms are labeled with the suffix A.

The dihedral angle between the planes formed by the cobalt center together with both donor atoms of the six-membered chelate rings is 77° , significantly larger compared to the homologous dinuclear copper complex $\text{Cu}_2\text{L}_2^{\text{tBusal}}$ (**9**). Thus the coordination polyhedra can be best described as distorted tetrahedral. This is in agreement with the angles in the coordination polyhedra all ranging from 95° to 129° . The salicylidene ligand side chains are twisted with respect to the central *meta*-phenylene bridge with dihedral angles of about 58° for both coordinating and 47° for the non-coordinating side chains. The non-coordinating binding pocket is aligned at opposite sites of the bridging plane. The *meta*-phenylene rings of the ligands are parallel to each other at a distance of 325 pm and shifted. Again this *anti*-orientation leads to an offset π - π interaction with a centroid–centroid distance of 408 pm shown in figure 3.15. Compared to the copper complex $\text{Cu}_2\text{L}_2^{\text{tBusal}}$ (**9**) both intramolecular distances are larger due to the distorted tetrahedral coordination geometry of the cobalt centers. In analogy to the copper complex $\text{Cu}_2\text{L}_2^{\text{tBusal}}$ (**9**) the complex molecules are well isolated in the crystal packing with a large intermolecular $\text{Co} \cdots \text{Co}$ separation of 1000 pm, compared to the intramolecular separation of 732 pm.

[Cu₄(L₂^{tBusal})₂(hfac)₂(MeOH)₂] (Cu₄L₂^{tBusal}) (11)

The tetranuclear complex $Cu_4L_2^{tBusal}$ was obtained as crystals containing a high amount of co-crystallized chloroform and methanol molecules with the resulting composition of $[Cu_4(L_2^{tBusal})_2(hfac)_2(MeOH)_2] \cdot 5CHCl_3 \cdot 3MeOH$. Four copper centers are chelated and bridged by two ligand molecules in a *meta*-phenylene arrangement. The molecular structure of the complex molecule as well as the atom labeling scheme is depicted in figure 3.16. Selected bond lengths and angles are listed in table 3.5. The complex crystallizes in the triclinic space group $P\bar{1}$ again as a centrosymmetric complex. The asymmetric unit contains only half of the tetranuclear complex molecule. Analogous to the dinuclear complex $Cu_2L_2^{tBusal}$ (9) two crystallographically identical copper centers Cu1 and Cu1A are coordinated by two ligand molecules under formation of a metallamacrocycle. The third binding pocket of each ligand molecule binds one copper ion together with the deprotonated hfac co-ligand.

Again the copper center Cu1 adopts a distorted tetragonal coordination environment with very similar bond lengths and angles. Hence the dihedral angle between the planes formed by the copper center and the donor atoms of the six-membered chelate rings of

Table 3.5: Selected bond lengths [pm] and angles [°] for complex $Cu_4L_2^{tBusal}$ (11).

Cu1–O1	188.8(3)	Cu1–O2A	190.1(3)
Cu1–N1	196.8(4)	Cu1–N2A	195.9(4)
Cu2–O3	186.8(3)	Cu2–O4	195.1(4)
Cu2–O5	200.6(4)	Cu2–O6	229.7(4)
Cu2–N3	196.8(4)		
O1–Cu1–O2A	92.39(14)	O1–Cu1–N1	93.42(14)
O1–Cu1–N2A	146.17(16)	N1–Cu1–O2A	148.81(16)
N1–Cu1–N2A	99.71(15)	O2A–Cu1–N2A	92.19(14)
O3–Cu2–O4	170.01(17)	O3–Cu2–O5	88.63(16)
O3–Cu2–O6	95.71(16)	O3–Cu2–N3	92.08(15)
O4–Cu2–O5	88.17(17)	O4–Cu2–O6	93.66(16)
O4–Cu2–N3	89.70(15)	O5–Cu2–O6	88.65(18)
O5–Cu2–N3	171.43(18)	O6–Cu2–N3	99.77(17)

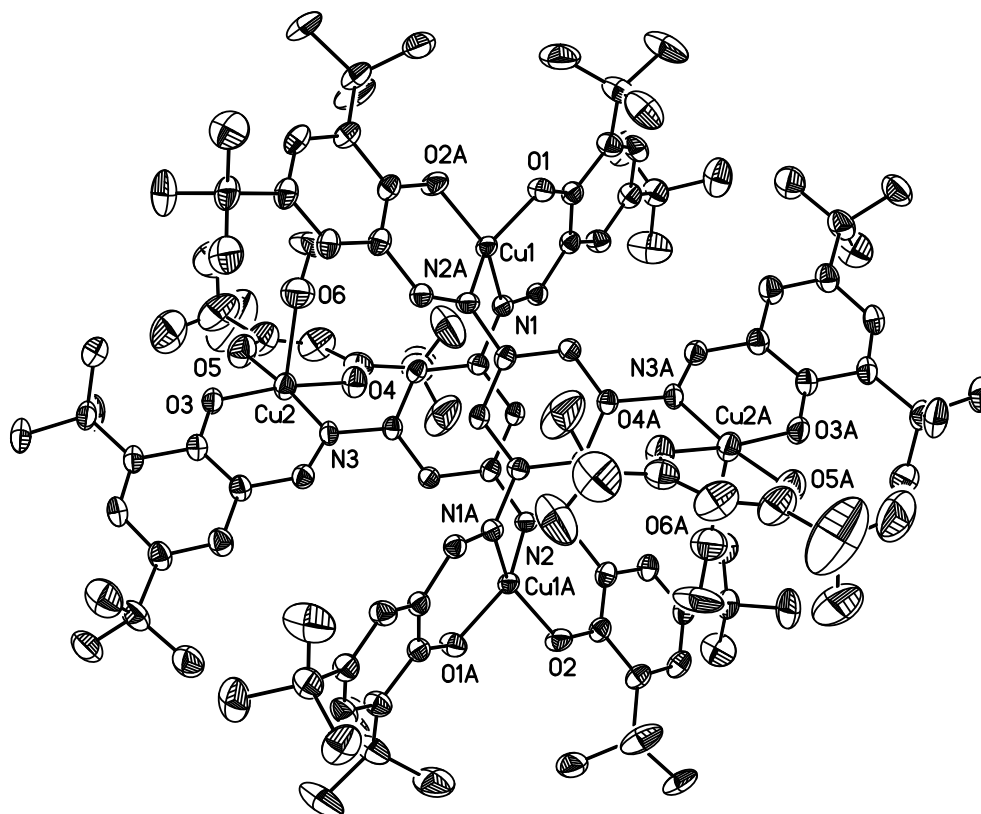


Figure 3.16: Molecular structure of the complex $\text{Cu}_4\text{L}_2^{4\text{Basal}}$ (**11**). Thermal ellipsoids are drawn at the 50% probability level. Solvent molecules as well as hydrogen atoms are omitted for clarity. Symmetry equivalent atoms are labeled with the suffix A.

each ligand molecule is only slightly different with 45° . The copper ions Cu2 possess an almost ideal square-pyramidal coordination environment. The basal plane is formed by the phenolate oxygen atom and the imine nitrogen atom of the ligand together with both carbonyl oxygen atoms of the deprotonated hfac co-ligand with bond lengths ranging between 187 and 201 pm. The copper ion is displaced out of the basal plane by 15 pm towards the apical position occupied by a methanol oxygen atom at a larger distance of 230 pm. The *trans* angles are very similar with 170° for O3–Cu2–O4 and 171° for O5–Cu2–N3 indicating only a slight distortion of the basal plane. The distortion of the square-pyramidal coordination environment can be quantified by the Addison distortion index τ of 0.02 confirming the almost perfect square pyramidal coordination geometry of the copper centers ($\tau = 0$ for an ideal tetragonal pyramid, $\tau = 1$ for an ideal trigonal bipyramid^[209]).

The phenylene rings of the salicylidene ligand side chains, which are coordinated to the bridging copper ions Cu1 and Cu1A, are twisted with respect to the central *meta*-phenylene bridging unit with dihedral angles of about 58° and 42° . This leads to a Cu...Cu separation of 742 pm. The third salicylidene side chain is twisted towards the opposite site of the bridge with a smaller dihedral angle of 34° . This leads to shorter interatomic separations of 611 pm for Cu1...Cu2 and longer distances of 714 pm for Cu1...Cu2A. The central *meta*-phenylene rings are parallel but *anti*-oriented at a distance of 303 pm with an offset π - π interaction between them. The centroid-centroid distance between both bridging phenylene rings is 343 pm very similar as in the dinuclear complex $\text{Cu}_2\text{L}_2^{\dagger\text{Busal}}$ (9).

In the crystal packing the neutral tetranuclear molecules assemble parallel without significant interactions between them, illustrated in figure 3.17. This results in an large separation of the complex molecules with the shortest intermolecular Cu...Cu distance of 853 pm. Due to the missing intermolecular interactions, the co-crystallized chloroform molecules are all highly disordered over several positions which unfortunately could not be fully resolved. Due to this fact the ωR_2 value is rather high. Nevertheless this does not have an influence on the bond lengths and angles within the tetranuclear complex molecule.

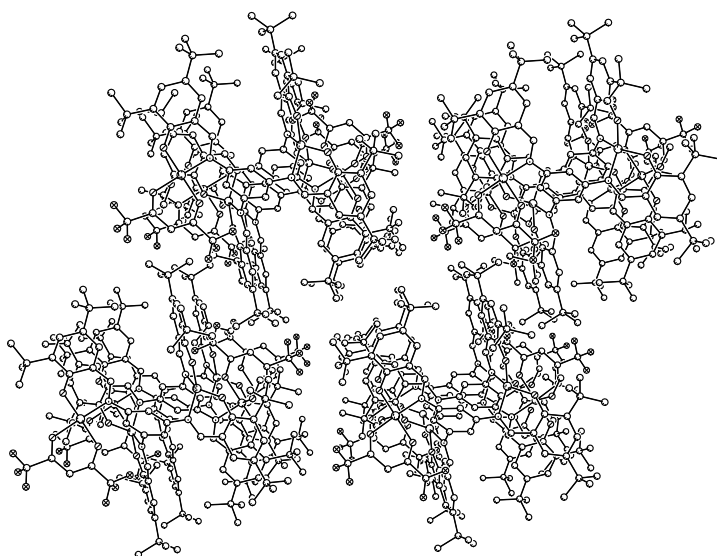


Figure 3.17: Crystal packing of complex $\text{Cu}_4\text{L}_2^{\dagger\text{Busal}}$ (11). Solvent molecules as well as hydrogen atoms are omitted for clarity. Viewing along the [010] direction of the unit cell.

3.3.3 Magnetic Properties

Dinuclear Copper(II) Complex

The magnetic data of complex $\text{Cu}_2\text{L}_2^{\text{Busal}}$ (**9**) is depicted in figure 3.18 as $\chi_M = f(T)$ and $\chi_M T = f(T)$ plots. The experimental $\chi_M T$ value at room temperature is $0.94 \text{ cm}^3 \text{ K mol}^{-1}$, which is slightly above the theoretical spin-only value expected for two independent copper(II) ions. Upon lowering the temperature $\chi_M T$ decreases reaching a minimum value of $0.86 \text{ cm}^3 \text{ K mol}^{-1}$ at 40 K and then rapidly increases to $0.98 \text{ cm}^3 \text{ K mol}^{-1}$ at 2 K. The minimum $\chi_M T$ value at 40 K is close to the spin-only value of two independent copper(II) ions and the subsequent increase below 30 K indicates ferromagnetic exchange interactions between both copper centers. Therefore the decrease of $\chi_M T$ in the high temperature region can be assigned to a temperature independent paramagnetism consistent with the higher room temperature $\chi_M T$ value.

In order to interpret the magnetic properties the experimental $\chi_M T$ data was analyzed using the Bleaney-Bowers equation for isolated dinuclear copper(II) complexes ($\hat{H} = -J\hat{S}_1\hat{S}_2$ with $S_1 = S_2 = 1/2$).^[210] Due to the course of the magnetic data the contribution of the temperature independent paramagnetism (χ_{TIP}) was also taken into account in equation 3.5 for $\chi_M = f(T)$.

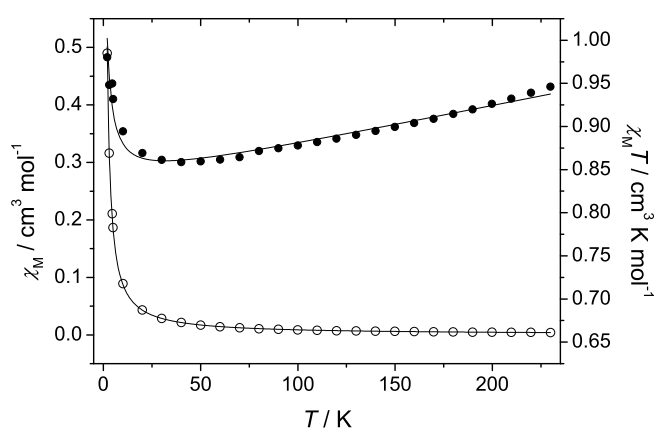


Figure 3.18: Plot of the thermal dependence of χ_M (empty circles, \circ) and $\chi_M T$ (black filled circles, \bullet) for complex $\text{Cu}_2\text{L}_2^{\text{Busal}}$ (**9**) measured with an applied magnetic field of 2000 Oe. The corresponding fit functions according to the Bleaney-Bowers equation 3.5 are drawn as solid lines (for parameters see text).

$$\chi_{\text{M}} = \frac{2N_{\text{A}}\beta^2g^2}{kT} \frac{1}{3 + \exp(-J/kT)} + \chi_{\text{TIP}} \quad (3.5)$$

The best fit obtained for the dinuclear complex $\text{Cu}_2\text{L}_2^{\dagger\text{Busal}}$ (**9**) results in $J = +1.5(1) \text{ cm}^{-1}$, $g = 2.105(6)$, and $\chi_{\text{TIP}} = 4.5(1) \cdot 10^{-4} \text{ cm}^3 \text{ mol}^{-1}$ with $r^2 = 0.99228$.

For the dinuclear complex a positive coupling constant is obtained which reveals ferromagnetic interactions between both copper centers leading to an $S = 1$ triplet ground state. The exchange interaction is ascribed to spin polarization effects through the aromatic *meta*-phenylene linkage.^[196] The observed intradimer coupling is weakly ferromagnetic in contrast to reported dinuclear complexes with double Schiff-base ligands of 1,3-phenylenediamine and salicylic aldehydes all exhibiting very weak antiferromagnetic exchange interactions with very similar J of about -1.0 cm^{-1} .^[119,120,124] This can be ascribed to different distortions of the copper coordination geometries within each complex, which affect the orientation of the magnetic orbitals of both copper centers in relation to the bridging benzene rings. Moreover, DFT calculations on a similar dinuclear copper(II) complex result in weak ferromagnetic interactions with $J = +1.7 \text{ cm}^{-1}$, which is in excellent agreement with the obtained coupling constant of $J = +1.5 \text{ cm}^{-1}$.^[123] Furthermore the ferromagnetic exchange interaction falls well within the broad range of $-1 < J < +17 \text{ cm}^{-1}$ reported for dinuclear *meta*-phenylene-bridged copper(II) complexes.^[119-124,206]

Dinuclear Cobalt(II) Complex

Variable temperature (2-300 K) magnetic susceptibility data collected on a polycrystalline sample of the dinuclear cobalt complex $\text{Co}_2\text{L}_2^{\dagger\text{Busal}}$ (**10**) is depicted in figure 3.19 as $\chi_{\text{M}} = f(T)$ and $\chi_{\text{M}}T = f(T)$. The experimental $\chi_{\text{M}}T$ value at 300 K is $5.25 \text{ cm}^3 \text{ K mol}^{-1}$, which is in good agreement with the theoretical spin-only value expected for two independent cobalt(II) ions with $S = 3/2$ and confirms the high-spin character of both cobalt(II) centers in the complex. On decreasing temperature the $\chi_{\text{M}}T$ value slightly decrease to $4.64 \text{ cm}^3 \text{ K mol}^{-1}$ at 50 K and then rapidly decreases to $2.04 \text{ cm}^3 \text{ K mol}^{-1}$ at 2 K. The slight decrease upon cooling in the high temperature region can be ascribed to a temperature independent paramagnetism, as also observed in the dinuclear copper(II)

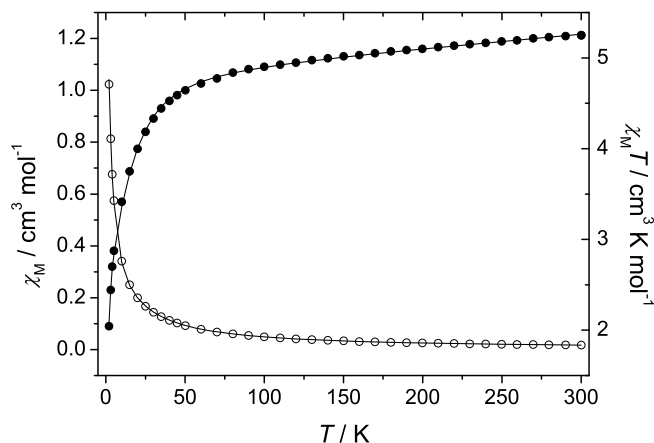


Figure 3.19: Plot of the thermal dependence of χ_M (empty circles, \circ) and $\chi_M T$ (black filled circles, \bullet) for complex $\text{Co}_2\text{L}_2^{\dagger\text{Busal}}$ (**10**) measured with an applied magnetic field of 2000 Oe. The data were fitted with the program package DAVE using the spin Hamiltonian given in equation 3.6 (fit functions drawn as solid lines; for parameters see text).

complex $\text{Cu}_2\text{L}_2^{\dagger\text{Busal}}$ (**9**). Moreover the rapid decrease at lower temperatures might be either attributed to antiferromagnetic exchange interactions between the cobalt centers or to large local zero-field splitting (ZFS) characteristic for cobalt(II) ions. A mixture of both is also possible.

In order to explain this magnetic behavior for cobalt(II) complexes the ZFS of the cobalt(II) ions has to be considered especially in the cases of weak exchange interactions. Due to the large separation between both cobalt(II) ions of about 732 pm only a weak interaction is expected, as in the dinuclear copper complex $\text{Cu}_2\text{L}_2^{\dagger\text{Busal}}$ (**9**). The experimental magnetic data has been successfully simulated using the anisotropic spin Hamiltonian given in equation 3.6 in a full matrix diagonalization approach including the ZFS and Zeeman effects. To avoid overparametrization only an axial ZFS was initially assumed with one D equal for both cobalt centers, due to the centrosymmetry of the complex molecule.

$$\hat{H} = -J\hat{S}_1\hat{S}_2 + \sum_{i=1}^2 D_i[\hat{S}_{z,i}^2 - \frac{1}{3}(S_i(S_i + 1))] + \sum_{i=1}^2 g_i\beta\hat{S}_i\vec{H} \quad (3.6)$$

Fitting the parameters to the experimental data using the full matrix diagonalization routine DAVE^[177] whilst the temperature independent paramagnetism (χ_{TIP}) is taking into

account gives the following results: $J = -0.2 \text{ cm}^{-1}$, $g = 2.27$, $D = -20.4 \text{ cm}^{-1}$, and $\chi_{TIP} = 1.5 \cdot 10^{-3} \text{ cm}^3 \text{ mol}^{-1}$. The later inclusion of a rhombic ZFS with the spin Hamiltonian $\hat{H}_{ZFS} = D[S_z^2 - \frac{1}{3}S(S+1) + E/D(\hat{S}_x^2 - \hat{S}_y^2)]$ which accounts for the distorted tetrahedral geometry, leads to the parameters $D = -20.4 \text{ cm}^{-1}$ and $E/D = 3 \cdot 10^{-5}$. This confirms the predominate presence of an axial ZFS within the dinuclear complex. As the variations of the χ_{MT} are in general not very sensitive to the sign of D , it can not be unambiguously determined.^[178] Therefore the reversal sign for the D parameter was tested which lead to an only marginal worse fit of the experimental data with very similar values for all other parameters. Nevertheless the large D value is consistent with the observed distorted tetrahedral coordination geometry of the cobalt(II) ions and further with reported distorted tetrahedral cobalt(II) complexes.^[211,212]

The isotropic exchange between the cobalt centers is very weak compared to the ZFS. An alternative fit assuming exclusively ZFS under consideration of the temperature independent paramagnetism did not reproduce the course of the experimental χ_{MT} data. This confirms further the presence of a weak antiferromagnetic coupling between both cobalt centers mediated through the bridging ligand. The rather large χ_{TIP} can be attributed to spin orbit coupling characteristic for cobalt(II) complexes. The exchange interaction between both cobalt centers is very weak antiferromagnetic compared to the corresponding copper complex with ferromagnetic exchange interactions. Moreover the coupling is slightly weaker compared to reported dinuclear *meta*-phenylenediimine-bridged metallamacrocyclic cobalt(II) complexes with coupling constants of about $J = -1.3 \text{ cm}^{-1}$.^[125] This might be attributed to the almost ideal tetrahedral coordination environments of the cobalt centers within these complexes compared to the stronger distorted geometry within complex $\mathbf{Co}_2\mathbf{L}_2^{\dagger\text{Busal}}$ (10).

Tetranuclear Copper(II) Complex

The magnetic data of complex $\mathbf{Cu}_4\mathbf{L}_2^{\dagger\text{Busal}}$ (11) is depicted in figure 3.20 as $\chi_M = f(T)$ and $\chi_{MT} = f(T)$ plots. The χ_{MT} value appears to be roughly invariant at $1.8 \text{ cm}^3 \text{ K mol}^{-1}$ between 300 and 50 K, which is in good agreement with the spin-only value expected for four independent copper(II) ions with $S = 1/2$. Below 50 K the χ_{MT} value rapidly increases up to $3.15 \text{ cm}^3 \text{ K mol}^{-1}$ at 2 K, indicating a ferromagnetic exchange interaction between the copper centers mediated through the *meta*-phenylenetriimine bridges. The value is close to that expected for a $S = 2$ ground state indicating a ferromagnetic coupling between all four copper centers.

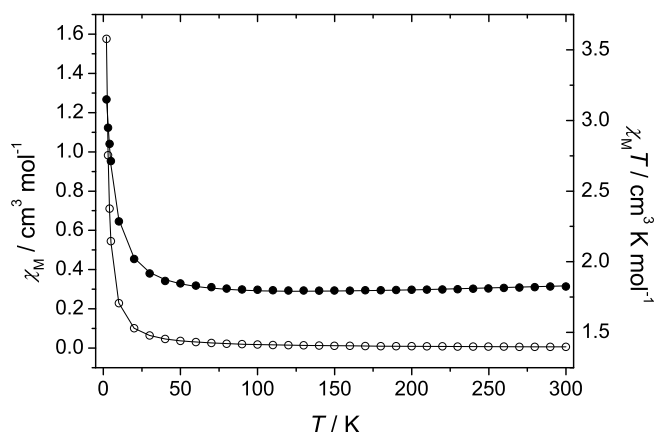


Figure 3.20: Plot of the thermal dependence of χ_M (empty circles, \circ) and $\chi_M T$ (black filled circles, \bullet) for complex $\text{Cu}_4\text{L}_2^{t\text{Busal}}$ (**11**) measured with an applied magnetic field of 2000 Oe. The data were fitted with the program package DAVE using the isotropic spin Hamiltonian given in equation 3.7 (fit functions drawn as solid lines; for parameters see text).

Besides, an unusual temperature dependent magnetic behavior is observed for the tetranuclear complex $\text{Cu}_4\text{L}_2^{t\text{Busal}}$ shown in figure 3.21. Complex cooling for five days at 4 K and subsequent warming leads to a different course of $\chi_M T$ value between 50 and 160 K. From 50 K the $\chi_M T$ value increases to a maximum followed by a steadily decrease to the final value measured during the cooling process at 160 K. The increase is dependent on the cooling time and the applied cooling temperature but independent on the strength of the magnetic field. Furthermore the magnitude is influenced by details within the preparation of the complex, which are not completely understood yet. In all cases the process is completely reversible, which means that warming above 160 K and the subsequent cooling results in a normal course of the magnetic data as shown in figure 3.20. A similar magnetic behavior is also observed for the dinuclear complex $\text{Cu}_2\text{L}_2^{t\text{Busal}}$ (**9**). Such a magnetic behavior was not yet reported, which makes the complex very interesting for further studies. The anomaly is ascribed to structural changes within the coordination geometry of the copper centers.^[213] In cooperations with other work groups further studies using differential scanning calorimetry (DSC) and X-ray powder diffraction at low temperatures are still under investigation. Nevertheless cooling of the complex from 300 to 2 K within the time scale of the magnetization measurement results in the normal course of the $\chi_M T$ value enabling an interpretation of the magnetic data (see figure 3.20).

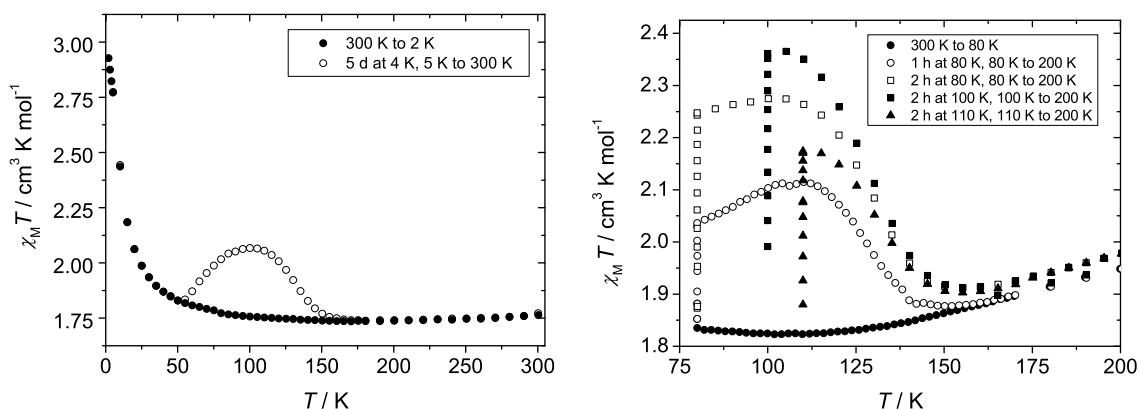


Figure 3.21: Left: Plot of the thermal dependence of $\chi_{\text{M}}T$ for complex $\text{Cu}_4\text{L}_2^{\dagger\text{Busal}}$ (11) measured with an applied magnetic field of 5000 Oe. Temperature dependence upon cooling from 300 to 2 K (black filled circles, ●) and cooling for five days at 4 K followed by warming up to 300 K (empty circles, ○). Right: Magnetic anomaly as a function of the cooling time as well as cooling temperature.

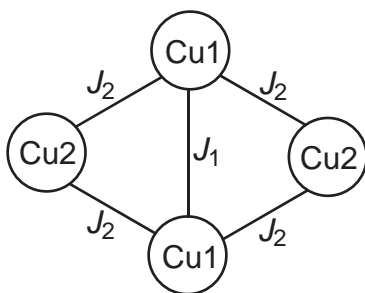


Figure 3.22: The spin topology of the employed two- J model for the tetranuclear copper complex $\text{Cu}_4\text{L}_2^{\dagger\text{Busal}}$ (11).

In the tetranuclear complex two equivalent triangular *meta*-phenylene-bridged Cu_3 subunits are connected in an edge sharing manner. Hence a two- J model is employed in order to interpret the magnetic data which is shown in figure 3.22. The experimental data was analyzed using the full matrix diagonalization routine DAVE^[177] with the corresponding isotropic spin Hamiltonian given in equation 3.7 under consideration of additional Zeeman interactions.

$$\hat{H} = -J_1 \hat{S}_1 \hat{S}_2 - J_2 (\hat{S}_1 \hat{S}_3 + \hat{S}_2 \hat{S}_4 + \hat{S}_2 \hat{S}_3 + \hat{S}_1 \hat{S}_4) + \sum_{i=1}^4 g_i \beta \hat{S}_i \vec{H} \quad (3.7)$$

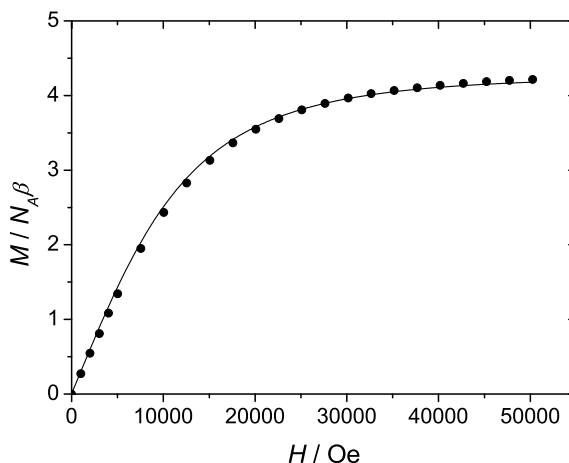


Figure 3.23: Field dependence of the magnetization for complex $\text{Cu}_4\text{L}_2^{\dagger\text{Busal}}$ (11) at 2 K (\bullet). The Brillouin function for $S = 2$ and $g = 2.12$ is plotted as solid line.

Due to slight decrease of the $\chi_{\text{M}}T$ value upon cooling in the high temperature region an additional temperature independent paramagnetism (χ_{TIP}) is also considered. The best fit of the experimental data of complex $\text{Cu}_4\text{L}_2^{\dagger\text{Busal}}$ (11) results in the parameters $J_1 = +12.0 \text{ cm}^{-1}$, $J_2 = +2.7 \text{ cm}^{-1}$, $g = 2.12$, and $\chi_{\text{TIP}} = 4.0 \cdot 10^{-4} \text{ cm}^3 \text{ mol}^{-1}$.

The overall observed ferromagnetic coupling within the Cu_4 core is consistent with magnetization measurements at 2 K, depicted in figure 3.23, confirming the $S = 2$ ground state. Ferromagnetic interaction is ascribed to spin polarization through both *meta*-phenylenetriimine bridges. The ferromagnetic coupling J_1 between the central copper centers Cu1 and Cu2 is stronger compared to the coupling J_2 with the peripheral copper centers Cu3 and Cu4. Both copper centers are aligned at the same site relating to the benzene bridge, whereas the peripheral ones are arranged at the opposite site. This coupling is significantly stronger compared to the dinuclear copper complex $\text{Cu}_2\text{L}_2^{\dagger\text{Busal}}$ (9) with $J = +1.5 \text{ cm}^{-1}$, which might be ascribed to an overall stronger tetrahedral distortion of the coordination geometry of the copper centers leading to a better exchange interaction through the spin polarization mechanism. Compared to the rather large $\text{Cu} \cdots \text{Cu}$ separations between 611 and 742 pm in the tetranuclear complex, all ferromagnetic couplings are rather strong. This ligand mediates efficient exchange interactions between the copper centers through spin polarization mechanism.

4 Triaminoguanidine-Bridged Complexes

4.1 Ligand and Complex Design

Another bridging unit capable of a tritopic coordination of transition metal ions is the triaminoguanidine. Three ligands differing in the ligand side chains were synthesized, shown in figure 4.1. Triple Schiff-base ligands of triaminoguanidine are capable to coordinate three transition metal ions in close proximity. Müller *et al.* have published the synthesis of the ligands $\text{H}_5\text{L3}^{\text{Brsal}}$ and $\text{H}_5\text{L3}^{\text{Hsal}}$ easily accessible through Schiff-base condensation of salicylic aldehyde derivatives with triaminoguanidine.^[91,92] The ligands are isolated in form of their hydrochloride salts $\text{H}_5\text{L3}^{\text{Hsal}} \cdot \text{HCl}$ and $\text{H}_5\text{L3}^{\text{Brsal}} \cdot \text{HCl}$. In fact every salicylic aldehyde derivative can be reacted with triaminoguanidine affording similar ligands with different substituents in the side chains.^[132,137,139,214] The ligands possess three equivalent binding pockets each with a N_2O donor set. After deprotonation the ligands can coordinate three metal ions in their pentaanionic forms. The reaction with divalent transition metal ions needs neutral co-ligands while trivalent metal ions demand ionic co-ligands as all isolated complexes are exclusively monocationic or neutral. Trinuclear complexes with divalent cations are well known, while the trivalent analogues are still rare. Therefore the coordination of iron(III) ions was investigated. The ligand $\text{H}_2\text{L3}^{\text{py}}$ was also synthesized through Schiff-base condensation reaction of pyridine-2-carbalydehyde and triaminoguanidine. Again the ligand was isolated as the hydrochloride salt $\text{H}_2\text{L3}^{\text{py}} \cdot \text{HCl}$. The coordination behavior towards different transition metal ions was studied and trinuclear transition metal complexes were synthesized. Moreover the defined linkage of these complexes into higher aggregates will be demonstrated.

The triaminoguanidine-based ligands geared towards the generation of strong antiferromagnetic coupled triangular complexes, in contrast to the previously discussed *meta*-phenylene-bridged complexes aiming for ferromagnetic exchange interactions through spin polarization. It is interesting to mention, that all complexes were prepared apply-

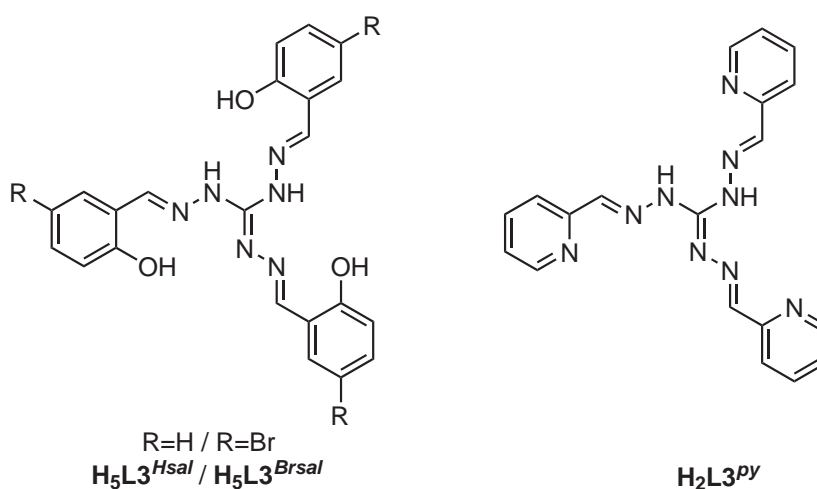


Figure 4.1: Schematic representation of the tritopic ligands based on triaminoguanidine.

ing a directed synthetic route and not by serendipity. Due to the different synthetic approaches, the results are discussed in separate groups in the following sections.

4.2 Iron(III) Complexes with the Ligand $\text{H}_5\text{L}_3^{\text{Brsal}}$

4.2.1 Synthesis and Characterization

Various trinuclear copper(II) and nickel(II) complexes with different tris-salicylidene-amino-guanidine ligands were prepared by our group in a directed synthesis approach using additional capping co-ligands, like 2,2'-bipyridine and 2,4,6-tris(2-pyridyl)-1,3,5-triazine.^[139–141] In contrast to this just two structurally characterized iron(III) complexes are obtained through serendipitous assembly.^[139] The reproducibility of both complex syntheses is difficult due to extreme long crystallization times of four and eleven months in combination with the self-assembly process.

The synthesis of the iron(III) complexes is much more difficult compared to the copper(II) and nickel(II) complexes. This is caused by the higher acidity of the iron(III) ion in combination with the imine functionalities in the ligands sensitive for hydrolysis. Moreover a cyclization reaction of the ligand has been observed in the presence of iron(III) ions.^[139] Due to the fact, that additional base is needed for the deprotonation of the ligand, predominantly insoluble iron(III) oxo-hydroxo species precipitated

from the reaction solutions performing the synthesis in protic polar solvents like alcohols or water. Furthermore the resulting iron(III) complexes are only sparingly soluble in most common organic solvents and even less soluble in dimethylsulfoxide as well as dimethylformamide making the structural characterization more difficult. These are only a few facts that complicate the synthesis and crystallization of trinuclear iron(III) complexes. Therefore an alternative synthetic access to triaminoguanidine-bridged iron(III) complexes needs to be established.

A versatile access to trinuclear iron(III) complexes was found utilizing a rather unusual synthetic approach. Herein pyridine was used acting as solvent, base and co-ligand for the coordinative saturation of the iron centers within the trinuclear complex. As iron(III) source the metal chloride was dissolved in pyridine leading to the formation of a soluble iron(III)-chloro-pyridinium complex. The chloride anions further act as co-ligands and counterbalance the resulting highly charged trinuclear cation after complex formation through coordination to the iron centers. Moreover the extreme excess of pyridine prevents the uncontrolled polymerization of the trinuclear complexes in solution.

For the complex synthesis iron(III) chloride hexahydrate was dissolved in pyridine resulting in a red colored solution. Subsequently a solution of the ligand $H_5L3^{Brsal} \cdot HCl$ in pyridine was added dropwise, accompanied by an immediate color change to deep green. This indicates a coordination of the iron ions by the ligand. Then sodium perchlorate monohydrate was added to improve the crystallization by the use of a low-coordinating counteranion. Finally the diffusion of methanol into the reaction solution resulted in green hexagonal prism of the trinuclear iron(III) complex $[Fe_3(L3^{Brsal})(py)_6Cl_3]ClO_4$ (Fe_3L3^{Brsal}) (**12**) in high yield of 64 % based on crystalline material. As expected the pyridine molecules and chloride ions act as co-ligands. The complex is nearly insoluble in most common organic solvents including dimethylformamide as well as dimethylsulfoxide, but soluble in pyridine.

Due to the lability of both co-ligands, which is evident from the complex formation reaction, they can be easily exchanged by chelating co-ligands. A first attempt was carried out with 8-hydroxyquinoline (Hq). The addition into a solution of the iron complex Fe_3L3^{Brsal} (**12**) led to the formation of the neutral trinuclear complex $[Fe_3(L3^{Brsal})(q)_3(py)_2Cl]$ ($Fe_3L3^{Brsal}q_3$) (**13**). One chloride ion together with one pyridine molecule were each replaced by the deprotonated 8-hydroxyquinoline co-ligand. More-

over a coordinated chloride ion counterbalances the positive charge of the trinuclear unit resulting in a neutral complex molecule. Hence the trinuclear complex $\text{Fe}_3\text{L3}^{Brsal}$ (**12**) provides an easy access to the targeted synthesis of trinuclear iron(III) complexes with various bis- as well as tris-chelating co-ligands.

In addition a hexanuclear iron(III) complex was obtained performing the synthesis analogous to the trinuclear iron complex $\text{Fe}_3\text{L3}^{Brsal}$ (**12**) but without sodium perchlorate monohydrate. The reaction of $\text{FeCl}_3 \cdot 6\text{H}_2\text{O}$ with the ligand $\text{H}_5\text{L3}^{Brsal} \cdot \text{HCl}$ in pyridine followed by addition of methanol into the reaction mixture afforded green prism of complex $[\text{Fe}_6(\text{L3}^{Brsal})_2(\mu\text{-OMe})_2(\text{py})_8\text{Cl}_6]$ ($\text{Fe}_6\text{L3}_2^{Brsal}$) (**14**). Herein two trinuclear iron(III) complex molecules are connected through two methanolate bridges.

The three complexes were characterized by X-ray structural analysis, elemental analysis, and IR spectroscopy. Due to the above mentioned poor solubility of the trinuclear iron complex $\text{Fe}_3\text{L3}^{Brsal}$ (**12**), no signals were detected in the ESI mass spectra measured in different solvents and even mixtures of them. This was the same for the other complexes as well. Furthermore FAB mass spectra did not show any signals of the complexes. The crystals of complexes $\text{Fe}_3\text{L3}^{Brsal}$ (**12**) and $\text{Fe}_6\text{L3}_2^{Brsal}$ (**14**) stay intact after isolation from the reaction solution, whereas complex $\text{Fe}_3\text{L3}^{Brsal}\mathbf{q}_3$ (**13**) loses the co-crystallized solvent molecules which is in agreement with the elemental analyses data.

In the IR spectrum of the ligand the $\tilde{\nu}_{\text{C}=\text{N}}$ stretching vibration is observed at 1665 cm^{-1} . Upon coordination to iron(III) ions this band is shifted to frequencies lower than 1600 cm^{-1} . In addition, characteristic bands assigned to stretching vibrations of the triaminoguanidine core ligand are also slightly shifted. These bands are mixed with the vibration bands of the pyridine co-ligands preventing an unambiguously assignment to an individual vibration mode. The IR spectra of the trinuclear complex $\text{Fe}_3\text{L3}^{Brsal}$ (**12**) and the hexanuclear complex $\text{Fe}_6\text{L3}_2^{Brsal}$ (**14**) are very similar and are dominated by the pyridine co-ligands. Additionally in complex $\text{Fe}_3\text{L3}^{Brsal}$ (**12**) a strong band is observed at 1096 cm^{-1} , characteristic for the stretching vibration of unbound perchlorate counterions in the crystal lattice. In the IR spectrum of the trinuclear complex $\text{Fe}_3\text{L3}^{Brsal}\mathbf{q}_3$ (**13**) an additional strong band is observed at 1107 cm^{-1} due to the $\tilde{\nu}_{\text{C}-\text{O}}$ stretching vibration. The perchlorate stretching vibration is absent.

4.2.2 Crystal Structures

 $[Fe_3(L3^{Brsal})(py)_6Cl_3]ClO_4$ (Fe_3L3^{Brsal}) (12)

In the complex Fe_3L3^{Brsal} (12) three iron(III) ions are coordinated by the penta-deprotonated triaminoguanidine ligand, each within one tridentate binding pocket. The molecular structure and labeling scheme of the complex cation $[Fe_3(L3^{Brsal})(py)_6Cl_3]^+$ is depicted in figure 4.2. Selected bond lengths and angles are listed in table 4.1. The complex crystallizes in the hexagonal space group $P\bar{3}$ with an C_3 axis through the central carbon atom C1. Consequently the three iron(III) centers are crystallographically equivalent.

The iron centers possess a distorted octahedral coordination geometry with a N_4OCl donor set. Three coordination sites at the iron(III) ion are coordinated by the N_2O donor set of the triaminoguanidine ligand with bite angles of 85° for $O1-Fe1-N2$ and 73° for $N2-Fe1-N1A$. The fourth position within the tetragonal plane is occupied by a chloride ion at a distance of 229 pm. The octahedral geometry is completed by two pyridine molecules, which bind at distances of 220 pm (N3) and 218 pm (N4) in the axial positions. The bond lengths to the ligand donor atoms are shorter ranging from 190 to 214 pm. All distances are in the usually observed range for octahedral iron(III) complexes

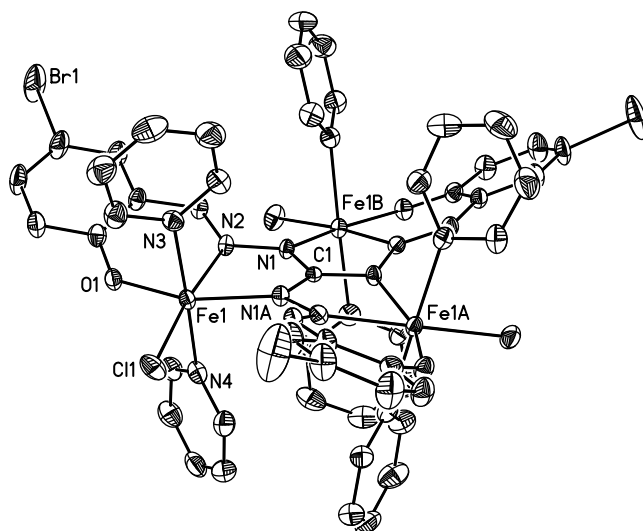


Figure 4.2: Molecular structure of the complex cation of Fe_3L3^{Brsal} (12). Thermal ellipsoids are drawn at the 50% probability level. The hydrogen atoms are omitted for clarity. Symmetry equivalent atoms are labeled with the suffixes A and B.

Table 4.1: Selected bond lengths [pm] and angles [°] for complex **Fe₃L3^{Brsal}** (12).

Fe1–O1	190.0(3)	Fe1–N1A	209.0(3)
Fe1–N2	214.0(4)	Fe1–N3	220.0(4)
Fe1–N4	217.6(4)	Fe1–Cl1	228.98(12)
O1–Fe1–N1A	158.21(13)	O1–Fe1–N2	85.28(13)
O1–Fe1–N3	88.11(14)	O1–Fe1–N4	89.92(14)
O1–Fe1–Cl1	100.42(10)	N2–Fe1–N1A	73.32(13)
N2–Fe1–N3	93.01(14)	N2–Fe1–N4	87.15(14)
N2–Fe1–Cl1	173.78(10)	N3–Fe1–N1A	88.94(14)
N3–Fe1–N4	178.01(14)	N3–Fe1–Cl1	89.69(10)
N4–Fe1–N1A	93.01(14)	N4–Fe1–Cl1	90.35(11)
Cl1–Fe1–N1A	101.15(10)		

indicating the iron center to be in the high-spin state.^[215–220] The iron center is perfectly situated within the tetragonal plane. The three *trans* angles are 158° (O1–Fe1–N1A), 174° (N2–Fe1–Cl1), and 178° (N3–Fe1–N4) indicating a distortion of the octahedral geometry mainly caused by the rigid ligand binding pocket.

The triaminoguanidine ligand is bowl-shaped, due to the coordination of the iron centers. The bromo substituent is displaced out of the least square plane of the central CN₆ core by 246 pm, resulting in a dihedral angle of 27° between the central CN₆ core and the salicylidene rings. The dihedral angle between the tetragonal planes of the iron centers is 22°, which leads to an interatomic Fe···Fe separation of 509 pm and Fe–N–N–Fe torsion angles of 161°. The axial pyridine molecules are twisted against each other with a dihedral angle of 75°. The positive charge of the complex cation is counterbalanced by a perchlorate ion also situated on a C₃ axis. In the crystal packing the complex molecules assemble through slipped face-to-face π - π interactions between the axial pyridine molecules with distances of 338 and 348 pm. This leads to the formation of a 3D network illustrated in figure 4.3. Furthermore the perchlorate ion establishes hydrogen bonding interactions with the pyridine hydrogen atoms in distances of 322 pm (C_{py}···O). Therefore the perchlorate ion do not show a disorder. Within this network the trinuclear complex core units are well separated with the shortest intermolecular Fe···Fe contacts of 796 pm.

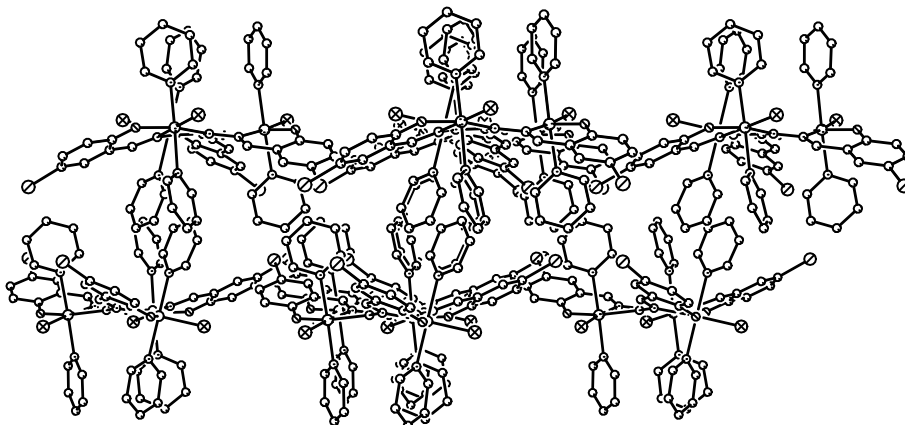


Figure 4.3: Supramolecular structure representing the π - π interactions of the complex cations of Fe_3L3^{Brsal} (**12**). The hydrogen atoms are omitted for clarity.

$[Fe_3(L3^{Brsal})(q)_3(py)_2Cl] (Fe_3L3^{Brsal}q_3)$ (13**)**

The molecular structure as well as the labeling scheme of complex $Fe_3L3^{Brsal}q_3$ (**13**) is depicted in figure 4.4. Selected bond lengths and angles are listed in table 4.2. Three iron(III) ions are coordinated by the deprotonated triaminoguanidine ligand and linked through N-N diazine bridges into a triangular arrangement. Each iron center is coordinated in a distorted octahedral geometry. Three coordination sites at the iron centers are occupied by the N_2O donor set of the triaminoguanidine ligand, as previously described for complex Fe_3L3^{Brsal} (**12**), with averaged bite angles of 87° and 75° for O-Fe-N and N-Fe-N, respectively. The fourth positions within the ligand planes are occupied by the phenolate oxygen atom of the deprotonated 8-hydroxyquinoline co-ligands, whereas the pyridine nitrogen atom coordinates in the axial positions with bite angles of about 79° . The second axial position at the iron centers Fe2 and Fe3 is occupied by pyridine molecules in distances of 216 pm (Fe2-N10) and 219 pm (Fe3-N11). The iron center Fe1 is coordinated by a chloride ion at a distance of 233 pm counterbalancing the positive charge of the trinuclear complex. The donor-iron distances within the tetragonal planes are very similar for each iron center. The bond lengths range between 191 and 213 pm, with shorter Fe-O distances situated on the lower and longer Fe-N distances situated on the upper end of this range. The distances to the axial pyridine nitrogen atoms of the co-ligands are clearly longer ranging between 219 to 225 pm. This is caused by the rigidity of the 8-hydroxyquinoline co-ligand forming a five-membered chelate ring with the metal center in combination with a short Fe-O distance. As expected the distances

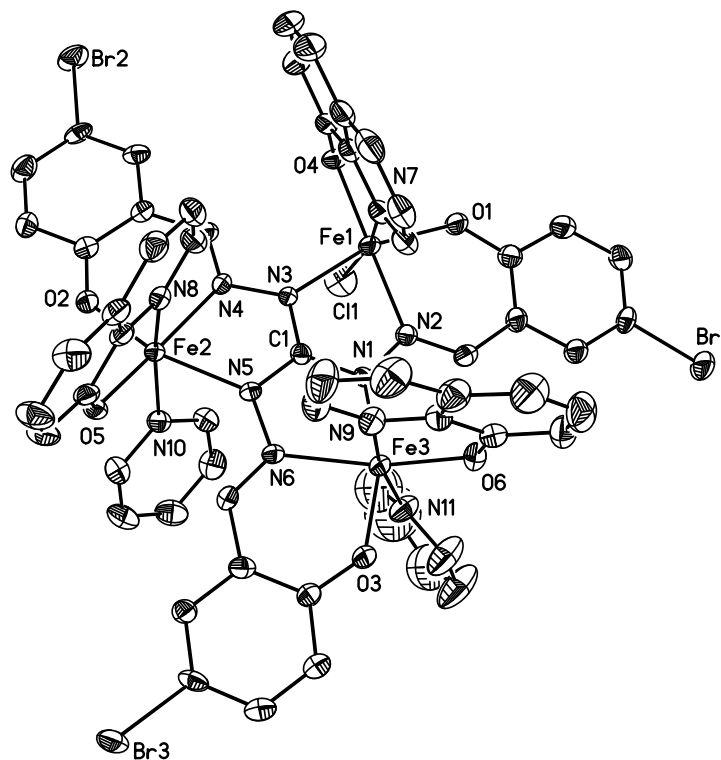


Figure 4.4: Molecular structure of the complex $\text{Fe}_3\text{L3}^{\text{Brsal}}\text{q}_3$ (**13**). Thermal ellipsoids are drawn at the 50% probability level. The co-crystallized solvent molecules as well as the hydrogen atoms are omitted for clarity.

Table 4.2: Selected bond lengths [pm] and angles [$^\circ$] for complex $\text{Fe}_3\text{L3}^{\text{Brsal}}\text{q}_3$ (**13**).

Fe1–O1	192.1(3)	Fe2–O2	191.0(3)	Fe3–O3	190.5(3)
Fe1–O4	193.9(3)	Fe2–O5	193.8(3)	Fe3–O6	193.0(3)
Fe1–N2	212.6(3)	Fe2–N4	211.2(3)	Fe3–N1	204.6(3)
Fe1–N3	212.0(3)	Fe2–N5	211.4(3)	Fe3–N6	212.9(3)
Fe1–N7	225.0(4)	Fe2–N8	219.2(4)	Fe3–N9	221.5(4)
Fe1–Cl1	233.09(14)	Fe2–N10	215.6(3)	Fe3–N11	219.1(4)
O1–Fe1–N3	160.60(12)	O2–Fe2–N5	160.43(12)	O3–Fe3–N1	159.44(13)
O4–Fe1–N2	160.43(13)	O5–Fe2–N4	168.19(12)	O6–Fe3–N6	162.78(12)
N7–Fe1–Cl1	169.43(10)	N8–Fe2–N10	165.21(12)	N9–Fe3–N11	170.56(14)

to the ligand donor atoms as well as the pyridine co-ligands are very similar to those in the symmetric trinuclear iron complex $Fe_3L3^{Brsal}q_3$ (**12**). Moreover all are in the expected range for high-spin iron(III) complexes.^[215–220] The tetragonal plane of each iron center exhibits a slight tetrahedral distortion with dihedral angles of 20° (Fe1), 13° (Fe2), and 18° (Fe3). The iron ions Fe2 and Fe3 are displaced out of the least square tetragonal plane by 6 pm and 9 pm towards the axial positions occupied by the pyridine molecules. The iron ion Fe1 shows a larger displacement of 22 pm towards the coordinated chloride ion. The *trans* angles range from 159° to 171° indicating a distortion from the octahedral geometry.

The ligand molecule is rather flat compared to the bowl shape within the trinuclear iron complex Fe_3L3^{Brsal} (**12**). A slight propeller-like distortion exists with averaged dihedral angles of 10° between the phenylene rings and the central CN_6 core. The iron centers are arranged in an almost isosceles triangle linked through N–N diazine bridges with two equivalent interatomic FeFe distances of 511 pm (Fe1...Fe2, Fe2...Fe3) and one elongated basal edge with 506 pm (Fe1...Fe3). Consequently two different Fe–N–N–Fe torsion angles of 180° (Fe1–N3–N4–Fe2, Fe2–N5–N6–Fe3) and 171° (Fe1–N2–N1–Fe3) are present within the complex.

In the crystal packing the trinuclear complex molecules assemble to chains through π – π interactions between the quinoline co-ligands bound at the iron centers Fe1 and Fe2. These chains run along the [110] direction of the unit cell with perfect face-to-face π – π interactions in a distance of 334 pm (figure 4.5). Therefore the trinuclear complex core units are well separated with the shortest intermolecular Fe...Fe distance of 851 pm within and 837 pm between these parallel aligned chains.

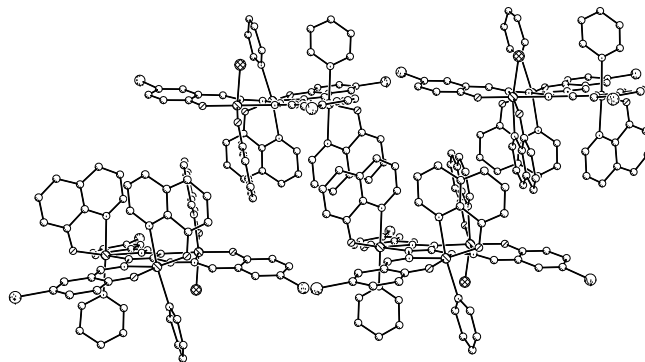


Figure 4.5: Supramolecular arrangement of the trinuclear complex molecules of $Fe_3L3^{Brsal}q_3$ (**13**). The co-crystallized solvent molecules as well as the hydrogen atoms are omitted for clarity.

$[\text{Fe}_6(\text{L3}^{\text{Brsal}})_2(\mu\text{-OMe})_2(\text{py})_8\text{Cl}_6]$ ($\text{Fe}_6\text{L3}_2^{\text{Brsal}}$) (14)

The molecular structure and the heteroatom labeling scheme of the hexanuclear complex $\text{Fe}_6\text{L3}_2^{\text{Brsal}}$ (14) is depicted in figure 4.6. The complex crystallizes in the orthorhombic space group $Pbca$ as a dimer of two crystallographically equivalent trinuclear complex moieties linked through two methanolate bridges.

Each iron center possesses a distorted octahedral geometry. The iron(III) ions are coordinated by the ON_2 donor set of the penta-deprotonated triaminoguanidine ligand as previously described. The coordination polyhedra of Fe2 and Fe3 are nearly identical to those of the symmetric trinuclear complex $\text{Fe}_3\text{L3}^{\text{Brsal}}$ (12) with similar bond lengths and angles listed in table 4.3. Again the fourth position within the ligand plane is occupied by a chloride ion in a larger distance of about 231 pm compared to all other ranging between 191 to 214 pm. The iron centers are displaced out of the corresponding tetragonal plane by 1 pm (Fe2) and 3 pm (Fe3). Both axial positions are occupied by pyridine molecules in distances of about 220 pm completing the distorted octahedral geometry. Again these are twisted with dihedral angles of 45° (Fe2) and 52° (Fe3).

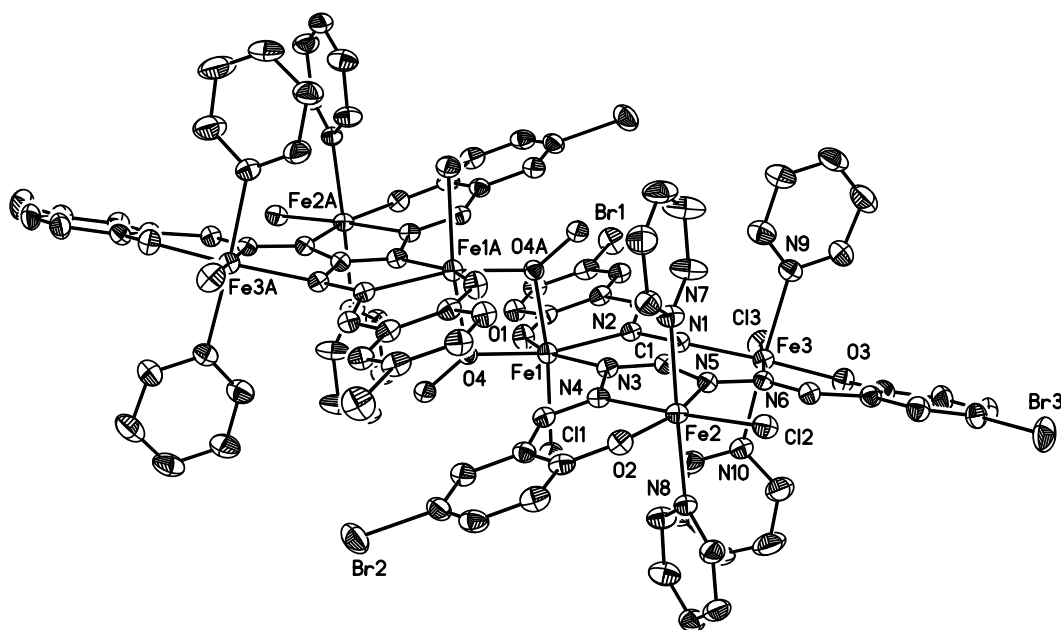


Figure 4.6: Molecular structure of complex $\text{Fe}_6\text{L3}_2^{\text{Brsal}}$ (14). Thermal ellipsoids are drawn at the 30% probability level. The co-crystallized solvent molecules as well as the hydrogen atoms are omitted for clarity. Symmetry equivalent atoms are labeled with the suffix A.

Table 4.3: Selected bond lengths [pm] and angles [$^\circ$] for complex $Fe_6L3_2^{Brsal}$ (**14**).

Fe1–O1	191.5(4)	Fe2–O2	190.0(4)	Fe3–O3	191.1(4)
Fe1–O4	198.6(3)	Fe2–N4	213.5(4)	Fe3–N1	209.1(4)
Fe1–O4A	205.0(3)	Fe2–N5	210.8(4)	Fe3–N6	213.8(4)
Fe1–N2	215.6(4)	Fe2–N7	220.8(4)	Fe3–N9	220.2(5)
Fe1–N3	212.3(4)	Fe2–N8	218.0(4)	Fe3–N10	219.6(5)
Fe1–Cl1	236.90(15)	Fe2–Cl2	232.08(14)	Fe3–Cl3	230.91(15)
O1–Fe1–N3	157.40(16)	O2–Fe2–N5	159.35(16)	O3–Fe3–N1	160.11(15)
O4–Fe1–N2	167.12(14)	N4–Fe2–Cl2	176.87(12)	N6–Fe3–Cl3	176.56(12)
O4A–Fe1–Cl1	167.90(11)	N7–Fe2–N8	176.69(17)	N9–Fe3–N10	177.25(19)

The octahedral coordination geometry at the iron ion Fe1 is completed by two methanolate molecules and one chloride ion. Both methanolate molecules bridge two trinuclear complex moieties through coordination in the fourth positions within the ligand plane together with the axial coordination to the symmetry equivalent iron center resulting in a methanolate-bridged hexanuclear complex. The axial bond length to the methanolate oxygen atom is slightly elongated with 205 pm compared to the equatorial distance with 199 pm leading to a Fe1–O4–Fe1A bridging angle of 105° . Moreover the distance to the chloride ion is slightly elongated with 237 pm compared to those of the iron centers Fe2 and Fe3. The equatorial plane shows a slight tetrahedral distortion with a dihedral angle of about 13° . The iron is displaced out of the idealized plane by 11 pm towards the axial positioned chloride ion. Thus the octahedral coordination environment of the iron ion Fe1 shows a higher distortion compared to the iron centers Fe2 and Fe3, both nearly equal. This is further confirmed by the *trans* angles ranging from 157° to 168° for the iron center Fe1, whereas for both other Fe2 and Fe3 these are much larger ranging from 166° to 177° .

Again the ligand molecule shows a distortion from planarity resulting in a bowl-shaped arrangement, but less pronounced as in the symmetric trinuclear complex Fe_3L3^{Brsal} (**12**). The dimerisation through the methanolate bridges causes an irregular distortion of the ligand molecules indicated by the different dihedral angles between the idealized tetragonal planes of the iron centers within each trinuclear complex unit of 6° (Fe1Fe2), 16° (Fe2Fe3) and 20° (Fe1Fe3). Moreover this leads to interatomic Fe...Fe

separations of 513 pm (Fe1···Fe2), 508 pm (Fe1···Fe3), and 514 pm (Fe2···Fe3) as well as Fe–N–N–Fe torsion angles of 174° (Fe1–N3–N4–Fe2), 152° (Fe1–N2–N1–Fe3), and 170° (Fe2–N5–N6–Fe3). In contrast, the distance between the methanolate-bridged iron centers is clearly shorter with 319 pm.

4.2.3 Magnetic Properties

Trinuclear Iron(III) Complexes

The magnetic properties of both trinuclear iron containing complexes $\text{Fe}_3\text{L3}^{\text{Brsal}}$ (12) and $\text{Fe}_3\text{L3}^{\text{Brsal}}\mathbf{q}_3$ (13) were determined by magnetic measurements in a temperature range from 2 to 300 K. The temperature dependencies for both complexes of the molar susceptibility χ_M and its product $\chi_M T$ are shown in figure 4.7. The magnetic behavior of the complexes is very similar, in line with what is expected considering the highly related structural arrangements of the iron centers. At 300 K the $\chi_M T$ value is $9.21 \text{ cm}^3 \text{ K mol}^{-1}$ for complex $\text{Fe}_3\text{L3}^{\text{Brsal}}$ (12) and $9.60 \text{ cm}^3 \text{ K mol}^{-1}$ for $\text{Fe}_3\text{L3}^{\text{Brsal}}\mathbf{q}_3$ (13). Upon lowering the temperature $\chi_M T$ decreases continuously reaching a value of $0.31 \text{ cm}^3 \text{ K mol}^{-1}$ at 2 K in both complexes. The high temperature values are much larger compared to the spin-only value of three independent low-spin iron(III) centers with $S = 1/2$ ($\chi_M T = 1.13 \text{ cm}^3 \text{ K mol}^{-1}$ assuming that $g = 2$). This is consistent with the crystal structure data indicating all iron centers to be in the high-spin state. However these values are smaller than the calculated value for three uncoupled high-spin iron(III)

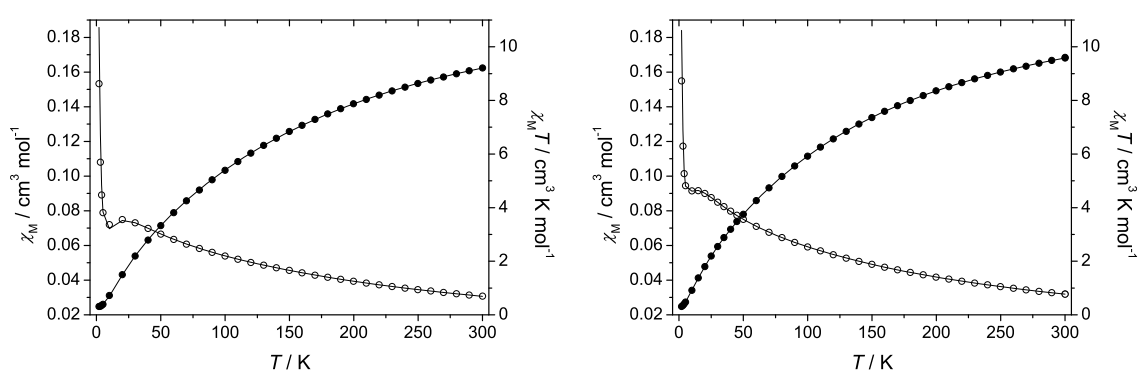


Figure 4.7: Plot of the thermal dependence of χ_M (empty circles, \circ) and $\chi_M T$ (black filled circles, \bullet) for complex $\text{Fe}_3\text{L3}^{\text{Brsal}}$ (12) (left) and complex $\text{Fe}_3\text{L3}^{\text{Brsal}}\mathbf{q}_3$ (13) (right) measured with an applied magnetic field of 2000 Oe. The solid lines represents the best fit to the experimental data (for parameters see text).

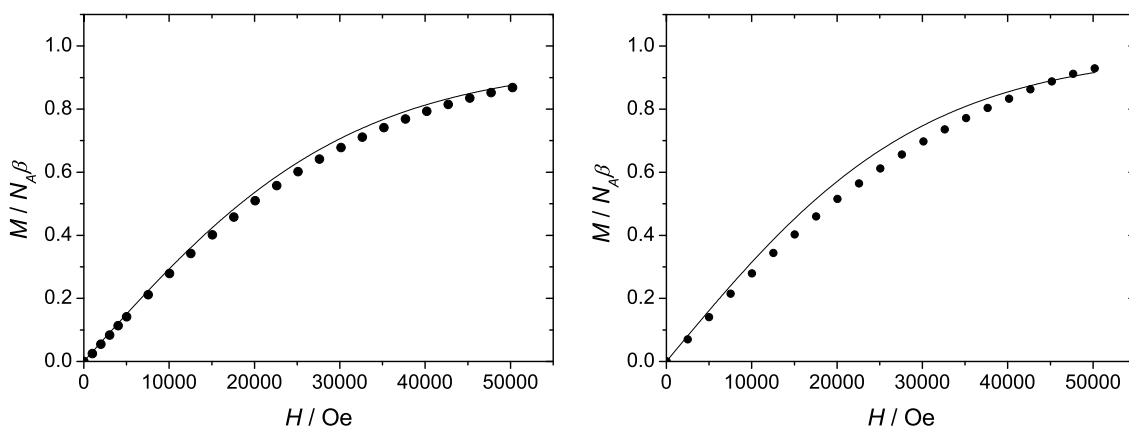


Figure 4.8: Field dependence of the magnetization for complex **Fe₃L3^{Brsal}** (**12**) (left) and complex **Fe₃L3^{Brsal}q₃** (**13**) (right) at 2 K. The Brillouin functions for $S = 1/2$ and the appropriate g values are plotted as solid line (see text).

centers with $S = 5/2$ ($\chi_M T = 13.13 \text{ cm}^3 \text{ K mol}^{-1}$ assuming that $g = 2$) indicating antiferromagnetic exchange interactions between the three iron centers, which is in agreement with the gradual decrease of the $\chi_M T$ values observed upon cooling. The antiferromagnetic exchange coupling between the three iron(III) ions is mediated by the diazine N–N bridges. Moreover the low temperature values are close to the spin-only value of $S = 1/2$, which is consistent with magnetization measurements at 2 K depicted in figure 4.8. These confirm the $S = 1/2$ ground state of both complexes.

Based on the crystallographic data the three iron centers in complex **Fe₃L3^{Brsal}** (**12**) are equivalent. Therefore the triangular unit Fe_3 within the complex cation $[\text{Fe}_3(\text{L3}^{\text{Brsal}})(\text{py})_6\text{Cl}_3]^+$ can be treated as an equilateral triangle with three equal pairwise magnetic interactions. In order to obtain the exchange coupling constant J the temperature dependence of $\chi_M T$ was simulated with the corresponding spin Hamiltonian by a full-matrix diagonalization approach including isotropic exchange and Zeeman interactions with the programm package DAVE.^[177]

$$\hat{H} = -J(\hat{S}_1\hat{S}_2 + \hat{S}_1\hat{S}_3 + \hat{S}_2\hat{S}_3) + \sum_{i=1}^3 g_i\beta\hat{S}_i\vec{H} \quad (4.1)$$

The best fit is obtained with parameters $J = -12.7 \text{ cm}^{-1}$ and $g = 1.99$, which excellently reproduces the course of the experimental magnetic data in the whole temperature range.

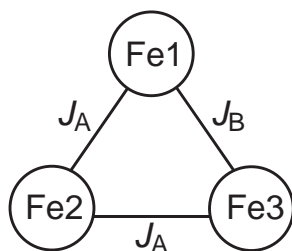


Figure 4.9: The spin topology of the employed two- J model for complex $\text{Fe}_3\text{L}_3^{\text{Brsal}}\mathbf{q}_3$ (13).

In complex $\text{Fe}_3\text{L}_3^{\text{Brsal}}\mathbf{q}_3$ (13) the three iron centers are crystallographically independent. The iron centers are arranged as almost perfect isosceles triangle linked through N–N diazine bridges with two different interatomic Fe \cdots Fe separations of 511 pm (Fe1 \cdots Fe2, Fe2 \cdots Fe3) and 506 pm (Fe1 \cdots Fe3) as well as Fe–N–N–Fe torsion angles of 180° (Fe1–N3–N4–Fe2, Fe2–N5–N6–Fe3) and 171° (Fe1–N2–N1–Fe3) are observed (see section 4.2.2). Therefore a two- J model is employed as spin topology, representing an isosceles triangle which is illustrated in figure 4.9. In this model the different octahedral coordination environments of the iron centers with a $\text{N}_3\text{O}_2\text{Cl}$ donor set for Fe1 and a N_4O_2 donor set for both Fe2 and Fe3 was neglected, since the exchange interactions are dominated by the bridging triaminoguanidine core unit. The corresponding spin Hamiltonian with $J_A = J_{12} = J_{23}$ and $J_B = J_{13}$ is given in equation 4.2.

$$\hat{H} = -J_A(\hat{S}_1\hat{S}_2 + \hat{S}_2\hat{S}_3) - J_B(\hat{S}_1\hat{S}_3) + \sum_{i=1}^3 g_i\beta\hat{S}_i\vec{H} \quad (4.2)$$

Using the program package DAVE the best fit is obtained with parameters $J_A = -9.8 \text{ cm}^{-1}$, $J_B = -11.1 \text{ cm}^{-1}$, and $g = 1.98$. Although the spin topology leads to an excellent agreement with the experimental magnetic data, the two coupling constants can not unambiguously be assigned to J_A and J_B based on the structural features.

For both complexes $\text{Fe}_3\text{L}_3^{\text{Brsal}}$ (12) and $\text{Fe}_3\text{L}_3^{\text{Brsal}}\mathbf{q}_3$ (13) a negative coupling constant is obtained which reveals antiferromagnetic interactions between the iron(III) centers resulting in $S = 1/2$ ground states. Within the C_3 symmetric complex $\text{Fe}_3\text{L}_3^{\text{Brsal}}$ (12) the spin is delocalized though all three iron centers leading to spin frustration.^[71] Due to

the spin ground state of $S = 1/2$ in combination with the equilateral triangular spin topology this complex might be an interesting target as a qubit in the field of quantum computation.^[84,85,144,145,147]

In the symmetric trinuclear complex Fe_3L3^{Brsal} (**12**) the coupling $J = -12.6 \text{ cm}^{-1}$ is slightly stronger compared to complex $Fe_3L3^{Brsal}q_3$ (**13**). This is assigned to differences in the Fe–N–N–Fe torsion angles and hence the interatomic Fe···Fe separations. The smaller the torsion angle the smaller is the distance between the iron centers. The torsion angles in complex Fe_3L3^{Brsal} (**12**) are 161° , which are significantly smaller compared to 180° and 171° in complex $Fe_3L3^{Brsal}q_3$ (**13**).

To summarize, the smaller the Fe–N–N–Fe torsion angle in the trinuclear triamino-guanidine-based iron(III) complexes the stronger is the antiferromagnetic exchange interaction. The same trend has also been observed in N–N diazine-bridged iron(III) azacrown complexes where the exchange interactions are generally slightly weaker in the range $7.7 < -J < 9.3 \text{ cm}^{-1}$.^[140,221,222]

Hexanuclear Iron(III) Complex

Variable temperature (2–300 K) magnetic susceptibility data collected on a polycrystalline sample of the hexanuclear complex $Fe_6L3_2^{Brsal}$ (**14**) is depicted in figure 4.10. The experi-

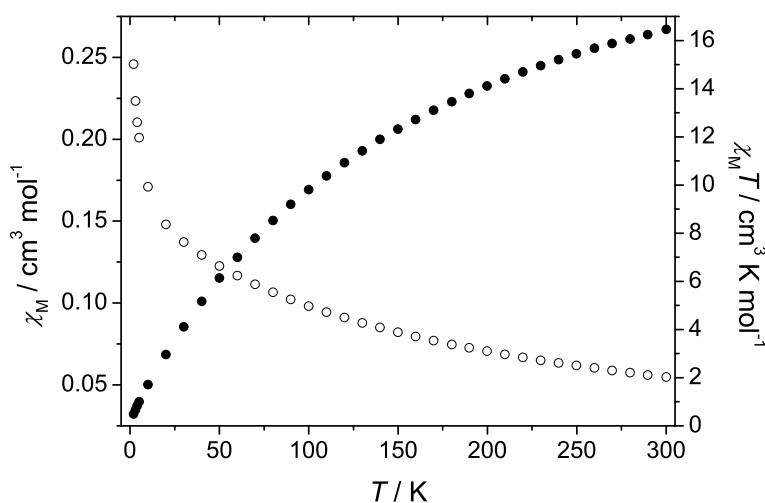


Figure 4.10: Plot of the thermal dependence of χ_M (empty circles, ○) and $\chi_M T$ (black filled circles, ●) for complex $Fe_6L3_2^{Brsal}$ (**14**) measured with an applied magnetic field of 2000 Oe.

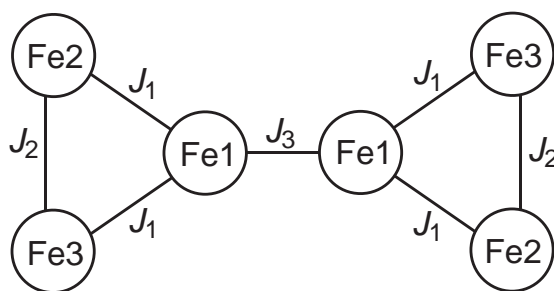


Figure 4.11: The spin topology of the employed three- J model for the hexanuclear iron(III) complex $\text{Fe}_6\text{L3}_2^{\text{Brsal}}$ (**14**).

mental value $\chi_{\text{M}}T$ at 300 K is $16.65 \text{ cm}^3 \text{ K mol}^{-1}$. Upon lowering the temperature, $\chi_{\text{M}}T$ reaches a minimum value of $0.50 \text{ cm}^3 \text{ K mol}^{-1}$ at 2 K. The high temperature value is lower than the spin-only value for six uncoupled high-spin iron(III) ions with $S = 5/2$ ($26.26 \text{ cm}^3 \text{ K mol}^{-1}$ assuming that $g = 2$), but much higher than the spin-only value for six uncoupled low-spin iron(III) ions with $S = 1/2$ ($2.25 \text{ cm}^3 \text{ K mol}^{-1}$ assuming that $g = 2$). The gradual decrease indicates an antiferromagnetic exchange interaction within the trinuclear subunits mediated by the N–N diazine bridges, which is in agreement with the lower high temperature value for six independent high-spin iron(III) centers. The centrosymmetry of the complex molecule leads to an antiparallel alignment of the spins $S = 1/2$ of each triangular subunit resulting in an $S = 0$ ground state. This is further confirmed by the low temperature value.

Due to the structure of the complex a three- J model is necessary for the interpretation of the magnetic data, which is shown in figure 4.11. Beside the couplings within the trinuclear subunits J_1 and J_2 mediated through the N–N diazine bridges of the ligand molecules an additional coupling J_3 between the doubly methanolate-bridged iron centers has to be considered. This can be simplified into a two- J model assuming an averaged coupling within the trinuclear subunits with $J_1 = J_2$. Unfortunately no analytic expressions are known for hexanuclear high-spin iron(III) complexes due to the high dimension of the resulting matrix. Therefore only an estimation of the exchange interactions could be given. For both trinuclear complexes $\text{Fe}_3\text{L3}^{\text{Brsal}}$ (**12**) and $\text{Fe}_3\text{L3}^{\text{Brsal}}\mathbf{q}_3$ (**13**) coupling constants of -12.6 cm^{-1} and -10.2 cm^{-1} (averaged) are obtained, which predominantly depend on the Fe–N–N–Fe torsion angles. Within the trinuclear subunits

of the hexanuclear complex the averaged torsion angle with about 165° is very similar to complex $Fe_3L_3^{Brsal}$ (12) with 161° , which should lead to a similar averaged coupling constant. This is supported by the temperature dependence of the magnetic data compared to the trinuclear complexes.

The exchange coupling J_3 represents the superexchange pathway through the methanolate bridges, which predominantly depend on the iron–oxygen distance and the iron–oxygen–iron angle. Most attempts to establish magnetostructural correlations have focused on dinuclear oxo-, hydroxo- and alkoxo-bridged iron(III) complexes. In all cases, empirical and semiempirical relationships have been established between exchange coupling constant J and the iron–oxygen–iron angle (α) or the iron–oxygen distance (r) in the bridges.^[223–227]

For oxo-bridged dinuclear iron(III) complexes an empirical correlation has been published between the coupling constant J and the averaged iron–oxygen distance (r).^[225] An exponential dependence was established, wherein the magnitude of the antiferromagnetic coupling increases with decreasing r . The Fe–O–Fe angle α was found to have only second-order effects on J . Angular variation is important only when r is large as it is the case in the hexanuclear complex.

A systematic study has been performed with a series of binuclear alkoxo-bridged complexes with similar r , and α varying between 102° and 106° , while J varies between -15 and -21 cm^{-1} . The simplest correlation was found to be of the type given in equation 4.3.^[226]

$$-J = 1.48\alpha - 135 \quad (4.3)$$

In the hexanuclear complex $Fe_6L_3^{Brsal}$ (14) the bridging angle α is 105° , which results in a coupling constant of $J = -20.4 \text{ cm}^{-1}$ between the methanolate-bridged iron centers.

Weihe and Güdel used a formulation based on the angular overlap model to derive an expression for J including both parameters r as well as α represented in equation 4.4.^[228]

$$-J = A(B + C\cos\alpha + \cos^2\alpha)\exp(Dr) \quad (4.4)$$

In effect, the correlation was established for iron dimers whose iron centers are also involved in additional bridging interactions with other iron centers. It indicates that the antiferromagnetic interaction is stronger as α increases and r decreases. Moreover this correlation was applied to hexanuclear mixed oxo-hydroxo-bridged iron(III) complexes.^[229] The regression of the semiempirical calculated coupling constants for the spin Hamilto-

nian $\hat{H} = -J(\hat{S}_1\hat{S}_2)$ resulted in the parameters $A = 4 \cdot 10^7 \text{ cm}^{-1}$, $B = 0.2$, $C = -1$ and $D = -7 \text{ \AA}^{-1}$. For the hexanuclear complex $\text{Fe}_6\text{L3}_2^{\text{Brsal}}$ (**14**) with $r = 2.02 \text{ \AA}$ and $\alpha = 105^\circ$ this leads to the coupling constant of $J = -15.2 \text{ cm}^{-1}$ between the methanolate-bridged iron centers.

Both independent correlations predict similar magnitudes of the antiferromagnetic exchange interaction through the methanolate bridges. Moreover the coupling constant is in the same range as expected for the intratrimer coupling mediated through the N–N diazine bridges. In the hexanuclear complex $\text{Fe}_6\text{L3}_2^{\text{Brsal}}$ the resulting $S = 1/2$ spins within each trinuclear subunit are aligned antiparallel in agreement with the symmetry of the hexanuclear complex. This leads to a $S = 0$ ground state.

4.3 Pentanuclear Heterometallic Complexes with the Ligands

$\text{H}_5\text{L3}^{\text{Brsal}}$ and $\text{H}_5\text{L3}^{\text{Hsal}}$

4.3.1 Synthesis and Characterization

The C_3 symmetric triaminoguanidine-based Schiff-base ligands $\text{H}_5\text{L3}^{\text{Brsal}} \cdot \text{HCl}$ and $\text{H}_5\text{L3}^{\text{Hsal}} \cdot \text{HCl}$ possess three equivalent binding pockets. After total deprotonation the ligands coordinate to three transition metal ions in their penta-anionic form. Since the ligands have been used as hydrochloride salt, at least six equivalents of base are needed for both deprotonation of the amine groups of the guanidine moiety and the phenolic hydroxy groups in order to favor the coordination of the metal ions. Two different complex structures as shown in figure 4.12 have been obtained with nickel(II) ions. The trinuclear nickel(II) complexes have been isolated by the addition of three equivalents of capping co-ligands like 2,2'-bipyridine and 2,4,6-tris(2-pyridyl)-1,3,5-triazine (tptz).^[141] Moreover pentanuclear nickel(II) complexes are accessible, wherein two trinuclear subunits are cross-linked through a common nickel(II) ion.^[140]

Utilizing a directed successive synthesis route an extension to heterometallic complexes is possible due to the different nature of the three amine protons of the triaminoguanidine moiety. The hydrochloride can be easily removed by the addition of one equivalent of triethylamine as base, while both other amine nitrogen atoms remain protonated. From

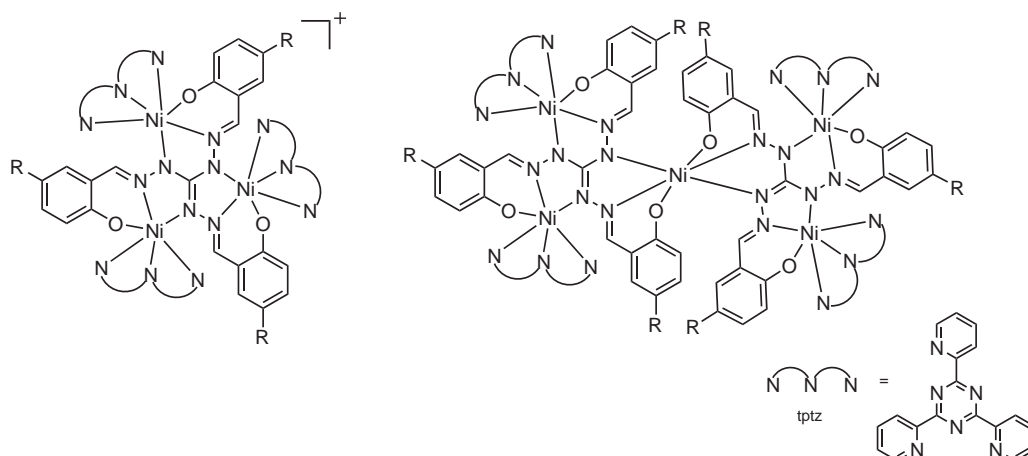


Figure 4.12: Schematic representation of the two different complex structures obtained with nickel(II) ions, the trinuclear cationic complex (left) and the neutral pentanuclear complex (right).

methanolic solutions the hydrochloride free ligands crystallized within a few minutes, which was proven by NMR spectroscopy. The control of the acidity of the reaction solution by successive stoichiometric addition of triethylamine as base provides the stepwise accessibility of the binding pockets by deprotonation. In addition, phenolic groups are known to be strongly acidic and they were easily deprotonated during complexation reaction even without additional base.

These characteristics were utilized for stepwise coordination of different transition metal ions. Three heterometallic pentanuclear complexes with the same structural motif of the general formula $[M^{III}Ni_4^{II}(L3)_2(tptz)_4](ClO_4)_x(Cl)_{1-x}$ with $M = Fe, Mn, Co$ were synthesized following the directed *step-by-step* synthesis shown in figure 4.13. Herein two nickel complex subunits are linked by the central trivalent metal ion. Starting from the triaminoguanidine ligands the hydrochloride was removed by one equivalent of triethylamine leading to the unsymmetrical free ligands H_5L3^{Hsal} and H_5L3^{Brsal} with only one binding pocket accessible in a tridentate fashion. Both amine nitrogen groups remain protonated and therefore both of the other binding pockets are not accessible for the coordination of a metal ion in a tridentate fashion. Consequently, the reaction with half an equivalent of iron(II)-, manganese(II)- or cobalt(II) perchlorate in the presence of one equivalent of triethylamine resulted in the formation of mononuclear complexes wherein the metal ions are coordinated by two ligand molecules in an octahedral environment. Only one binding pocket of each ligand is occupied due to the above men-

4 Triaminoguanidine-Bridged Complexes

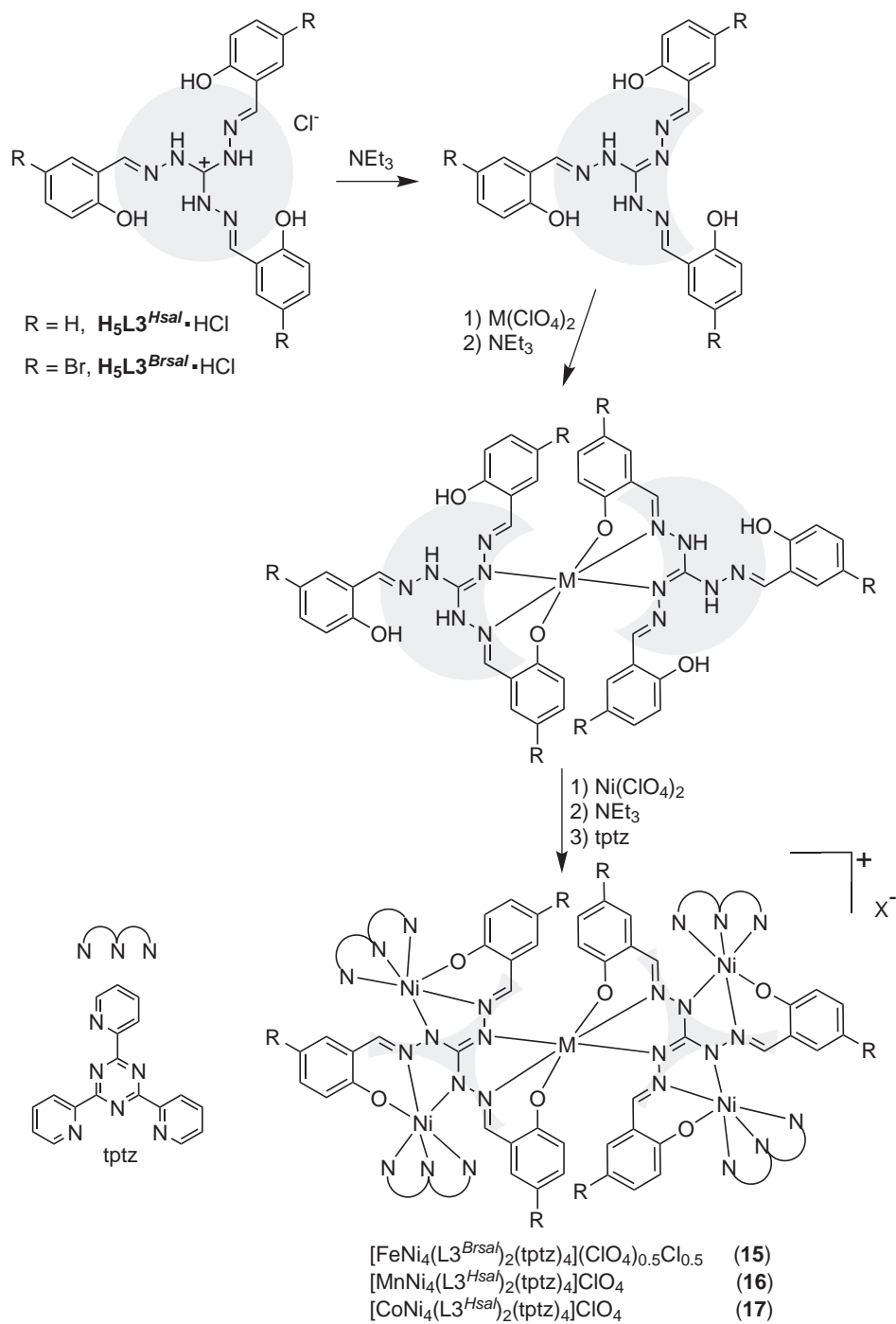


Figure 4.13: Schematic *step-by-step* synthesis of the heterometallic pentanuclear complexes **FeNi₄L3₂^{Brsal}** (15), **MnNi₄L3₂^{Hsal}** (16) and **CoNi₄L3₂^{Hsal}** (17) in dimethylformamide-methanol-mixture. Abbreviations herein: NEt₃ = triethylamine and tptz = 2,4,6-tris(2-pyridyl)-1,3,5-triazine.

tioned protonation of both amine nitrogen atoms of each ligand. The following reaction with two equivalents nickel(II) perchlorate and additional four equivalents triethylamine for deprotonation of the remaining hydroxy and amine protons yielded discrete pentanuclear complexes. During the complexation reaction the central metal ions were oxidized. This oxidation process led to a higher stability of the central metal ion against metal exchange reaction with the nickel ions. To prevent higher aggregation 2,4,6-tris(2-pyridyl)-1,3,5-triazine (tptz) was utilized as co-ligand.^[141] Moreover tptz is well known for its ability to support crystallization by an appropriate crystal packing via π - π interactions.^[180,230–232] Tptz possesses free donor sites after coordinative saturation of the pentanuclear core unit which could be utilized for further complexation reaction and defined aggregation.^[233–235]

The complex $[\text{FeNi}_4(\text{L3}^{\text{Brsal}})_2(\text{tptz})_4](\text{ClO}_4)_{0.5}\text{Cl}_{0.5}$ ($\text{FeNi}_4\text{L3}_2^{\text{Brsal}}$) (15) was isolated using iron(II) perchlorate and $\text{H}_5\text{L3}^{\text{Brsal}} \cdot \text{HCl}$ as ligand. The reaction of the ligand $\text{H}_5\text{L3}^{\text{Hsal}} \cdot \text{HCl}$ with manganese(II) and cobalt(II) perchlorate resulted in the complexes $[\text{MnNi}_4(\text{L3}^{\text{Hsal}})_2(\text{tptz})_4]\text{ClO}_4$ ($\text{MnNi}_4\text{L3}_2^{\text{Hsal}}$) (16) and $[\text{CoNi}_4(\text{L3}^{\text{Hsal}})_2(\text{tptz})_4]\text{ClO}_4$ ($\text{CoNi}_4\text{L3}_2^{\text{Hsal}}$) (17) after drying in air.

All complexes were obtained as pure crystalline solids. Crystals suitable for X-ray crystallography were only obtained for $\text{FeNi}_4\text{L3}_2^{\text{Brsal}}$ (15). The complexes $\text{MnNi}_4\text{L3}_2^{\text{Hsal}}$ (16) and $\text{CoNi}_4\text{L3}_2^{\text{Hsal}}$ (17) were recrystallized from chloroform-methanol-mixture resulting in large well defined crystals. Unfortunately these were also not suitable for X-ray crystallography.

The formation of all complexes is also confirmed by ESI mass spectrometry, IR spectroscopy and elemental analysis. Each mass spectra shows predominantly one signal which is equal to the corresponding complex cation. The isotope patterns are in excellent agreement with the calculated ones and are unambiguously assigned to the corresponding heterometallic pentanuclear complex cations $[\text{MNi}_4(\text{L3})_2(\text{tptz})_4]^+$ (see figures 4.14, 4.15 and 4.16). All spectra confirm the exclusive formation of the heterometallic complexes and their stability in solution.

The IR spectrum of $\text{FeNi}_4\text{L3}_2^{\text{Brsal}}$ (15) is similar to them of $\text{MnNi}_4\text{L3}_2^{\text{Hsal}}$ (16) and $\text{CoNi}_4\text{L3}_2^{\text{Hsal}}$ (17), which are nearly identical. The $\tilde{\nu}_{(\text{C}=\text{N})}$ stretching vibration is shifted from 1665 cm^{-1} in the ligand to frequencies lower than 1600 cm^{-1} in the complex due to the coordination of the imine nitrogen atoms to the metal centers. In addition, char-

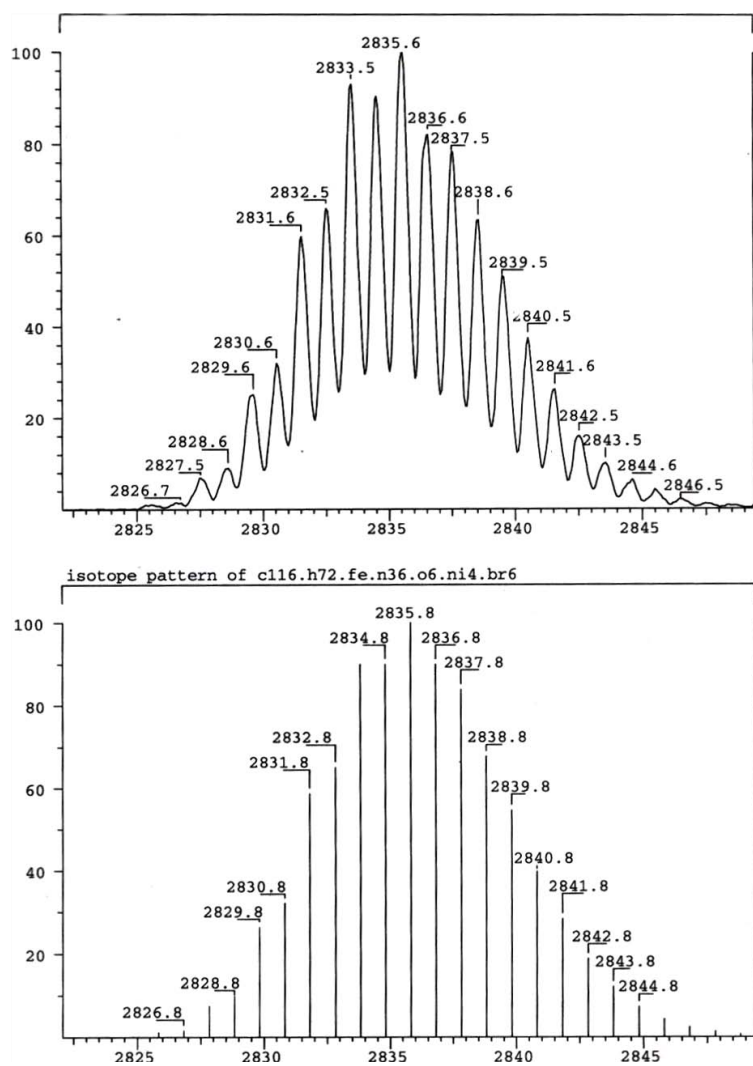


Figure 4.14: Measured (top) and calculated (bottom) isotope pattern of the pentanuclear complex cation $[\text{FeNi}_4(\text{L3}^{\text{Brsal}})_2(\text{tptz})_4]^+$ of $\text{FeNi}_4\text{L3}^{\text{Brsal}}$ (**15**) in ESI mass spectrum. The calculation is based on $\text{C}_{116}\text{H}_{72}\text{FeN}_{36}\text{O}_6\text{Ni}_4\text{Br}_6$.

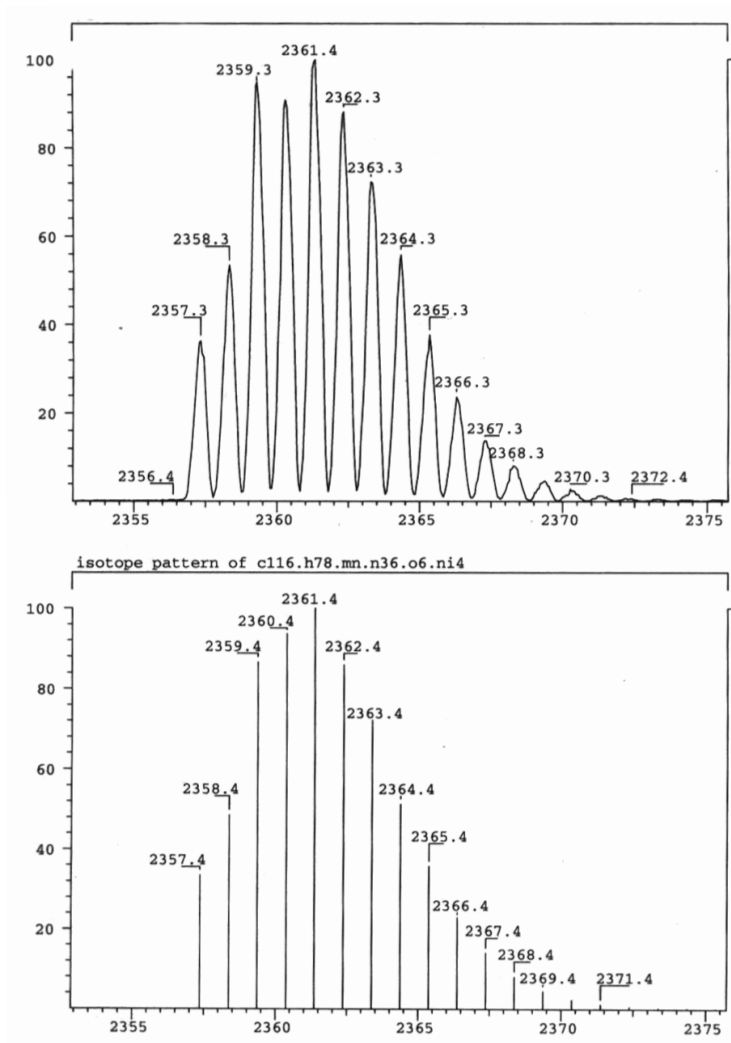


Figure 4.15: Measured (top) and calculated (bottom) isotope pattern of the pentanuclear complex cation $[MnNi_4(L3^{Hsal})_2(tptz)_4]^+$ of $MnNi_4L3^{Hsal}$ (**16**) in ESI mass spectrum. The calculation is based on $C_{116}H_{78}MnN_{36}O_6Ni_4$.

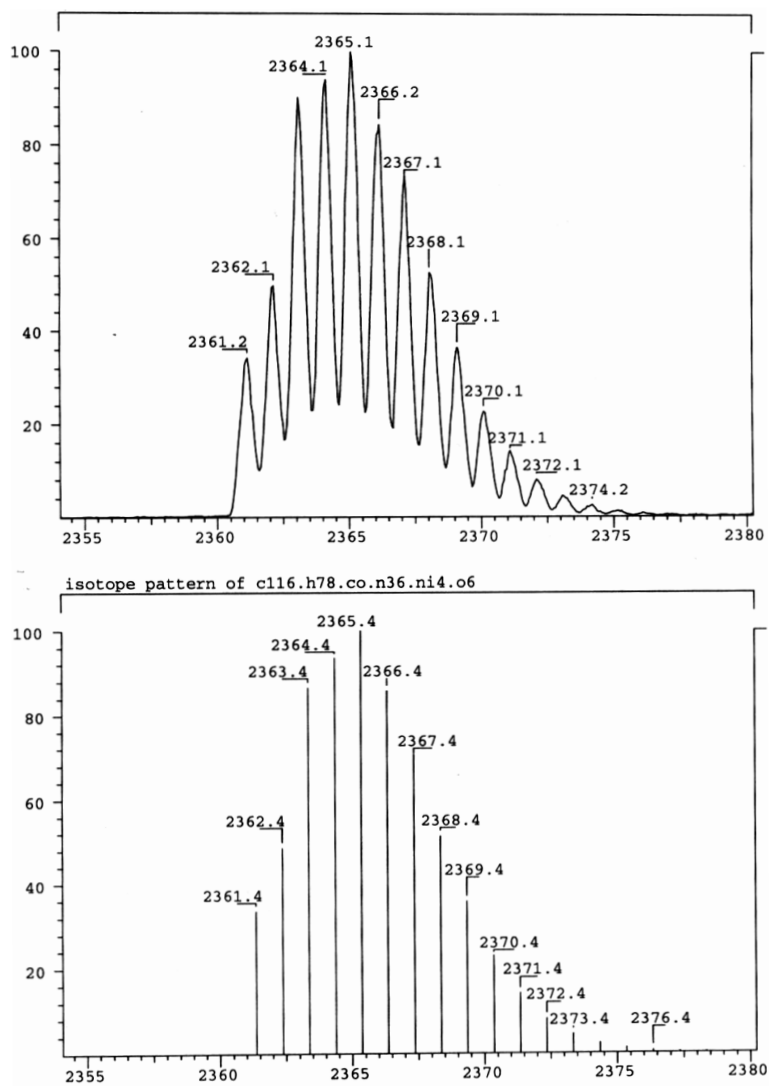
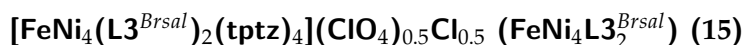


Figure 4.16: Measured (top) and calculated (bottom) isotope pattern of the pentanuclear complex cation $[\text{CoNi}_4(\text{L3}^{\text{Hsal}})_2(\text{tptz})_4]^+$ of $\text{CoNi}_4\text{L3}^{\text{Hsal}}$ (**17**) in ESI mass spectrum. The calculation is based on $\text{C}_{116}\text{H}_{78}\text{CoN}_{36}\text{O}_6\text{Ni}_4$.

acteristic bands assigned to stretching vibrations of the triaminoguanidine core ligand are also slightly shifted upon coordination. Furthermore vibrations characteristic for the tptz co-ligand appear in the same region. Therefore the bands could not be unambiguously determined. The IR spectrum exhibits a broad band observed at around 3435 cm^{-1} characteristic for the crystallized water molecules present in the complex structure. An additional strong band is observed at 1669 cm^{-1} assigned to the $\tilde{\nu}_{(C=O)}$ stretching vibration of the crystallized dimethylformamide molecules. In addition a characteristic band at around 1100 cm^{-1} is observed which can be attributed to the $\tilde{\nu}_{(Cl-O)}$ stretching vibration of the perchlorate counterion. The IR spectra of the complexes $MnNi_4L3_2^{Hsal}$ (16) and $CoNi_4L3_2^{Hsal}$ (17) exhibit all bands present in complex $FeNi_4L3_2^{Brsal}$ (15) except the $\tilde{\nu}_{(C=O)}$ stretching vibration of the dimethylformamide molecules at 1669 cm^{-1} confirming the structural similarity. They only differ slightly in the strength of the bands.

The elemental analysis also confirms the X-ray crystallography structural data for $FeNi_4L3_2^{Brsal}$ (15). In this context, the final complex compositions concerning the water content and the counteranion of $MnNi_4L3_2^{Hsal}$ (16) and $CoNi_4L3_2^{Hsal}$ (17) are postulated from the elemental analyses. According to the presence of perchlorate and chloride counteranions in complex structure of $FeNi_4L3_2^{Brsal}$ (15), the exact nature of the counteranion can not be unambiguously determined from this data. It might also be possible, that the charge is partially counterbalanced by chloride ions in connection with a slightly higher water content in both complexes. Nevertheless the effect on the molar mass of the two complexes is negligible. Only the molar mass in combination with the structure of the central core unit is essential for the interpretation of the magnetic data.

4.3.2 Crystal Structure



Molecular structure and heteroatom labeling scheme of the pentanuclear complex cation $[FeNi_4(L3^{Brsal})_2(tptz)_4]^+$ of $FeNi_4L3_2^{Brsal}$ (15) is depicted in figure 4.17, the central pentanuclear core unit is enlarged and simplified shown in figure 4.18. Selected bond lengths and angles are listed in table 4.4. Complex $FeNi_4L3_2^{Brsal}$ (15) crystallizes in the triclinic space group $P\bar{1}$. Two triangular $[FeNi_2(L3^{Brsal})_2(tptz)_2]$ -subunits are interconnected by a common iron(III) ion accommodated in two tridentate pockets of both triaminoguanidine-based ligand moieties in a N_4O_2 environment.

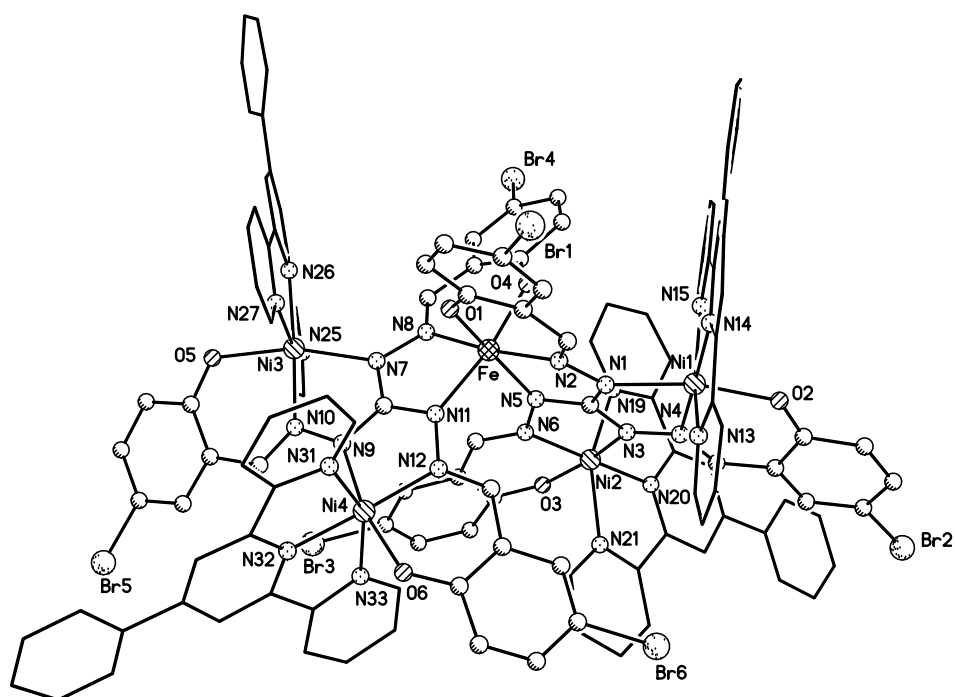


Figure 4.17: Molecular structure of the complex cation of $\text{FeNi}_4\text{L}_3^{\text{Brsal}}$ (**15**). The tptz co-ligands are illustrated as sticks except the coordinating nitrogen atoms. Furthermore all hydrogen atoms are omitted for clarity.

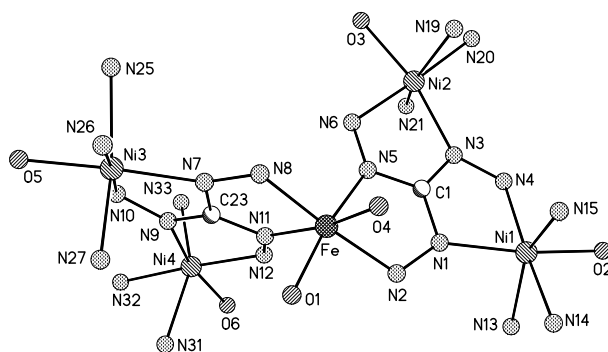


Figure 4.18: Representation of the pentanuclear core of $\text{FeNi}_4\text{L}_3^{\text{Brsal}}$ (**15**) together with the coordination environments of the peripheral nickel ions.

Table 4.4: Selected bond lengths [pm] and angles [$^\circ$] for complex $FeNi_4L3_2^{Brsal}$ (15).

Fe–O1	189.4(5)	Ni1–O2	200.1(5)	Ni2–O3	201.3(5)
Fe–O4	190.6(5)	Ni1–N1	207.2(6)	Ni2–N3	207.9(6)
Fe–N2	199.6(6)	Ni1–N4	200.8(6)	Ni2–N6	201.7(5)
Fe–N5	200.5(5)	Ni1–N13	223.5(6)	Ni2–N19	219.6(7)
Fe–N8	199.0(6)	Ni1–N14	201.3(6)	Ni2–N20	199.9(6)
Fe–N11	197.8(6)	Ni1–N15	216.4(7)	Ni2–N21	216.7(7)
		Ni3–O5	202.0(6)	Ni4–O6	200.0(5)
		Ni3–N7	206.6(6)	Ni4–N9	207.1(6)
		Ni3–N10	201.2(6)	Ni4–N12	199.5(7)
		Ni3–N25	218.8(6)	Ni4–N31	215.7(6)
		Ni3–N26	200.5(6)	Ni4–N32	199.1(7)
		Ni3–N27	215.4(6)	Ni4–N33	218.3(7)
O1–Fe–N5	168.8(3)	O2–Ni1–N1	166.9(2)	O3–Ni2–N3	167.6(2)
O4–Fe–N11	168.4(2)	N4–Ni1–N14	173.4(2)	N6–Ni2–N20	176.7(3)
N2–Fe–N8	173.0(3)	N13–Ni1–N15	151.6(2)	N19–Ni2–N21	152.1(2)
		O5–Ni3–N7	164.6(2)	O6–Ni4–N9	168.0(2)
		N10–Ni3–N26	175.9(2)	N12–Ni4–N32	176.5(2)
		N25–Ni3–N27	152.2(2)	N31–Ni4–N33	152.6(3)

The central iron(III) ion is coordinated in an slightly distorted octahedral environment as indicated by the observed *cis* angles ranging from 78° to 108° and *trans* angles varying from 168° to 173° . The ligands are coordinated in a meridional fashion forming two five- and two six-membered chelate rings at the iron(III) center with bite angles of 78° (N2–Fe–N5, N8–Fe–N11), 90° (O1–Fe–N2) and 92° (O4–Fe–N8), respectively. The distances to both phenolate oxygen atoms are very similar with about 190 pm. Furthermore, the bond lengths of the nitrogen donor atoms are longer ranging from 198 to 200 pm. All are in very good agreement to literature values indicating the iron(III) ion to be in the low-spin state.^[236]

The peripheral nickel(II) ions are surrounded by a N_5O donor atom set arranged in an distorted octahedral coordination environment with similar *trans* angles ranging from 152° to 177° . Three coordination sites at each nickel are occupied by the N_2O donor set of

the triaminoguanidine ligand including the phenolate oxygen atom, the imine nitrogen atom and the amine nitrogen atom. The octahedral geometry is completed by three nitrogen atoms of the tptz co-ligand coordinating in a terpyridine-like chelating meridional fashion. The equatorial positions are occupied by the corresponding ligand donor atoms and the triazine nitrogen atom of the tptz co-ligands with bond lengths between 200 and 208 pm. The distances to the amine nitrogen atoms are longer than the other, all located on the lower end of the range. Both axial positions are occupied by the pyridine nitrogen atoms of the co-ligands with longer distances ranging from 215 to 224 pm and *trans* angles of about 152°. The nickel ions are displaced out of the corresponding N₃O tetragonal plane, defined by the four equatorial donor atoms, by 15 pm (Ni1), 14 pm (Ni2), 24 pm (Ni3) and 29 pm (Ni4), respectively.

The dihedral angle between the idealized planes formed by each ligand including the CN₆ triaminoguanidine moiety is about 89°, very close to perpendicular orientation of the two interlocked trinuclear [FeNi₂(L3^{Brsal})(tptz)₂]-subunits. Within both subunits the tetragonal planes of the nickel centers are nearly coplanar with dihedral angles of 15° between Ni1 and Ni2 as well as 19° between Ni3 and Ni4, which is consistent with the expected planarity of the corresponding trinuclear core subunits. In addition, the tetragonal planes of the nickel ions and the central iron ion, formed by the corresponding phenolate oxygen, imine nitrogen and amine nitrogen ligand donor atom together with the coplanar amine nitrogen atom of the second ligand, are also slightly twisted with dihedral angles of 27° for Ni1, 21° for Ni2, 25° for Ni3 and 18° for Ni4. The nickel centers Ni1 and Ni3 are arranged in line with the central iron ion. In addition, the Ni2 and Ni4 are situated within the idealized plane of the iron center including both phenolate oxygen atoms O1/O4 and both amine nitrogen atoms N5/N11 with a minimal deviation of 1 pm each.

The interatomic M··M separations and the M–N–N–M torsion angles between neighboring metal centers are listed in table 4.5. Within both trinuclear subunits the metal ions are arranged as nearly isosceles triangles with two almost equivalent Fe··Ni distances and a longer Ni··Ni distance due to shorter bond lengths of the iron center compared to them of the nickel centers. The nickel distances are with about 497 pm nearly equal to a reported trinuclear nickel complex with this ligand^[141]. The Ni–N–N–Ni torsion angles of 164° and 171° are also in the expected range. In addition the Fe–N5–N6–Ni2 and Fe–N11–N12–Ni4 torsion angles are nearly identical to them, while the Fe–N2–N1–Ni1

Table 4.5: Interatomic M...M separations [pm] and the torsion angles M–N–N–M [°] in complex $FeNi_4L3_2^{Brsal}$ (15).

Fe...Ni1	491.6	Fe–N2–N1–Ni1	154.6
Fe...Ni2	489.5	Fe–N5–N6–Ni2	170.7
Fe...Ni3	490.1	Fe–N8–N7–Ni3	154.6
Fe...Ni4	486.7	Fe–N11–N12–Ni4	169.2
Ni1...Ni2	497.5	Ni1–N4–N3–Ni2	169.5
Ni3...Ni4	496.2	Ni3–N10–N9–Ni4	163.5

and Fe–N8–N7–Ni3 ones are with 155° distinctly smaller but still in the *trans* orientation related to the N–N diazine bridge. Due to the bulky tptz, the pentanuclear core units are well separated with the shortest intermolecular Ni...Ni distance of 928 pm.

The pentanuclear complex cation $[FeNi_4(L3^{Brsal})_2(tptz)_4]^+$ crystallizes together with one counteranion as a statistical distribution of perchlorate as well as chloride ions. The ratio of the counterions was refined as one-to-one. The complex cations assemble through π - π interactions as a result of face-to-face orientation of the tptz moieties of two parallel layers. Moreover a point-to-face arrangement of the pyridine rings of tptz co-ligands to the phenylene rings of the tris-*N*-(5-bromo-salicylidene)-amino-guanidine ligands is formed.^[237] The co-crystallized dimethylformamide, water and methanol molecules are situated in between and are predominantly disordered over several crystallographic positions.

4.3.3 Magnetic Properties

Variable temperature (2–300 K) magnetic susceptibility data was collected on powder samples for the three complexes $FeNi_4L3_2^{Brsal}$ (15), $MnNi_4L3_2^{Hsal}$ (16), and $CoNi_4L3_2^{Hsal}$ (17). The magnetic data is shown in figure 4.19, 4.20 and 4.21 as $\chi_M = f(T)$ and $\chi_M T = f(T)$ plots. All complexes show a monotonous decline upon lowering the temperature. This indicates antiferromagnetic interactions through the N–N diazine bridges of the triaminoguanidine ligand scaffold as found in other compounds. Due to the heterometallic nature of the complexes in connection with various exchange pathways between the metal centers the analysis and interpretation of the magnetic data is not straightforward. A comparative study of the magnetic data of the three complexes

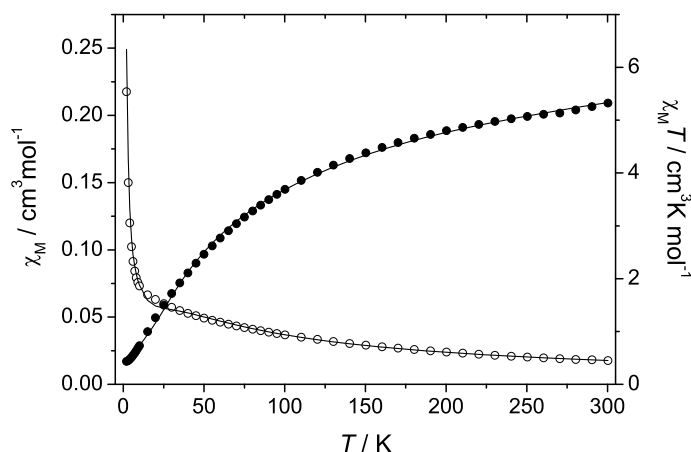


Figure 4.19: Plot of the thermal dependence of χ_M (empty circles, \circ) and $\chi_M T$ (black filled circles, \bullet) for complex $\text{FeNi}_4\text{L3}_2^{\text{Brsal}}$ (**15**) measured with an applied magnetic field of 2000 Oe. The corresponding fit functions are drawn as solid lines (for parameters see text).

was done by *Eike T. Spielberg*.^[213] Therefore the results are only presented in conclusion. For further details and discussions please refer to his thesis.

In the cobalt containing complex $\text{CoNi}_4\text{L3}_2^{\text{Hsal}}$ (**17**) the cobalt(III) ion is in the low-spin state with $S = 0$. The experimental data was analyzed with the help of a full matrix least square routine which also accounts for the paramagnetic impurity α .^[238] The measured values can be reproduced quite nicely using the parameters $J_{\text{NiNi}} = -35.8 \text{ cm}^{-1}$ and $g_{\text{Ni}} = 2.111$ with $\alpha = 7.3\%$.

In the heterometallic manganese complex $\text{MnNi}_4\text{L3}_2^{\text{Hsal}}$ (**16**) the manganese(III) ion is in the high-spin state with $S = 2$. Fitting the parameters to the data using the full matrix diagonalization routine DAVE and considering also temperature independent paramagnetism (χ_{TIP}) and intermolecular interactions via the mean field approach (λ) gives the following results: $g_{\text{Mn}} = 1.997$, $g_{\text{Ni}} = 2.114$, $J_{\text{NiNi}} = -34.0 \text{ cm}^{-1}$, $J_{\text{MnNi}} = +1.3 \text{ cm}^{-1}$, $\chi_{\text{TIP}} = 3.1 \cdot 10^{-3} \text{ cm}^3 \text{ mol}^{-1}$, and $\lambda = -0.03 \text{ K}$.^[177]

In the iron containing heteronuclear complex $\text{FeNi}_4\text{L3}_2^{\text{Brsal}}$ (**15**) the iron(III) center is in the low-spin state with $S = 1/2$. Fitting of the magnetic data utilizing a full matrix diagonalization routine DAVE leads to the following parameters $J_{\text{NiNi}} = -33.2 \text{ cm}^{-1}$, $J_{\text{FeNi}} = -39.9 \text{ cm}^{-1}$, $g = 2.298$, and $\chi_{\text{TIP}} = 6.9 \cdot 10^{-3} \text{ cm}^3 \text{ K mol}^{-1}$.^[177]

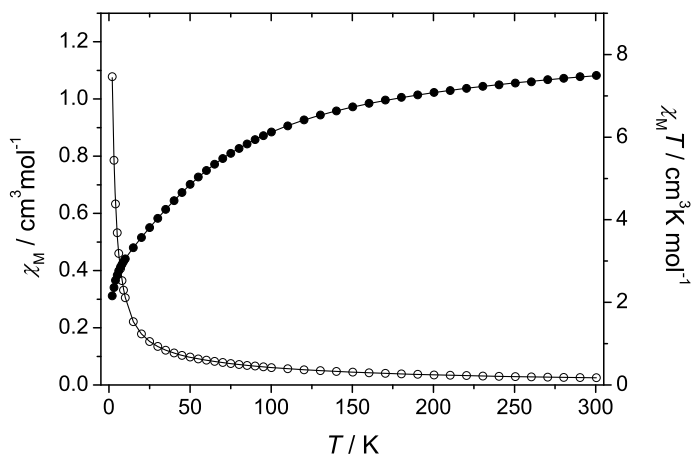


Figure 4.20: Plot of the thermal dependence of χ_M (empty circles, \circ) and $\chi_M T$ (black filled circles, \bullet) for complex $MnNi_4L3_2^{Hsal}$ (**16**) measured with an applied magnetic field of 2000 Oe. The corresponding fit functions are drawn as solid lines (for parameters see text).

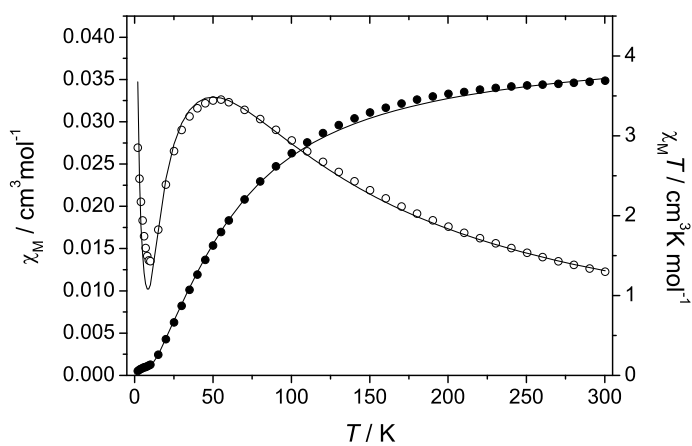


Figure 4.21: Plot of the thermal dependence of χ_M (empty circles, \circ) and $\chi_M T$ (black filled circles, \bullet) for complex $CoNi_4L3_2^{Hsal}$ (**17**) measured with an applied magnetic field of 2000 Oe. The corresponding fit functions are drawn as solid lines (for parameters see text).

As expected the coupling constant J_{NiNi} between the nickel ions is nearly equal for each complex due to the structural similarities. This data clearly shows that the magnitude of the nickel nickel interactions resembles very well the one found for the reported trinuclear compounds.^[140,141] Within the manganese complex $\text{MnNi}_4\text{L3}_2^{\text{Hsal}}$ (**16**) only a very weak antiferromagnetic exchange interaction between the manganese ion and the nickel centers is observed leading to a cancelation of the nickel contribution. This results in a manganese-type ground state. Moreover the coupling between the iron ion and the nickel centers in complex $\text{FeNi}_4\text{L3}_2^{\text{Brsal}}$ (**15**) is stronger than the nickel nickel interactions resulting in a strong admixture of nickel wave functions into the ground state. This leads to a delocalized, degenerated $S = 1/2$ spin ground state, which makes the iron compound an interesting target as a qubit in the field of quantum computation.^[84,85,144,145,147]

4.4 Trinuclear Transition Metal Complexes with the Ligand

$\text{H}_2\text{L3}^{\text{py}}$

4.4.1 Synthesis and Characterization

The ligand $\text{H}_2\text{L3}^{\text{py}}$, previously shown in figure 4.1, was synthesized through Schiff-base condensation of triaminoguanidine with pyridine-2-carbaldehyde isolated as the hydrochloride salt $\text{H}_2\text{L3}^{\text{py}} \cdot \text{HCl}$. The synthesis was performed at 45°C in a methanol-water-mixture leading to a yellow solid after evaporation of the solvent. The water was removed by addition of ethanol and subsequent evaporation of the solvent in vacuum. This was repeated two times leaving the microcrystalline ligand co-crystallized with ethanol. Due to the pyridine side chains the ligand acts as base. The addition of hydrochloric acid into a methanolic solution led to the crystallization of the tetrahydrochloride salt $\text{H}_2\text{L3}^{\text{py}} \cdot 4\text{HCl}$. The ligand is excellent soluble in most polar organic solvents, like methanol, ethanol, water, dimethylformamide and dimethylsulfoxide. In contrast to the known tris-*N*-salicylidene-aminoguanidine ligands with various substituents in the side chains, this ligand possess an N_3 donor set within each binding pocket forming two five-membered chelate rings with the coordinated metal ions. Therefore the binding pocket is larger, which is favorable for the complexation of larger metal ions, e.g. cobalt(II) as well as manganese(II). Especially cobalt(II) complexes

are very interesting for magnetochemistry due to the high anisotropy of the cobalt(II) ion. The deprotonated ligand coordinates to three metal ions in the di-anionic form. Due to the lower overall charge of the ligand molecule within the complex, reaction with divalent transition metal ions leads to the formation of a tetra-cationic trinuclear precursor complex. Therefore additional anionic co-ligands can be easily introduced into trinuclear complexes.

Trinuclear complexes of different divalent transition metal ions were synthesized with this ligand. Utilizing the synthetic strategy similar to what is described for the trinuclear iron(III) complex Fe_3L3^{Brsal} (**12**) in section 4.2 trinuclear complexes of copper(II), nickel(II), cobalt(II), and manganese(II) were obtained.

For the syntheses of the copper and nickel complexes three equivalents of the metal(II) chloride salt were dissolved in pyridine. Subsequently a solution of the ligand was added accompanied by a color change. Slow evaporation of the solvent afforded the trinuclear copper complex $[Cu_3(L3^{py})(py)_2Cl_4]$ (Cu_3L3^{py}) (**18**) and the corresponding nickel complex $[Ni_3(L3^{py})(py)_6Cl_3]Cl$ (Ni_3L3^{py}) (**19**). Again pyridine and chloride function as co-ligands.

For the synthesis of the copper complex Cu_3L3^{py} the ligand was dissolved in pyridine. The resulting complex crystallizes from the reaction solution within a few hours. The nickel complex Ni_3L3^{py} could be obtained in an analogous synthesis. Due to the excellent solubility of this complex in pyridine, the complex crystallizes after evaporation of the pyridine solution to nearly dryness. Moreover the pyridine hydrochloride byproduct also crystallized from the reaction mixture. Therefore the synthesis was performed in a methanol-pyridine-mixture leading to large single crystals of the complex. Both complexes were obtained in excellent yields of about 75 % related to pure crystalline material. Further crops, increasing the yield up to nearly 90 %, were obtained by evaporation of the reaction mixtures to dryness and subsequent washing with methanol. In the copper complex all four chloride ions are bound to the copper centers leading to a neutral trinuclear complex, whereas in the nickel complex one chloride ion is unbounded counterbalancing the positive charge of the complex cation.

The corresponding cobalt(II) and manganese(II) complexes were synthesized in pyridine under argon atmosphere using standard Schlenk techniques to avoid an oxidation of the metal ions. Utilizing the metal(II) chlorides only microcrystalline precipitates could

be isolated. Due to the preferred octahedral coordination environments of cobalt(II) and manganese(II) ions, the complex should be structurally very similar to them of the nickel containing compound $\text{Ni}_3\text{L3}^{py}$ (**19**). Therefore additional perchlorate was added to improve the crystallization through exchange of the chloride counteranion. This could be realized by addition of sodium perchlorate or ammonium perchlorate to the reaction solution. Unfortunately they are only poorly soluble in pyridine. To keep the complexation reaction as simple as possible, 1 : 2 mixtures of the metal(II) perchlorate and metal(II) chloride salts were utilized for the synthesis of the complexes. This led to the formation of the trinuclear cobalt(II) complex $[\text{Co}_3(\text{L3}^{py})(\text{py})_6\text{Cl}_3]\text{ClO}_4$ ($\text{Co}_3\text{L3}^{py}$) (**22**) as well as the trinuclear manganese(II) complex $[\text{Mn}_3(\text{L3}^{py})(\text{py})_6\text{Cl}_3]\text{ClO}_4$ ($\text{Mn}_3\text{L3}^{py}$) (**23**). The positive charge of each complex cation is counterbalanced by one perchlorate ion. Both complexes were isolated in excellent yields of about 75 % related to crystalline material.

All complexes were characterized by elemental analysis, IR spectroscopy, mass spectrometry and X-ray crystallography. The crystals of the nickel complex $\text{Ni}_3\text{L3}^{py}$ (**19**) stay intact without the loss of co-crystallized solvents, which is confirmed by the elemental analysis data. All other complexes lose the co-crystallized solvent molecules consistent with the elemental analysis data. Furthermore, upon drying in air for some days, the copper complex $\text{Cu}_3\text{L3}^{py}$ loses the coordinated pyridine molecules resulting in the final complex composition of $[\text{Cu}_3(\text{L3}^{py})\text{Cl}_4]$ (**18a**). The IR spectra of the copper complex $\text{Cu}_3\text{L3}^{py}$ (**18**) and the nickel complex $\text{Ni}_3\text{L3}^{py}$ (**19**) are very similar. The $\tilde{\nu}_{(\text{C}=\text{N})}$ stretching vibration band situated at 1643 cm^{-1} in the ligand is weakened and shifted to about 1600 cm^{-1} in complexes, due to the coordination of the imine nitrogen atoms to the metal centers. In addition, both spectra are dominated by the stretching vibrations within the pyridine coligands as well as ligand side chains. Hence the spectra contain rather less bands. Bands are observed at about 1480 , 1440 , 1400 , and 1340 cm^{-1} which can be attributed to the stretching vibrations within the pyridine moieties. The IR spectra of the cobalt complex $\text{Co}_3\text{L3}^{py}$ and the manganese complex $\text{Mn}_3\text{L3}^{py}$ are also nearly equal and furthermore very similar to them of the nickel complex $\text{Ni}_3\text{L3}^{py}$ due to the structural similarities. An additional band is observed at about 1100 cm^{-1} unambiguously assigned to the perchlorate stretching vibration of the counteranion. In the ESI mass spectra of the copper complex $\text{Cu}_3\text{L3}^{py}$ (**18**) a signal was detected at $m/z = 665$ which can be assigned to the complex cation $[\text{Cu}_3(\text{L3}^{py})\text{Cl}_3]^+$. The spectrum of the nickel complex $\text{Ni}_3\text{L3}^{py}$ (**19**) shows

a signal at $m/z = 649$ assigned to the trinuclear complex cation $[Ni_3(L3^{py})Cl_3]^+$ again without the pyridine molecules. In the ESI mass spectra of both other complexes no signal of the complex cation could be detected. This might be ascribed to the oxidation of the metal centers in combination with the decomposition of the complexes in solution.

Based on the mass spectrometry data in combination with the properties of the structurally similar trinuclear iron(III) complex $[Fe_3(L3^{Brsal})(py)_6Cl_3]ClO_4$ (**12**), previously discussed in section 4.2, the pyridine molecules and chloride ions of these complexes can be easily replaced by other ligands. Thus they provide a clever access to the targeted synthesis of various trinuclear complexes as well as higher aggregates with adjustable connectivities using either capping or bridging co-ligands.

Due to the nearly equal structures of the nickel(II), cobalt(II) and manganese(II) complex the ligand exchange was exemplarily tested at the trinuclear nickel complex Ni_3L3^{py} (**19**). Two different co-ligands were utilized. The azide ion was used as an example of an anionic monodentate co-ligand and the bis(pyridin-2-ylcarbonyl)-amide (Hbpca) able to coordinate in a terpyridine-like tris-chelating fashion (see figure 4.22).^[239] Although both co-ligands are known for the bridging coordination of various transition metal ions,^[240,241] the reaction conditions were optimized towards the synthesis of the trinuclear complexes. The bridging coordination of the Hbpca co-ligand is introduced in the next section.

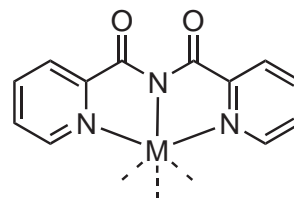


Figure 4.22: The terpyridine-like coordination mode of bpca.

The reaction of the in situ prepared nickel complex Ni_3L3^{py} (**19**) with three equivalents of sodium azide under addition of sodium perchlorate led to the formation of extremely large red cubic prism. Single X-ray structural analysis reveals the exchange of the coordinated chloride ions against end-on bound azide ions resulting in the final complex composition of $[Ni_3(L3^{py})(py)_6(N_3)_3]ClO_4$ ($Ni_3L3^{py}(N_3)_3$) (**20**). The positive charge of the complex cation is counterbalanced by a perchlorate ion. In the IR spectrum a strong characteristic band is observed at 2053 cm^{-1} which is assigned to the azide stretching vibration ($\tilde{\nu}_{(N\equiv N)}$). Furthermore the $\tilde{\nu}_{(Cl-O)}$ stretching vibration of the perchlorate counterion is observed at 1093 cm^{-1} . The rest of the spectrum is nearly identical to them of the trinuclear nickel complex Ni_3L3^{py} (**19**). The ESI mass spectrum in methanol shows

only one intense signal at $m/z = 674$ assigned to the complex cation $[\text{Ni}_3(\text{L3}^{py})(\text{N}_3)_3]^+$ without the coordinated pyridine molecules.

The reaction of the trinuclear nickel complex $\text{Ni}_3\text{L3}^{py}$ (**19**) with three equivalents of Hbpca under addition of ammonium hexafluorophosphate led to the formation of red prism of $[\text{Ni}_3(\text{L3}^{py})(\text{bpca})_3]\text{PF}_6$ ($\text{Ni}_3\text{L3}^{py}(\text{bpca})_3$) (**21**) after slow evaporation of the reaction solution. The positive charge of the trinuclear complex cation is counterbalanced by a hexafluorophosphate anion. The IR spectrum is dominated by the vibrations of the coordinated bpca co-ligands. A strong band is observed at 1695 cm^{-1} , which can be attributed to the $\tilde{\nu}_{(\text{C}=\text{O})}$. The stretching vibrations assigned to the pyridine moieties of the ligands and the co-ligands are only slightly shifted compared to the trinuclear nickel complex $\text{Ni}_3\text{L3}^{py}$ (**19**). An additional characteristic band is observed at 846 cm^{-1} due to the stretching vibration $\tilde{\nu}_{(\text{P}-\text{F})}$ in the hexafluorophosphate counteranion.

4.4.2 Crystal Structures

$[\text{Cu}_3(\text{L3}^{py})(\text{py})_2\text{Cl}_4]$ ($\text{Cu}_3\text{L3}^{py}$) (**18**)

The trinuclear complex $\text{Cu}_3\text{L3}^{py}$ (**18**) crystallizes in the triclinic space group $P\bar{1}$ with three crystallographically independent copper ions. Three copper ions are coordinated by the double deprotonated triaminoguanidine-based ligand connected through N–N diazine bridges into an equilateral triangle. The positive charge is counterbalanced by chloride ions coordinated to the copper centers resulting in a neutral complex. The molecular structure as well as the labeling scheme of the complex molecule is depicted in figure 4.23. Selected bond lengths and angles are listed in table 4.6.

Table 4.6: Selected bond lengths [pm] and angles [°] for complex $\text{Cu}_3\text{L3}^{py}$ (**18**).

Cu1–N2	199.0(2)	Cu2–N5	198.3(2)	Cu3–N1	202.0(2)
Cu1–N3	204.7(2)	Cu2–N6	203.7(2)	Cu3–N8	197.8(2)
Cu1–N4	203.4(2)	Cu2–N7	200.7(2)	Cu3–N9	203.6(2)
Cu1–Cl1	223.76(8)	Cu2–N11	228.0(2)	Cu3–N11	224.3(2)
Cu1–Cl4	252.65(8)	Cu2–Cl2	224.15(8)	Cu3–Cl3	224.64(8)
N3–Cu1–N4	151.77(9)	N6–Cu2–N7	151.92(9)	N1–Cu3–N9	154.40(9)
N2–Cu1–Cl1	166.20(7)	N5–Cu2–Cl2	173.48(7)	N8–Cu3–Cl3	168.88(7)

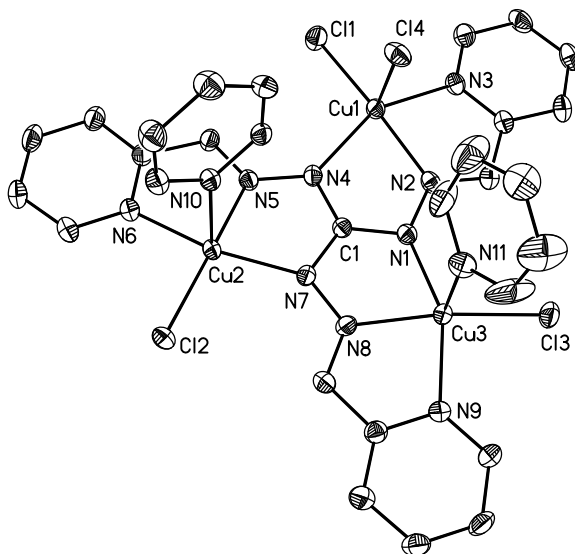


Figure 4.23: Molecular structure of the complex molecule Cu_3L3^{py} (**18**). Thermal ellipsoids are drawn at the 50% probability level. Hydrogen atoms and solvent molecules are omitted for clarity.

All copper centers are placed in a distorted square pyramidal coordination environment. Within the basal plane three coordination sites at each copper ion are occupied by the nitrogen atoms of the tridentate binding pocket of the ligand with bond lengths ranging from 198 to 204 pm. The fourth position is occupied by a chloride ion in a larger distance of about 224 pm. The apical positions are occupied by a chloride ion in a distance of 253 pm at the copper center Cu1 and pyridine molecules in distances of 228 pm and 224 pm at the copper centers Cu2 and Cu3, respectively. These bond lengths are elongated indicating a strong Jahn-Teller effect at all copper centers, typical for copper(II) complexes.

The ligand molecule is nearly planar with a mean deviation of about 8 pm from the least square plane including all ligand atoms. Moreover all apical donors are arranged at the same site of the ligand plane. The *trans* angles vary between 152° and 174° indicating a distortion of the basal planes. Thus the copper centers are displaced from their corresponding best least square planes by 28 pm (Cu1), 20 pm (Cu2), and 22 pm (Cu3) towards the apical positions. The coordination polyhedra of each copper center can be best described as distorted square pyramidal further indicated by similar τ values of $\tau_{Cu1} = 0.24$, $\tau_{Cu2} = 0.36$, and $\tau_{Cu3} = 0.24$. This leads to similar torsion angles of 158° (Cu1–N4–N5–Cu2), 162° (Cu1–N2–N1–Cu3), and 161° (Cu2–N7–N8–Cu3) as well as in-

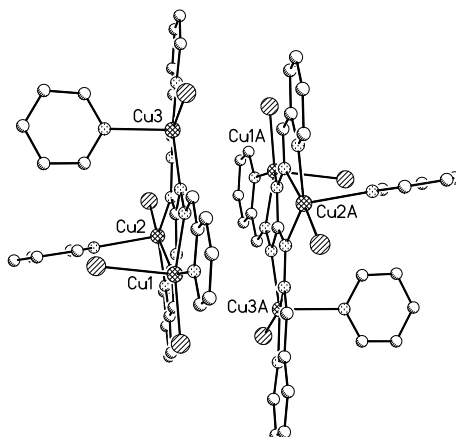


Figure 4.24: Supramolecular arrangement of two complex molecules $[\text{Cu}_3(\text{L3}^{\text{py}})(\text{py})_2\text{Cl}_4]$ of $\text{Cu}_3\text{L3}^{\text{py}}$ (**18**). Hydrogen atoms are omitted for clarity. Symmetry equivalent atoms are labeled with the suffix A.

teratomic $\text{Cu}\cdots\text{Cu}$ distances of 489 pm ($\text{Cu1}\cdots\text{Cu2}$), 490 pm ($\text{Cu1}\cdots\text{Cu3}$), and 487 pm ($\text{Cu2}\cdots\text{Cu3}$) within the copper triangle.

In the crystal packing the complex molecules assemble coplanar in relation to the above defined ligand planes. Two molecules are arranged in close proximity with a interplanar distance of about 300 pm illustrated in figure 4.24 leading to short intermolecular $\text{Cu}\cdots\text{Cu}$ separations of 446 pm ($\text{Cu1}\cdots\text{Cu3A}$) and 472 pm ($\text{Cu1}\cdots\text{Cu2A}$). These dimeric units further assemble to 1D chains through weak π - π interactions of the apical coordinated pyridine molecules in a distance of about 385 pm between the planes of pairwise interacting pyridine co-ligands (see figure 4.25).

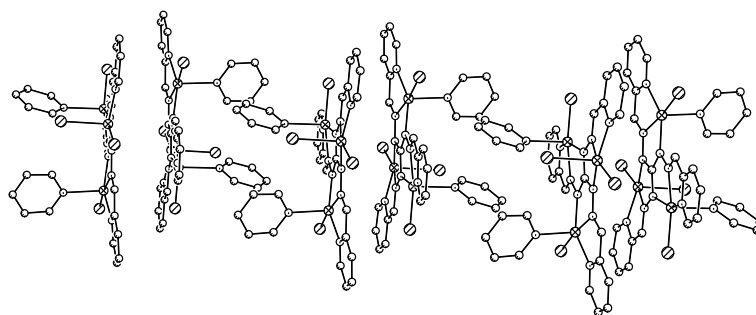


Figure 4.25: Representation of the π - π interactions between the pyridine co-ligands of $[\text{Cu}_3(\text{L3}^{\text{py}})(\text{py})_2\text{Cl}_4]$ in the crystal structure of $\text{Cu}_3\text{L3}^{\text{py}}$ (**18**). Hydrogen atoms are omitted for clarity.

$[Ni_3(L3^{py})(py)_6Cl_3]Cl$ (Ni_3L3^{py}) (19)

The molecular structure of the complex cation $[Ni_3(L3^{py})(py)_6Cl_3]^+$ of complex Ni_3L3^{py} (19) is depicted in figure 4.26. Selected bond lengths and angles are listed in table 4.7. The complex crystallizes in the monoclinic space group $P2_1/c$. Three nickel centers are coordinated and linked through N–N diazine bridges of the double deprotonated triaminoguanidine-based ligand into a triangle. Although the complex possess no crystallographically C_3 symmetry, the three nickel centers within the asymmetric unit are nearly equal.

Each nickel possess a distorted octahedral geometry with a N_5Cl donor set. Three coordination sites are occupied by the N_3 donor set of the ligand within one binding pocket. The distance to the imine nitrogen atom with about 202 pm is rather short compared to the bond lengths to the pyridine and the guanidine nitrogen atoms with about 210 pm. This is mainly caused by the large binding pocket forming two five-membered chelate rings with each nickel center. The octahedral coordination geometry is completed by a chloride ion, which is bound in a distance of about 238 pm and two pyridine molecules with averaged bond lengths of 216 pm. The chloride ion occupies the fourth position within the plane of the three nitrogen donor atoms of the central ligand molecule and

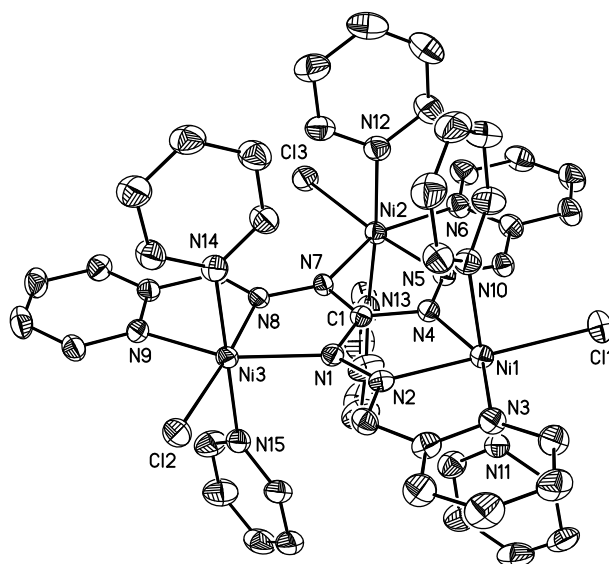


Figure 4.26: Molecular structure of the complex cation $[Ni_3(L3^{py})(py)_6Cl_3]^+$ of Ni_3L3^{py} (19). Thermal ellipsoids are drawn at the 50% probability level. Hydrogen atoms are omitted for clarity.

Table 4.7: Selected bond lengths [pm] and angles [°] for complex **Ni₃L3^{py}** (**19**).

Ni1–N2	202.0(3)	Ni2–N5	202.7(3)	Ni3–N1	208.6(3)
Ni1–N3	210.1(3)	Ni2–N6	212.3(3)	Ni3–N8	201.8(3)
Ni1–N4	209.7(3)	Ni2–N7	209.8(3)	Ni3–N9	209.6(3)
Ni1–N10	215.9(3)	Ni2–N12	214.8(4)	Ni3–N14	216.3(3)
Ni1–N11	214.8(3)	Ni2–N13	216.3(4)	Ni3–N15	216.0(3)
Ni1–Cl1	237.88(11)	Ni2–Cl3	238.07(11)	Ni3–Cl2	237.29(10)
N2–Ni1–Cl1	176.83(9)	N5–Ni2–Cl3	175.07(9)	N1–Ni3–N9	154.51(12)
N3–Ni1–N4	154.28(13)	N6–Ni2–N7	153.15(12)	N14–Ni3–N15	179.71(13)
N10–Ni1–N11	178.80(12)	N12–Ni2–N13	175.20(13)	N8–Ni3–Cl2	175.15(9)

the nickel center Ni3 perfectly situated within this plane. Furthermore the nickel centers Ni1 and Ni2 are only slightly displaced out of their corresponding averaged planes by 1 pm and 2 pm towards their apical positions occupied by the pyridine nitrogen atoms N11 and N12, respectively. Compared to the trinuclear copper complex **Cu₃L3^{py}** (**18**) all bond lengths within the equatorial plane are significantly longer, whereas the axial bond lengths are shorter.

The *trans* angles are between 153° and 180° indicating a distortion of the octahedral environment. The distortion is due to the rigid binding pocket of the triaminoguanidine ligand forming two five-membered chelate rings with the nickel ion, while all other *trans* angles are situated at the upper end of this range. The ligand molecule is nearly planar leading to torsion angles of 169° (Ni1–N4–N5–Ni2), 175° (Ni1–N2–N1–Ni3) and 180° (Ni2–N7–N8–Ni3). This results in nearly equal interatomic Ni···Ni separations of about 504 pm within the nickel triangle. Due to the octahedral coordination environments of the nickel centers compared to the square pyramidal geometry within the trinuclear copper complex (**18**), the torsion angles and hence the interatomic distances are significantly larger. The axial pyridine molecules at each nickel center are twisted with an dihedral angle of 87° (Ni1), 78° (Ni2) and 70° (Ni3). Due to this the complex does not exhibit *C*₃ symmetry, although the coordination geometries including all bond lengths and angles are very similar for each nickel center within the trinuclear cationic molecule. The positive charge of the complex cation is counterbalanced by one chloride ion, disordered over three crystallographic positions.

$[Ni_3(L3^{py})(py)_6(N_3)_3]ClO_4$ ($Ni_3L3^{py}(N_3)_3$) (20)

The molecular structure of the trinuclear complex cation $[Ni_3(L3^{py})(py)_6(N_3)_3]^+$ of compound $Ni_3L3^{py}(N_3)_3$ (20) is depicted in figure 4.27. Selected bond lengths and angles are listed in table 4.8. The structure is similar to the trinuclear nickel complex Ni_3L3^{py} (19), wherein the coordinated chloride ion at each nickel center is replaced by an azide ion. The complex crystallizes in the cubic space group $Pa\bar{3}$ with a C_3 axis through the central carbon atom C1 of the guanidine moiety with three crystallographically equivalent nickel centers.

The nickel center within the asymmetric unit is coordinated in a distorted octahedral geometry. The bond lengths to the nitrogen donors of the ligand as well as the pyridine molecules are nearly the same compared to complex Ni_3L3^{py} (19). The azide ion is bound in a distance of 210 pm within the plane defined by the nitrogen donor atoms of the ligand binding pocket, leading to an N_6 donor set at the nickel center. As expected also the angles are very similar. Again the $N3-Ni1-N1A$ *trans* angle within the rigid ligand binding pocket is with 155° rather small compared to the $N2-Ni1-N6$ and $N4-Ni1-N5$ angles with about 177° . The nickel ion is nearly perfect arranged within the tetragonal plane, defined by the nitrogen atoms of the tridentate binding pocket together with the azide nitrogen atom, with a displacement of only 1 pm towards the apical position occupied by the pyridine nitrogen atom N4 in a distance of 214 pm. Hence the distance to the

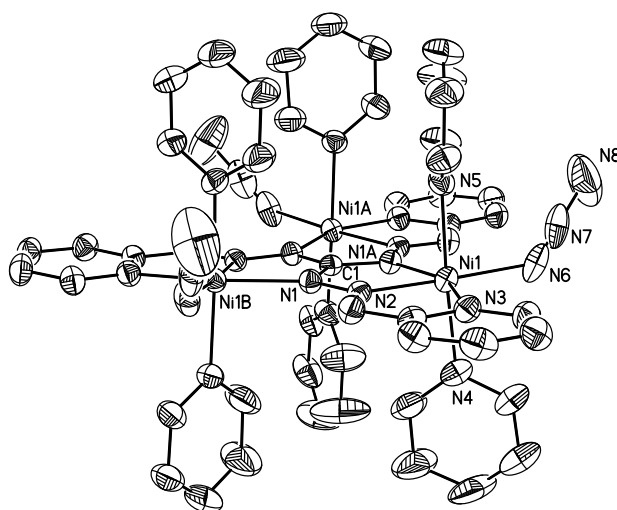


Figure 4.27: Molecular structure of the complex cation $[Ni_3(L3^{py})(py)_6(N_3)_3]^+$ of $Ni_3L3^{py}(N_3)_3$ (20). Thermal ellipsoids are drawn at the 50% probability level. Hydrogen atoms are omitted for clarity.

Table 4.8: Selected bond lengths [pm] and angles [°] for complex $\text{Ni}_3\text{L3}^{py}(\text{N}_3)_3$ (**20**).

Ni1–N1A	208.5(3)	Ni1–N2	201.6(3)
Ni1–N3	209.3(3)	Ni1–N4	213.8(3)
Ni1–N5	217.6(3)	Ni1–N6	209.4(4)
N2–Ni1–N1A	75.90(11)	N2–Ni1–N3	78.65(11)
N2–Ni1–N4	93.42(12)	N2–Ni1–N5	89.36(11)
N2–Ni1–N6	176.80(13)	N3–Ni1–N1A	154.44(11)
N3–Ni1–N4	87.39(11)	N3–Ni1–N5	91.47(11)
N3–Ni1–N6	99.17(12)	N4–Ni1–N1A	91.75(11)
N4–Ni1–N5	176.73(12)	N4–Ni1–N6	88.80(15)
N5–Ni1–N1A	90.59(11)	N5–Ni1–N6	88.35(14)
N6–Ni1–N1A	106.36(12)		

second axial pyridine nitrogen atom N15 is slightly longer with about 218 pm. The apical pyridine molecules retains the twisted arrangement with an dihedral angle of 82°. The Ni–N–Ni torsion angle with 174° is in agreement with the planarity of the complex molecule, which leads to an interatomic Ni···Ni separation of 503 pm.

The complex cation crystallizes with one perchlorate counterion situated at a C_3 axis. Within the crystal packing the complex molecules are well separated with additional hydrogen bonding interaction between the oxygen atom O1M of the co-crystallized methanol molecule and the azide ion in a distance of 287 pm (O1M···N8) stabilizing the angled coordination at the nickel center.

$[\text{Ni}_3(\text{L3}^{py})(\text{bpca})_3]\text{PF}_6$ ($\text{Ni}_3\text{L3}^{py}(\text{bpca})_3$) (**21**)

The molecular structure of the trinuclear complex cation $[\text{Ni}_3(\text{L3}^{py})(\text{bpca})_3]^+$ of compound $\text{Ni}_3\text{L3}^{py}(\text{bpca})_3$ (**21**) is depicted in figure 4.28. Selected bond lengths and angles are listed in table 4.9. Although the three nickel ions are crystallographically independent the complex molecule possess a pseudo C_3 symmetry with nearly equal nickel centers.

The nickel ions are embedded in a distorted octahedral environment with a N_6 donor set. Three coordination sites at each nickel center are occupied by the nitrogen atoms

of the tridentate binding pocket of the ligand molecule. The deprotonated bis(pyridin-2-ylcarbonyl)-amide co-ligand completes the octahedral environment through coordination in a terpyridine-like chelating fashion. The bond lengths are between 201 and 216 pm. The distances to the imine nitrogen atoms of the ligand as well as the amide nitrogen atoms of the co-ligand are all situated at the lower end of the respective range whereas the distances to the pyridine nitrogen atoms of the ligand are elongated with values at the upper end of the range. All other distances are very similar with averaged 208 pm. As expected the bond lengths and angles with the donor atoms of the triaminoguanidine ligand are nearly equal to both other complexes Ni_3L3^{py} (19) and $Ni_3L3^{py}(N_3)_3$ (20). The *trans* angles range from 154° to 179° , wherein the angles within the binding pockets of the triaminoguanidine ligand as well as the angles within the bpca co-ligands are situated at the lower end.

Analogous to complex Ni_3L3^{py} (19) the nickel ion Ni3 is perfectly situated within the tetragonal plane defined by the nitrogen atoms of the tridentate binding pocket and the amide nitrogen atom of the co-ligand. The Ni1 and Ni2 are displaced out by 2 pm towards their apical positions occupied by the pyridine nitrogen atoms N12 and N13, which is consistent with the expected planarity of the ligand molecule. Hence the tor-

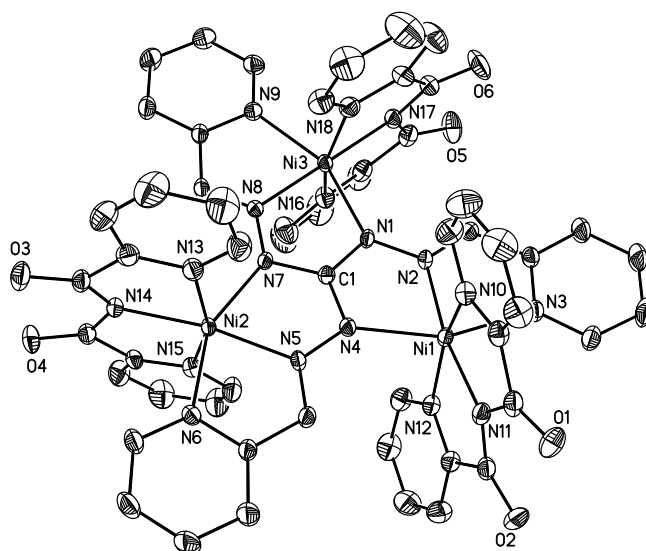


Figure 4.28: Molecular structure of the complex cation $[Ni_3(L3^{py})(bpca)_3]^+$ of $Ni_3L3^{py}(bpca)_3$ (21). Thermal ellipsoids are drawn at the 50% probability level. Hydrogen atoms are omitted for clarity.

Table 4.9: Selected bond lengths [pm] and angles [°] for complex **Ni₃L3^{py}(bpca)₃ (21)**.

Ni1–N2	201.3(2)	Ni2–N5	201.9(2)	Ni3–N1	210.3(2)
Ni1–N3	215.8(2)	Ni2–N6	214.3(2)	Ni3–N8	201.2(2)
Ni1–N4	208.8(2)	Ni2–N7	209.0(2)	Ni3–N9	209.3(2)
Ni1–N10	208.2(2)	Ni2–N13	207.4(2)	Ni3–N16	208.5(2)
Ni1–N11	200.7(2)	Ni2–N14	201.4(2)	Ni3–N17	201.4(2)
Ni1–N12	208.2(2)	Ni2–N15	207.5(2)	Ni3–N18	208.1(2)
N2–Ni1–N11	170.57(9)	N5–Ni2–N14	170.81(9)	N1–Ni3–N9	154.71(9)
N3–Ni1–N4	154.04(9)	N6–Ni2–N7	153.70(9)	N8–Ni3–N17	178.78(9)
N10–Ni1–N12	159.40(9)	N13–Ni2–N15	159.24(9)	N16–Ni3–N18	159.95(10)

sion angles differ only slightly with 178° (Ni1–N4–N5–Ni2), 173° (Ni1–N2–N1–Ni3) and 177° (Ni2–N7–N8–Ni3) leading to an interatomic Ni···Ni separation of 502 pm. The positive charge is counterbalanced by a hexafluorophosphate anion situated above the central carbon atom C1 of the ligand. Together with the co-crystallized water molecules these are involved in hydrogen bonding interactions resulting in a 3D network. Due to this the hexafluorophosphate anion is fixed within the crystallographic position and does not show any disorder.

[Co₃(L3^{py})(py)₆Cl₃]ClO₄ (Co₃L3^{py}) (22)

The trinuclear complex **Co₃L3^{py} (22)** crystallizes in the chiral monoclinic space group C2 consistent with the presence of solely one enantiomeric form. The molecular structure as well as the labeling scheme of the complex cation [Co₃(L3^{py})(py)₆Cl₃]⁺ is depicted in figure 4.29. Selected bond lengths and angles are listed in table 4.10.

Three cobalt(II) ions are coordinated by one triaminoguanidine ligand linked through N–N diazine bridges. Each cobalt ion is coordinated in a distorted octahedral environment with a N₅Cl donor set equal to the nickel centers in complex **Ni₃L3^{py} (19)**. Three coordination sites are occupied by the tridentate binding pocket of the ligand as previously described with bond lengths ranging from 210 to 216 pm. The fourth position within this plane is occupied by a chloride ion in a distance of about 235 pm. The dis-

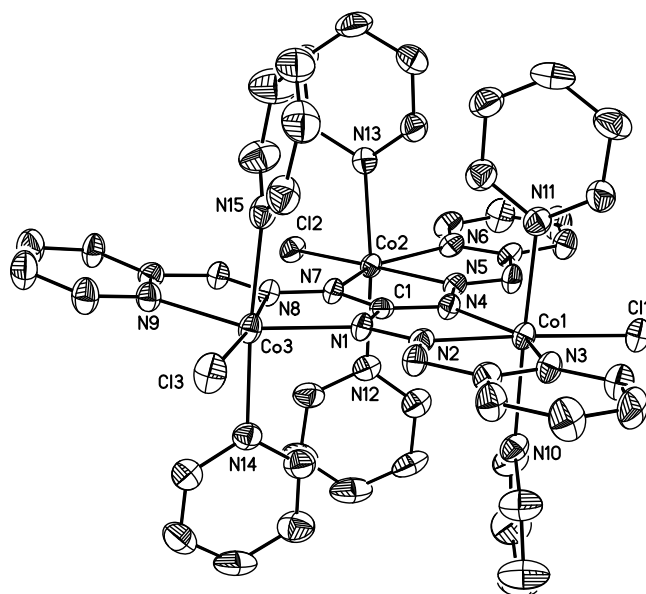


Figure 4.29: Molecular structure of the complex cation $[Co_3(L3^{py})(py)_6Cl_3]^+$ of Co_3L3^{py} (**22**). Thermal ellipsoids are drawn at the 50% probability level. Hydrogen atoms are omitted for clarity.

Table 4.10: Selected bond lengths [pm] and angles [$^\circ$] for complex Co_3L3^{py} (**22**).

Co1–N2	210.2(3)	Co2–N5	211.7(3)	Co3–N1	210.3(3)
Co1–N3	215.6(3)	Co2–N6	214.7(4)	Co3–N8	210.6(3)
Co1–N4	214.6(3)	Co2–N7	212.7(3)	Co3–N9	213.8(3)
Co1–N10	220.5(4)	Co2–N12	219.2(4)	Co3–N14	222.5(4)
Co1–N11	222.2(4)	Co2–N13	221.6(4)	Co3–N15	227.9(4)
Co1–Cl1	235.24(12)	Co2–Cl2	236.08(10)	Co3–Cl3	233.92(11)
N4–Co1–N3	149.01(13)	N5–Co2–Cl2	171.74(10)	N1–Co3–N9	148.54(12)
N2–Co1–Cl1	175.66(9)	N7–Co2–N6	147.83(12)	N8–Co3–Cl3	172.34(9)
N10–Co1–N11	177.65(12)	N12–Co2–N13	174.01(14)	N14–Co3–N15	174.79(14)

tances to axial pyridine nitrogen atoms vary between 220 and 228 pm. All donor-cobalt distances are longer compared to the trinuclear nickel complex $\text{Ni}_3\text{L3}^{py}$ (**19**), except the distances to the chloride ions which are nearly identical. Hence the *trans* angles within the tridentate binding pockets are with about 148° rather small due to the rigidity of the ligand molecule. Moreover the other *trans* angles are between 172° and 178° . All cobalt ions are arranged nearly perfect in the corresponding tetragonal planes with maximal displacements of 4 pm. The torsion angles are very similar with 179° (Co1–N4–N5–Co2) and 178° (Co1–N2–N1–Co3, Co2–N7–N8–Co3). This leads to interatomic Co...Co separations of 517 pm (Co1...Co2) and 513 pm (Co1...Co3, Co2...Co3), respectively. The axial pyridine molecules at each cobalt ion are twisted with dihedral angles between 28° and 81° .

Although the complex molecule includes a lot of pyridine and co-crystallizes with pyridine molecules, no π - π interactions are observed within the crystal packing. The trinuclear complex molecules assemble through hydrogen bonding interaction between the coordinated chloride ions and the pyridine hydrogen atoms in distances ranging from 357 to 363 pm ($\text{C}_{py}\cdots\text{Cl}$). The perchlorate oxygen atoms are further involved with smaller distances from 319 to 345 pm ($\text{C}_{py}\cdots\text{O}$). Both distances are within the expected range of C–H...anion hydrogen bonding interaction.^[169,242] It should be noted that the perchlorate counterion does not show any disorder, presumably due to the bridging connectivity within the hydrogen bonding network.

$[\text{Mn}_3(\text{L3}^{py})(\text{py})_6\text{Cl}_3]\text{ClO}_4$ ($\text{Mn}_3\text{L3}^{py}$) (**23**)

The complex $\text{Mn}_3\text{L3}^{py}$ (**23**) crystallizes in the chiral monoclinic space group $P2_1$ consistent with the presence of solely one enantiomeric form. The molecular structure of the complex cation $[\text{Mn}_3(\text{L3}^{py})(\text{py})_6\text{Cl}_3]^+$ as well as the heteroatom labeling scheme of $\text{Mn}_3\text{L3}^{py}$ (**23**) is depicted in figure 4.30. Selected bond lengths and angles are listed in table 4.11.

The complex structure is very similar to those of the cobalt complex $\text{Co}_3\text{L3}^{py}$ (**22**) and nickel complex $\text{Ni}_3\text{L3}^{py}$ (**19**). Each manganese(II) ion is coordinated in a distorted octahedral coordination environment. The fourth positions within the tetragonal planes are occupied by the nitrogen donor atoms of the ligand binding pocket with Mn–N distances ranging from 222 to 230 pm and a chloride ion in a distance of about 240 pm. The man-

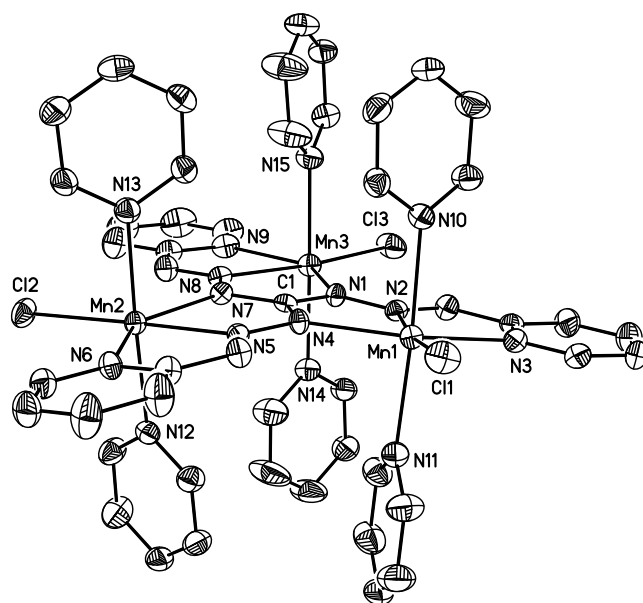


Figure 4.30: Molecular structure of the complex cation $[Mn_3(L3^{py})(py)_6Cl_3]^+$ of Mn_3L3^{py} (**23**). Thermal ellipsoids are drawn at the 50% probability level. Hydrogen atoms are omitted for clarity.

Table 4.11: Selected bond lengths [pm] and angles [$^\circ$] for complex Mn_3L3^{py} (**23**).

Mn1–N2	226.0(2)	Mn2–N5	225.8(2)	Mn3–N1	222.7(2)
Mn1–N3	229.1(2)	Mn2–N6	225.7(2)	Mn3–N8	224.0(2)
Mn1–N4	224.4(2)	Mn2–N7	222.0(2)	Mn3–N9	230.2(3)
Mn1–N10	231.4(2)	Mn2–N12	233.9(2)	Mn3–N14	233.4(2)
Mn1–N11	232.6(2)	Mn2–N13	234.2(2)	Mn3–N15	233.3(2)
Mn1–Cl1	240.75(8)	Mn2–Cl2	240.94(8)	Mn3–Cl3	239.62(8)
N2–Mn1–Cl1	172.72(6)	N6–Mn2–N7	140.62(8)	N1–Mn3–N9	141.08(8)
N3–Mn1–N4	140.15(8)	N5–Mn2–Cl2	173.54(6)	N8–Mn3–Cl3	172.63(6)
N10–Mn1–N11	175.88(9)	N12–Mn2–N13	176.33(8)	N14–Mn3–N15	178.98(9)

ganese centers are arranged nearly perfect within the corresponding plane with minimal displacements of 4 pm (Mn1), 1 pm (Mn2), and 2 pm (Mn3). The axial positions are occupied by pyridine nitrogen atoms with similar bond lengths of about 233 pm. Again these pyridine molecules are twisted with dihedral angles between 25° and 63°. All donor-manganese distances are longer compared to the cobalt complex **Co₃L3^{py}** (**22**). Therefore the *trans* angle within the ligand binding pocket is somewhat smaller with about 141° indicating a strong distortion of the octahedral geometry. All other *trans* angles vary between 173° and 179°. The above defined tetragonal planes are nearly coplanar with dihedral angles from 5° to 14°, which is consistent with the expected planarity of the trinuclear core fragment. This leads to similar interatomic Mn···Mn separations of 541 pm (Mn1···Mn2), 538 pm (Mn1···Mn3), and 536 pm (Mn2···Mn3) as well as Mn–N–N–Mn torsion angles of 174° (Mn1–N4–N5–Mn2), 176° (Mn1–N2–N1–Mn3), and 172° (Mn2–N7–N8–Mn3). The positive charge of the complex cation is counterbalanced by a perchlorate ion.

Analogous to the cobalt complex **Co₃L3^{py}** (**22**) no π - π interactions are present in the crystal packing. The complex molecules assemble through C–H···anion hydrogen bonding interactions involving the coordinated chloride as well as the perchlorate counterion in distances of 343 pm (C_{py}···Cl) as well as 322 to 342 pm (C_{py}···O). Due to this the perchlorate ion is fixed within its position in the crystal packing and does not show any disorder. The distances are within the expected range of C–H···anion hydrogen bonding interaction.^[169,242]

4.4.3 Magnetic Properties

Trinuclear Copper(II) Complex

Temperature dependent magnetic susceptibility data for the copper complex **Cu₃L3^{py}** (**18**) is shown as $\chi_M = f(T)$ and $\chi_M T = f(T)$ plots in figure 4.31. The measurements were performed on a freshly prepared powdered sample immobilized in paraffin, to prevent the loss of the coordinated pyridine molecules in vacuum. The $\chi_M T$ value at 300 K is 0.72 cm³ K mol⁻¹, which is significantly lower than the spin-only value for three independent copper(II) ions with $S = 1/2$. Upon lowering the temperature the $\chi_M T$ value steadily decreases reaching 0.45 cm³ K mol⁻¹ at 40 K and then rapidly decreases to 0.25 cm³ K mol⁻¹ at 2 K. The gradual decrease to 40 K indicate strong antiferromag-

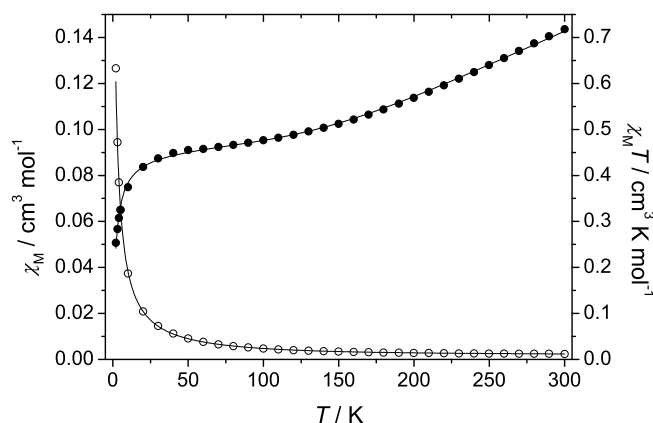


Figure 4.31: Plot of the thermal dependence of χ_M (empty circles, \circ) and $\chi_M T$ (black filled circles, \bullet) for complex Cu_3L3^{py} (**18**) measured with an applied magnetic field of 2000 Oe. The corresponding fit functions according to equation 4.6 taken only a single exchange coupling $J = J_A = J_B$ into account are drawn as solid lines (for parameters see text).

netic exchange interactions between the three copper(II) centers mediated by the N–N diazine bridges. Moreover this is in agreement with the lower room temperature value of $\chi_M T$. The value at 40 K is close to the spin-only value of one independent copper(II) ion with $S = 1/2$. It is assumed that the rapid decrease at lower temperature is caused by intermolecular antiferromagnetic exchange interactions between the resulting $S = 1/2$ ground spin states.

In complex Cu_3L3^{py} (**18**) the apical positions of the penta-coordinated copper ions Cu2 and Cu3 are occupied by pyridine molecules, whereas a chloride ion coordinates to the copper ion Cu1. Therefore a two- J model is employed as spin topology depicted in figure 4.32. The corresponding isotropic spin Hamiltonian is given in equation 4.5 with $J_A = J_{12} = J_{13}$ and $J_B = J_{23}$.

$$\hat{H} = -J_A(\hat{S}_1\hat{S}_2 + \hat{S}_1\hat{S}_3) - J_B(\hat{S}_2\hat{S}_3) \quad (4.5)$$

This leads to the expression for $S_1 = S_2 = S_3 = 1/2$ given in equation 4.6 under consideration of temperature independent paramagnetism (χ_{TIP}), intermolecular exchange interaction (θ) and paramagnetic impurity (ρ) with the abbreviations: $A = (J_A - J_B)/kT$ and $B = 3J_A/2kT$.

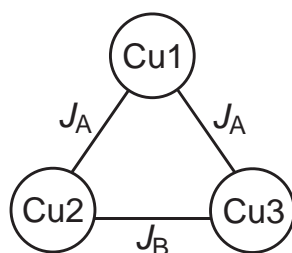


Figure 4.32: The spin topology of the employed two- J model for the trinuclear copper complex **Cu₃L3^{py}** (18).

$$\chi_M = \frac{N_A \beta^2 g^2}{4k(T - \theta)} \frac{1 + \exp A + 10 \exp B}{1 + \exp A + 2 \exp B} (1 - \rho) + \frac{3N_A \beta^2 g^2}{4kT} \rho + \chi_{TIP} \quad (4.6)$$

The fit of the experimental data according to equation 4.6 reveals a strong correlation between both exchange coupling constants J_A and J_B . Therefore an equilateral triangle with three equal pairwise magnetic exchange interactions is assumed. Moreover this is in agreement with the structural data exhibiting three nearly identical interatomic Cu...Cu distances of 489 pm (Cu1...Cu2), 490 pm (Cu1...Cu3), and 487 pm (Cu2...Cu3) as well as torsion angles of 158° (Cu1-N4-N5-Cu2), 162° (Cu1-N2-N1-Cu3), and 161° (Cu2-N7-N8-Cu3). The apical co-ligands are only weakly bound with minor influence on the tetragonal coordination of each copper center. The best fit according to equation 4.6 assuming only a single exchange coupling $J = J_A = J_B$ results in $J = -299(9) \text{ cm}^{-1}$, $g = 2.13(3)$, $\theta = -2.0(2) \text{ K}$, $\rho = 0.02(1)$ and $\chi_{TIP} = 3.1(6) \cdot 10^{-4} \text{ cm}^3 \text{ mol}^{-1}$ with $r^2 = 0.99902$.

Very strong antiferromagnetic exchange interactions are obtained between the three copper centers leading to an $S = 1/2$ ground state. Therefore this complex might be an interesting target as a qubit in the field of quantum computation.^[84,85,144,145,147] The strength of the coupling is comparable to them in the trinuclear copper complexes based on tris-*N*-salicylidene-aminoguanidine together with 2,2'-bipyridine co-ligands in the range $309 < -J < 335 \text{ cm}^{-1}$.^[139] This is due to nearly equal structural arrangements within the triaminoguanidine-bridged triangular copper core unit. The coupling is only slightly influenced by the ligand side chain as well as the applied co-ligands.

Trinuclear Nickel(II) Complexes

The magnetization of polycrystalline samples of the trinuclear nickel complexes Ni_3L3^{py} (**19**), $Ni_3L3^{py}(N_3)_3$ (**20**), and $Ni_3L3^{py}(bpca)_3$ (**21**) was measured in a temperature range between 2 and 300 K. For complex Ni_3L3^{py} (**19**) the temperature dependence of the paramagnetic molar susceptibility χ_M and its product with temperature $\chi_M T$ are depicted in figure 4.33. A very similar magnetic behavior is observed for the compounds $Ni_3L3^{py}(N_3)_3$ (**20**) and $Ni_3L3^{py}(bpca)_3$ (**21**) shown in figure 4.34. The experimental $\chi_M T$ values at 300 K are $2.91 \text{ cm}^3 \text{ K mol}^{-1}$ for Ni_3L3^{py} (**19**), $3.00 \text{ cm}^3 \text{ K mol}^{-1}$ for $Ni_3L3^{py}(N_3)_3$ (**20**), and $2.96 \text{ cm}^3 \text{ K mol}^{-1}$ for $Ni_3L3^{py}(bpca)_3$ (**21**) close to the spin-only value of three uncoupled nickel(II) ions with $S = 1$. Upon lowering the temperature, $\chi_M T$ continuously decreases approaching values close to zero. This behavior is characteristic for an antiferromagnetic exchange interaction between the three nickel(II) centers with a $S = 0$ ground state.

The complex $Ni_3L3^{py}(N_3)_3$ (**20**) has a crystallographic C_3 symmetry. Although both other complexes Ni_3L3^{py} (**19**) and $Ni_3L3^{py}(bpca)_3$ (**21**) possess no crystallographically imposed symmetry, the three nickel centers within each complex are nearly identical with equal interatomic $Ni \cdots Ni$ separations. Therefore the Ni_3 triangular unit of each complex can be treated as an equilateral triangle with three equal pairwise magnetic interactions. The

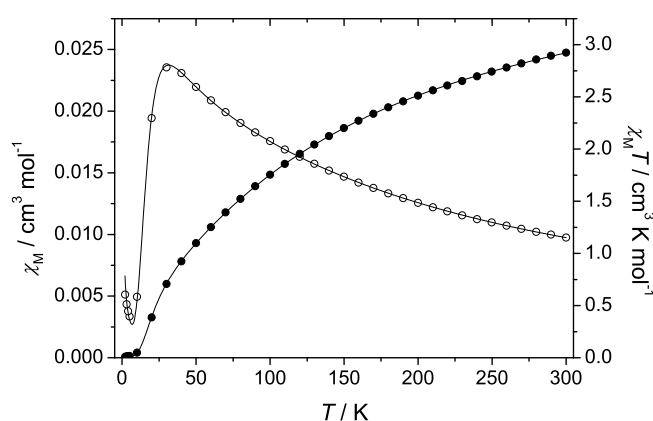


Figure 4.33: Plot of the thermal dependence of χ_M (empty circles, \circ) and $\chi_M T$ (black filled circles, \bullet) for complex Ni_3L3^{py} (**19**) measured with an applied magnetic field of 2000 Oe. The solid lines represent the best fit to the experimental data according to equation 4.8 (for parameters see text and table 4.12).

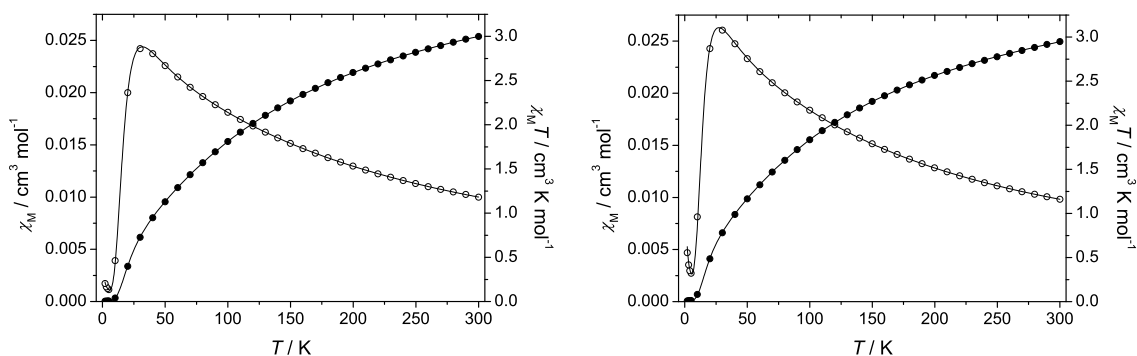


Figure 4.34: Plot of the thermal dependence of χ_M (empty circles, \circ) and $\chi_M T$ (black filled circles, \bullet) for the complexes $\text{Ni}_3\text{L3}^{py}(\text{N}_3)_3$ (**20**) (left) and $\text{Ni}_3\text{L3}^{py}(\text{pbca})_3$ (**21**) (right) measured with an applied magnetic field of 2000 Oe. The solid lines represents the best fit to the experimental data according to equation 4.8 (for parameters see text and table 4.12).

corresponding isotropic spin Hamiltonian has the following expression:

$$\hat{H} = -J(\hat{S}_1\hat{S}_2 + \hat{S}_1\hat{S}_3 + \hat{S}_2\hat{S}_3) \quad (4.7)$$

For $S_1 = S_2 = S_3 = 1$ this leads to the expression given in equation 4.8 under consideration of paramagnetic impurities ρ and temperature independent paramagnetism χ_{TIP} . Herein the abbreviations stand for $A = J/kT$, $B = 3J/kT$, and $C = 6J/kT$.

$$\chi_M T = \frac{2N_A\beta^2 g^2}{k} \frac{3\exp A + 10\exp B + 14\exp C}{1 + 9\exp A + 10\exp B + 7\exp C} (1 - \rho) + \frac{8N_A\beta^2}{k} \rho + \chi_{TIP} T \quad (4.8)$$

In each case the obtained fit function shows an excellent agreement with the experimental values with coefficients of determination $r^2 \geq 0.99999$. The resulting fit parameters for the three complexes are summarized in table 4.12.

The exchange coupling constants J are the same for both trinuclear complexes $\text{Ni}_3\text{L3}^{py}$ (**19**) and $\text{Ni}_3\text{L3}^{py}(\text{N}_3)_3$ (**20**) with $J = -42 \text{ cm}^{-1}$. In complex $\text{Ni}_3\text{L3}^{py}(\text{pbca})_3$ (**21**) the coupling is slightly weaker with $J = -36 \text{ cm}^{-1}$. This might be ascribed to a weak influence of the chelating co-ligand, due to the fact that no significant structural difference exist between the three N–N diazine-bridged nickel triangles. Moreover all couplings are stronger compared to trinuclear nickel(II) complexes based on bromo-substituted tris-*N*-salicylidene-aminoguanidine ligands ranging from -27 to -34 cm^{-1} .^[141,243]

Table 4.12: Fit parameters of the magnetic data for the trinuclear nickel complexes Ni_3L3^{py} (19), $Ni_3L3^{py}(N_3)_3$ (20), and $Ni_3L3^{py}(bpca)_3$ (21) according to equation 4.8.

	(19)	(20)	(21)
$J [cm^{-1}]$	-41.7(2)	-41.7(1)	-36.0(1)
g	2.173(5)	2.220(3)	2.126(4)
ρ	0.0039(4)	0.0008(3)	0.0029(4)
$\chi_{TIP} [cm^3 mol^{-1}]$	$7.4(3) \cdot 10^{-4}$	$6.1(2) \cdot 10^{-4}$	$9.2(3) \cdot 10^{-4}$
r^2	0.99999	1	0.99999

Trinuclear Cobalt(II) Complex

The magnetic data for complex Co_3L3^{py} (22) is depicted in figure 4.35 as temperature dependent plots of χ_M and $\chi_M T$. The room temperature value of $\chi_M T$ is $7.73 cm^3 K mol^{-1}$. Upon lowering the temperature, the $\chi_M T$ value continuously decreases reaching a minimum of about $1.05 cm^3 K mol^{-1}$ at 2 K. The room temperature value is close to the spin-only value for three independent high-spin cobalt(II) centers with $S = 3/2$ ($7.44 cm^3 K mol^{-1}$ assuming that $g = 2.3$). This is in agreement with the crystallographic data confirming the high-spin character of all three cobalt(II) ions. The course of the $\chi_M T$ value is indicative for antiferromagnetic exchange interactions between the three cobalt centers mediated through the N–N diazine bridges.

According to the rather similar interatomic Co...Co distances of 517 pm (Co1...Co2) and 513 pm (Co1...Co3, Co2...Co3) as well as Co–N–N–Co torsion angles of 179° (Co1–N4–N5–Co2) and 178° (Co1–N2–N1–Co3, Co2–N7–N8–Co3) within the complex cation, an equilateral triangular spin topology with three equal cobalt(II) ions is assumed. The experimental data was analyzed by a full-matrix diagonalization approach using the program package DAVE.^[177] The corresponding isotropic spin Hamiltonian, including Zeeman interactions, is given in equation 4.9 with $S_1 = S_2 = S_3 = 3/2$.

$$\hat{H} = -J(\hat{S}_1\hat{S}_2 + \hat{S}_1\hat{S}_3 + \hat{S}_2\hat{S}_3) + \sum_{i=1}^3 g_i\beta\hat{S}_i\vec{H} \quad (4.9)$$

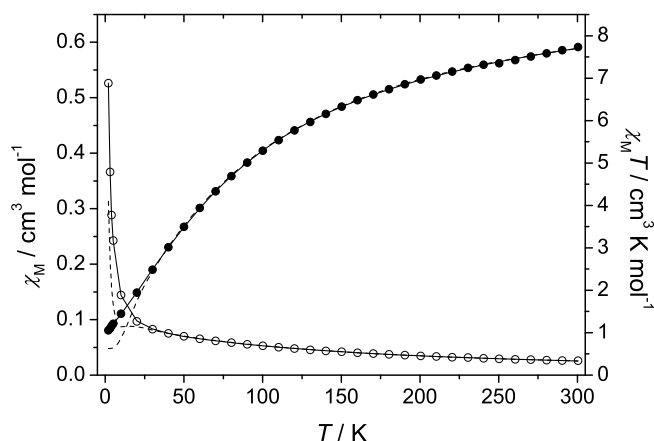


Figure 4.35: Plot of the thermal dependence of χ_M (empty circles, \circ) and $\chi_M T$ (black filled circles, \bullet) for complex $\text{Co}_3\text{L3}^{py}$ (**22**) measured with an applied magnetic field of 2000 Oe. The data were fitted with the program package DAVE. The dashed lines represents the best fit using the isotropic spin Hamiltonian given in equation 4.9. Moreover the solid lines represents the best fit to the experimental data taken the antisymmetric exchange into account according to equation 4.12 (for parameters see text).

The analysis of the experimental data set of $\chi_M T$ resulted in parameters $J = -16.9 \text{ cm}^{-1}$ and $g = 2.59$. The calculated values agree well with the experimental data of $\chi_M T$ in the temperature range between 30 and 300 K. Below 30 K the fit function drops down to $0.63 \text{ cm}^3 \text{ K mol}^{-1}$ at 2 K equal to a ground spin state of $S = 1/2$ (see dashed lines in figure 4.35). Alternative analysis using an isosceles triangular spin topology derived from equation 4.10 to take into account the slight variations in $\text{Co} \cdots \text{Co}$ distances as well as Co-N-N-Co torsion angles results in an improved fit due to higher number of refined parameters but reproduced worse the experimental $\chi_M T$ data over the whole temperature range.

$$\hat{H} = -J_1(\hat{S}_1\hat{S}_3 + \hat{S}_2\hat{S}_3) - J_2(\hat{S}_1\hat{S}_2) + \sum_{i=1}^3 g_i\beta\hat{S}_i\vec{H} \quad (4.10)$$

The almost two times higher experimental value of $\chi_M T$ at 2 K can be ascribed to a strong zero-field splitting (ZFS) which is characteristic for cobalt(II) ions. Furthermore in triangular antiferromagnetically coupled complexes with half-integer spins intramolecular antisymmetric exchange interactions (AE) between the metal centers has

been observed,^[244,245] These were predominantly reported for trinuclear copper(II) complexes,^[75,79,81–83,246] beside a few iron(III) and cobalt(II) complexes.^[194,247,248] Moreover in antiferromagnetically coupled D_3 symmetric triangular copper(II) complexes symmetry lowering was observed at low temperature.^[75,77] The possibility of magnetic Jahn-Teller effect has been proposed suggesting that a minimal distortion of about 1 pm should occur in the ground state of any antiferromagnetically coupled trinuclear complexes to remove the three-fold symmetry.^[249] The cobalt complex exhibits only a pseudo C_3 symmetry. Therefore the magnetic data was analyzed taken both effects into account and assuming an isosceles triangular spin topology according to equation 4.10. The appropriate spin hamiltonian that accounts for ZFS and AE interactions is given in equation 4.11.

$$\hat{H} = \hat{H}_{HDVV} + \hat{H}_{ZFS} + \hat{H}_{AE} + \hat{H}_{Zeeman} \quad (4.11)$$

Due to the triangular spin topology of the complex cation the ZFS and AE are assumed to be predominantly axial. To avoid overparametrization the local anisotropy of the g value was neglected assuming only an averaged g for all three cobalt centers. This results in the expression for the spin Hamiltonian given in equation 4.12. The AE follows a set of symmetry rules.^[244] The effective antisymmetric exchange constant G of the trimer is proportional to the sum of the components of two center interactions G_{ij} leading to the expression $G([S_1 \times S_2] + [S_2 \times S_3] + [S_3 \times S_1])$.^[246,247]

$$\begin{aligned} \hat{H} = & -J_1(\hat{S}_1\hat{S}_3 + \hat{S}_2\hat{S}_3) - J_2(\hat{S}_1\hat{S}_2) + \sum_{i=1}^3 D_i[S_{z,i}^2 - \frac{1}{3}S_i(S_i + 1)] \\ & + \sum_{ij} G_{ij}[S_i \times S_j] + \sum_{i=1}^3 g_i\beta\hat{S}_i\vec{H} \end{aligned} \quad (4.12)$$

The best fit of the experimental data is obtained with the parameters $J_1 = -17.9 \text{ cm}^{-1}$, $J_2 = -11.9 \text{ cm}^{-1}$, $g = 2.58$, $D = 26.8 \text{ cm}^{-1}$, and $G = \pm 0.2 \text{ cm}^{-1}$. The antisymmetric exchange is extremely weak compared to the anisotropic zero-field splitting. Hence G could be neglected, which leads to a marginally worse fit with similar parameters of $J_1 = -17.9 \text{ cm}^{-1}$, $J_2 = -12.0 \text{ cm}^{-1}$, $g = 2.58$, and $D = 26.5 \text{ cm}^{-1}$. Moreover an alternative fit assuming exclusively antisymmetric exchange interaction did not reproduce the

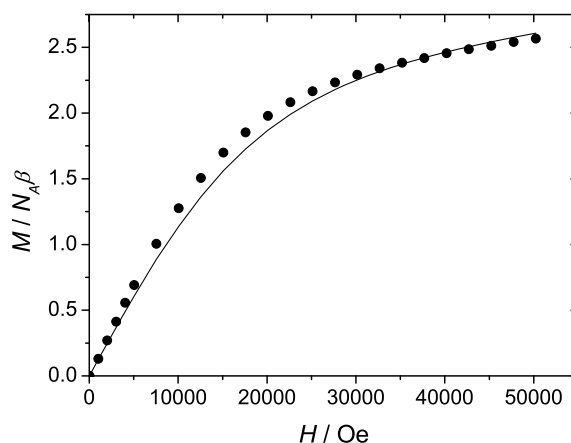


Figure 4.36: Field dependence of the magnetization for complex $\text{Co}_3\text{L3}^{py}$ (**22**) at 2 K (\bullet). The solid line represents the simulated data with the parameters $J_1 = -17.9 \text{ cm}^{-1}$, $J_2 = -12.0 \text{ cm}^{-1}$, $g = 2.58$, and $D = 26.5 \text{ cm}^{-1}$ using the program package julX.^[238]

course of the experimental $\chi_{\text{M}}T$ data in the low temperature region. This confirms further that the low temperature magnetic behavior of the trinuclear complex is dominated by the ZFS of the cobalt(II) ions. The observed antiferromagnetic couplings in combination with the large ZFS is consistent with magnetization measurements at 2 K shown in figure 4.36. The data, analyzed with the program package julX, shows a good agreement between the experimental and simulated data.^[238]

The negative coupling constants J reveals antiferromagnetic exchange interactions between the three cobalt centers. These isotropic exchange interactions through the N–N diazine bridges of the ligand are very strong compared to the only magnetically characterized triangular complexes with a tetrahedral coordination geometry with J values of -2.8 and -0.7 cm^{-1} .^[194,248] The experimental $\chi_{\text{M}}T$ values could be almost perfectly reproduced over the whole temperature range taken only additional ZFS into account, as the AE is rather weak. Moreover the magnitude of the D parameter is larger compared to the isotropic exchange interactions J .

The D value of about 30 cm^{-1} is consistent with the observed distorted octahedral coordination environment of the cobalt(II) ions and a reported triangular arrangement of octahedral coordinated cobalt(II) centers with $D = 39 \text{ cm}^{-1}$.^[93] Moreover the D value is in the reported wide range for cobalt(II) complexes of $-36 < D < 83 \text{ cm}^{-1}$.^[211,250–253] The trinuclear cobalt(II) complex is the first structurally as well as magnetochemically

characterized example of a triangular antiferromagnetically coupled complex with octahedral coordinated cobalt centers.

Trinuclear Manganese(II) Complex

The magnetic data for complex Mn_3L3^{py} (**23**) is depicted as temperature dependent plots of χ_M and $\chi_M T$ in figure 4.37. The $\chi_M T$ curve appears to be roughly invariant at $12.8 \text{ cm}^3 \text{ K mol}^{-1}$ from 300 K down to about 75 K, which is in good agreement with the spin-only value of three independent manganese ions with $S = 5/2$. Moreover this corroborates the high-spin character of the manganese centers assumed from the crystallographic data. Below 75 K the $\chi_M T$ value rapidly drops to $1.80 \text{ cm}^3 \text{ K mol}^{-1}$ at 2 K, indicating a weak antiferromagnetic interaction between the three manganese centers.

In the complex the three manganese centers are nearly equal leading to an equilateral triangular spin topology. The experimental data was analyzed by a full-matrix diagonalization approach using the program package DAVE.^[177] The corresponding isotropic spin Hamiltonian, including Zeeman interactions, with $S_1 = S_2 = S_3 = 5/2$ is given in equation 4.9. The best fit of the susceptibility data results in the parameters $J = -1.1 \text{ cm}^{-1}$,

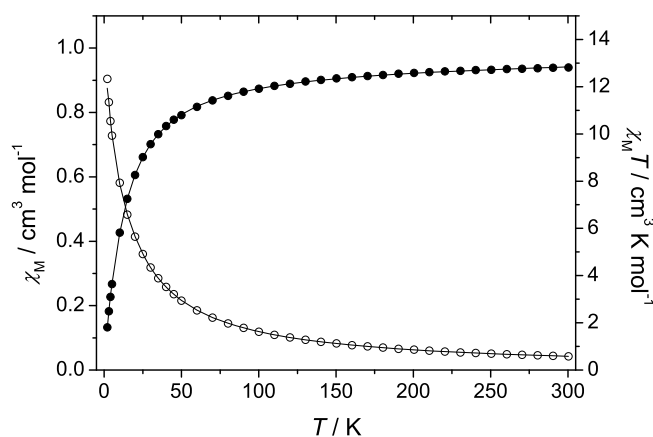


Figure 4.37: Plot of the thermal dependence of χ_M (empty circles, \circ) and $\chi_M T$ (black filled circles, \bullet) for complex Mn_3L3^{py} (**23**) measured with an applied magnetic field of 2000 Oe. The solid lines represents the best fit to the experimental data (for parameters see text).

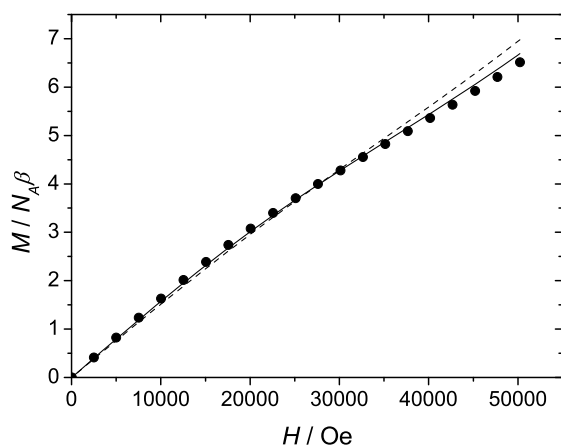


Figure 4.38: Field dependence of the magnetization for complex $\text{Mn}_3\text{L3}^{py}$ (**23**) at 2 K (\bullet). The lines represents the calculated data with the program package julX.^[238] The dashed line represents the course taken only the isotropic exchange interaction into account and the solid line considering additional ZFS with $D = 0.6 \text{ cm}^{-1}$ (for further parameters see text).

$g = 1.99$, and $\chi_{TIP} = 8.0 \cdot 10^{-4} \text{ cm}^3 \text{ mol}^{-1}$. The antiferromagnetic coupling through the N–N diazine bridges is very weak compared to all other trinuclear transition metal complexes based on triaminoguanidine. Due to these weak exchange interactions the ZFS has to be taken into account in order to reliably determine the exchange parameter.^[175,176] Inclusion of additional axial ZFS with $\hat{H}_{ZFS} = \sum_{i=1}^3 D_i [\hat{S}_{z,i}^2 - \frac{1}{3}(S_i(S_i + 1))]$ due to the pseudo C_3 symmetry of the complex results in the parameters $J = -1.1 \text{ cm}^{-1}$, $g = 1.99$, $D = 0.6 \text{ cm}^{-1}$ and $\chi_{TIP} = 7.1 \cdot 10^{-4} \text{ cm}^3 \text{ mol}^{-1}$. As expected, the inclusion of ZFS effects leads to a fit improvement. The coupling constant J and the g value are unchanged. Nevertheless, the non-zero value of D confirms the assumption of a significant ZFS contribution in this complex. It should be noted, that the sign of D can not be determined from the magnetic susceptibility data. In accordance to the very weak exchange interactions the magnetization at 2 K shows no saturation within the measured range (see figure 4.38). The isotropic splitting of the energy levels is weaker than the Zeeman splitting caused by the magnetic field. Consequently no linear dependence of the magnetization from the magnetic field is observed. The data was analyzed with the program package julX, which further confirms the presence of a weak axial ZFS. The inclusion of $D = 0.6 \text{ cm}^{-1}$ into the calculation results in an excellent agreement with the course of the experimental magnetization values (see figure 4.38).^[238]

4.5 Coordination Polymers Based on Trinuclear Complex Units with the Ligand H_2L3^{py}

4.5.1 Synthesis and Characterization

In the previous section the syntheses of various novel trinuclear complexes with the ligand H_2L3^{py} are presented which exhibit labile pyridine and chloride co-ligands accessible for ligand exchange. The isolated trinuclear complexes are fully characterized. Within this section the connection of these molecules into coordination polymers is investigated. The trinuclear complexes are exclusively cationic due to the dianionic charge of the deprotonated ligand molecule. Therefore anionic bridging co-ligands are utilized for the linkage of the triangular complex units into coordination polymers.

The oxalate dianion has been intensely studied as bridging ligand.^[254–271] A large number of bridging binding modes have been observed.^[272] Selected ones are illustrated in figure 4.39. Herein the symmetric μ -ox bidentate coordination of two metal centers (mode A) is by far the most frequently observed one. Especially in copper(II) complexes additional terminal di- or tridentate ligands with nitrogen donor atoms favors this bridging mode

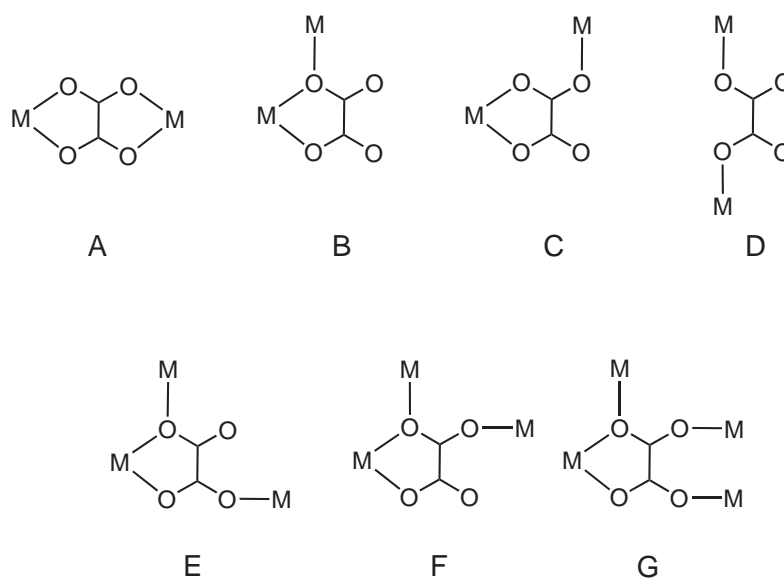


Figure 4.39: Different coordination modes of the oxalate ligand.

due to the preferred square planar or square pyramidal coordination geometry of the copper ions.^[273–275] The trinuclear copper complex $[\text{Cu}_3(\text{L}3^{py})\text{Cl}_4]$ (**18a**) possesses weakly bound chloride ions in combination with free apical coordination sites at two copper centers, which are accessible for the coordination of bis-chelating co-ligands. Therefore the oxalate dianion should be suitable to cross-link the trinuclear copper complex units into a coordination polymer.

The reaction of the copper complex **18a** with sodium oxalate in water-ethanol-mixture results in the formation of green crystals suitable for X-ray crystallography. These are obtained through addition of the complex into a refluxing solution of sodium oxalate. Slowly cooling of the reaction mixture yielded the polymer complex $\{[\text{Cu}_3(\text{L}3^{py})(\mu\text{-ox})(\text{ox})(\text{H}_2\text{O})_2]\}_n$ ($\{\text{Cu}_3\text{L}3^{py}\}_n$) (**24**). Herein the chloride ions are replaced by oxalate dianions coordinated in a bridging mode (mode A) to two copper centers. Moreover within the trinuclear subunits one oxalate is coordinated to one copper center as terminal capping ligand counterbalancing the positive charge. This leads to the formation of a neutral oxalato-bridged 1D chain built up of trinuclear complex molecules.

The complex was also characterized by IR spectroscopy and elemental analysis. The crystals stay intact after isolation from the reaction mixture without losing the co-crystallized solvents. This is confirmed by the elemental analysis data. The IR spectrum shows two strong broad bands at 1646 cm^{-1} and 1419 cm^{-1} which can be attributed to the asymmetric and symmetric stretching vibration of the oxalate anion ($\tilde{\nu}_{\text{COO}^-}$). The $\tilde{\nu}_{\text{C=N}}$ stretching vibration is observed at 1608 cm^{-1} only slightly shifted compared to the trinuclear copper complex **18a** at 1606 cm^{-1} . All other characteristic bands are also only slightly shifted.

The second bridging co-ligand is the bis(pyridin-2-ylcarbonyl)-amine (Hbpca) which provides two different binding pockets, an oxygen rich double-chelating acetylacetonone-like and a nitrogen rich tris-chelating terpyridine-like binding pocket accessible after deprotonation (see figure 4.40). The reaction with various different transition metal ions results in the formation of mononuclear complexes of the general formula $[\text{M}(\text{bpca})_2]$.^[239,276–278] Exciting reports show that this simple complex can be successfully used as ligand for the coordination of further metal ions, due to the free acetylacetonone-like chelating binding

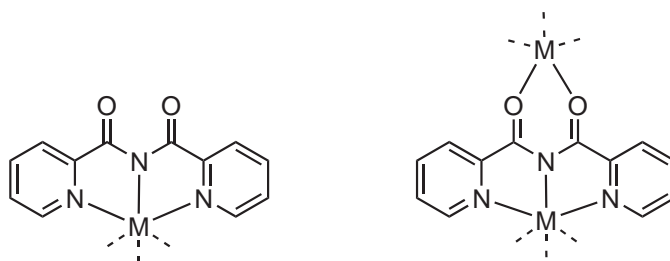


Figure 4.40: The terminal tris-chelating terpyridine-like coordination and the bridging coordination modes of the anionic bpca ligand.

pockets leading to extended structural assemblies in a controlled manner.^[239,241,279,280] Moreover coordination polymers are also accessible.^[281–283] In all previous mentioned compounds the bpca ligand mediates rather efficient magnetic exchange interactions between the bridged coordinated metal ions. Indeed some of these complexes are highly attractive showing single-molecule magnet (SMM) or single-chain magnet (SCM) behavior.^[284–286]

The trinuclear nickel complex $[Ni_3(L3^{py})(bpca)_3]PF_6$ (**21**) providing three free acetylacetonone-like chelating binding pockets was studied towards the coordination of metal ions. This should lead either to hexanuclear complexes under addition of capping co-ligands or coordination polymers.

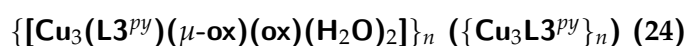
As a potential access to hexanuclear complexes, 1,1,1,5,5,5-hexafluoroacetylacetonone (Hhfac) was used as capping co-ligand. The reaction with cobalt(II) or manganese(II) ions leads to the formation of a neutral mononuclear complex with the general constitution $[M(hfac)_2(H_2O)_2]$ with two *cis*-positioned water molecules at the metal centers.^[287,288] These can be easily replaced by stronger mono- and bidentate ligands. Thus, the subsequent reaction with the trinuclear nickel complex **21** should result in a hexanuclear complex. Unfortunately this was not the case. No reaction was observed. Other approaches utilizing the corresponding lanthanide complexes of the general constitution $[M(hfac)_3(H_2O)_2]$ were also not successful.^[289] Only the trinuclear nickel precursor complex was isolated. This can be attributed to steric effects between the hfac co-ligands and the pyridine side chains of the central triaminoguanidine-based ligand. Therefore the direct linkage of the trinuclear nickel complex molecules with *3d*-transition metal(II) ions was carried out. Again no coordination of a metal ion was observed. Only the trinuclear nickel complex was isolated after reaction.

Most transition metal ions are not very flexible concerning their coordination geometry. Predominantly an octahedral or tetrahedral geometry is preferred. Moreover the charge of the resulting coordination polymer might be too high, due to the cationic nature of the trinuclear nickel(II) precursor. Therefore sodium ions with their monoanionic nature together with a high flexible coordination geometry were tested as linkers. Especially in the case of vacant carbonyl groups intriguing supramolecular assemblies have been reported wherein sodium ions cross-link metal complexes of different nuclearity into 1D chains, 2D layers and 3D networks.^[63,290–292]

The reaction of the in situ prepared trinuclear nickel complex $[\text{Ni}_3(\text{L}3^{py})(\text{bpca})_3]\text{Cl}$ with two equivalents of sodium perchlorate monohydrate led to the formation of red crystals of $\{[\text{Ni}_3(\text{L}3^{py})(\text{bpca})_3]\text{Na}(\text{ClO}_4)_2(\text{H}_2\text{O})_2\}_n$ ($\{\text{Ni}_3\text{L}3^{py}\}_n$) (**25**). The sodium ions cross-link the trinuclear nickel complexes through coordination at the carbonyl groups resulting in a 3D network.

The complex was characterized by X-ray structural analysis, elemental analysis and IR spectroscopy. The crystals remained intact after isolation and subsequent drying in air without losing the coordinated as well as co-crystallized water molecules. This is also confirmed by the elemental analysis data. The co-crystallized water molecules are highly disordered over several positions, which have not been fully resolved during structural analysis. Consequently the slightly higher water content found in the elemental analysis can be ascribed to this, which is in agreement with the thermogravimetric analysis data. The IR spectrum shows all bands of the trinuclear nickel complex $\text{Ni}_3\text{L}3^{py}(\text{bpca})_3$ (**21**), except the PF_6 stretching vibration. Moreover these are situated at nearly the same wave number, except the carbonyl band of the co-ligands. This band is slightly shifted from 1695 cm^{-1} in complex **21** to 1690 cm^{-1} caused by the coordination of the sodium ions. An additional broad band centered at about 1093 cm^{-1} is observed, which can be assigned to the stretching vibration of the perchlorate counterions.

4.5.2 Crystal Structures



The complex $\{\text{Cu}_3\text{L}3^{py}\}_n$ (**24**) crystallizes in the triclinic space group $P\bar{1}$ forming an one-dimensional coordination polymer built up by the trinuclear complex entities

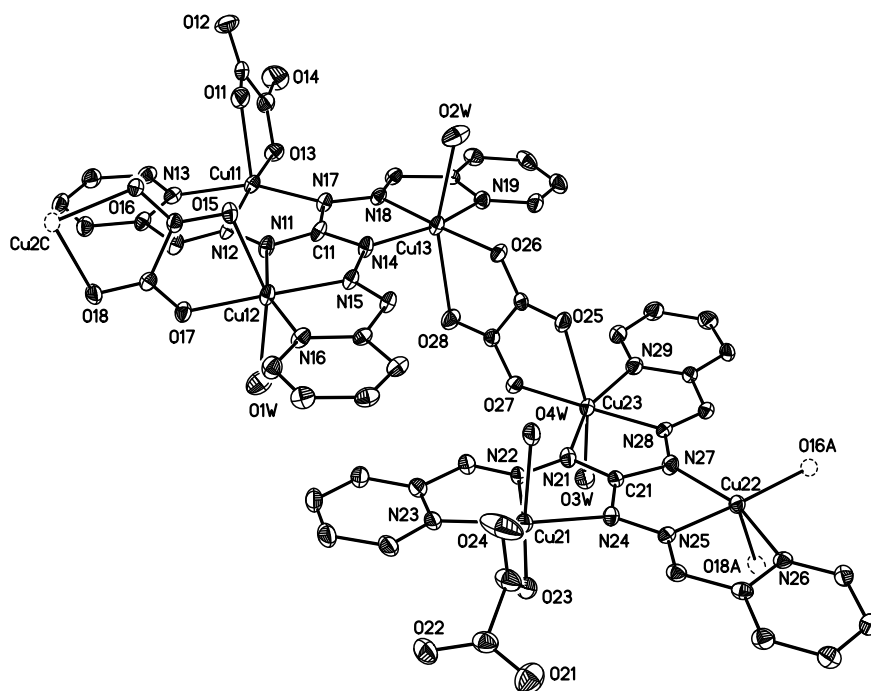


Figure 4.41: Structure of the asymmetric unit of the coordination polymer $\{Cu_3L3^{py}\}_n$ (**24**). Thermal ellipsoids are drawn at the 30% probability level. The co-crystallized solvent molecules and hydrogen atoms are omitted for clarity. Symmetry-related atoms are labeled with the suffix A and C.

$[Cu_3(L3^{py})(\mu\text{-ox})(\text{ox})(H_2O)_2]$. These are linked by a bridging oxalate. The molecular structure of the asymmetric unit as well as the atom numbering scheme of the heteroatoms is illustrated in figure 4.41.

The repeating unit contains six crystallographically independent copper atoms embedded in two ligands. The three binding sites of each triaminoguanidine-based ligand are occupied by the copper ions Cu_j1 , Cu_j2 , and Cu_j3 ($j = 1, 2$; running number assigned to the independent ligand moieties). The copper ions $Cu12$, $Cu13$, and $Cu23$ are placed in a distorted octahedral coordination geometry, whereas the copper ions $Cu11$, $Cu21$, and $Cu22$ possess a distorted square pyramidal coordination geometry. Three equatorial positions at each copper center are occupied by the nitrogen donor atoms of the ligand molecule coordinating in the classical tris-chelating manner. The fourth equatorial and one axial position of the copper centers $Cu12$, $Cu13$, $Cu22$, and $Cu23$ are occupied by the oxygen atoms of the bridging oxalate which leads to the formation of 1D chains. Furthermore the second axial position of $Cu12$, $Cu13$, and $Cu23$ are occupied by a water molecule

resulting in a distorted octahedral geometry. The copper centers Cu11 and Cu21 are each coordinated by a capping oxalate. The distorted square-pyramidal coordination geometry of Cu11 is completed by the oxygen atoms of the oxalate molecule, whereas Cu21 is coordinated only in the equatorial position. The apical position is occupied by a water molecule.

Selected bond lengths and angles for complex $\{\text{Cu}_3\text{L3}^{py}\}_n$ are summarized in table 4.13. Due to the rigid and planar coordination mode of the triaminoguanidine ligand the structural parameters of the equatorial coordination planes of all six copper centers are very similar. Significant variations are only found for the axial donors. The donor-copper distances within the tetragonal planes are similar for both complex entities and each copper ion ranging from 195 to 203 pm. Herein the distances to the nitrogen donor atoms of the ligand binding pockets are nearly the same to complex $\text{Cu}_3\text{L3}^{py}$ (18). The axial bond lengths vary from 217 to 250 pm and are significantly longer caused by the weaker coordination of the water molecules and the typical Jahn-Teller distortion of the copper(II) ion. The distance to the oxygen atom of the capping oxalate molecule is rather short with 217 pm (Cu11–O11) compared to both bridging oxalate ranging from 226 to 250 pm. Furthermore the bond lengths to the water molecules differ only slightly ranging from 232 to 239 pm.

The copper centers Cu11 and Cu21, coordinated by a capping oxalate molecule, are displaced out of the equatorial plane by 18 pm. The other copper centers are well arranged within their corresponding planes with a minimal displacement of less than 7 pm. Hence the Cu–N–N–Cu torsion angles are very similar varying between 172° and 180° which is consistent with the expected planarity of the ligand (see table 4.14). The *trans* angles within the tetragonal planes of each copper ion range from 156° up to 178° indicating a slight tetrahedral distortion. Furthermore the axial *trans* angles in the octahedra of Cu12, Cu13, and Cu23 vary between 155° and 161° indicating an additional axial distortion. Within the 1D polymer the trinuclear complex entities are nearly coplanar with a dihedral angle of 4° concerning the best least square plane defined by all ligand atoms. The chains run along the [110] direction of the unit cell. These are linked to double-chains through weak axial contacts between the copper center Cu2 and the oxalate oxygen atom O16 of an adjacent chain with a distance of 276 pm (see figure 4.42). This leads to short intermolecular Cu22...Cu22A separations of 359 pm compared to the nearly equal separations within the trinuclear complex moieties of about 490 pm. The non-covalent dis-

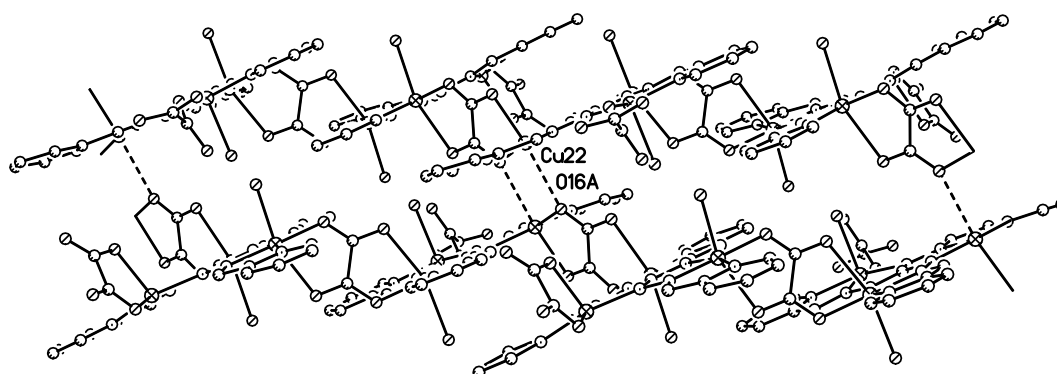
Table 4.13: Selected bond lengths [pm] and angles [$^\circ$] for complex $\{Cu_3L3^{py}\}_n$ (**24**).

Cu11–O11	216.8(5)	Cu21–O23	192.9(4)
Cu11–O13	195.2(4)	Cu21–O4W	233.8(4)
Cu11–N12	196.0(5)	Cu21–N22	195.2(5)
Cu11–N13	203.4(5)	Cu21–N23	203.0(5)
Cu11–N17	200.3(4)	Cu21–N24	199.9(4)
Cu12–O17	196.2(4)	Cu22–O16A	196.7(3)
Cu12–O15	250.1(6)	Cu22–O18A	225.9(4)
Cu12–O1W	239.3(5)	Cu22–N25	195.3(4)
Cu12–N11	199.6(5)	Cu22–N26	202.7(5)
Cu12–N15	196.2(4)	Cu22–N27	199.6(5)
Cu12–N16	202.0(5)	Cu23–O25	239.3(4)
Cu13–O26	195.5(4)	Cu23–O27	196.6(4)
Cu13–O28	240.2(4)	Cu23–O3W	235.7(5)
Cu13–O2W	232.4(5)	Cu23–N21	199.4(5)
Cu13–N14	201.6(4)	Cu23–N28	197.5(4)
Cu13–N18	197.1(5)	Cu23–N29	202.1(5)
Cu13–N19	203.0(5)		
O13–Cu11–N12	170.63(19)	O23–Cu21–N22	167.31(19)
N13–Cu11–N17	155.74(20)	N23–Cu21–N24	158.71(22)
O15–Cu12–O1W	154.74(15)	O16A–Cu22–N25	170.90(18)
O17–Cu12–N15	177.97(19)	N26–Cu22–N27	159.88(18)
N11–Cu12–N16	158.68(18)	O25–Cu23–O3W	161.46(15)
O26–Cu13–N18	177.76(18)	O27–Cu23–N28	177.67(19)
O28–Cu13–O2W	159.86(16)	N21–Cu23–N29	158.56(19)
N14–Cu13–N19	157.52(19)		

Table 4.14: Selected interatomic distances [pm] and torsion angles [°] for both independent complex molecules in polymer complex $\{\text{Cu}_3\text{L3}^{py}\}_n$ (**24**).

Cu11···Cu12	486.3	Cu21···Cu22	484.0
Cu11···Cu13	488.4	Cu21···Cu23	487.9
Cu12···Cu13	488.2	Cu22···Cu23	487.9
Cu13···Cu23	562.3	Cu22···Cu12	561.9
Cu11–N12–N11–Cu12	179.9	Cu21–N24–N25–Cu22	171.5
Cu11–N17–N18–Cu13	179.1	Cu21–N22–N21–Cu23	171.9
Cu12–N15–N14–Cu13	171.8	Cu22–N27–N28–Cu23	179.7

tances through the oxalate bridges are clearly longer with about 562 pm. The 1D chains are further linked through strong hydrogen bonding interactions established between the oxalate oxygen atom O22 and the coordinated water molecule O3W of adjacent chains in a distance of 268 pm. This is shown in figure 4.43. Moreover additional interchain hydrogen bonding interactions are established including the co-crystallized water and ethanol molecules. This leads to the formation of an extended 3D hydrogen bonding network.

**Figure 4.42:** Supramolecular double-chains of the 1D coordination polymer $\{\text{Cu}_3\text{L3}^{py}\}_n$ (**24**). Solvent molecules and hydrogen atoms are omitted for clarity. Dashed lines indicate weak inter-chain interactions between the copper center Cu22 and the oxalate oxygen atom O16 with a distance of 275.9 pm.

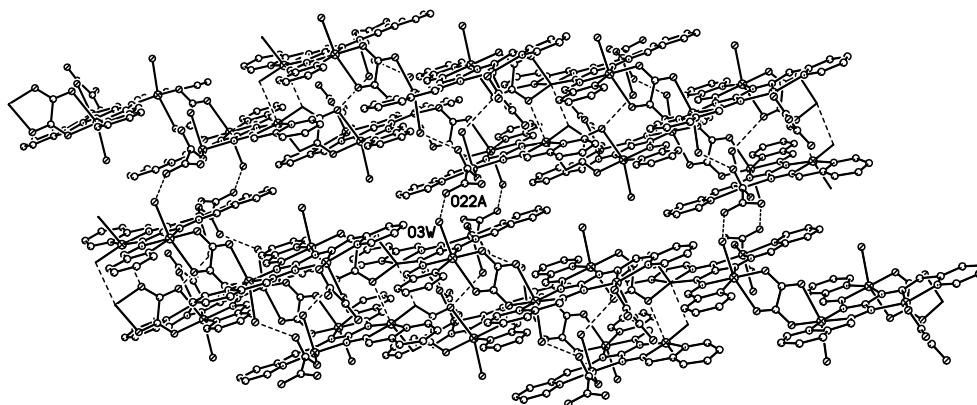
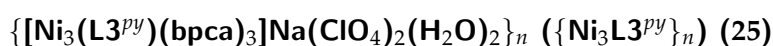


Figure 4.43: Supramolecular structure of the 1D coordination polymer $\{Cu_3L3^{py}\}_n$ (**24**). Solvent molecules and hydrogen atoms are omitted for clarity. Dashed lines indicate hydrogen bonding interactions. Pertinent distance: $O3W \cdots O22A$ 268.4 pm.



The complex $\{Ni_3L3^{py}\}_n$ (**25**) crystallizes in the monoclinic space group $P2_1/c$. The cationic trinuclear nickel complex units $[Ni_3(L3^{py})(bpca)_3]^+$ are cross-linked through sodium ions coordinated to the carbonyl oxygen atoms of the bpca co-ligands forming a 3D network. The molecular structure of the asymmetric unit containing six crystallographically independent nickel atoms embedded in two ligands together with two sodium ions, four perchlorate and four water molecules is shown in figure 4.44.

As expected the trinuclear complex cations are almost identical to complex $Ni_3L3^{py}(bpca)_3$ (**21**) with very similar bond lengths and angles. Again three nickel ions are coordinated by the triaminoguanidine ligand linked through N–N diazine bridges under formation of an equilateral triangle. The octahedral coordination environment of each nickel ion is completed by a bpca co-ligand. These trinuclear cationic molecules are cross-linked through coordination of the sodium ions to the carbonyl oxygen atoms of the bpca co-ligands. Three cationic trinuclear complex molecules are assembled around each sodium ion, two in the bidentate and one in a monodentate binding mode, resulting in a 3D network depicted in figure 4.45.

The contacts of the sodium ions are summarized in table 4.15. Each of the two independent sodium atoms is surrounded by six oxygen donor atoms, five carbonyl as well as an additional water molecule O1W at the sodium atom Na1 and a perchlorate ion O21P at the sodium atom Na2. The distances to the carbonyl oxygen donor atoms range from

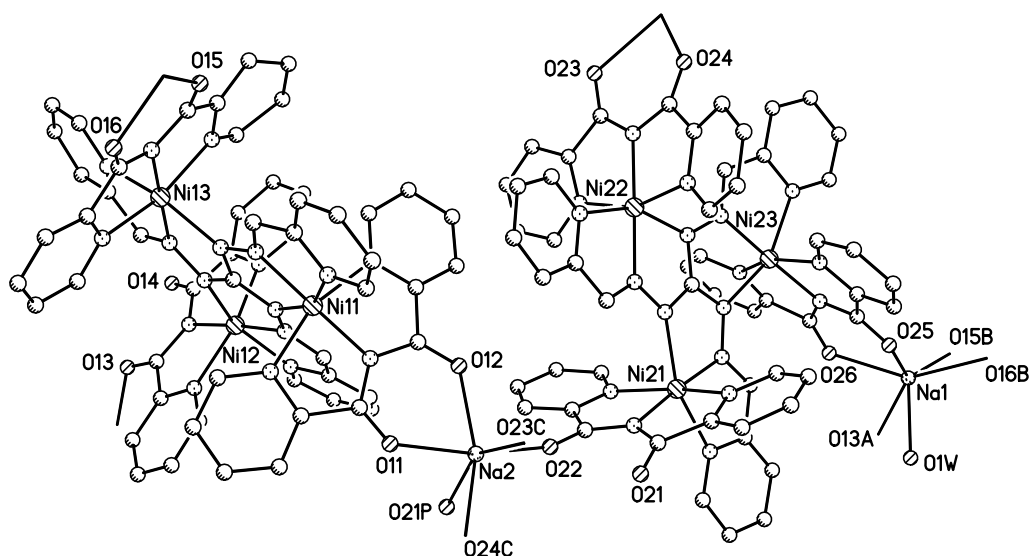


Figure 4.44: Structure of the asymmetric unit of complex $\{\text{Ni}_3\text{L3}^{py}\}_n$ (**25**). The non-coordinating perchlorate ions as well as water molecules are omitted for clarity. The hydrogen atoms are also not shown. Symmetry-related atoms are labeled with the index A to C. O21P denotes the oxygen atom of the coordinated perchlorate ion and O1W the coordinated water molecule.

233 to 253 pm for Na1 and are somewhat longer compared to them of the Na2 ranging from 226 to 243 pm. Moreover the water molecule is coordinated at a distance of 242 pm, whereas the perchlorate oxygen atom, disordered over two positions, exhibits larger distances of 255 and 259 pm, respectively. The network is very compact and the remaining perchlorate counterions as well as water molecules occupy the small void.

Table 4.15: Sodium donor distances [pm] in complex $\{\text{Ni}_3\text{L3}^{py}\}_n$ (**25**). Symmetry equivalent atoms are labeled with suffix A to C. O21P denotes the perchlorate oxygen atom disordered over two close together lying positions.

Na1–O13A	253.3(3)	Na2–O11	227.2(3)
Na1–O15B	233.4(3)	Na2–O12	236.9(3)
Na1–O16B	238.4(3)	Na2–O22	225.5(4)
Na1–O25	235.4(4)	Na2–O23C	243.2(4)
Na1–O26	236.3(3)	Na2–O24C	238.4(4)
Na1–O1W	241.8(5)	Na2–O21P	258.7(19)/254.1(26)

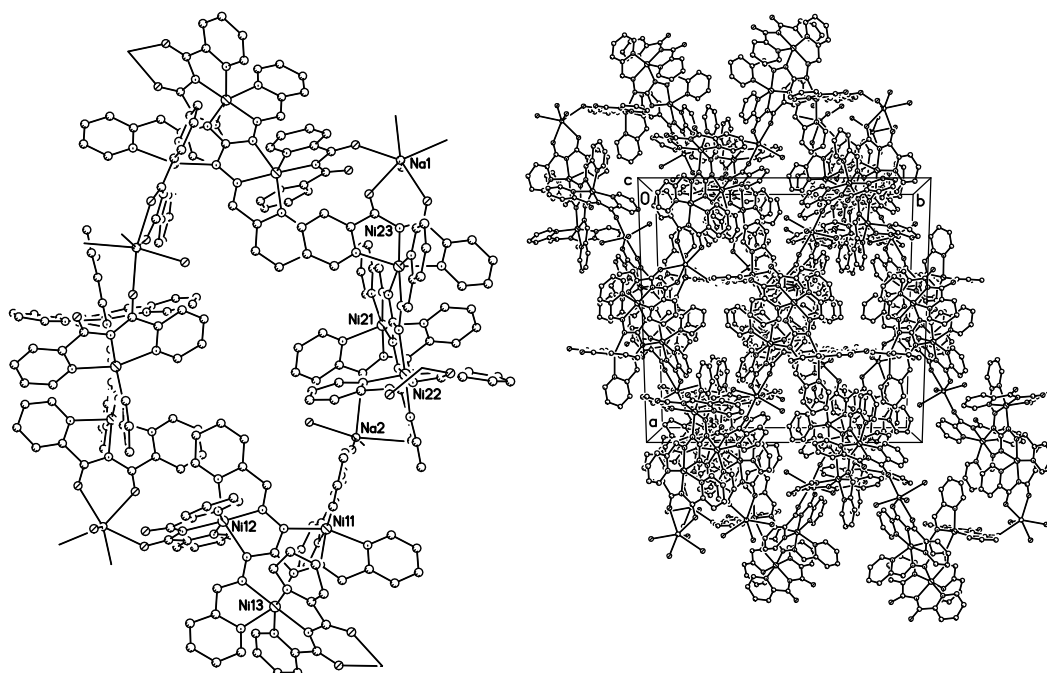


Figure 4.45: Polymer structure of complex $\{Ni_3L3^{py}\}_n$ (25). The non-coordinating perchlorate ions as well as water molecules are omitted for clarity. The hydrogen atoms are also not shown.

4.5.3 Magnetic Properties

For the coordination polymer $\{Cu_3L3^{py}\}_n$ (24) the temperature dependence of the paramagnetic molar susceptibility χ_M , which is based on the constituting trinuclear building block, and its product with temperature $\chi_M T$ are depicted in figure 4.46. At 300 K the $\chi_M T$ value is $0.69 \text{ cm}^3 \text{ K mol}^{-1}$, which is far from the expected spin-only value for three independent copper(II) centers with $S = 1/2$. Upon cooling the $\chi_M T$ value rapidly decreases to $0.43 \text{ cm}^3 \text{ K mol}^{-1}$ at 75 K and then slightly decreases to $0.40 \text{ cm}^3 \text{ K mol}^{-1}$ at 25 K. The lower room temperature value together with the gradual decrease is indicative for strong antiferromagnetic exchange interactions. The value of the plateau is in good agreement with the spin-only value of one single spin $S = 1/2$, confirming the antiferromagnetic exchange. Below 25 K the experimental $\chi_M T$ value also decrease rapidly, indicating an additional antiferromagnetic exchange interaction.

This overall course of the experimental data is very similar to the trinuclear copper complex Cu_3L3^{py} (18). Moreover from the observed plateau in the $\chi_M T = f(T)$ plot it is

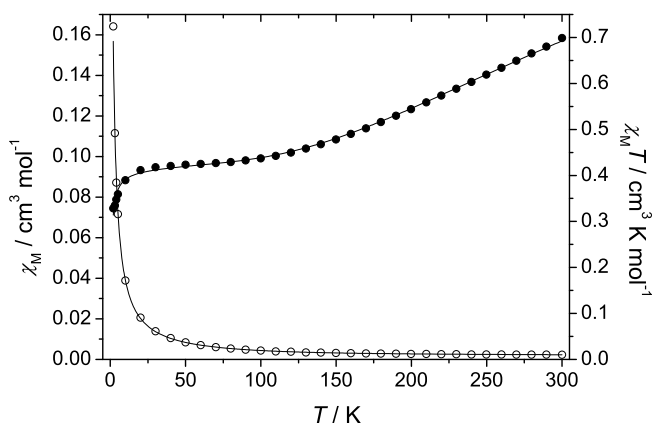


Figure 4.46: Plot of the thermal dependence of χ_M (empty circles, \circ) and $\chi_M T$ (black filled circles, \bullet) for complex $\{\text{Cu}_3\text{L3}^{py}\}_n$ (**24**) measured with an applied magnetic field of 2000 Oe. The corresponding fit functions according to equation 4.13 are drawn as solid lines (for parameters see text).

evident, that the magnetic interactions within the trinuclear copper units dominate the system and that the coupling through the oxalate bridges must be considerably lower in magnitude. The oxalato-bridged copper centers possess a Jahn-Teller distorted (4+2) octahedral coordination geometry. Due to the nearly perpendicular arrangement of the oxalate bridges with respect to the cheating ligand plane, these are not capable to transmit an efficient overlap between the relevant magnetic orbitals of the two copper(II) centers.^[255] Hence the magnetic interaction is negligible weak. Therefore the coordination polymer can be treated as an isolated trinuclear copper complex. Within the trinuclear units the copper centers are arranged in an almost equilateral triangle linked through the N–N diazine bridges of the triaminoguanidine-based ligand. The corresponding spin Hamiltonian $\hat{H} = -J(\hat{S}_1\hat{S}_2 + \hat{S}_1\hat{S}_3 + \hat{S}_2\hat{S}_3)$ with $S_1 = S_2 = S_3 = 1/2$ leads to the analytical expression given in equation 4.13 under consideration of additional temperature independent paramagnetism (χ_{TIP}) and intermolecular exchange interactions (θ).

$$\chi_M = \frac{N_A \beta^2 g^2}{4k(T - \theta)} \frac{5 + \exp(-3J/2kT)}{1 + \exp(-3J/2kT)} + \chi_{TIP} \quad (4.13)$$

The best fit of the experimental data set for the theoretical expression given in equation 4.13 results in parameters $J = -282(9) \text{ cm}^{-1}$, $g = 2.13(1)$, $\theta = -0.34(4) \text{ K}$, and $\chi_{TIP} = 3.0(6) \cdot 10^{-4} \text{ cm}^3 \text{ mol}^{-1}$ with $r^2 = 0.99712$.

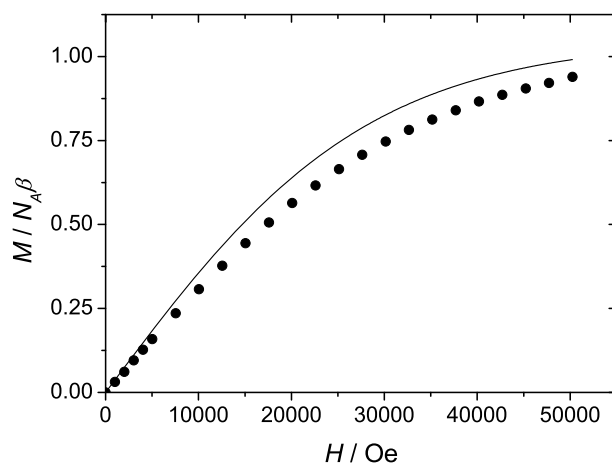


Figure 4.47: Field dependence of the magnetization for complex $\{Cu_3L3^{py}\}_n$ (**24**) at 2 K (\bullet). The Brillouin function for $S = 1/2$ and $g = 2.13$ is plotted as solid line.

Due to the very good agreement of the calculated curve with the experimental data, the interaction through the oxalate bridges is negligible, as assumed. Analogous to the trinuclear copper complex Cu_3L3^{py} (**18**) very strong antiferromagnetic exchange interactions are present between the three copper centers leading to an $S = 1/2$ within each trinuclear unit. This is confirmed by magnetization measurements at 2 K shown in figure 4.47. Furthermore the other parameters are very similar. The θ is smaller due to the larger separation between the trinuclear units in the polymer chains. In addition to this the θ might be also ascribed to very weak interchain interactions between the trinuclear complex moieties mediated through the oxalate bridges.

The strong antiferromagnetic interaction within the trinuclear complex moieties leads to spin frustration of the resulting $S = 1/2$ spin. Hence this complex might also be another interesting target as a qubit in the field of quantum computation.^[84,85,144,145,147]

5 Conclusion

This thesis comprises the targeted synthesis and characterization of trinuclear transition metal complexes of C_3 symmetric ligands. In certain cases the defined linkage of these complexes was successful utilizing different *step-by-step* synthetic strategies. The complexes were characterized with respect to their magnetic properties. Three different types of bridging ligands based on phloroglucinol, triaminobenzene and triaminoguanidine were utilized. According to the bridging units this thesis can be divided into three parts.

Phloroglucinol-bridged complexes: Chapter 2 describes the synthesis and characterization of a series of trinuclear phloroglucinol-bridged copper(II) and nickel(II) complexes. Various Schiff-base ligands were synthesized differing in the donor atoms in the ligand side chains as shown in figure 5.1. Planar trinuclear copper(II) complexes were obtained and assemble into 1D networks through weak coordination of adjacent trinuclear complex molecules in the axial positions of the copper centers. The synthesis of trinuclear octahedral nickel(II) complexes was successful by the addition of tris-chelating co-ligands.

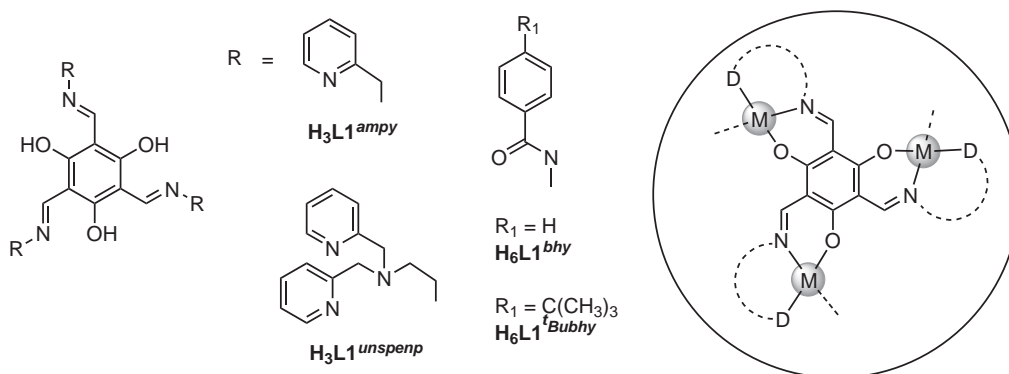


Figure 5.1: Synthesized phloroglucinol-based ligands. Circled: Schematic representation of the trinuclear core unit in the transition metal complexes.

Moreover the use of the ligand $\text{H}_3\text{L1}^{unspenp}$ offers direct access to the trinuclear complex without the addition of a co-ligand. The structural analysis of all complexes reveal that the core is based on a *meta*-phenylene arrangement of three metal ions linked through a central phloroglucinol backbone.

The hydrazide based ligands $\text{H}_3\text{L1}^{bhy}$ and $\text{H}_3\text{L1}^{tBubhy}$ are further suitable for the coordination of trivalent metal ions due to additional acidic amide protons within the ligand side chains. Based on this the first phloroglucinol-bridged trinuclear cobalt(III) complex was synthesized and structurally characterized.

Temperature dependent magnetic measurements of the complexes show predominantly weak antiferromagnetic exchange interactions between the three metal centers, which is contrary to the expectations from spin polarization between *meta*-phenylene-bridged metal ions. Due to the almost orthogonal orientation of the magnetic orbitals in relation to the bridging π -system, only an indirect spin polarization exchange is present which is less effective. The competing superexchange interaction predominately led to antiferromagnetic interactions. Moreover in the nickel complexes strong zero-field splitting is observed due to the distorted octahedral coordination geometry, significantly stronger than the isotropic exchange interactions. Nevertheless only a slight deviation from the planarity within one trinuclear copper(II) complex strengthens the exchange through spin polarization and led to overall weak ferromagnetic exchange interactions.

Triaminobenzene-bridged complexes: As a continuation of the approach utilized in the previous chapter with *meta*-phenylene-bridging arrangement of three metal centers, triaminobenzene was applied in *chapter 3*. Two different types of ligands were synthesized with one additional donor atom within each side chain; the Schiff-base ligand $\text{H}_3\text{L2}^{tBusal}$ and the amide ligand $\text{H}_3\text{L2}^{pic}$ shown in figure 5.2. The reaction with copper(II) ions provided a directed access to two different complex topologies. A C_3 symmetric trinuclear and a centrosymmetric dinuclear metallamacrocyclic complex was obtained depending on the dimension of the formed chelate rings upon coordination of the copper(II) ions. The five-membered chelate rings led to a *syn*-orientation of the aromatic bridging units whereas six-membered ones favored the *anti*-arrangement (see figure 5.2).

The ligand $\text{H}_3\text{L2}^{pic}$ formed a C_3 symmetric trinuclear metallamacrocyclic complex, wherein three copper centers are chelated and bridged by two ligand molecules. The

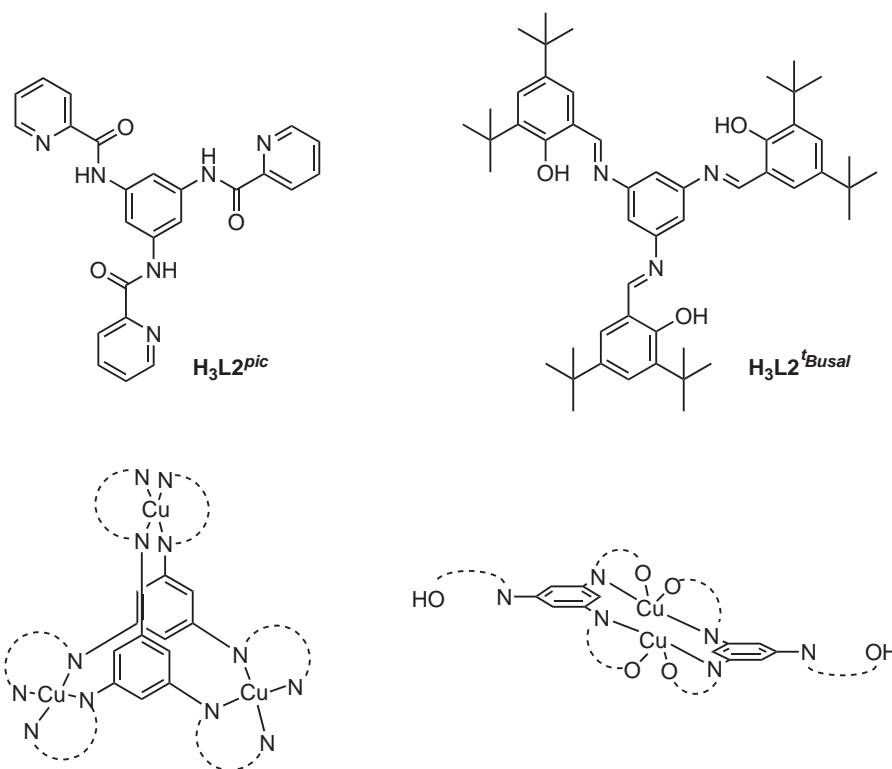


Figure 5.2: Schematic representation of the triaminobenzene-based ligands, shown on top of the figure, and the resulting two different copper complex structures. Left: Trinuclear 1,3,5-metallacyclophane structure with *syn*-oriented bridging benzene rings. Right: Dinuclear metallamacrocyclic complex with *anti*-oriented bridging benzene rings.

stoichiometric reaction led to the programmed *syn*-arrangement of two ligands resulting in a rare example of a 1,3,5-metallacyclophane. Due to the rigid nature of the ligand in connection with steric effects of the side chains, the copper centers exhibit a distorted tetragonal coordination geometry almost half way between square pyramidal and tetrahedral. Dimethylsulfoxide molecules are additionally weakly bound leading to a rather unusual highly distorted (4+1) coordination geometry of each copper center.

Besides, a novel tetranuclear metallamacrocycle complex of the amide ligand H_3L2^{pic} is obtained through self-assembly process. Two copper centers are coordinated by two ligands in a highly distorted coordination geometry analogous to them in the trinuclear complex. Moreover the two other copper centers are coordinated by the ligands, each within one binding pocket, and further linked through an asymmetrical di- μ -OH- $\mu_{1,3}$ -N₃-bridge. These possess a square pyramidal coordination geometry.

Temperature-dependent magnetic measurements revealed ferromagnetic exchange interactions in both complexes resulting from the spin polarization. Compared to the phloroglucinol-bridged complexes the couplings are clearly stronger. Within the 1,3,5-metallacyclophane the coupling is quite strong with $J = +25 \text{ cm}^{-1}$. Up to now this is by far the strongest coupling which has been reported for a complex resulting from the spin polarization. Within the tetranuclear complex the asymmetrical double-bridge causes a very strong antiferromagnetic exchange interaction between the two copper ions with $J < -1000 \text{ cm}^{-1}$. Again both other copper ions are strongly ferromagnetic coupled with $J = +18 \text{ cm}^{-1}$.

In contrast the Schiff-base ligand $\text{H}_3\text{L}2^{\text{Busal}}$ forms a dinuclear metallamacrocyclic copper complex wherein the bridging phenylene rings are *anti*-oriented. Similarly both copper centers exhibit a highly distorted tetragonal coordination geometry nearly half between square pyramidal and tetrahedral. Moreover the third binding pocket of each ligand remains unoccupied without hydrolysis.

This complex provides an easy access to tetranuclear complexes due to the two free binding pockets. The reaction with copper(II) ions under addition of the co-ligand 1,1,1,5,5,5-hexafluoroacetylacetone (Hhfac) resulted in the formation of a tetranuclear complex.

A metallamacrocyclic dinuclear cobalt(II) complex was also synthesized similar to the dinuclear copper(II) complex. Herein both cobalt centers are coordinated by two ligand molecules in a distorted tetrahedral geometry.

Again temperature-dependent magnetic measurements in both copper complexes revealed ferromagnetic exchange interactions as a result of the spin polarization. The exchange interactions are weaker with J values ranging from $+1.5$ up to $+12.0 \text{ cm}^{-1}$ compared to those in the copper(II) complexes with the amide ligand. In contrast to this very weak antiferromagnetic couplings with J close to zero are observed in the cobalt(II) complex. Additionally a large zero-field splitting with $|D| = 20 \text{ cm}^{-1}$ is observed within the complex, resulting from the distorted tetrahedral coordination geometry of the cobalt centers.

Triaminoguanidine-bridged complexes: *Chapter 4* describes the synthesis of trinuclear transition metal complexes based on triaminoguanidine and the defined linkage of these

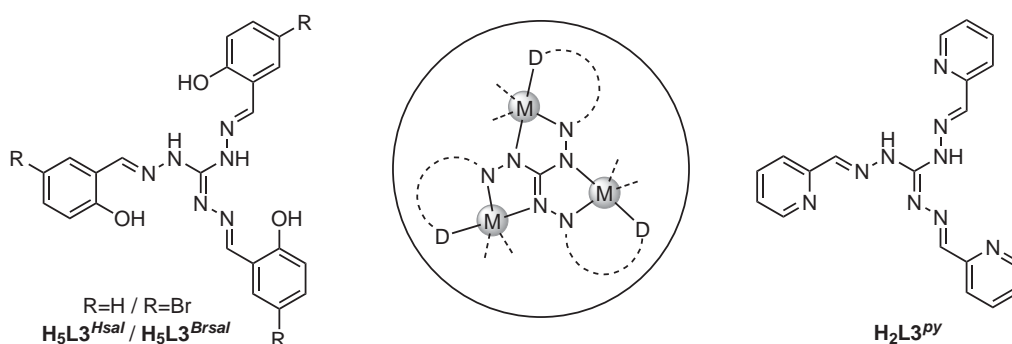


Figure 5.3: Triaminoguanidine-based ligands used in this work. Circled: Schematic representation of the trinuclear core unit in transition metal complexes.

trinuclear subunits into oligonuclear complexes as well as coordination polymers. Beside the known triple Schiff-base ligands $\mathbf{H}_5\mathbf{L3}^{Hsal}$ and $\mathbf{H}_5\mathbf{L3}^{Brsal}$ with salicylidene side chains, the ligand $\mathbf{H}_2\mathbf{L3}^{py}$ with pyridine side chains was synthesized all depicted in figure 5.3. The subsequent reaction with various transition metal ions under the addition of co-ligands provides an access to trinuclear complexes, wherein the metal ions are bridged in close proximity. Depending on the reaction conditions the directed synthesis of various complex topologies A to F was presented (see figure 5.4). Both bridging units utilized in the previous chapters take advantage of the spin polarization as a potential access to ferromagnetic coupled complexes. In contrast these ligands mediate exclusively anti-ferromagnetic exchange interactions through superexchange interactions over the N–N diazine bridges leading to a directed generation of magnetic molecules that show spin frustration within the $S = 1/2$ ground state.

A C_3 symmetric trinuclear iron(III) complex was prepared with the ligand $\mathbf{H}_5\mathbf{L3}^{Brsal}$ and labile pyridine and chloride co-ligands utilizing a non-conventional synthesis approach. This starts from a solution of the iron(III) chloride in pyridine. Herein pyridine simultaneously acts as solvent, base and co-ligand. In addition the chloride ions act as additional co-ligands counterbalancing the positive charged complex cation. Both co-ligands of the complex can be easily replaced providing an access to various complexes. The reaction of 8-hydroxyquinoline results in the formation of the corresponding trinuclear iron(III) complex. Moreover under addition of methanol two trinuclear iron complexes were cross-linked leading to a hexanuclear complex (schematic B in figure 5.4). Herein the subunits are connected through two methanolate bridges.

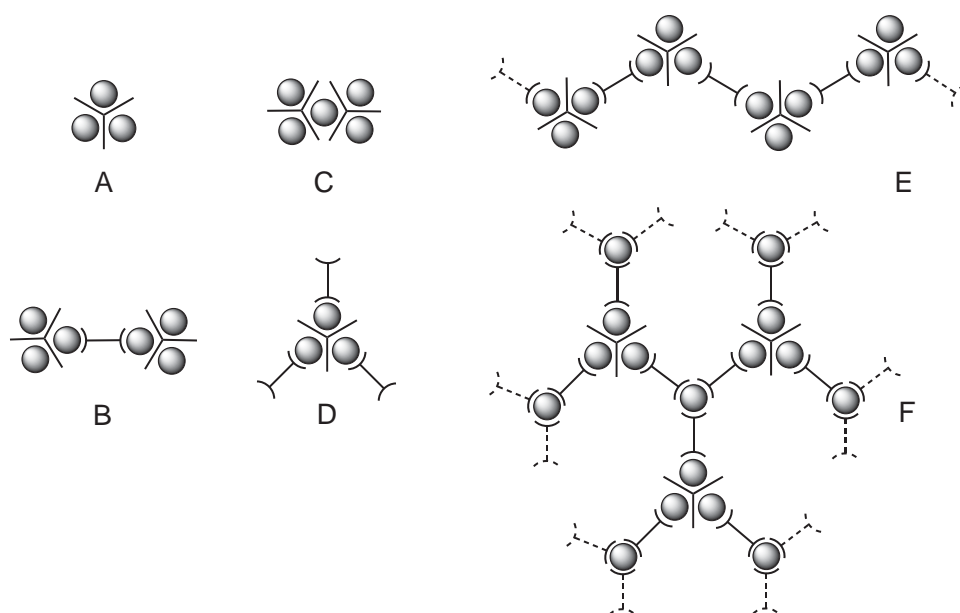


Figure 5.4: Schematic representation of the different complex topologies.

Temperature-dependent magnetic measurements reveal efficient antiferromagnetic exchange interactions within the three complexes with an $S = 1/2$ ground state for both trinuclear complexes and $S = 0$ ground state for the hexanuclear iron complex. The crystallographically C_3 symmetric iron complex possesses a spin frustrated $S = 1/2$ ground state and might provide therefore interesting electronic properties for potential applications as qubit in the research field of quantum computation.

Utilizing this ligand provides a clever access to heterometallic pentanuclear complexes. As an important result of this thesis a new facile synthetic approach towards these complexes was developed based on the stepwise deprotonation of the ligand and subsequent addition of different $3d$ -transition metal ions. The key step is the in situ formation of a mononuclear complex, wherein the metal ion is octahedrally coordinated by two ligand molecules. During complexation the metal center was oxidized leading to a higher stability of the complex against metal exchange reactions. The subsequent addition of nickel(II) ions followed by a chelating co-ligand 2,4,6-tris(2-pyridyl)-1,3,5-triazine (tptz) resulted in the pentanuclear complexes of the general formula $[M^{III}Ni^{II}_4(L3)_2(tptz)_4](ClO_4)_x(Cl)_{1-x}$ with $M = Fe, Mn, Co$. Two triangular subunits are interconnected by a common trivalent metal ion (schematic C in figure 5.4).

The ligand $\text{H}_2\text{L3}^{py}$ is accessible through Schiff-base condensation. In contrast to the known ligands providing phenolate oxygen atoms as donors within the salicylidene side chains, this ligand offers exclusively nitrogen donor atoms and therefore coordinate three metal centers in its dianionic form. A series of trinuclear $3d$ -transition metal complexes were synthesized utilizing the synthesis approach analogous to the trinuclear iron(III) complex. Complexes of copper(II), nickel(II), cobalt(II) and manganese(II) were isolated and structurally characterized. Again the metal centers are coordinatively saturated by labile chloride and pyridine co-ligands. These can be replaced by other ligands thus offering an access to various complexes. Besides other trinuclear complexes, the linkage into coordination polymers was realized.

The substitution of these labile co-ligands was verified on the nickel complex. The reaction with azide ions resulted in substitution of the coordinated chloride ions. Moreover the use of the co-ligand bis(pyridin-2-ylcarbonyl)-amine (Hbpca) yielded the trinuclear complex, wherein all pyridine and chloride ions were replaced by the co-ligands. This complex possess three free acetylacetonelike binding pockets derived from the coordinated co-ligand (schematic D in figure 5.4). The complex was cross-linked through sodium ions leading to a 3D network (schematic F in figure 5.4). Furthermore a 1D coordination polymer resulting from the bridging coordination of oxalate to the trinuclear copper complex units was obtained (schematic E in figure 5.4).

As expected the temperature-dependent magnetization measurements reveal exclusively antiferromagnetic exchange interactions in all complexes. The magnitude of the coupling constant J becomes smaller with the increasing spin of the transition metal ions, due to the higher number of superexchange pathways. In the copper complex the coupling is very strong with $J = -299 \text{ cm}^{-1}$ leading to a $S = 1/2$ spin ground state. The coupling within the nickel complexes with $-42 \leq J \leq -36 \text{ cm}^{-1}$ is dominated by the bridging ligand and does not reflect the change of the co-ligands. The cobalt complex shows a large zero-field splitting with $D = 27 \text{ cm}^{-1}$, significantly stronger compared to the isotropic exchange interactions of $J_1 = -18 \text{ cm}^{-1}$ and $J_2 = -12 \text{ cm}^{-1}$ within the isosceles triangle. In the manganese complex a very weak coupling is observed with $J = -1 \text{ cm}^{-1}$ together with a small zero-field splitting of $|D| = 0.6 \text{ cm}^{-1}$. Due to the very weak interactions the Zeeman splitting dominates the field-dependent magnetization resulting in a non linear increase without reaching the saturation. Both latter compounds are the first structurally and magnetically characterized triaminoguanidine-bridged cobalt and manganese complexes.

From a magnetochemical point of view, the 1D polymer copper complex behaves as a trinuclear complex due to the fact, that the oxalate bridges are perpendicular to the ligand plane. The strong coupling with $J = -282 \text{ cm}^{-1}$ within the trinuclear units leads to a $S = 1/2$ ground state of isolated copper(II) triangles. This complex therefore warrants further investigations into the spin frustration phenomenon with specific attention to the current research field of quantum computation.

In summary, new C_3 symmetric ligands mediating magnetic exchange interactions were introduced. Based on these various trinuclear transition metal complexes were prepared utilizing directed synthesis approaches. Furthermore the defined linkage of the trinuclear subunits into higher aggregates as well as coordination polymers was presented. Hence this thesis makes a considerable contribution to the directed synthesis of homo- as well as heterometallic complexes based on triangular building blocks. In addition a directed access to strongly ferromagnetic coupled high-spin compounds utilizing the spin polarization effect as well as antiferromagnetic coupled triangular compounds with a resulting $S = 1/2$ ground state was pointed out. Some of these compounds possess intriguing magnetic properties for later applications.

6 Zusammenfassung

Diese Dissertation umfasst die gezielte Synthese und Charakterisierung von dreikernigen Übergangsmetallkomplexen mit C_3 -symmetrischen Liganden. In einigen Fällen war die gezielte Verknüpfung der dreikernigen Einheiten unter Anwendung von verschiedenen *step-by-step* Synthesestrategien erfolgreich. Darüber hinaus wurden die Komplexe hinsichtlich ihren magnetischen Eigenschaften untersucht. Drei verschiedene Typen von verbrückenden Liganden basierend auf Phloroglucin, Triaminobenzen und Triaminoguanidin wurden verwendet. Bezüglich dieser verbrückenden Einheiten lässt sich die Disseration in drei Bereiche unterteilen.

Phloroglucin-verbrückte Komplexe: *Kapitel 2* beschreibt die Synthese und Charakterisierung einer Serie von dreikernigen phloroglucin-verbrückten Kupfer(II)- und Nickel(II)komplexen. Verschiedene Schiff-Base Liganden mit unterschiedlichen Donor-Atomen in den Seitenketten wurden synthetisiert, welche in *Abbildung 6.1* dargestellt sind. Planare trinukleare Kupfer(II)komplexe wurden charakterisiert, welche durch

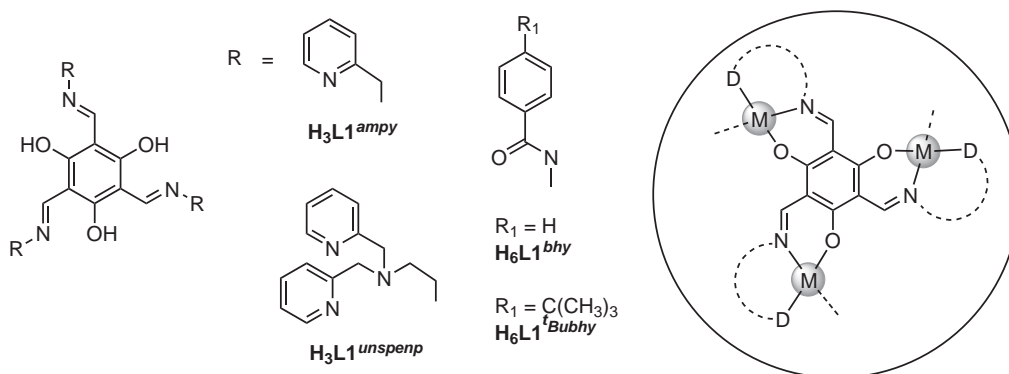


Abbildung 6.1: Synthetisierte phloroglucin-basierte Liganden. Eingekreist: Schematische Darstellung der trinuklearen Kerneinheit in den Übergangsmetallkomplexen.

schwache Koordination von benachbarten Molekülen in den axialen Positionen der Kupferionen 1D Netzwerke ausbilden. Die Darstellung dreikerniger Nickel(II)komplexe war durch Zugabe von chelatisierenden Koliganden erfolgreich. Darüber hinaus bietet der Ligand $\text{H}_3\text{L1}^{unspenp}$ einen gezielten Zugang zum entsprechenden dreikernigen Nickel(II)komplex ohne die Zugabe eines Koliganden.

Die Hydrazid-basierten Liganden $\text{H}_6\text{L1}^{bhy}$ und $\text{H}_6\text{L1}^{tBubhy}$ sind darüber hinaus aufgrund zusätzlicher azider Amidprotonen in den Ligandseitenketten geeignet, dreiwertige Metallzentren zu koordinieren. Davon ausgehend wurde der erste strukturell charakterisierte, phloroglucin-verbrückte trinukleare Kobalt(III)komplex dargestellt.

Temperaturabhängige Messungen der Magnetisierung an diesen Komplexen haben hauptsächlich antiferromagnetische Wechselwirkungen zwischen den drei Metallzentren ergeben, welche gegensätzlich zu den Erwartungen aus der Spinpolarisation zwischen *meta*-phenylen-verbrückten Metallionen sind. Aufgrund der annähernd orthogonalen Orientierung der magnetischen Orbitale bezüglich des verbrückenden π -Systems findet einzig eine indirekte Wechselwirkung über Spinpolarisation statt, die sehr schwach ist. Die konkurrierende Wechselwirkung über Superaustausch resultiert vorrangig in einer antiferromagnetischen Wechselwirkung. Daneben wird in den Nickelkomplexen eine große Nullfeldaufspaltung beobachtet, die in der verzerrten oktaedrischen Koordinationsgeometrie der Nickelzentren begründet ist. Diese ist deutlich stärker als die isotropen Wechselwirkungen über den Brückenliganden. Dennoch begünstigt innerhalb der Kupfer(II)komplexe schon eine minimale Abweichung von der Planarität die Wechselwirkungen über Spinpolarisation und führt zu schwach ferromagnetischen Kopplungen in einem Komplex.

Triaminobenzen-verbrückte Komplexe: Als eine Erweiterung der *meta*-phenylen-Verbrückung von drei Metallzentren wurde in *Kapitel 3* Triaminobenzen untersucht. Dazu wurden zwei verschiedene Typen von Liganden mit einem zusätzlichen Donoratom in jeder Seitenkette synthetisiert; der Schiff-Baseligand $\text{H}_3\text{L2}^{tBusal}$ und der Amidligand $\text{H}_3\text{L2}^{pic}$, dargestellt in *Abbildung 6.2*. Die Reaktion mit Kupfer(II)ionen bietet einen gezielten Zugang zu zwei unterschiedlichen Komplextopologien. Es wurde ein C_3 -symmetrischer trinuklearer und ein zentrosymmetrischer dinuklearer metallamakrocyclischer Komplex erhalten, abhängig von der Größe des mit dem Kupfer(II)ion aus-

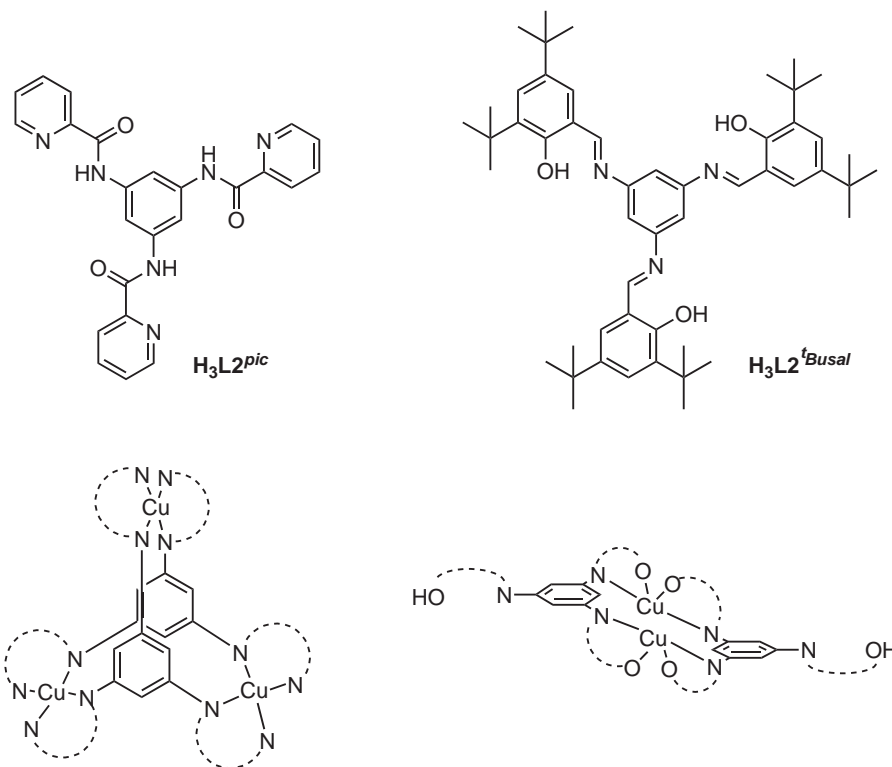


Abbildung 6.2: Schematische Darstellung der triaminobenzene-basierten Liganden, gezeigt im oberen Bereich der Abbildung, und die daraus resultierenden Kupferkomplexe. Links: Struktur des dreikernigen 1,3,5-Metallacyclophan mit *syn*-orientierten verbrückenden Benzenringen. Rechts: Zweikerniger metallamakrocyclischer Komplex mit *anti*-orientierten verbrückenden Benzenringen.

gebildeten Chelatrings. Fünfgliedrige Chelatrings führen zu einer *syn*-Anordnung der verbrückenden Benzenringe, währenddessen sechsgliedrige Ringe die *anti*-Anordnung begünstigen (vgl. Abbildung 6.2).

Der Ligand H_3L2^{pic} bildet einen C_3 -symmetrischen trinuklearen metallamakrocyclischen Komplex, indem drei Kupferionen durch zwei Liganden verbrückend koordiniert werden. Der stöchiometrische Umsatz ergibt durch die *syn*-Anordnung der verbrückenden Benzenringe beider Liganden ein äußerst seltenes 1,3,5-Metallacyclophan. Die Kupferzentren sind in einer verzerrten tetragonalen Koordinationsgeometrie zwischen quadratisch planar und tetraedisch komplexiert. Diese wird durch die Rigidität des Liganden in Verbindung mit sterischen Effekten der Seitenketten verursacht. Darüber hinaus ist noch Dimethylsulfoxid schwach an die Kupferzentren koordiniert, dass eine un-

gewöhnliche stark verzerrte (4+1) Koordinationsgeometrie an jedem Kupferion zur Folge hat.

Daneben wurde ein neuartiger vierkerniger metallamakrocyclischer Komplex mit dem Amidliganden $\text{H}_3\text{L}2^{\text{pic}}$ durch Selbstorganisation erhalten. Zwei Kupferzentren werden von jeweils zwei Ligandmolekülen in einer stark verzerrten tetragonalen Koordinationsgeometrie komplexiert, ähnlich der im dreikernigen Komplex. Die beiden anderen Kupferzentren werden von den Liganden jeweils in einer Bindungstasche komplexiert und sind darüber hinaus durch eine unsymmetrische $\mu\text{-OH-}\mu_{1,3}\text{-N}_3$ -Brückeneinheit verbunden. Diese besitzen eine (4+1) quadratisch-pyramidale Koordinationsgeometrie durch zusätzliche Koordination eines Wasser- und Dimethylformamidmoleküls in den apicalen Positionen der Kupferzentren.

Temperaturabhängige Messungen der Magnetisierung haben in allen Komplexen ferromagnetische Wechselwirkungen ergeben, hervorgerufen durch die Spinpolarisation. Die Kopplungen sind deutlich stärker verglichen mit den phloroglucin-verbrückten Komplexen. Im 1,3,5-Metallacyclophan sind die Kopplungen verglichen mit den großen Kupfer-Kupfer-Abständen von 670 pm mit $J = +25 \text{ cm}^{-1}$ sehr stark. Diese ist bis jetzt die mit Abstand stärkste Kopplung, welche für einen Komplex resultierend aus der Spinpolarisation berichtet worden ist. Im tetranuklearen Komplex verursacht die unsymmetrische Doppelbrücke eine sehr starke antiferromagnetische Wechselwirkung zwischen den zwei Kupferzentren mit $J < -1000 \text{ cm}^{-1}$. Die beiden anderen Kupferionen sind wiederum stark ferrmagnetisch mit $J = +18 \text{ cm}^{-1}$ gekoppelt.

Im Gegensatz dazu bildet der Schiff-Baseligand $\text{H}_3\text{L}2^{\text{Busal}}$ einen dinukleareren metallamakrocyclischen Komplex, worin die verbrückenden Benzenringe *anti*-positioniert sind. Wiederum besitzen beide Kupferzentren eine verzerrte tetragonale Koordinationsgeometrie zwischen quadratisch planar und tetraedrisch. Die dritte Bindungstasche der Liganden ist unbesetzt und hydrolysiert nicht. Dieser Komplex bietet einen eleganten Zugang zu tetranuklearen Komplexen, aufgrund der zwei freien Bindungstaschen. Tatsächlich ergibt die Umsetzung mit Kupfer(II)ionen unter Zugabe des Koliganden 1,1,1,5,5,5-Hexafluoracetylaceton (Hhfac) einen vierkernigen Komplex.

Darüber hinaus wurde ein dinuklearer Kobalt(II)komplex mit dem Schiff-Baseliganden $\text{H}_3\text{L}2^{\text{Busal}}$ synthetisiert. Die Struktur ist sehr ähnlich zu der des Kupfer(II)komplexes. Beide Kobaltzentren werden von zwei Liganden in einer verzerrten tetraedrischen Koordinationsgeometrie komplexiert.

Wiederum haben temperaturabhängige Messungen der Magnetisierung in beiden Kupferkomplexen eine ferromagnetische Wechselwirkung aufgrund der Spinpolarisation ergeben. Im Vergleich zu den Kupfer(II)komplexen mit dem Amidliganden sind die Austauschwechselwirkungen mit J zwischen $+1.5$ und $+12.0 \text{ cm}^{-1}$ schwächer. Im Gegensatz dazu wird im Kobalt(II)komplex eine sehr schwache antiferromagnetische Wechselwirkung mit J nahe Null beobachtet. Hervorgerufen durch die verzerrte tetraedrische Koordinationsgeometrie der Kobalt(II)ionen, besitzt der Komplex eine große Anisotropie mit $|D| = 20 \text{ cm}^{-1}$.

Triaminoguanidin-verbrückte Komplexe: *Kapitel 4* beschreibt die Synthese und Charakterisierung von dreikernigen Übergangsmetallkomplexen basierend auf Triaminoguanidin und deren gezielte Verknüpfung in oligonukleare Komplexe und Koordinationspolymere. Neben den bereits bekannten Schiff-Baseliganden $\mathbf{H}_5\mathbf{L3}^{Hsal}$ und $\mathbf{H}_5\mathbf{L3}^{Brsal}$ mit Salicylidenseitenketten wurde der Ligand $\mathbf{H}_2\mathbf{L3}^{py}$ mit Pyridinseitenketten synthetisiert (Abbildung 6.3). Die nachfolgende Reaktion mit verschiedensten Übergangsmetallionen unter Zugabe von Koliganden bietet einen Zugang zu trinuklearen Komplexen in denen drei Metallionen nah beieinander verbrückend koordiniert werden. Abhängig von den Reaktionsbedingungen ist die gezielte Darstellung von verschiedensten Komplextopologien A bis F vorgestellt worden (Abbildung 6.4). Beide in den vorangegangenen Kapiteln verwendeten verbrückenden Einheiten nutzen die Spinpolarisation als einen potentiellen Zugang zu ferromagnetisch gekoppelten Komplexen aus. Im Gegensatz dazu vermitteln diese Liganden ausschließlich antiferromagnetische Wechselwirkungen durch Superaustausch über die N–N Diazinbrücken. Dies ermöglicht die gezielte Darstellung von magnetischen Molekülen die Spinfrustration innerhalb des $S = 1/2$ Grundzustandes zeigen.

Unter Anwendung eines speziellen Syntheseansatzes ist ein C_3 -symmetrischer trinuklearer Eisen(III)komplex mit dem Liganden $\mathbf{H}_5\mathbf{L3}^{Brsal}$ und labilen Chlorid- und Pyridinkoliganden hergestellt worden. Dieser geht von einer Lösung des Eisen(III)chlorids in Pyridin aus. Pyridin fungiert gleichzeitig als Lösungsmittel, Base und Koligand. Daneben fungieren die Chloridionen als zusätzliche Koliganden zum Ausgleich der positiven Ladung des Komplexkations. Beide Koliganden im Komplex können leicht ersetzt werden

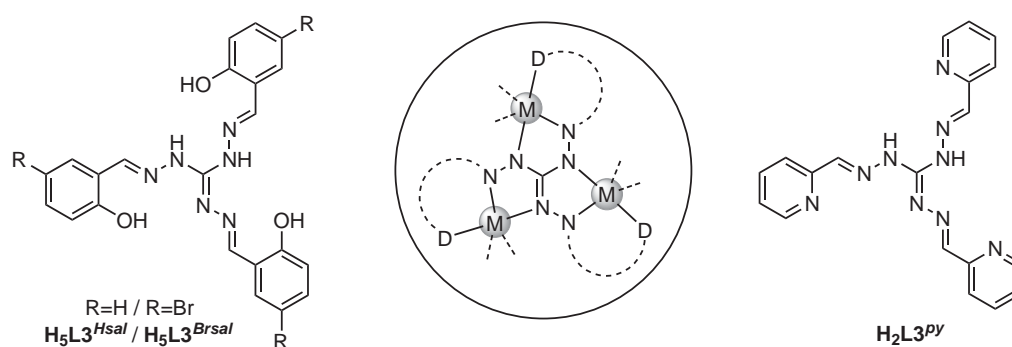


Abbildung 6.3: Triaminoguanidin-basierte Liganden. Eingekreist: Schematische Darstellung der trinuklearen Kerneinheit in den Übergangsmetallkomplexen.

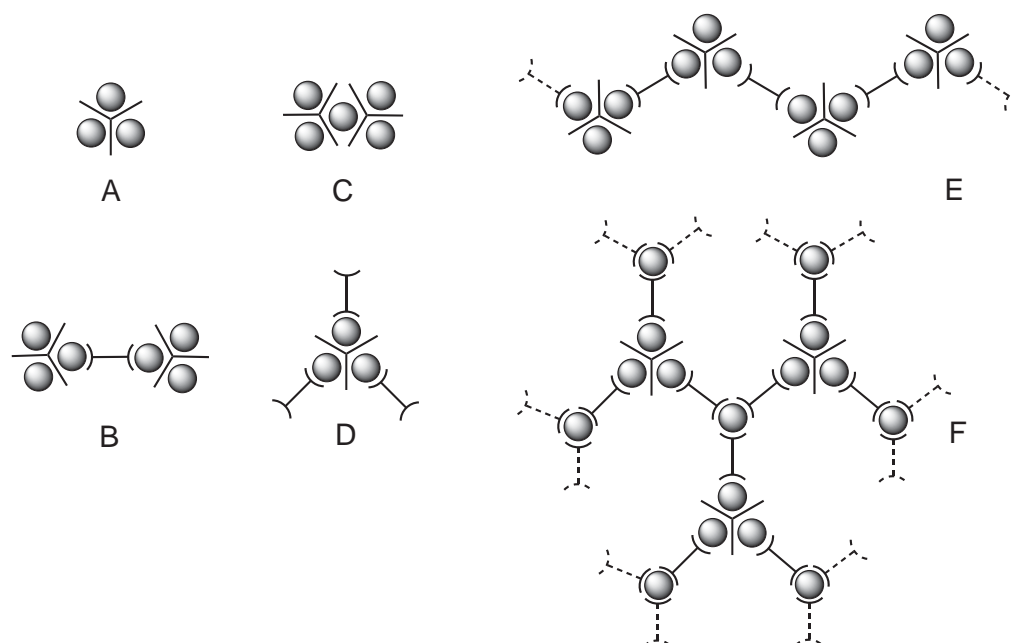


Abbildung 6.4: Schematische Darstellung der verschiedenen Komplextopologien.

und bieten einen eleganten Zugang zu verschiedenen weiteren Komplexen. Die Reaktion mit 8-Hydroxychinolin ergibt den entsprechenden dreikernigen Eisen(III)komplex. Darüber hinaus werden zwei trinukleare Eisenkomplexe durch Zugabe von Methanol unter Erhalt eines sechskernigen Komplexes verbunden. Die Komplex-Untereinheiten sind über zwei Methanolatbrücken verbunden (Vgl. B in Abbildung 6.4).

Die temperaturabhängige Messung der Magnetisierung ergibt in allen drei Komplexen antiferromagnetische Wechselwirkungen mit einem $S = 1/2$ Grundzustand in beiden trinuklearen Komplexen und einem $S = 0$ Grundzustand in dem hexanuklearen Komplex. Speziell der C_3 -symmetrische Komplex besitzt einen spinfrustrierten $S = 1/2$ Grundzustand und bietet deshalb interessante elektronische Eigenschaften für potentielle Anwendungen als Qubit für den Bereich der Quantencomputer.

Die Verwendung des Liganden bietet einen Zugang zu heterometallischen fünfkernigen Komplexen. Als ein bedeutendes Ergebnis dieser Dissertation wurde ein neuer einfacher synthetischer Zugang zu diesen Komplexen entwickelt, basierend auf der schrittweisen Deprotonierung des Liganden und daran anschließende Zugabe von verschiedenen Übergangsmetallionen. Der Schlüsselschritt ist die in-situ Bildung eines einkernigen Komplexes, worin das Metallion oktaedrisch von zwei Liganden koordiniert wird. Im Verlauf der Komplexbildung wird das Metallzentrum oxidiert, was zu einer erhöhten Stabilität gegenüber Metallaustausch führt. Die nachfolgende Zugabe von Nickel(II)ionen gefolgt von dem chelatisierenden Koliganden 2,4,6-Tris(2-pyridyl)-1,3,5-triazin (tptz) führt zu den Komplexen $[M^{III}Ni_4^{II}(L_3)_2(tptz)_4](ClO_4)_x(Cl)_{1-x}$ mit $M = Fe, Mn, Co$. Die zwei dreiseitigen Untereinheiten sind über ein gemeinsames dreiwertiges Metallion verbunden (Vgl. C in Abbildung 6.4).

Der Ligand $H_2L_3^{py}$ ist durch Schiff-Basekondensation zugänglich. Im Gegensatz zu den bekannten Liganden mit Phenolatsauerstoffatomen als Donoren innerhalb der Salicylidenseitenketten bietet dieser Ligand ausschließlich Stickstoffdonoren und koordiniert deshalb als Dianion. Unter Verwendung des Syntheseansatzes analog zum trinuklearen Eisen(III)komplex ist eine Serie von trinuklearen Komplexen mit zweiwertigen Übergangsmetallionen synthetisiert worden. Komplexe von Kupfer(II), Nickel(II), Kobalt(II) und Mangan(II) sind isoliert und strukturell charakterisiert worden. Wiederum sind die Metallzentren koordinativ von labilen Chlorid- und Pyridinkoliganden abgesättigt. Diese

können gegen andere Liganden ausgetauscht werden und bieten deshalb einen Zugang zu verschiedensten Komplexen.

Die Substitution der labilen Koliganden ist am Nickelkomplex bewiesen worden. Die Reaktion mit Azidionen führt zum selektiven Austausch der Chloridionen. Daneben wird unter Verwendung von Bis(pyridin-2-ylcarbonyl)-amin (Hbpca) ein trinuklearer Komplex erhalten indem alle Pyridine und Chloridionen durch den Koliganden ersetzt sind. Dieser Komplex besitzt drei freie acetylacetonartige Bindungstaschen (Vgl. D in Abbildung 6.4). Durch Zugabe von Natriumionen können diese Komplexmoleküle unter Erhalt eines 3D Netzwerkes quervernetzt werden (F in Abbildung 6.4). Weiterhin wurde ein 1D Koordinationspolymer durch die verbrückende Koordination von Oxalat an die trinuklearen Kupferkomplexeinheiten erhalten (Vgl. E in Abbildung 6.4).

Wie erwartet zeigen die temperaturabhängigen Messungen der Magnetisierungen ausschließlich antiferromagnetische Wechselwirkungen innerhalb der Komplexe. Die Größe der Kopplungskonstante sinkt mit steigendem Spin der Metallionen aufgrund der größeren Anzahl von Superaustauschpfaden. Im Kupferkomplex ist die Kopplung mit $J = -299 \text{ cm}^{-1}$ sehr stark resultierend in einem $S = 1/2$ Grundzustand. Die Kopplungen innerhalb der Nickelkomplexe mit $-42 \leq J \leq -36 \text{ cm}^{-1}$ werden vom Liganden dominiert und spiegeln nicht den Austausch der Koliganden wieder. Im Kobaltkomplex wird eine große Nullfeldaufspaltung mit $D = 27 \text{ cm}^{-1}$ beobachtet, welche deutlich stärker ist als die isotropen Wechselwirkungen mit $J_1 = -18 \text{ cm}^{-1}$ und $J_2 = -12 \text{ cm}^{-1}$ innerhalb des gleichseitigen Dreiecks. Im Mangankomplex wird eine sehr schwache Kopplung mit $J = -1 \text{ cm}^{-1}$ zusammen mit einer kleinen Nullfeldaufspaltung von $|D| = 0.6 \text{ cm}^{-1}$ beobachtet. Aufgrund der beiden sehr schwachen Wechselwirkungen wird die feldabhängige Magnetisierung von der Zeemanaufspaltung dominiert. Die beiden letzteren Verbindungen sind die ersten strukturell und magnetisch charakterisierten triaminoguanidinverbrückten Kobalt- und Mangankomplexe.

Ausgehend vom magnetochemischen Standpunkt verhält sich das 1D Kupferkoordinationspolymer wie ein dreikerniger Komplex, da die Oxalatbrücken senkrecht zur Ligandenebene stehen. Die starke Kopplung von $J = -282 \text{ cm}^{-1}$ innerhalb der trinuklearen Einheiten resultiert in einem $S = 1/2$ Grundzustand von isolierten Kupfer-Dreiecken. Folglich ist auch dieser Komplex interessant um das Phänomen der Spinfrustration im Hinblick auf das aktuelle Forschungsfeld der Quantencomputer zu untersuchen.

Abschließend lässt sich festhalten, dass neue C_3 -symmetrische Liganden vorgestellt wurden, die magnetische Wechselwirkungen zwischen den koordinierten Metallzentren vermitteln. Basierend auf diesen wurden gezielt verschiedenste trinukleare Übergangsmetallkomplexe hergestellt. Des Weiteren wurde die definierte Verknüpfung der trinuklearen Einheiten sowohl in höhere Aggregate als auch Koordinationspolymere dargestellt. Folglich beinhaltet diese Dissertation einen beachtlichen Beitrag zur gezielten Darstellung homo- und heterometallischer Komplexe basierend auf dreikernigen Bausteinen. Daneben wurde ein Zugang sowohl zu stark ferromagnetisch gekoppelten Verbindungen unter Ausnutzung der Spinpolarisation als auch antiferromagnetisch gekoppelten triangularen Verbindungen mit einem resultierenden $S = 1/2$ Grundzustand aufgezeigt. Einige dieser Verbindungen besitzen höchst interessante magnetische Eigenschaften für spätere Anwendungen.

7 Future Perspective

In this research, various trinuclear transition metal complexes were synthesized utilizing directed synthetic approaches. Moreover the linkage into higher aggregates was demonstrated providing many points of contacts for the directed syntheses of various complex topologies through the variation of co-ligands and metal centers.

Based on the synthesized copper(II) complexes, described in *chapter 2*, the use of bridging bis-chelating co-ligands like oxalate or oxamide might lead to trinuclear precursors, which can be cross-linked through addition of transition metal or lanthanide ions. For the nickel(II) complexes the tris-chelating tptz co-ligand holds a lot of promise due to its known bridging coordination of two metal centers and mediation of magnetic interactions (see figure 7.1).^[233–235,293,294] An extension provides the ligand 2,4,6-tris(2-pyrimidyl)-1,3,5-triazine (tpymt), potential to coordinate three metal ions in terpyridine-like binding pockets.^[295,296] The synthesized trinuclear cobalt complex is already one step ahead. Each coordinated bpca co-ligands possess a free acetylacetonone-like chelating binding pocket, which might provide an access to hexanuclear homo as well as heterometallic complexes under addition of capping co-ligands. Although all cobalt(III) centers are in the low-spin state, the complex promises interesting magnetic properties as a result of the reduction into cobalt(II). Moreover the coordination of iron(II) ions might result in an interesting heterometallic electron-transfer system.

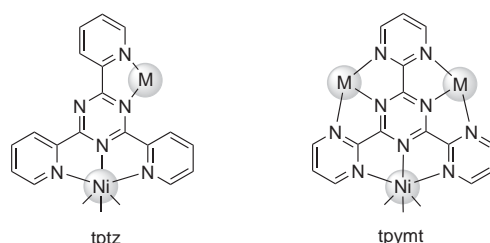
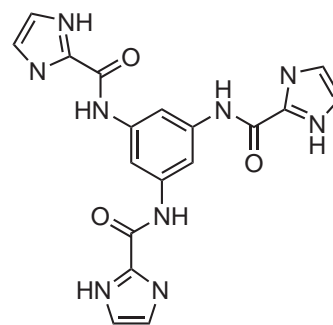


Figure 7.1: Schematic representation of the bridging coordination of the tptz and tpymt co-ligands.

The trinuclear metallacyclophane copper(II) complex, characterized in *chapter 3*, exhibits a very strong ferromagnetic coupling resulting from the spin polarization. Hence the analogous cobalt(II) and manganese(III) complexes are potential high-spin molecules providing an access to a new class of SMMs.

Ligands with other side chains are also promising for the synthesis of strongly coupled high-spin complexes. The analogous ligand with imidazole side chains provides additional [NO] binding pockets beside the three known bidentate [N₂] binding pockets, all accessible after deprotonation. The stepwise deprotonation might lead to 1,3,5-metallacyclophane complexes which can be utilized as precursors for the directed synthesis of enneanuclear homo as well as heterometallic transition metal complexes.^[90]



The dinuclear metallamacrocyclic copper(II) and cobalt(II) complexes possess two free binding pockets. Under appropriate conditions these seem to be likely candidates for the directed synthesis of heterometallic tetranuclear complexes. In addition the analogous dinuclear copper(II) complexes with other substituents within the salicylidene ligand side chains are very interesting in the light of further investigation of the magnetic anomaly phenomenon.

In the *chapter 4* trinuclear triaminoguanidine-bridged complexes with labile pyridine and chloride co-ligands were presented. An exchange against appropriate capping co-ligands might result in complexes with intriguing magnetic properties, e.g. trinuclear spin-crossover or radical complexes.^[297,298] Especially for the iron(III) complex, utilization of the ligands *N*-(8-quinolyl)salicylaldimine and *N*-(pyridin-2-ylmethyl)salicylaldimine that show spin-crossover behavior with hysteresis loops in the corresponding mononuclear complexes hold a lot of promise.^{[299–301] [302–304]}

The trinuclear cobalt(II) and manganese(II) complexes combine chirality and magnetic properties because the crystallization occurred in chiral space groups with the exclusive presence of one enantiomeric form. Therefore both might be interesting for the current research field of magnetochirality.

With regard to the potential application of the triangular complexes as qubits, quantum coherence is essential as one criteria formulated by David P. DiVincenzo.^[305,306] In this

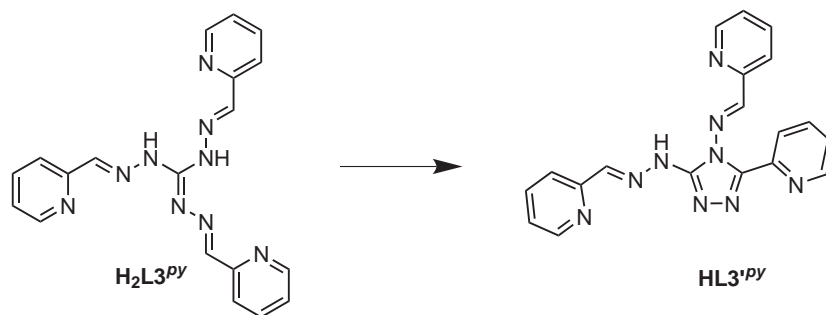


Figure 7.2: Schematic representation of the cyclization of ligand H_2L3^{py} .

context lanthanide complexes are promising candidates due to their proposed long decoherence times.^[307,308] Trials to utilize the synthetic route with pyridine as solvent were unfortunately not successful. In the presence of gadolinium chloride the ligand underwent an oxidative cyclization illustrated in figure 7.2. This has been also reported for the tris-*N*-(salicylidene)-amino-guanidine ligand under various reaction conditions.^[92,136,139] Nevertheless under appropriate conditions the ligand seem to be suitable for the synthesis of trinuclear complexes due to the large binding pockets forming exclusively five-membered chelate rings with the metal centers.

– Experimental –

8 General

Abbreviations used throughout the text:

unspenp = *N,N*-bis(pyridin-2-ylmethyl)-ethylenediamine,

Hbpea = bis(pyridin-2-ylethyl)-amine,

Hbpca = bis(pyridin-2-ylcarbonyl)-amine,

Hhfac = 1,1,1,5,5,5-hexafluoroacetylacetone,

Hq = 8-hydroxyquinoline,

tptz = 2,4,6-tris(2-pyridyl)-1,3,5-triazine,

H₃L1^{ampy} = 2,4,6-tris(pyridin-2-ylmethyliminomethyl)-phloroglucinol,

H₃L1^{unspenp} = 2,4,6-tris{2-[bis(pyridine-2-ylmethyl)amino]ethyliminomethyl}-phloroglucinol,

H₃L1^{bhy} = 2,4,6-tris(benzhydrazidiminomethyl)-phloroglucinol,

H₃L1^{tBubhy} = 2,4,6-tris(4-*tert*-butylbenzhydrazidiminomethyl)-phloroglucinol,

H₃L2^{pic} = *N,N',N''*-tris(2-pyridinecarboxamide)-1,3,5-benzene,

H₃L2^{tBusal} = *N,N',N''*-tris(3,5-di-*tert*-butylsalicylidene)-amino-1,3,5-benzene,

H₅L3^{Hsal} = tris-*N*-(salicylidene)-amino-guanidine,

H₅L3^{Brsal} = tris-*N*-(5-bromo-salicylidene)-amino-guanidine,

H₂L3^{py} = tris-*N*-(pyridin-2-ylmethylidene)-amino-guanidine.

9 Physical Measurements

Melting points were determined *via* a VEB Analytik Dresden HMK 72/41555 and are given uncorrected.

Thermogravimetric analyses (TGA) for powdered samples were performed on a Netzsch STA409PC Luxx apparatus under constant flow of nitrogen.

IR spectra were measured on a Bruker IFS55/Equinox spectrometer with a Raman unit FRA 106/S on samples prepared as KBr pellets.

^1H , ^{13}C , $^1\text{H}\{^1\text{H}\}$ COSY, and $^1\text{H}\{^{13}\text{C}\}$ HSQC NMR experiments were carried out on a Bruker AVANCE 200 and 400 spectrometer. The chemical shifts were referenced to tetramethylsilane.

Mass spectra were measured on a Bruker MAT SSQ 710 spectrometer for FAB measurements and on a MAT95XL Finnigan instrument for electron spray ionization.

Elemental analyses (C, H, N) were acquired by use of a Leco CHNS-932 and a Vario EL III elemental analyzer.

Magnetic susceptibilities were obtained from powdered samples in gelatin capsules using a Quantum-Design MPMSR-5S SQUID magnetometer equipped with a 5 Tesla magnet in the range from 300 to 2 K. The measured data was corrected for diamagnetism of the capsules and the intrinsic diamagnetism of the sample, estimated by measurements on a similar ligand system.

The molar susceptibility data of the complexes is based on the molecular weights calculated from the elemental analyses data. All coupling constants J in this thesis are related to the Heisenberg-Dirac-van Vleck-Hamiltonian in the form of

$$\hat{H} = -J\hat{S}_i\hat{S}_j.$$

10 Crystal Structure Determinations

Single crystals were selected while covered with mother liquor under a polarizing microscope and fixed on fine glass fibers. The crystallographic data was collected on a Nonius KappaCCD diffractometer using graphite-monochromated Mo-K α radiation ($\lambda = 71.073$ pm). A summary of crystallographic and structure refinement data is given in appendix A.3. Data was corrected for Lorentz and polarization effects, but not for absorption effects.^[309–311] The structures were solved by direct methods with SHELXS-97 and refined by full-matrix least-squares techniques against F_o^2 using SHELXL-97.^[312] The program XP (SIEMENS Analytical X-ray Instruments, Inc.) was used for structure representations.

Anisotropic thermal parameters were used for all non-hydrogen atoms except for the solvent molecules on partially occupied positions. These were refined isotropically. Hydrogen atoms were calculated and treated as riding atoms with fixed thermal parameters except the hydrogen atoms of water molecules in complexes **Cu₃L1^{ampy} (1)**, **Ni₃L1^{unspenp} (3)** and **Cu₄L2₂^{pic} (8)**, including both coordinated as well as co-crystallized ones. These were found during structure solution and refined isotropically.

11 Syntheses

11.1 Materials

2,4,6-Triformylphloroglucinol^[148], Hbpea^[313], Hbpca^[239], and unspenp^[314] were prepared according to published procedures. 1,3,5-Triaminobenzene was synthesized in a two step synthesis via 1,3,5-cyclohexanetrione trioxime^[187,188]. Triaminoguanidine^[315] and the corresponding Schiff-base ligands $\text{H}_5\text{L}_3^{\text{Hsal}} \cdot \text{HCl}$ ^[92] and $\text{H}_5\text{L}_3^{\text{Brsal}} \cdot \text{HCl}$ ^[91] were also synthesized according to literature procedures. Commercial available pyridine-2-carbaldehyde and pyridine were distilled prior to use. All other chemicals and solvents are commercially available and were used as received without further purification, unless stated differently.

11.2 Syntheses of the Ligands

11.2.1 Phloroglucinol-Based Ligands

$\text{H}_3\text{L}_1^{\text{ampy}}$

2,4,6-Triformylphloroglucinol (0.50 g, 2.4 mmol) suspended in ethanol (50 mL) was mixed with a solution of 2-aminomethylpyridine (0.76 g, 7.0 mmol) in ethanol (5 mL) accompanied by a color change from colorless to yellow. The resulting mixture was stirred for 24 h resulting in a dissolution of the 2,4,6-triformylphloroglucinol. The volatile components were removed in vacuum leaving the ligand as yellow oil in quantitative yield. The ligand solidified upon storage in the freezer at $-25\text{ }^\circ\text{C}$.

Yield: 1.10 g. IR (KBr, cm^{-1}): $\tilde{\nu} = 3420$ m br, 3230 w br (NH), 3052 w (CH arom.), 3010 w (CH arom.), 2925 w (CH_2), 1675 w (C=O), 1608 vs (C=C), 1545 m, 1457 w, 1437 m, 1350 m, 1320 m, 1199 m, 835 w, 753 w. ^1H NMR (400 MHz, DMSO- d_6): 4.76 (m, 6H, CH_2), 7.30–7.49 (m, 12H, $\text{C}^{3,5}\text{H}_{\text{py}}$), 7.81 and 7.87 (m, 3H, $\text{C}^4\text{H}_{\text{py}}$), 8.22 (m, 3H, CH-NH), 8.56 and 8.62 (m, 3H, $\text{C}^6\text{H}_{\text{py}}$), 11.18 and 11.62 (m, 3H, NH) ppm. ^{13}C NMR (100 MHz, DMSO- d_6):

53.8 and 54.0 (CH₂), 104.8 and 104.9 (C²_{ph}), 122.3, 122.4, 123.0, 123.3, 123.3 and 123.8 (all C^{3,5}H_{py}), 137.6 and 137.7 (C⁴H_{py}), 149.4 and 149.9 (C⁶H_{py}), 154.0, 157.2, 157.2, 157.7, 157.8 and 158.2 (all C²H_{py} and CH-NH), 181.5, 184.5 and 187.5 (all C=O) ppm.

H₃L1^{unspenp}

To a suspension of 2,4,6-triformylphloroglucinol (0.33 g, 1.5 mmol) in ethanol (100 mL) a solution of unspenp (1.15 g, 4.5 mmol) in ethanol (20 mL) was added accompanied by a color change from colorless to yellow. The resulting mixture was stirred for 24 h leading to a dissolution of the 2,4,6-triformylphloroglucinol. The volatile components were removed in vacuum leaving the ligand as yellow oil in quantitative yield.

Yield: 1.30 g. IR (KBr, cm⁻¹): $\tilde{\nu}$ = 3420 m br, 3230 w br (NH), 3056 w (CH arom.), 3011 w (CH arom.), 2929 m (CH₂), 2826 m (CH₂), 1685 w (C=O), 1608 vs (C=C), 1546 m, 1473 w, 1436 m, 1351 m, 1320 m, 1203 m, 1149 m, 1127 m, 835 w, 764 m. ¹H NMR (400 MHz, DMSO-d₆): 2.70 (m, 6H, CH₂-NH), 3.64 (m, 6H, CH₂-N), 3.81 and 3.82 (s, 12H, CH₂-py), 7.13 and 7.25 (m, 6H, C⁵H_{py}), 7.45–7.76 (m, 12 H, C^{3,4}H_{py}), 8.20 (m, 3H, CH-NH), 8.43 and 8.50 (m, 6H, C⁶H_{py}), 11.00 and 11.39 (m, 3H, NH) ppm. ¹³C NMR (100 MHz, DMSO-d₆): 47.2 (CH₂-NH), 54.6 (CH₂-N), 59.7 and 60.0 (CH₂-py), 104.5, 104.5 and 104.6 (all C²_{ph}), 122.3, 122.5, 122.7, 123.1, 123.1 and 123.4 (all C^{3,5}H_{py}), 136.8, 136.9 and 137.0 (all C⁴H_{py}), 148.9, 149.1 and 149.2 (all C⁶H_{py}), 159.3, 159.3, 159.4 and 159.4 (all C²H_{py} and CH-NH), 181.5, 184.6 and 187.5 (all C=O) ppm.

H₆L1^{bhy}

2,4,6-Triformylphloroglucinol (0.34 g, 1.6 mmol) was suspended in ethanol (75 mL) and a solution of benzhydrazide (1.14 g, 8.3 mmol) in ethanol (80 mL) was added accompanied by a color change from colorless to yellow. The resulting mixture was stirred for 24 h in which the 2,4,6-triformylphloroglucinol dissolved and the ligand precipitated. The yellow solid was filtered off, intensely washed with ethanol, and finally dried in vacuum. Yield: 0.53 g (58 %). M.p. > 250 °C. IR (KBr, cm⁻¹): $\tilde{\nu}$ = 3435 m br (OH), 3232 w br (NH), 3062 w (CH arom.), 3029 vw (CH arom.), 1653 vs (Amid I, C=N), 1647 vs (Amid I, C=N), 1635 s (C=C), 1603 m (C=C), 1540 m (Amid II), 1332 m, 1283 s, 1188 m, 688 w, 680 w. ¹H NMR (200 MHz, DMSO-d₆): 7.55 (m, 9H, CH_{ph}), 7.92 (m, 6H, CH_{ph}), 8.91 (s, 3H, CH=N), 12.22 (s, 3H, NH) 13.88 (s, 3H, OH) ppm. ¹³C NMR (50 MHz, DMSO-d₆): 98.9, 127.5,

128.5, 131.9, 132.4, 145.0, 161.5, 162.3 ppm. Elemental analysis calcd (%) for $C_{30}H_{24}N_6O_6$ (564.55 g/mol): C 63.82, H 4.28, N 14.89; found: C 63.31, H 4.42, N 14.76.

H_6L1^{tBubhy}

2,4,6-Triformylphloroglucinol (0.50 g, 2.4 mmol) suspended in methanol (100 mL) was reacted with 4-*tert*-butyl-benzhydrazide (1.37 g, 7.1 mmol) accompanied by a color change from colorless to yellow. The resulting mixture was stirred for 24 h in which the 2,4,6-triformylphloroglucinol dissolved and the ligand precipitated. The yellow solid was filtered off, intensely washed with ethanol, and finally dried in vacuum.

Yield: 1.20 g (69%). M.p. > 250 °C. IR (KBr, cm^{-1}): $\tilde{\nu}$ = 3435 m br (OH), 3219 m br (NH), 3059 vw (CH arom.), 3033 vw (CH arom.), 2964 vs (CH₃), 2905 w (CH₃), 2869 w (CH₃), 1653 vs (Amid I, C=N), 1649 vs (Amid I, C=N), 1610 s (C=C), 1539 m (Amid II), 1507 m, 1458 w, 1364 vw, 1328 m, 1301 m, 1273 s, 1188 m, 888 w, 848 w. ¹H NMR (200 MHz, DMSO-*d*₆): 1.29 (s, 27H, CH₃), 7.52 (m, 6H, ³J_{AB} = 8.5 Hz, CH_{ph}), 7.86 (m, 6H, ³J_{AB} = 8.5 Hz, CH_{ph}), 8.89 (s, 3H, CH=N), 12.14 (s, 3H, NH) 13.88 (s, 3H, OH) ppm. ¹³C NMR (50 MHz, DMSO-*d*₆): 30.8 (CH₃), 34.6 (C_{tBu}), 98.9, 125.2, 127.4, 129.6, 144.8, 154.8, 161.4, 162.2 ppm. Elemental analysis calcd (%) for $H_6L1^{tBubhy} \cdot 0.5H_2O$, $C_{42}H_{49}N_6O_{6.5}$ (741.88 g/mol): C 68.00, H 6.66, N 11.33; found: C 67.88, H 6.68, N 11.17.

11.2.2 Triaminobenzene-Based Ligands

H_3L2^{pic}

The synthesis was carried out under argon atmosphere. 1,3,5-Triaminobenzene (0.96 g, 7.8 mmol) dissolved in dry pyridine (10 mL) was mixed with a solution of 2-pyridine-carboxylic acid (2.88 g, 23.4 mmol) in dry pyridine (10 mL). Triphenyl phosphite (7.25 g, 23.4 mmol) was added and the reaction mixture was heated to 100 °C and kept at this temperature for 4 h while a colorless solid precipitated. After stirring over night at ambient temperature the solid was filtered off, washed with pyridine followed by methanol, and finally dried in vacuum.

Yield: 3.12 g (91%). M.p. > 200 °C. IR (KBr, cm^{-1}): $\tilde{\nu}$ = 3435 w br (OH, H₂O), 3335 s (NH), 3090 vw (CH arom.), 3064 w (CH arom.), 1686 vs (AMID I), 1613 s (C=C), 1591 m (C=C), 1570 m (C=C), 1542 vs (AMID II), 1446 s, 1425 vs, 1283 w, 1234 w, 1189 w, 1042 w, 879 w, 844 w, 785 m, 688 m, 621 m, 580 m. ¹H NMR (400 MHz, DMSO-*d*₆): δ = 7.71 (t,

3H, $^3J = 8.0$ Hz, C^5H_{py}), 8.10 (t, 3H, $^3J = 8.0$ Hz C^4H_{py}), 8.17 (s, 3H, CH_{ph}), 8.18 (d, 3H, $^3J = 8.0$ Hz, C^3H_{py}), 8.77 (d, 3H, $^3J_t = 4.0$ Hz, C^6H_{py}), 10.59 (s, 3H, NH) ppm. Elemental analysis calcd (%) for $H_3L2^{pic} \cdot 0.33H_2O$, $C_{24}H_{18.66}N_6O_{3.33}$ (444.44 g/mol): C 64.86, H 4.23, N 18.91; found: C 64.86, H 4.10, N 18.86.

H_3L2^{tBusal}

Under inert atmosphere, a solution of 1,3,5-triaminobenzene (0.62 mg, 5.0 mmol) in methanol (30 mL) was mixed with a solution of 3,5-di-*tert*-butylsalicylaldehyde (3.54 g, 15.1 mmol) in methanol (20 mL), accompanied by a color change to intense yellow. The reaction mixture was stirred for 24 h at ambient temperatures. During this time the ligand crystallized as yellow needles. The ligand was filtered off, washed two times with methanol, and finally dried in vacuum.

Yield: 3.47 g (90%). M.p. > 200 °C. IR (KBr, cm^{-1}): $\tilde{\nu} = 3425$ w br, 2959 vs (CH_3), 2907 m (CH_3), 2871 m (CH_3), 1619 s, 1571 vs (all C=N, C=C), 1467 m (C=C), 1439 m, 1362 m, 1231 m, 1175 m, 1139 m. 1H NMR (400 MHz, $CDCl_3$): 1.34 (s, 27H, CH_3), 1.47 (s, 27H, CH_3), 7.16 (s, 3H, CH_{ph}), 7.26 (m, 3H, CH_{sal}), 7.48 (m, 3H, CH_{sal}), 7.16 (s, 3H, CH_{sal}), 8.76 (s, 3H, $CH=N$), 13.53 (s, 3H, OH) ppm. ^{13}C NMR (100 MHz, $CDCl_3$): 29.4 (CH_3), 31.4 (CH_3), 34.2 (C_{tBu}), 35.1 (C_{tBu}), 112.1 (CH_{ph}), 118.1, 127.1 (CH_{sal}), 128.5 (CH_{sal}), 137.1, 140.7, 150.6, 158.4 (C-OH), 164.6 (CH=N) ppm. MS (FAB in nba): $m/z = 772$ [$H_3L2^{tBusal} + H$] $^+$. Elemental analysis calcd (%) for $C_{51}H_{69}N_3O_3$ (772.11 g/mol): C 79.33, H 9.01, N 5.44; found: C 79.40, H 9.09, N 5.48.

11.2.3 Triaminoguanidine-Based Ligands

$H_2L3^{py} \cdot HCl$

A solution of triaminoguanidine hydrochloride (3.01 g, 21 mmol) in water (30 mL) was added dropwise to a stirred solution of pyridine-2-carbaldehyde (6.90 g, 64 mmol) in methanol (150 mL). The color changed immediately to yellow. The solution was heated at 45 °C for 2 h. After removing the volatile components in vacuum at ambient temperature, the crude product was obtained as yellow powder. This was redissolved twice in ethanol (100 mL) and evaporated to dryness finally yielding a microcrystalline solid. After drying in vacuum, the ligand was obtained in quantitative yield together with co-crystallized ethanol in the resulting constitution of $H_2L3^{py} \cdot HCl \cdot 1.5EtOH$.

Yield: 10.20 g. TGA: Weight loss up to 150 °C: 14.3% (calcd for 1.5 EtOH 14.5%), decomposition > 204 °C. IR (KBr, cm^{-1}): $\tilde{\nu} = 3421$ vs br (O-H, EtOH), 3051 m (CH arom.), 1643 vs (C=N), 1619 s (C=C), 1588 s (C=C), 1566 w, 1475 w, 1437 w, 1119 w, 1090 w, 773 w. ^1H NMR (400 MHz, DMSO- d_6): 7.53 (m, 3H, C^5H_{py}), 8.01 (m, 3H, C^4H_{py}), 8.53 (m, 3H, C^3H_{py}), 8.69 (m, 3H, C^6H_{py}), 8.91 (s, 3H, CH=N) ppm. ^{13}C NMR (100 MHz, DMSO- d_6): 122.3 (C^3H_{py}), 125.7 (C^5H_{py}), 137.7 (C^4H_{py}), 149.8 (C^6H_{py}), 150.5 (C_{tag}), 151.4 (CH=N), 152.4 (C^2H_{py}) ppm. MS (DEI): $m/z = 372$ ($[\text{H}_2\text{L3}^{py} + \text{H}]^+$). Elemental analysis calcd (%) for $\text{H}_2\text{L3}^{py} \cdot \text{HCl} \cdot 1.5\text{EtOH}$, $\text{C}_{22}\text{H}_{27}\text{ClN}_9\text{O}_3$ (476.97 g/mol): C 55.40, H 5.71, N 26.43; found: C 54.78, H 5.97, N 25.79.

The ligand was crystallized by dissolution in methanol and subsequent addition of HCl_{aq} . Yellow needles were formed which were collected by filtration, washed with methanol, and dried in vacuum. The ligand was obtained as tetra hydrochloride salt in the constitution of $\text{H}_2\text{L3}^{py} \cdot 4\text{HCl} \cdot \text{H}_2\text{O}$. TGA: Decomposition > 237 °C. IR (KBr, cm^{-1}): $\tilde{\nu} = 3436$ s br (O-H, H_2O), 3100–2500 vs (NH^+), 1646 s, 1622 vs, 1606 s, 1592 vs (all C=N, C=C), 1523 m, 1458 s, 1370 w, 1319 s, 1295 s, 1256 w, 1126 s, 1087 w, 958 vw, 780 s, 717 vw, 666 vw, 449 vw. ^1H NMR (400 MHz, D_2O): 7.71 (m, 3H, $^3J = 8.0$ Hz, CH_{py}), 7.93 (m, 3H, $^3J = 8.0$ Hz, CH_{py}), 8.29 (m, 3H, $^3J = 8.0$ Hz, CH_{py}), 8.37 (s, 3H, CH=N), 8.45 (m, 3H, $^3J = 4.0$ Hz, CH_{py}) ppm. ^{13}C NMR (100 MHz, D_2O): 127.7, 140.7, 142.8, 144.1, 147.1, 151.7 ppm (CH=N). Elemental analysis calcd (%) for $\text{H}_2\text{L3}^{py} \cdot 4\text{HCl} \cdot \text{H}_2\text{O}$, $\text{C}_{19}\text{H}_{23}\text{Cl}_4\text{N}_9\text{O}$ (535.26 g/mol): C 42.63, H 4.33, N 23.55; found: C 42.94, H 4.15, N 23.61.

11.3 Syntheses of the Complexes

11.3.1 Phloroglucinol-Bridged Complexes

$[\text{Cu}_3(\text{L1}^{ampy})(\text{MeCN})(\text{H}_2\text{O})_2](\text{ClO}_4)_3$ ($\text{Cu}_3\text{L1}^{ampy}$) (1)

A solution of the ligand $\text{H}_3\text{L1}^{ampy}$ (69 mg, 144 μmol) in methanol (5 mL) was added dropwise to a vigorously stirred solution of $\text{Cu}(\text{ClO}_4)_2 \cdot 6\text{H}_2\text{O}$ (159 mg, 3 equiv) in acetonitrile (5 mL). The addition of aqueous ammonia (25 μL , 3 equiv) caused the precipitation of a green solid which immediately redissolved after complete addition. The green solution was stirred for further 5 min. Slow evaporation afforded green crystals of $[\text{Cu}_3(\text{L1}^{ampy})(\text{MeCN})(\text{H}_2\text{O})_2](\text{ClO}_4)_2(\text{ClO}_4) \cdot 2.25\text{H}_2\text{O}$ within three days suitable for X-ray crystallography. The crystals were isolated, washed with water, and dried in air.

Yield: 50 mg (34%). IR (KBr, cm^{-1}): $\tilde{\nu} = 3425$ s br (OH, H_2O), 2905 vw (CH_2), 2322 vw ($\text{C}\equiv\text{N}$), 2295 vw ($\text{C}\equiv\text{N}$) 1601 vs (C=N, C=C), 1569 m (C=C), 1503 vs, 1446 w, 1424 w, 1372 s, 1343 vw, 1247 w, 1121 vs, 1108 vs (Cl-O ClO_4), 1091 vs (ClO_4), 626 m. MS (micro-ESI in MeOH): $m/z = 784$ (100%, $[\text{Cu}_3(\text{L1}^{\text{ampy}})(\text{MeCN})(\text{OH})_2+\text{Na}]^+$). Elemental analysis calcd (%) for $[\text{Cu}_3(\text{L1}^{\text{ampy}})(\text{MeCN})(\text{H}_2\text{O})_2](\text{ClO}_4)_3 \cdot 2.25\text{H}_2\text{O}$, $\text{C}_{29}\text{H}_{32.50}\text{Cl}_3\text{Cu}_3\text{N}_7\text{O}_{19.25}$ (1084.09 g/mol): C 32.13, H 3.02, N 9.04; found: C 32.16, H 2.75, N 8.91.

$[\text{Ni}_3(\text{L1}^{\text{ampy}})(\text{Hbpea})_3](\text{ClO}_4)_3$ ($\text{Ni}_3\text{L1}^{\text{ampy}}$) (2)

To a stirred solution of the ligand $\text{H}_3\text{L1}^{\text{ampy}}$ (55 mg, 115 μmol) aqueous ammonia (23 μL , 3 equiv) was added followed by a solution of $\text{Ni}(\text{ClO}_4)_2 \cdot 6\text{H}_2\text{O}$ (130 mg, 3 equiv) in methanol (5 mL). This caused the formation of a rose precipitate which completely redissolved during stirring for 10 min at ambient temperature. Hbpea (78 mg, 3 equiv) dissolved in methanol (3 mL) was added leading to the formation of a precipitate which completely redissolved upon addition of acetonitrile (2 mL). Over night red-brown prism suitable for X-ray crystallography were obtained which were collected by filtration, washed with methanol, and dried in air.

Yield: 62 mg (35%). IR (KBr, cm^{-1}): $\tilde{\nu} = 3429$ s br (O-H, H_2O), 3252 m br (NH), 3073 w (CH arom.), 2939 m (CH_2), 2872 m (CH_2), 1605 vs (C=N, C=C), 1567 s (C=C), 1546 m, 1492 vs (C=C), 1444 s, 1369 s, 1293 m, 1086 vs br (Cl-O ClO_4), 764 m, 624 m. Elemental analysis calcd (%) for $[\text{Ni}_3(\text{L1}^{\text{ampy}})(\text{Hbpea})_3](\text{ClO}_4)_3 \cdot 6\text{H}_2\text{O}$, $\text{C}_{69}\text{H}_{84}\text{Cl}_3\text{Ni}_3\text{N}_{15}\text{O}_{21}$ (1741.93 g/mol): C 47.58, H 4.86, N 12.06; found: C 47.49, H 4.11, N 12.04.

$[\text{Ni}_3(\text{L1}^{\text{unspenp}})(\text{H}_2\text{O})_3](\text{ClO}_4)_3$ ($\text{Ni}_3\text{L1}^{\text{unspenp}}$) (3)

To a stirred solution of the ligand $\text{H}_3\text{L1}^{\text{unspenp}}$ (92 mg, 104 μmol) aqueous ammonia (27 μL , 3 equiv) was added followed by a solution of $\text{Ni}(\text{ClO}_4)_2 \cdot 6\text{H}_2\text{O}$ (123 mg, 3 equiv) in methanol (5 mL). The solution was stirred for further 1 min and stood undisturbed in a closed vessel. Within one week rose needles were formed, which were filtered, washed with methanol, and dried in air. These were redissolved in acetonitrile. Slow evaporation afforded red block prism suitable for X-ray crystallography.

Yield: 108 mg (73%). IR (KBr, cm^{-1}): $\tilde{\nu} = 3436$ vs br (O-H, H_2O), 2910 m (CH_2), 2860 m (CH_2), 1606 vs (C=N, C=C), 1495 vs (C=C), 1446 s, 1364 s, 1331 m, 1253 m, 1090 vs br (Cl-O ClO_4), 768 m, 625 s. MS (micro-ESI in MeOH): $m/z = 1253$ (50%, $[\text{Ni}_3(\text{L1}^{\text{unspenp}})(\text{ClO}_4)_2]^+$). Elemental analysis calcd (%) for

$[\text{Ni}_3(\text{L1}^{unspenp})(\text{H}_2\text{O})_3](\text{ClO}_4)_3 \cdot \text{H}_2\text{O}$, $\text{C}_{51}\text{H}_{59}\text{Cl}_3\text{Ni}_3\text{N}_{12}\text{O}_{19}$ (1426.52 g/mol): C 42.94, H 4.17, N 11.78; Found: C 42.79, H 3.85, N 11.46.

$[\text{Cu}_3(\text{H}_2\text{L1}^{bhy})(\text{Him})_3](\text{ClO}_4)_2$ ($\text{Cu}_3\text{L1}^{bhy}$) (4)

The ligand $\text{H}_6\text{L1}^{bhy}$ (83 mg, 147 μmol) was suspended in methanol (5 mL) followed by the addition of solid $\text{Cu}(\text{ClO}_4)_2 \cdot 6\text{H}_2\text{O}$ (163 mg, 3 equiv) and aqueous ammonia (51 μL , 4 equiv). The mixture was stirred for 5 min in which the ligand dissolved leading to a green colored solution. Subsequently, imidazole (30 mg, 3 equiv) and acetonitrile (3 mL) was added and the solution was stirred for further 5 min. Slow evaporation of the reaction solution afforded green crystals within one week suitable for X-ray crystallography. The crystals were isolated, washed with methanol, and dried in air affording the solvent free complex.

Yield: 62 mg (32 %). IR (KBr, cm^{-1}): $\tilde{\nu}$ = 3400 s br, 3257 m br (N-H), 3070 w (CH arom.), 2970 w, 2853 w (both imidazole), 1605 m, 1588 m, 1558 vs, 1496 vs, 1482 vs (all Amid I, C=N, C=C), 1352 vs, 1245 m, 1121 s, 1108 s (Cl-O ClO_4), 1092 s (ClO_4), 1066 s (ClO_4), 625 m, 423 m. MS (micro-ESI in DMF/MeOH): m/z = 969 (10 %, $[\text{Cu}_3(\text{HL1}^{benzhy})(\text{DMF})_3]^+$), 964 (8 %, $[\text{Cu}_3(\text{HL1}^{benzhy})(\text{Him})(\text{DMF})_2]^+$). Elemental analysis calcd (%) for $[\text{Cu}_3(\text{H}_2\text{L1}^{benzhy})(\text{Him})_3](\text{ClO}_4)_2$, $\text{C}_{39}\text{H}_{50}\text{Cl}_2\text{Cu}_3\text{N}_{12}\text{O}_{23}$ (1154.29 g/mol): C 40.58, H 2.79, N 14.56; found: C 40.59, H 3.25, N 14.56.

$[\text{Ni}_3(\text{H}_3\text{L1}^{bhy})(\text{Hbpea})_3](\text{ClO}_4)_3$ ($\text{Ni}_3\text{L1}^{bhy}$) (5)

To a suspension of the ligand $\text{H}_6\text{L1}^{bhy}$ (59 mg, 105 μmol) in methanol (10 mL) $\text{Ni}(\text{ClO}_4)_2 \cdot 6\text{H}_2\text{O}$ (116 mg, 3 equiv) dissolved in methanol (5 mL) was added followed by aqueous ammonia (25 μL , 3 equiv). The mixture was stirred for 10 min at ambient temperature which leads to a dissolution of the ligand resulting in a yellow solution. Hbpea (72 mg, 3 equiv) dissolved in methanol (5 mL) was added dropwise followed by further aqueous ammonia (25 μL , 3 equiv). The solution was stirred for 10 min. Within three days, slow evaporation afforded red needles which were isolated, washed with methanol, and dried in air. Single crystals were obtained through vapor diffusion of diethylether into a methanol-acetonitrile solution of the complex.

Yield: 138 mg (75 %). IR (KBr, cm^{-1}): $\tilde{\nu}$ = 3437 s br, 3254 m br (N-H), 3066 w (CH arom.), 2944 w (CH_2), 2875 w (CH_2), 1608 s, 1583 s, 1549 vs, 1495 vs, 1482 vs (all Amid I, C=N, C=C), 1445 m, 1346 vs, 1243 m, 1108

vs br (Cl-O ClO₄), 624 m. MS (micro-ESI in MeOH): m/z = 1616 (5%, [[Ni₃(H₃L1^{bhy})(Hbpea)₃](ClO₄)₂]⁺), 1517 (20%, [[Ni₃(H₂L1^{bhy})(Hbpea)₃](ClO₄)]⁺), 1416 (35%, [Ni₃(HL1^{bhy})(Hbpea)₃]⁺), 1189 (55%, [Ni₃(HL1^{bhy})(Hbpea)₂]⁺). Elemental analysis calcd (%) for [Ni₃(H₃L1^{benzhy})(Hbpea)₃](ClO₄)₃ · 3H₂O, C₇₂H₇₈Cl₃N₁₅Ni₃O₂₁ (1771.92 g/mol): C 48.80, H 4.44, N 11.86; found: C 48.67, H 4.41, N 11.73.

[Co₃(L1^{tBubhy})(bpca)₃] (Co₃L1^{tBubhy}) (6)

To a vigorously stirred suspension of the ligand H₆L1^{tBubhy} (57 mg, 77 μmol) in methanol (5 mL) a solution of CoCl₂ · 6H₂O (56 mg, 3 equiv) in methanol (5 mL) was added. Subsequently, aqueous ammonia (50 μL, 6 equiv) was added leading to a clear deep brown solution. Hbpca (52 mg, 3 equiv) dissolved in acetonitrile (10 mL) was added dropwise and the reaction mixture was stirred for further 5 min. Slow evaporation afforded brown crystals within one week suitable for X-ray crystallography. The crystals were isolated, washed with methanol, and dried in air.

Yield: 52 mg (41 %). IR (KBr, cm⁻¹): $\tilde{\nu}$ = 3438 s br, 3078 vw (CH arom.), 2962 m (CH₃), 1719 vs (C=O), 1635 m (C=N), 1607 m (C=C), 1507 vs (C=C bpca), 1487 vs (C=C bpca), 1348 vs, 1225 w. MS (micro-ESI in MeOH/CHCl₃): m/z = 1605 (100 %, [Co₃(L1^{tBubhy})(bpca)₃+Na]⁺). Elemental analysis calcd (%) for [Co₃(L1^{tBubhy})(bpca)₃] · 0.5CHCl₃, C_{78.5}H_{66.5}Cl_{1.5}Co₃N₁₅O₁₂ (1641.94 g/mol): C 57.42, H 4.08, N 12.80; found: C 57.46, H 4.47, N 12.77.

11.3.2 Triaminobenzene-Bridged Complexes

[Cu₃(L2^{pic})₂(DMSO)₃] (Cu₃L2^{pic}) (7)

To a suspension of the ligand H₃L2^{pic} (41 mg, 92 μmol) in dimethylsulfoxide (5 mL) a solution of Cu(ClO₄)₂ · 6H₂O (52 mg, 1.5 equiv) in dimethylsulfoxide (3 mL) was added. Subsequent addition of triethylamine (39 μL, 3 equiv) afforded a clear red-brown solution which was stirred for further 15 min. After one week at ambient temperature dark red-brown prisms of [Cu₃(L2^{pic})₂(DMSO)₃] · 3DMSO · 6H₂O suitable for X-ray diffraction were obtained. The crystals were isolated and washed with dimethylformamide followed by washing with methanol in which the crystals crumble into powder. This is caused by the loss of all dimethylsulfoxide molecules including both coordinated and crystallized ones affording the complex compound [Cu₃(L2^{pic})₂] · 7H₂O after drying in

air. The same complex was obtained performing the synthesis in dimethylformamide instead of dimethylsulfoxide. Crystallization occurred within one day in nearly quantitative yield.

Yield: 42 mg (77 %). TGA: Weight loss up to 100 °C: 10.5 % (calcd for 7H₂O 10.6 %). M.p. > 200 °C. IR (KBr, cm⁻¹): $\tilde{\nu}$ = 3420 vs br (H₂O), 3069 w (CH arom.), 1617 s, 1588 vs, 1565 vs (all C=N, C=C), 1437 s, 1363 vs, 1295 m, 758 m, 693 m. MS (micro-ESI in DMF/MeOH): m/z = 1084 (100 %, [Cu₃(L2^{pic})₂+Na]⁺), 1062 (20 %, [Cu₃(L2^{pic})₂+H]⁺). Elemental analysis calcd (%) for [Cu₃(L2^{pic})₂] · 7H₂O, C₄₈H₄₄N₁₂O₁₃Cu₃ (1187.57 g/mol): C 48.55, H 3.73, N 14.15; found: C 48.58, H 3.93, N 14.32.

[Cu₄(L2^{pic})₂(μ_{1,3}-N₃)(μ-OH)(H₂O)(DMF)] (Cu₄L2₂^{pic}) (8)

To a suspension of the ligand H₃L2^{pic} (61 mg, 137 μmol) in dimethylformamide (10 mL) a solution of Cu(ClO₄)₂ · 6 H₂O (154 mg, 3 equiv) in dimethylformamide (7 mL) was added. The subsequent addition of triethylamine (58 μL, 1 equiv) afforded a deep red-brown clear solution which was stirred for further 30 min at ambient temperature. Sodium azide (27 mg, 3 equiv) dissolved in water (1 mL) was added. After slow evaporation dark red-brown prism of the complex were obtained within one week. The crystals were isolated, washed with dimethylformamide followed by methanol, and finally dried in air. During the washing and drying process the crystals crumble into powder. This afforded the final complex compound [Cu₄(L2^{pic})₂(μ_{1,3}-N₃)(μ-OH)(H₂O)(DMF)] · 14H₂O.

Yield: 45 mg (43 %). TGA: Weight loss up to 100 °C: 10.5 % (calcd for 9H₂O 10.6 %), weight loss from 100 °C up to 250 °C: 14.6 % (calcd for 6H₂O + DMF + N₃ 14.6 %), decomposition > 150 °C. IR (KBr, cm⁻¹): $\tilde{\nu}$ = 3421 vs br (OH⁻, H₂O), 3076 w (CH arom.), 2037 s (N≡N, N₃), 1660 w (C=O, DMF), 1618 s, 1587 vs, 1566 vs (all C=N, C=C), 1437 s, 1370 s, 1294 m, 760 m, 690 m. MS (micro-ESI in DMSO/MeOH): m/z = 1084 (100 %, [Cu₃(L2^{pic})₂+Na]⁺). Elemental analysis calcd (%) for [Cu₄(L2^{pic})₂(μ_{1,3}-N₃)(μ-OH)(H₂O)(DMF)] · 14H₂O, C₅₁H₆₈N₁₆O₂₃Cu₄ (1527.36 g/mol): C 40.10, H 4.49, N 14.67; found: C 39.95, H 4.64, N 14.59.

[Cu₂(HL2^{tBusal})₂] (Cu₂L2₂^{tBusal}) (9)

To a stirred solution of the ligand H₃L2^{tBusal} (163 mg, 211 μmol) in chloroform (10 mL) a solution of Cu(ClO₄)₂ · 6H₂O (78 mg, 1 equiv) in methanol (10 mL) was added. Next,

triethylamine (59 μL , 2 equiv) was added leading immediately to a brown colored solution. Slow evaporation of the reaction mixture afforded brown needles within five days suitable for X-ray crystallography. The crystals were isolated, washed with methanol, and dried in air.

Yield: 163 mg (93%). IR (KBr, cm^{-1}): $\tilde{\nu} = 3446$ w br, 2957 s (CH_3), 2906 m (CH_3), 2870 m (CH_3), 1617 s, 1576 vs, 1526 vs (all $\text{C}=\text{N}$, $\text{C}=\text{C}$), 1426 s, 1386 m, 1362 m, 1271 s, 1174 s, 1130 m, 532 m. MS (micro-ESI in $\text{MeOH}/\text{CHCl}_3$): $m/z = 1689$ (100%, $[\text{Cu}_2(\text{HL}2^{\text{tBusal}})_2+\text{Na}]^+$), 1667 (20%, $[\text{Cu}_2(\text{HL}2^{\text{tBusal}})_2+\text{H}]^+$). Elemental analysis calcd (%) for $[\text{Cu}_2(\text{HL}2^{\text{tBusal}})_2] \cdot 0.5\text{CHCl}_3$, $\text{C}_{102.5}\text{H}_{134.5}\text{Cl}_{1.5}\text{Cu}_2\text{N}_6\text{O}_6$ (1726.98 g/mol): C 71.29, H 7.85, N 4.87; found: C 70.88, H 7.92, N 4.71.

$[\text{Co}_2(\text{HL}2^{\text{tBusal}})_2] (\text{Co}_2\text{L}2_2^{\text{tBusal}})$ (10)

A solution of the ligand $\text{H}_3\text{L}2^{\text{tBusal}}$ (77 mg, 100 μmol) in chloroform (10 mL) was added dropwise to a stirred solution of $\text{Co}(\text{CH}_3\text{COO})_2 \cdot 4\text{H}_2\text{O}$ (25 mg, 1 equiv) in dimethylformamide (15 mL). The resulting orange solution was heated at 100 $^\circ\text{C}$ for 30 min accompanied by a color change to deep red. A red microcrystalline solid precipitated within three days, which was filtered, washed with methanol, and dried in vacuum yielding the water containing complex $[\text{Co}_2(\text{HL}2^{\text{tBusal}})_2] \cdot \text{H}_2\text{O}$. Crystals of $[\text{Co}_2(\text{HL}2^{\text{tBusal}})_2] \cdot 4\text{DMF}$ suitable for X-ray crystallography were obtained by recrystallization from a hot dimethylformamide solution.

Yield: 75 mg (90%). IR (KBr, cm^{-1}): $\tilde{\nu} = 3447$ vw br, 2958 s (CH_3), 2906 m (CH_3), 2870 m (CH_3), 1617 m, 1574 vs, 1526 vs (all $\text{C}=\text{N}$, $\text{C}=\text{C}$), 1418 s, 1385 m, 1362 m, 1253 m, 1170 m, 1130 w. MS (micro-ESI in $\text{Aceton}/\text{MeOH}$): $m/z = 1680$ (10%, $[\text{Co}_2(\text{HL}2^{\text{tBusal}})_2+\text{Na}]^+$), 1657 (40%, $[\text{Co}_2(\text{HL}2^{\text{tBusal}})_2]^+$), 772 (100%, $[\text{H}_3\text{L}2^{\text{tBusal}}]^+$). Elemental analysis calcd (%) for $[\text{Co}_2(\text{HL}2^{\text{tBusal}})_2] \cdot \text{H}_2\text{O}$, $\text{C}_{102}\text{H}_{136}\text{Co}_2\text{N}_6\text{O}_7$ (1676.07 g/mol): C 73.09, H 8.18, N 5.01; found: C 73.12, H 8.26, N 4.77.

$[\text{Cu}_4(\text{L}2^{\text{tBusal}})_2(\text{hfac})_2(\text{MeOH})_2] (\text{Cu}_4\text{L}2_2^{\text{tBusal}})$ (11)

A solution of the ligand $\text{H}_3\text{L}2^{\text{tBusal}}$ (77 mg, 100 μmol) in chloroform (5 mL) was mixed with triethylamine (42 μL , 3 equiv). This solution was added dropwise to a stirred solution of $\text{CuCl}_2 \cdot 2\text{H}_2\text{O}$ (39 mg, 2 equiv) in methanol (15 mL) leading to a deep green-brown color. After 5 min stirring at ambient temperatures a solution of Hhfac (14 mg, 1 equiv) and triethylamine (14 μL , 1 equiv) in chloroform (5 mL) was added very slowly and

the reaction mixture was stirred for further 5 min. Within one week, slow evaporation afforded crystals of $[\text{Cu}_4(\text{L}2^{\text{tBusal}})_2(\text{hfac})_2(\text{MeOH})_2] \cdot 5\text{CHCl}_3 \cdot 3\text{MeOH}$ suitable for X-ray crystallography. The crystals were isolated, washed with a small amount of chloroform followed by methanol, and finally dried in air. During isolation and drying process of the crystals, the co-crystallized solvent molecules as well as both coordinated methanol molecules were lost affording the solvent free complex compound $[\text{Cu}_4(\text{L}2^{\text{tBusal}})_2(\text{hfac})_2]$. Yield: 82 mg (74 %). IR (KBr, cm^{-1}): $\tilde{\nu} = 3446$ w br, 2959 s (CH_3), 2907 m (CH_3), 2870 m (CH_3), 1645 m ($\text{C}=\text{O}$), 1619 s, 1577 vs, 1526 vs (all $\text{C}=\text{N}$, $\text{C}=\text{C}$), 1462 s, 1424 s, 1386 m, 1361 m, 1255 vs, 1174 s, 1158 s, 532 vw. MS (micro-ESI in $\text{CHCl}_3/\text{MeOH}$): $m/z = 2228$ (10 %, $[\text{Cu}_4(\text{L}2^{\text{tBusal}})_2(\text{hfac})_2 + \text{Na}]^+$), 1960 (20 %, $[\text{Cu}_3(\text{L}2^{\text{tBusal}})_2(\text{hfac}) + \text{Na}]^+$), 1752 (40 %, $[\text{Cu}_3(\text{L}2^{\text{tBusal}})_2 + \text{Na}]^+$), 1729 (60 %, $[\text{Cu}_3(\text{L}2^{\text{tBusal}})_2 + \text{H}]^+$), 1690 (70 %, $[\text{Cu}_2(\text{HL}2^{\text{tBusal}})_2 + \text{Na}]^+$), 1668 (38 %, $[\text{Cu}_2(\text{HL}2^{\text{tBusal}})_2]^+$). Elemental analysis calcd (%) for $[\text{Cu}_4(\text{L}2^{\text{tBusal}})_2(\text{hfac})_2]$, $\text{C}_{112}\text{H}_{134}\text{Cu}_4\text{F}_{12}\text{N}_6\text{O}_{10}$ (2206.46 g/mol): C 60.97, H 6.12, N 3.81; found: C 61.64, H 6.23, N 3.68.

11.3.3 Triaminoguanidine-Bridged Complexes

$[\text{Fe}_3(\text{L}3^{\text{Brsal}})(\text{py})_6\text{Cl}_3]\text{ClO}_4$ ($\text{Fe}_3\text{L}3^{\text{Brsal}}$) (12)

A solution of the ligand $\text{H}_5\text{L}3^{\text{Brsal}} \cdot \text{HCl}$ (179 mg, 260 μmol) in pyridine (10 mL) was added dropwise to a stirred solution of $\text{FeCl}_3 \cdot 6\text{H}_2\text{O}$ (210 mg, 3 equiv) in pyridine (10 mL). The resulting green colored solution was stirred for 10 min at ambient temperature. Then a solution of $\text{NaClO}_4 \cdot \text{H}_2\text{O}$ (37 mg, 1 equiv) in methanol (5 mL) was added dropwise and stirring continued for further 5 min. Within one week, slow diffusion of methanol into the reaction mixture afforded dark green hexagonal prisms suitable for X-ray crystallography. The crystals were isolated, washed with pyridine and methanol, and finally dried in air.

Yield: 260 mg (64 %). IR (KBr, cm^{-1}): $\tilde{\nu} = 3436$ m br, 3075 w (CH arom.), 1602 s, 1591 s, 1559 s (all $\text{C}=\text{N}$, $\text{C}=\text{C}$), 1458 vs, 1445 vs, 1393 m, 1363 s, 1294 m, 1187 m, 1096 s ($\text{Cl}-\text{O}-\text{ClO}_4$), 1011 m, 834 m, 756 m, 698 m, 672 s, 550 m. Elemental analysis calcd (%) for $[\text{Fe}_3(\text{L}3^{\text{Brsal}})(\text{py})_6\text{Cl}_3]\text{ClO}_4 \cdot 1.5\text{py}$ (1614.68 g/mol), $\text{C}_{59.5}\text{H}_{49.5}\text{Br}_3\text{Cl}_4\text{Fe}_3\text{N}_{13.5}\text{O}_7$: C 44.26, H 3.09, N 11.71; found: C 44.18, H 3.09, N 11.78.

[Fe₃(L3^{Brsal})(q)₃(py)₂Cl] (Fe₃L3^{Brsal}q₃) (13)

A solution of the ligand H₅L3^{Brsal} · HCl (133 mg, 193 μmol) in pyridine (5 mL) was added dropwise to a stirred solution of FeCl₃ · 6H₂O (156 mg, 3 equiv) in pyridine (5 mL). The resulting green colored solution was stirred for 10 min at ambient temperature. Subsequently, a solution of 8-hydroxyquinoline (Hq) (84 mg, 3 equiv) in pyridine (3 mL) was added dropwise and stirred for further 5 min. Dark green prism suitable for X-ray crystallography were obtained through slow diffusion of methanol into the reaction mixture within three days. The crystals were isolated, washed with pyridine followed by methanol, and finally dried in air.

Yield: 150 mg (54 %). IR (KBr, cm⁻¹): $\tilde{\nu}$ = 3435 m br, 3049 w (CH arom.), 1592 m, 1573 m, 1527 m (all C=N, C=C), 1496 s, 1459 vs, 1445 s, 1375 s, 1322 s, 1107 s (C-O), 823 m, 740 m, 673 m. Elemental analysis calcd (%) for [Fe₃(L3^{Brsal})(q)₃(py)₂Cl], C₅₉H₄₀Br₃ClFe₃N₁₁O₆ (1441.72 g/mol): C 49.15, H 2.80, N 10.69; found: C 49.16, H 3.06, N 10.73.

[Fe₆(L3^{Brsal})₂(μ-OMe)₂(py)₈Cl₆] (Fe₆L3^{Brsal}) (14)

A solution of the ligand H₅L3^{Brsal} · HCl (220 mg, 319 μmol) in pyridine (7 mL) was added dropwise to a stirred solution of FeCl₃ · 6H₂O (187 mg, 3 equiv) in pyridine (9 mL). The resulting green colored solution was stirred for 5 min at ambient temperature. Methanol (15 mL) was added and the reaction mixture was left undisturbed. Green prism suitable for X-ray crystallography were obtained within three days. These were isolated, washed with pyridine followed by methanol, and finally dried in air.

Yield: 330 mg (79 %). IR (KBr, cm⁻¹): $\tilde{\nu}$ = 3435 w br, 3071 w (CH arom.), 1593 s, 1528 s (all C=N, C=C), 1461 vs, 1444 vs, 1396 m, 1368 s, 1294 w, 1187 m, 820 w, 755 w, 697 m, 673 s, 549 w. Elemental analysis calcd (%) for [Fe₆(L3^{Brsal})₂(μ-OMe)₂(py)₈Cl₆] · py, C₉₁H₇₅Br₆Cl₆Fe₆N₂₁O₈ (2617.92 g/mol): C 41.75, H 2.89, N 11.24; found: C 41.95, H 3.04, N 11.23.

[FeNi₄(L3^{Brsal})₂(tptz)₄](ClO₄)_{0.5}Cl_{0.5} (FeNi₄L3^{Brsal}) (15)

To a DMF solution (10 mL) of the ligand H₅L3^{Brsal} · HCl (138 mg, 200 μmol) triethylamine (28 μL, 1 equiv) was added dropwise followed by a solution of Fe(ClO₄)₂ · 6H₂O (37 mg, 0.5 equiv) in methanol (5 mL). To the deep green solution further triethylamine (28 μL, 1 equiv) was added and the reaction mixture was stirred for 10 min at ambient

temperature. Afterwards this was added dropwise to a vigorously stirred solution of $\text{Ni}(\text{ClO}_4)_2 \cdot 6\text{H}_2\text{O}$ (146 mg, 2 equiv) in methanol (10 mL). Triethylamine (111 μL , 4 equiv) was added dropwise followed by 2,4,6-tris(2-pyridyl)-1,3,5-triazine (125 mg, 2 equiv) dissolved in methanol (10 mL). The resulting brown solution was stirred for further 10 min. Slow evaporation over a period of one month afforded brown block prism suitable for X-ray crystallography. The crystals were isolated, washed with methanol, and dried in air.

Yield: 224 mg (69%). IR (KBr, cm^{-1}): $\tilde{\nu} = 3435$ s br (H_2O), 3062 w (CH arom.), 1669 m (C=O, DMF), 1575 m, 1557 vs, 1531 vs (all C=N and C=C), 1469 vs, 1431 s, 1392 m, 1375 s, 1176 m (C-O), 1108 s (Cl-O ClO_4), 769 s, 666 m, 635 w. Elemental analysis calcd (%) for MS (micro-ESI in MeOH): $m/z = 2836$ (100%, $[\text{FeNi}_4(\text{L3}^{\text{Brsal}})_2(\text{tptz})_4]^+$), 335 (25%, $[\text{tptz} + \text{Na}]^+$). $[\text{FeNi}_4(\text{L3}^{\text{Brsal}})_2(\text{tptz})_4](\text{ClO}_4)_{0.5}\text{Cl}_{0.5} \cdot 2.5\text{DMF} \cdot 9\text{H}_2\text{O}$, $\text{C}_{123.5}\text{H}_{107.5}\text{Br}_6\text{ClFeN}_{38.5}\text{Ni}_4\text{O}_{19.5}$ (3248.42 g/mol): C 45.66, H 3.34, N 16.60; found: C 45.88, H 3.26, N 16.92.

$[\text{MnNi}_4(\text{L3}^{\text{Hsal}})_2(\text{tptz})_4]\text{ClO}_4$ ($\text{MnNi}_4\text{L3}_2^{\text{Hsal}}$) (16)

The synthesis is similar to the one of complex $\text{FeNi}_4\text{L3}_2^{\text{Brsal}}$ (15). As ligand $\text{H}_5\text{L3}^{\text{Hsal}} \cdot \text{HCl}$ was used instead of $\text{H}_5\text{L3}^{\text{Brsal}} \cdot \text{HCl}$ as ligand and as metal salt $\text{Mn}(\text{ClO}_4)_2 \cdot 6\text{H}_2\text{O}$ instead of $\text{Fe}(\text{ClO}_4)_2 \cdot 6\text{H}_2\text{O}$. After the addition of $\text{Mn}(\text{ClO}_4)_2 \cdot 6\text{H}_2\text{O}$ and triethylamine the mononuclear precursor complex precipitated from the reaction solution as fine yellow-brown needles. After 15 min stirring under ambient temperatures the resulting suspension was added to the solution of $\text{Ni}(\text{ClO}_4)_2 \cdot 6\text{H}_2\text{O}$ in methanol leading to a dissolution of the precipitate. Slow evaporation of the reaction solution afforded brown needles within two months, which were filtered off, washed with methanol, and dried in air. These were redissolved in chloroform-methanol-mixture (1 : 1, 20 mL). Subsequent slow evaporation at room temperature afforded brown needles which were unfortunately not suitable for X-ray crystallography. The crystals were isolated and dried in air affording $[\text{MnNi}_4(\text{L3}^{\text{Hsal}})_2(\text{tptz})_4]\text{ClO}_4 \cdot 8\text{H}_2\text{O}$.

Yield: 151 mg (58%). IR (KBr, cm^{-1}): $\tilde{\nu} = 3435$ vs br (H_2O), 3061 w (CH arom.), 1596 m, 1575 m, 1557 vs, 1531 vs (all C=N and C=C), 1472 vs, 1448 vs, 1392 w, 1375 s, 1193 m (C-O), 1099 s (Cl-O ClO_4), 769 s, 665 w, 634 w. MS (micro-ESI in MeOH): $m/z = 2360$ (100%, $[\text{MnNi}_4(\text{L3}^{\text{Hsal}})_2(\text{tptz})_4]^+$), 335 (40%, $[\text{tptz} + \text{Na}]^+$). Elemental analysis calcd (%) for $[\text{MnNi}_4(\text{L3}^{\text{Hsal}})_2(\text{tptz})_4]\text{ClO}_4 \cdot 8\text{H}_2\text{O}$, $\text{C}_{116}\text{H}_{94}\text{ClMnN}_{36}\text{Ni}_4\text{O}_{18}$ (2605.38 g/mol): C 53.48, H 3.64, N 19.35; found: C 53.20, H 3.52, N 18.93.

[CoNi₄(L3^{Hsal})₂(tptz)₄]ClO₄ (CoNi₄L3₂^{Hsal}) (17)

The synthesis is analogous to the one of complex **MnNi₄L3₂^{Hsal}** (16) using Co(ClO₄)₂ · 6H₂O instead of Mn(ClO₄)₂ · 6H₂O. Slow evaporation of the reaction solution afforded brown needles within two months, which were filtered, washed with methanol and dried in air. These were redissolved in chloroform-methanol-mixture (1 : 1, 20 mL). Subsequent slow evaporation at room temperature afforded brown block crystals which were unfortunately not suitable for X-ray crystallography. The crystals were isolated and dried in air affording [CoNi₄(L3^{Hsal})₂(tptz)₄]ClO₄ · 8H₂O.

Yield: 185 mg (71 %). IR (KBr, cm⁻¹): $\tilde{\nu}$ = 3402 vs br (H₂O), 3061 w (CH arom.), 1594 m, 1575 m, 1557 vs, 1532 vs (all C=N and C=C), 1476 vs, 1457 vs, 1392 w, 1375 s, 1194 m (C-O), 1108 s (Cl-O ClO₄), 769 s, 665 w, 634 w. MS (micro-ESI in MeOH): m/z = 2365 (100 %, [CoNi₄(L3^{Hsal})₂(tptz)₄]⁺), 335 (55 %, [tptz + Na]⁺). Elemental analysis calcd (%) for [CoNi₄(L3^{Hsal})₂(tptz)₄]ClO₄ · 8H₂O, C₁₁₆H₉₄ClCoN₃₆Ni₄O₁₈ (2609.38 g/mol): C 53.39, H 3.63, N 19.32; found: C 53.08, H 4.01, N 19.21.

[Cu₃(L3^{py})(py)₂Cl₄] (Cu₃L3^{py}) (18)

A solution of the ligand H₂L3^{py} · HCl (36 mg, 75 μmol) in pyridine (15 mL) was added to a stirred solution of CuCl₂ · 2H₂O (43 mg, 3 equiv) in pyridine (5 mL), accompanied by a color change from blue to brown. The reaction mixture was stirred for 5 min at ambient temperature and then stood in a closed vessel. Within one week brown prism of [Cu₃(L3^{py})(py)₂Cl₄] (18) were obtained. The crystals were isolated, washed with pyridine and dried in air. This led to the loss of both coordinated as well as co-crystallized pyridine molecules resulting in the final complex constitution [Cu₃(L3^{py})Cl₄] (18a).

Yield: 41 mg (78 %).

A second crystalline fraction was obtained after evaporation of the reaction mixture to dryness and subsequent washing with methanol.

Overall yield: 48 mg (90 %). IR (KBr, cm⁻¹): $\tilde{\nu}$ = 3435 w br, 3065 vw (CH arom.), 3016 w (CH arom.), 1606 m (C=N and C=C), 1481 s, 1417 vs, 1347 s, 1214 w, 1150 s, 783 vw. MS (micro-ESI in DMF/MeOH): m/z = 665 ([Cu₃(L3^{py})Cl₃]⁺). Elemental analysis calcd (%) for [Cu₃(L3^{py})Cl₄], C₁₉H₁₅Cl₄Cu₃N₉ (701.83 g/mol): C 32.52, H 2.15, N 17.96; found: C 32.90, H 2.32, N 17.80.

[Ni₃(L3^{py})(py)₆Cl₃]Cl (Ni₃L3^{py}) (19)

A solution of the ligand H₂L3^{py} · HCl (0.62 g, 1.31 mmol) in methanol (10 mL) was added dropwise to a stirred solution of NiCl₂ · 6H₂O (0.93 g, 3 equiv) in pyridine-methanol-mixture (1 : 1, 40 mL) accompanied by a color change from yellow to red. Triethylamine (0.55 mL, 3 equiv) was added and stirred for further 5 min at ambient temperature. After two weeks of slow evaporation, red crystals suitable for crystal structure determination were obtained. The crystals were isolated, washed with a small amount of methanol, and dried in air.

Yield: 1.16 g (72 %).

A second crystalline fraction was obtained after evaporation of the reaction mixture to dryness and subsequent washing with ice cold methanol.

Overall yield: 1.42 g (88 %). IR (KBr, cm⁻¹): $\tilde{\nu}$ = 3402 s br (O-H, H₂O), 3063 m (CH_{py}), 1602 s (C=N and C=C), 1476 m, 1442 s, 1400 vs, 1344 vs, 1165 vs, 1146 vs. MS (micro-ESI in MeOH): m/z = 649 ([Ni₃(L3^{py})Cl₃]⁺). Elemental analysis calcd (%) for [Ni₃(L3^{py})(py)₃Cl₃]Cl · 0.5MeOH · 3.5H₂O, C_{49.5}H_{53.5}Cl₄N₁₅Ni₃O₄ (1240.95 g/mol): C 47.91, H 4.39, N 16.93; found: C 47.81, H 4.46, N 17.12.

[Ni₃(L3^{py})(py)₆(N₃)₃]ClO₄ (Ni₃L3^{py}(N₃)₃) (20)

A solution of the ligand H₂L3^{py} · HCl (73 mg, 153 μmol) in methanol (10 mL) was added dropwise to a stirred solution of NiCl₂ · 6H₂O (109 mg, 3 equiv) in pyridine-methanol-mixture (1 : 1, 10 mL). Triethylamine (45 μL, 3 equiv) was added and the red solution was stirred for 5 min at ambient temperature. Afterwards a solution of NaClO₄ · H₂O (22 mg, 1 equiv) in methanol (2 mL) followed by NaN₃ (30 mg, 3 equiv) in water (5 mL) was added. Slow evaporation of the reaction mixture afforded red cubic prism suitable for X-ray crystallography. The crystals were isolated, washed with methanol, and finally dried in air.

Yield: 155 mg (75 %). IR (KBr): $\tilde{\nu}$ = 3436 m br, 3071 w (CH_{py}), 2053 vs (N≡N, N₃), 1600 s (C=N and C=C), 1477 m, 1443 s, 1398 vs, 1335 s, 1162 m, 1147 s, 1093 s (Cl-O ClO₄), 697 w cm⁻¹. MS (micro-ESI in MeOH): m/z = 674 (100 %, [Ni₃(L3^{py})(N₃)₃]⁺). Elemental analysis calcd (%) for [Ni₃(L3^{py})(py)₃(N₃)₃]ClO₄ · 3MeOH, C₅₂H₅₇ClN₂₄Ni₃O₇ (1341.70 g/mol): C 46.55, H 4.28, N 25.05; found: C 46.38, H 3.83, N 24.93.

[Ni₃(L3^{py})(bpca)₃]PF₆ (Ni₃L3^{py}(bpca)₃) (21)

To a solution of the nickel complex Ni₃L3^{py} (**19**) (99 mg, 80 μmol) in methanol (5 mL) Hbpca (55 mg, 3 equiv) in chloroform (3 mL) was added. Then triethylamine (33 μL, 3 equiv) was added followed by a solution of NH₄PF₆ (13 mg, 1 equiv) in water (2 mL). The resulting red solution was stirred for 5 min at ambient temperature. Slow evaporation of the reaction mixture afforded red prism suitable for X-ray crystallography. The crystals were isolated, washed with a small amount of methanol, and finally dried in air. Yield: 100 mg (88 %). IR (KBr, cm⁻¹): $\tilde{\nu}$ = 3469 m br, 3064 w (CH arom.), 3018 w (CH arom.), 1695 vs (C=O), 1600 s (C=N and C=C), 1568 w, 1472 w, 1444 w, 1395 vs, 1359 vs, 1336 vs, 1295 m, 1259 w, 1228 w, 1147 s, 1093 vw, 1021 vw, 846 s (P-F PF₆), 759 m, 712 w, 632 m, 558 m. MS (micro-ESI in MeOH/DMF): m/z = 1223 (100 % [Ni₃(L3^{py})(bpca)₃]⁺). Elemental analysis calcd (%) for [Ni₃(L3^{py})(bpca)₃]PF₆ · 2H₂O, C₅₅H₄₃F₆N₁₈Ni₃O₈P (1405.09 g/mol): C 47.01, H 3.08, N 17.94; found: C 47.15, H 2.90, N 17.91.

[Co₃(L3^{py})(py)₆Cl₃]ClO₄ (Co₃L3^{py}) (22)

The synthesis was carried out under argon atmosphere using standard schlenk techniques. Pyridine was distilled from calcium hydride and degassed in three freeze/pump/thaw cycles prior to use.

A mixture of Co(ClO₄)₂ · 6H₂O (49 mg, 134 μmol) and CoCl₂ · 6H₂O (64 mg, 2 equiv) was dissolved in pyridine (7 mL). The ligand H₂L3^{py} · HCl (70 mg, 1 equiv) was added in portions accompanied by a color change from colorless to red. The reaction mixture have been stirred for further 10 min. Single crystals suitable for X-ray crystallography were obtained within one week at ambient temperature. The crystals were filtered off, washed with pyridine, and dried in a stream of argon.

Yield: 120 mg (73 %). IR (KBr, cm⁻¹): $\tilde{\nu}$ = 3435 w br, 3067 w (CH arom.), 1602 s (C=N and C=C), 1480 m, 1442 s, 1404 vs, 1342 s, 1297 w, 1144 s, 1099 s (Cl-O ClO₄), 700 m, 635 vw, 623 m. Elemental analysis calcd (%) for [Co₃(L3^{py})(py)₆Cl₃]ClO₄, C₄₉H₄₅Cl₄Co₃N₁₅O₄ (1226.59 g/mol): C 47.98, H 3.70, N 17.13; found: C 47.87, H 3.50, N 17.02.

[Mn₃(L3^{py})(py)₆Cl₃]ClO₄ (Mn₃L3^{py}) (23)

The synthesis was performed analogous to the one of the corresponding cobalt complex **Co₃L3^{py} (22)** using a mixture of Mn(ClO₄)₂ · 6H₂O (53 mg, 146 μmol) and MnCl₂ · 4H₂O (58 mg, 2 equiv). Crystals suitable for X-ray crystallography were also obtained within one week at ambient temperature. These were filtered off, washed with pyridine, and dried in a stream of argon.

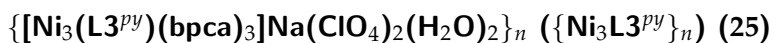
Yield: 135 mg (76 %). IR (KBr, cm⁻¹): $\tilde{\nu}$ = 3435 w br, 3066 w (CH arom.), 1599 s (C=N and C=C), 1479 m, 1442 s, 1398 vs, 1342 vs, 1298 m, 1136 vs, 1098 s (Cl-O ClO₄), 701 m, 635 w, 623 m. Elemental analysis calcd (%) for [Mn₃(L3^{py})(py)₆Cl₃]ClO₄, C₄₉H₄₅Cl₄Mn₃N₁₅O₄ (1214.61 g/mol): C 48.45, H 3.73, N 17.30; found: C 48.78, H 3.44, N 17.00.

{[Cu₃(L3^{py})(μ-ox)(ox)(H₂O)₂]}_n ({Cu₃L3^{py})}_n (24)

A solution of the ligand H₂L3^{py} · HCl (74 mg, 155 μmol) in methanol (8 mL) and triethylamine (66 μL, 3 equiv) was added dropwise to a solution of CuClO₄ · 6H₂O (175 mg, 3 equiv) in acetonitrile (10 mL) accompanied by a color change from yellow to green. The reaction mixture was stirred for 20 min at ambient temperature while a green solid precipitated. The resulting suspension was added dropwise into a stirred solution of Na₂ox (127 mg, 6 equiv) in water (17 mL) leading to the dissolution of the precipitate accompanied by the formation of a colorless precipitate identified as excess Na₂ox. Subsequently ethanol (3 mL) was added, the mixture was filtered and allowed to stand undisturbed. Over night a deep green microcrystalline solid precipitated which was filtered, washed with water, and finally dried in air.

Crystals suitable for X-ray crystallography were obtained starting from the trinuclear copper complex [Cu₃(L3^{py})Cl₄] (**18**) (10 μmol). This was added to a refluxing solution of Na₂ox (6 equiv) in ethanol-water-mixture (1 : 1, 10 mL). Within 30 min the complex dissolved leading to a green colored solution. Slowly cooling of the mixture afforded over night green block single crystals of {[Cu₃(L3^{py})(μ-ox)(ox)(H₂O)₂]}_n · 0.25nEtOH · 3.5nH₂O.

Yield: 84 mg (66 %). IR (KBr, cm⁻¹): $\tilde{\nu}$ = 3430 s br (O-H, H₂O), 1646 vs br (COO⁻), 1608 s (C=N and C=C), 1483 s, 1448 m, 1419 vs (COO⁻), 1346 s, 1155 s, 781 w. Elemental analysis calcd (%) for [Cu₃(L3^{py})(μ-ox)(ox)(H₂O)₂] · 0.25EtOH · 3.5H₂O, C_{23.5}H_{27.5}Cu₃N₉O_{13.75} (1693.32 g/mol): C 33.34, H 3.27, N 14.89; found: C 33.52, H 2.59, N 14.61.



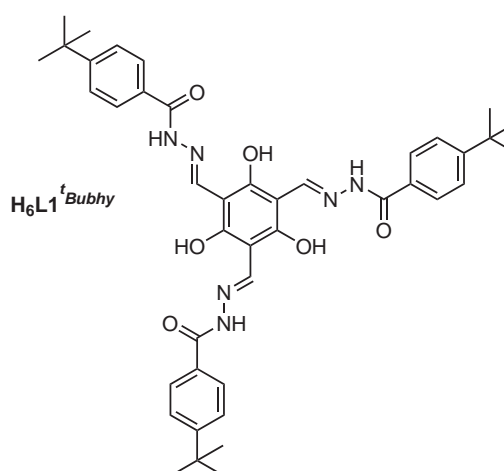
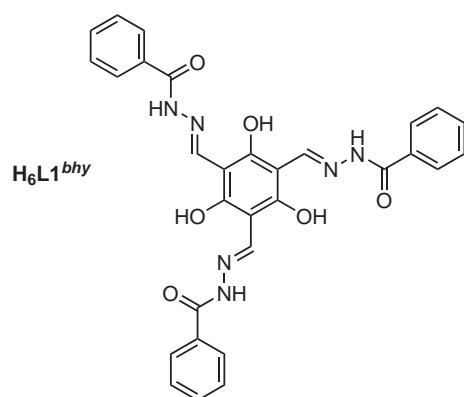
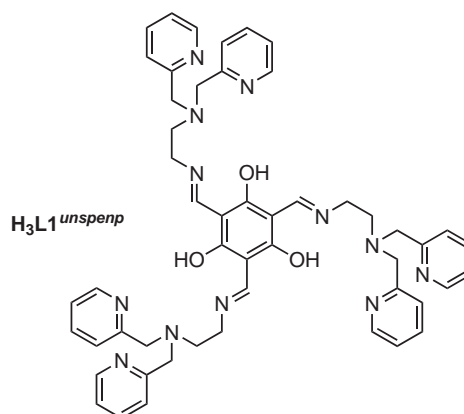
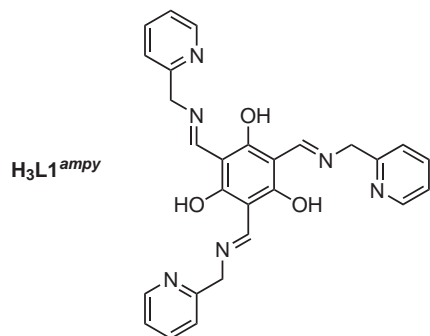
Hbpca (55 mg, 3 equiv) dissolved in chloroform (3 mL) was added to a stirred solution of the nickel complex $\text{Ni}_3\text{L3}^{py}$ (**19**) (99 mg, 78 μmol) in methanol (5 mL). Afterwards triethylamine (33 μL , 1 equiv) was added followed by a solution of $\text{NaClO}_4 \cdot \text{H}_2\text{O}$ (25 mg, 2 equiv) in methanol (2 mL) and the red solution was stirred for 5 min at ambient temperature. Slow evaporation of the reaction mixture led to the formation of red prism suitable for X-ray crystallography. The crystals were isolated, washed with a small amount of methanol, and finally dried in air.

Yield: 80 mg (68 %). TGA: Weight loss up to 150 °C: 3.6 % (calcd for $3\text{H}_2\text{O}$ 3.6 %). IR (KBr, cm^{-1}): $\tilde{\nu} = 3435$ s br (O-H, H_2O), 3066 m (CH arom.), 1690 vs (C=O), 1600 m (C=N and C=C), 1396 vs, 1366 vs, 1335 s, 1296 m, 1147 s, 1093 m br (Cl-O ClO_4), 633 m. MS (micro-ESI in MeOH): $m/z = 1223$ (100 %, $[\text{Ni}_3(\text{L3}^{py})(\text{bpca})_3]^+$). Elemental analysis calcd (%) for $[\text{Ni}_3(\text{L3}^{py})(\text{bpca})_3]\text{Na}(\text{ClO}_4)_2(\text{H}_2\text{O})_2 \cdot \text{H}_2\text{O}$, $\text{C}_{55}\text{H}_{45}\text{Cl}_2\text{N}_{18}\text{NaNi}_3\text{O}_{17}$ (1500.03 g/mol): C 44.04, H 3.02, N 16.81; found: C 43.69, H 2.63, N 16.36.

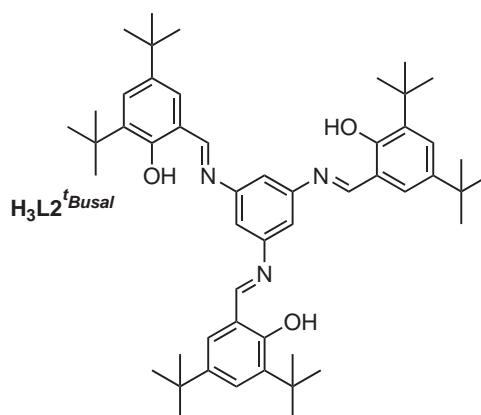
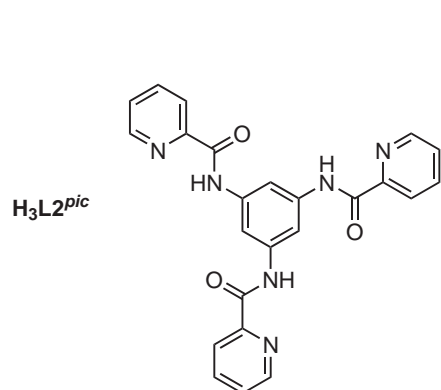
– Appendix –

A.1 Ligand-Overview

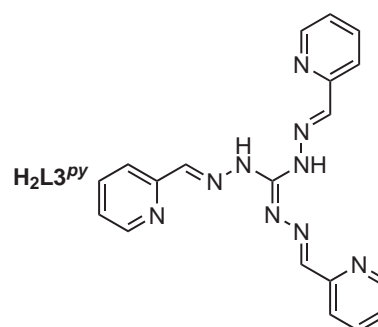
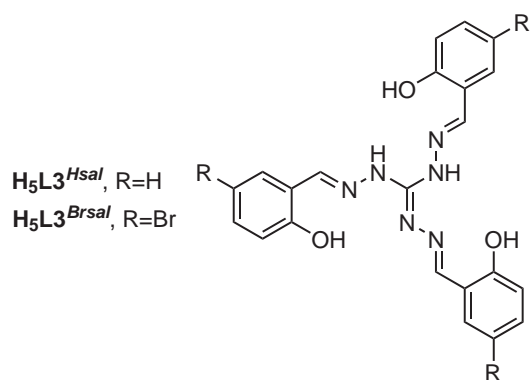
Phloroglucinol-Based Ligands



Triaminobenzene-Based Ligands



Triaminoguanidine-Based Ligands



A.2 Complex-Overview

Phloroglucinol-Bridged Complexes

1	$[\text{Cu}_3(\text{L1}^{ampy})(\text{MeCN})(\text{H}_2\text{O})_2](\text{ClO}_4)_3$	$(\text{Cu}_3\text{L1}^{ampy})$
2	$[\text{Ni}_3(\text{L1}^{ampy})(\text{Hbpea})_3](\text{ClO}_4)_3$	$(\text{Ni}_3\text{L1}^{ampy})$
3	$[\text{Ni}_3(\text{L1}^{unspenp})(\text{H}_2\text{O})_3](\text{ClO}_4)_3$	$(\text{Ni}_3\text{L1}^{unspenp})$
4	$[\text{Cu}_3(\text{H}_2\text{L1}^{bhy})(\text{Him})_3](\text{ClO}_4)_2$	$(\text{Cu}_3\text{L1}^{bhy})$
5	$[\text{Ni}_3(\text{H}_3\text{L1}^{bhy})(\text{Hbpea})_3](\text{ClO}_4)_3$	$(\text{Ni}_3\text{L1}^{bhy})$
6	$[\text{Co}_3(\text{L1}^{tBubhy})(\text{bpca})_3]$	$(\text{Co}_3\text{L1}^{tBubhy})$

Triaminobenzene-Bridged Complexes

7	$[\text{Cu}_3(\text{L2}^{pic})_2(\text{DMSO})_3]$	$(\text{Cu}_3\text{L2}_2^{pic})$
8	$[\text{Cu}_4(\text{L2}^{pic})_2(\mu_{1,3}\text{-N}_3)(\mu\text{-OH})(\text{H}_2\text{O})(\text{DMF})]$	$(\text{Cu}_4\text{L2}_2^{pic})$
9	$[\text{Cu}_2(\text{HL2}^{tBusal})_2]$	$(\text{Cu}_2\text{L2}_2^{tBusal})$
10	$[\text{Co}_2(\text{HL2}^{tBusal})_2]$	$(\text{Co}_2\text{L2}_2^{tBusal})$
11	$[\text{Cu}_4(\text{L2}^{tBusal})_2(\text{hfac})_2(\text{MeOH})_2]$	$(\text{Cu}_4\text{L2}_2^{tBusal})$

Triaminoguanidine-Bridged Complexes

12	$[\text{Fe}_3(\text{L3}^{Brsal})(\text{py})_6\text{Cl}_3]\text{ClO}_4$	$(\text{Fe}_3\text{L3}^{Brsal})$
13	$[\text{Fe}_3(\text{L3}^{Brsal})(\text{q})_3(\text{py})_2\text{Cl}]$	$(\text{Fe}_3\text{L3}^{Brsal}\text{q}_3)$
14	$[\text{Fe}_6(\text{L3}^{Brsal})_2(\mu\text{-OMe})_2(\text{py})_8\text{Cl}_6]$	$(\text{Fe}_6\text{L3}_2^{Brsal})$
15	$[\text{FeNi}_4(\text{L3}^{Brsal})_2(\text{tptz})_4](\text{ClO}_4)_{0.5}\text{Cl}_{0.5}$	$(\text{FeNi}_4\text{L3}_2^{Brsal})$
16	$[\text{MnNi}_4(\text{L3}^{Hsal})_2(\text{tptz})_4]\text{ClO}_4$	$(\text{MnNi}_4\text{L3}_2^{Hsal})$
17	$[\text{CoNi}_4(\text{L3}^{Hsal})_2(\text{tptz})_4]\text{ClO}_4$	$(\text{CoNi}_4\text{L3}_2^{Hsal})$
18	$[\text{Cu}_3(\text{L3}^{py})(\text{py})_2\text{Cl}_4]$	$(\text{Cu}_3\text{L3}^{py})$
19	$[\text{Ni}_3(\text{L3}^{py})(\text{py})_6\text{Cl}_3]\text{Cl}$	$(\text{Ni}_3\text{L3}^{py})$
20	$[\text{Ni}_3(\text{L3}^{py})(\text{py})_6(\text{N}_3)_3]\text{ClO}_4$	$(\text{Ni}_3\text{L3}^{py}(\text{N}_3)_3)$
21	$[\text{Ni}_3(\text{L3}^{py})(\text{bpca})_3]\text{PF}_6$	$(\text{Ni}_3\text{L3}^{py}(\text{bpca})_3)$
22	$[\text{Co}_3(\text{L3}^{py})(\text{py})_6\text{Cl}_3]\text{ClO}_4$	$(\text{Co}_3\text{L3}^{py})$
23	$[\text{Mn}_3(\text{L3}^{py})(\text{py})_6\text{Cl}_3]\text{ClO}_4$	$(\text{Mn}_3\text{L3}^{py})$
24	$\{[\text{Cu}_3(\text{L3}^{py})(\mu\text{-ox})(\text{ox})(\text{H}_2\text{O})_2]\}_n$	$(\{\text{Cu}_3\text{L3}^{py}\}_n)$
25	$\{[\text{Ni}_3(\text{L3}^{py})(\text{bpca})_3]\text{Na}(\text{ClO}_4)_2(\text{H}_2\text{O})_2\}_n$	$(\{\text{Ni}_3\text{L3}^{py}\}_n)$

A.3 Crystallographic Details

Table A.1: Crystallographic data and structure-refinement parameters for complex $[\text{Cu}_3(\text{L1}^{ampy})(\text{MeCN})(\text{H}_2\text{O})_2](\text{ClO}_4)_3 \cdot 2.25\text{H}_2\text{O}$ (**1**).

empirical formula	$\text{C}_{29}\text{H}_{32.50}\text{Cl}_3\text{Cu}_3\text{N}_7\text{O}_{19.25}$
formula weight (g mol^{-1})	1084.09
crystal system	triclinic
space group	$P\bar{1}$
a (pm)	1269.67(11)
b (pm)	1284.32(11)
c (pm)	1433.29(15)
α ($^\circ$)	91.786(6)
β ($^\circ$)	112.988(5)
γ ($^\circ$)	112.759(5)
V (nm^3)	1.9378(3)
Z	2
crystal size (mm)	0.6 x 0.6 x 0.4
D_{calcd} (Mg m^{-3})	1.858
μ (mm^{-1})	1.929
θ range of data collection ($^\circ$)	2.22, 27.44
measured reflections	12610
unique reflections/ R_{int}	8418/0.0363
goodness-of-fit on F^2	1.006
R indices (all data)	$R_1 = 0.0997, wR_2 = 0.1413$
final R indices ($F > 2\sigma(F)$)	$R_1 = 0.0535, wR_2 = 0.1183$
$R_1 = \sum(F_o - F_c) / \sum F_o , wR_2 = (\sum w(F_o^2 - F_c^2)^2 / \sum w(F_o^2)^2)^{\frac{1}{2}}$	

Table A.2: Crystallographic data and structure-refinement parameters for complex $[\text{Ni}_3(\text{L1}^{ampy})(\text{Hbpea})_3](\text{ClO}_4)_3 \cdot 1.75\text{MeCN} \cdot 1.75\text{MeOH} \cdot 0.375\text{H}_2\text{O}$ (**2**).

empirical formula	$\text{C}_{74.50}\text{H}_{86}\text{Cl}_3\text{N}_{16.75}\text{Ni}_3\text{O}_{17.38}$
formula weight (g mol^{-1})	1776.58
crystal system	monoclinic
space group	$P2_1/n$
a (pm)	3284.28(3)
b (pm)	1809.45(2)
c (pm)	3295.34(3)
α ($^\circ$)	90.00
β ($^\circ$)	117.910(1)
γ ($^\circ$)	90.00
V (nm^3)	17.3055(3)
Z	8
crystal size (mm)	0.4 x 0.4 x 0.3
D_{calcd} (Mg m^{-3})	1.364
μ (mm^{-1})	0.811
θ range of data collection ($^\circ$)	1.65, 27.48
measured reflections	103393
unique reflections/ R_{int}	39388/0.0635
goodness-of-fit on F^2	0.995
R indices (all data)	$R_1 = 0.1280, wR_2 = 0.2287$
final R indices ($F > 2\sigma(F)$)	$R_1 = 0.0717, wR_2 = 0.1956$
$R_1 = \sum(F_o - F_c) / \sum F_o , wR_2 = (\sum w(F_o^2 - F_c^2)^2 / \sum w(F_o^2)^2)^{\frac{1}{2}}$	

Table A.3: Crystallographic data and structure-refinement parameters for complex $[\text{Ni}_3(\text{L1}^{\text{unspenp}})(\text{H}_2\text{O})_3](\text{ClO}_4)_3 \cdot 3\text{MeCN} \cdot 0.5\text{H}_2\text{O}$ (**3**).

empirical formula	$\text{C}_{57}\text{H}_{67}\text{Cl}_3\text{N}_{15}\text{Ni}_3\text{O}_{18.5}$
formula weight (g mol^{-1})	1540.74
crystal system	rhombohedral
space group	$R\bar{3}$
a (pm)	2720.42(6)
b (pm)	2720.42(6)
c (pm)	1579.65(5)
α ($^\circ$)	90.00
β ($^\circ$)	90.00
γ ($^\circ$)	120.00
V (nm^3)	10.1243(4)
Z	6
crystal size (mm)	0.6 x 0.6 x 0.5
D_{calcd} (Mg m^{-3})	1.516
μ (mm^{-1})	1.027
θ range of data collection ($^\circ$)	2.63, 27.53
measured reflections	17854
unique reflections/ R_{int}	5131/0.0426
goodness-of-fit on F^2	0.949
R indices (all data)	$R_1 = 0.0563, wR_2 = 0.1236$
final R indices ($F > 2\sigma(F)$)	$R_1 = 0.0399, wR_2 = 0.1118$
$R_1 = \sum(F_o - F_c) / \sum F_o , wR_2 = (\sum w(F_o^2 - F_c^2)^2 / \sum w(F_o^2)^2)^{\frac{1}{2}}$	

Table A.4: Crystallographic data and structure-refinement parameters for complex $[\text{Cu}_3(\text{H}_2\text{L1}^{bhy})(\text{Him})_3](\text{ClO}_4)_2 \cdot 2\text{MeOH}$ (**4**).

empirical formula	$\text{C}_{41}\text{H}_{40}\text{Cl}_2\text{Cu}_3\text{N}_{12}\text{O}_{16}$
formula weight (g mol^{-1})	1218.37
crystal system	triclinic
space group	$P\bar{1}$
a (pm)	1509.76(4)
b (pm)	1838.75(5)
c (pm)	2129.84(6)
α ($^\circ$)	69.0210(10)
β ($^\circ$)	72.336(2)
γ ($^\circ$)	83.756(2)
V (nm^3)	5.2604(2)
Z	4
crystal size (mm)	0.6 x 0.6 x 0.5
D_{calcd} (Mg m^{-3})	1.538
μ (mm^{-1})	1.380
θ range of data collection ($^\circ$)	1.85, 27.49
measured reflections	35740
unique reflections/ R_{int}	23343/0.0332
goodness-of-fit on F^2	1.005
R indices (all data)	$R_1 = 0.1128, wR_2 = 0.2301$
final R indices ($F > 2\sigma(F)$)	$R_1 = 0.0692, wR_2 = 0.1946$
$R_1 = \sum(F_o - F_c) / \sum F_o , wR_2 = (\sum w(F_o^2 - F_c^2)^2 / \sum w(F_o^2)^2)^{\frac{1}{2}}$	

Table A.5: Crystallographic data and structure-refinement parameters for complex $[\text{Ni}_3(\text{H}_3\text{L1}^{bhy})(\text{Hbpea})_3](\text{ClO}_4)_3 \cdot 3\text{MeCN} \cdot 3.5\text{MeOH}$ (5).

empirical formula	$\text{C}_{81.50}\text{H}_{95}\text{Cl}_3\text{N}_{18}\text{Ni}_3\text{O}_{21.50}$
formula weight (g mol^{-1})	1953.23
crystal system	rhombohedral
space group	$R\bar{3}$
a (pm)	2111.87(2)
b (pm)	2111.87(2)
c (pm)	3716.81(4)
α ($^\circ$)	90.00
β ($^\circ$)	90.00
γ ($^\circ$)	120.00
V (nm^3)	14.3561(2)
Z	6
crystal size (mm)	0.3 x 0.3 x 0.3
D_{calcd} (Mg m^{-3})	1.356
μ (mm^{-1})	0.744
θ range of data collection ($^\circ$)	2.29, 27.87
measured reflections	21692
unique reflections/ R_{int}	7544/0.0601
goodness-of-fit on F^2	1.022
R indices (all data)	$R_1 = 0.0868, wR_2 = 0.1559$
final R indices ($F > 2\sigma(F)$)	$R_1 = 0.0534, wR_2 = 0.1376$
$R_1 = \sum(F_o - F_c) / \sum F_o , wR_2 = (\sum w(F_o^2 - F_c^2)^2 / \sum w(F_o^2)^2)^{\frac{1}{2}}$	

Table A.6: Crystallographic data and structure-refinement parameters for complex $[\text{Co}_3(\text{L1}^{t\text{Bubhy}})(\text{bpca})_3] \cdot 2.5\text{CHCl}_3 \cdot 4\text{MeOH} \cdot 3.25\text{H}_2\text{O}$ (**6**).

empirical formula	$\text{C}_{84.50}\text{H}_{91}\text{Cl}_{7.50}\text{Co}_3\text{N}_{15}\text{O}_{19.25}$
formula weight (g mol^{-1})	2067.39
crystal system	triclinic
space group	$P\bar{1}$
a (pm)	1615.36(4)
b (pm)	1696.84(5)
c (pm)	2076.29(6)
α ($^\circ$)	106.147(1)
β ($^\circ$)	102.471(1)
γ ($^\circ$)	101.166(1)
V (nm^3)	5.1386(2)
Z	2
crystal size (mm)	0.5 x 0.5 x 0.4
D_{calcd} (Mg m^{-3})	1.336
μ (mm^{-1})	0.742
θ range of data collection ($^\circ$)	3.98, 27.44
measured reflections	33515
unique reflections/ R_{int}	22179/0.0382
goodness-of-fit on F^2	1.095
R indices (all data)	$R_1 = 0.1261, wR_2 = 0.3021$
final R indices ($F > 2\sigma(F)$)	$R_1 = 0.1001, wR_2 = 0.2801$
$R_1 = \sum(F_o - F_c) / \sum F_o , wR_2 = (\sum w(F_o^2 - F_c^2)^2 / \sum w(F_o^2)^2)^{\frac{1}{2}}$	

Table A.7: Crystallographic data and structure-refinement parameters for complex $[\text{Cu}_3(\text{L}2^{pic})_2(\text{DMSO})_3] \cdot 3\text{DMSO} \cdot 6\text{H}_2\text{O}$ (7).

empirical formula	$\text{C}_{60}\text{H}_{78}\text{Cu}_3\text{N}_{12}\text{O}_{18}\text{S}_6$
formula weight (g mol^{-1})	1590.93
crystal system	cubic
space group	$Pa\bar{3}$
a (pm)	3145.28(2)
b (pm)	3145.28(2)
c (pm)	3145.28(2)
α ($^\circ$)	90
β ($^\circ$)	90
γ ($^\circ$)	90
V (nm^3)	31.1156(3)
Z	16
crystal size (mm)	0.8 x 0.8 x 0.6
D_{calcd} (Mg m^{-3})	1.399
μ (mm^{-1})	1.043
θ range of data collection ($^\circ$)	1.94 , 27.47
measured reflections	155394
unique reflections/ R_{int}	11843/0.0768
goodness-of-fit on F^2	1.056
R indices (all data)	$R_1 = 0.0932, wR_2 = 0.1743$
final R indices ($F > 2\sigma(F)$)	$R_1 = 0.0612, wR_2 = 0.1553$
$R_1 = \sum(F_o - F_c) / \sum F_o , wR_2 = (\sum w(F_o^2 - F_c^2)^2 / \sum w(F_o^2)^2)^{\frac{1}{2}}$	

Table A.8: Crystallographic data and structure-refinement parameters for complex $[\text{Cu}_4(\text{L}^{2pic})_2(\mu_{1,3}\text{-N}_3)(\mu\text{-OH})(\text{H}_2\text{O})(\text{DMF})] \cdot 2\text{DMF} \cdot 3\text{H}_2\text{O}$ (**8**).

empirical formula	$\text{C}_{57}\text{H}_{60}\text{Cu}_4\text{N}_{18}\text{O}_{14}$
formula weight (g mol^{-1})	1475.39
crystal system	monoclinic
space group	$P2_1/n$
a (pm)	1888.98(4)
b (pm)	1546.20(3)
c (pm)	2248.69(5)
α ($^\circ$)	90
β ($^\circ$)	114.1560(10)
γ ($^\circ$)	90
V (nm^3)	5.9927(2)
Z	4
crystal size (mm)	0.8 x 0.8 x 0.4
D_{calcd} (Mg m^{-3})	1.635
μ (mm^{-1})	1.483
θ range of data collection ($^\circ$)	2.38, 27.50
measured reflections	39996
unique reflections/ R_{int}	13718/0.0787
goodness-of-fit on F^2	1.016
R indices (all data)	$R_1 = 0.1038, wR_2 = 0.1312$
final R indices ($F > 2\sigma(F)$)	$R_1 = 0.0512, wR_2 = 0.1116$
$R_1 = \sum(F_o - F_c) / \sum F_o , wR_2 = (\sum w(F_o^2 - F_c^2)^2 / \sum w(F_o^2)^2)^{\frac{1}{2}}$	

Table A.9: Crystallographic data and structure-refinement parameters for complex $[\text{Cu}_2(\text{HL}2^{\text{tBusal}})_2] \cdot 10\text{CHCl}_3$ (**9**).

empirical formula	$\text{C}_{122}\text{H}_{144}\text{Cl}_{31}\text{Cu}_4\text{N}_6\text{O}_6$
formula weight (g mol^{-1})	2896.36
crystal system	monoclinic
space group	$P2_1/c$
a (pm)	1886.20(6)
b (pm)	3704.72(11)
c (pm)	1004.23(3)
α ($^\circ$)	90.00
β ($^\circ$)	100.918(2)
γ ($^\circ$)	90.00
V (nm^3)	6.8904(4)
Z	2
crystal size (mm)	0.5 x 0.5 x 0.3
D_{calcd} (Mg m^{-3})	1.396
μ (mm^{-1})	0.960
θ range of data collection ($^\circ$)	1.98, 27.50
measured reflections	23897
unique reflections/ R_{int}	14274/0.0423
goodness-of-fit on F^2	1.008
R indices (all data)	$R_1 = 0.1543, wR_2 = 0.2570$
final R indices ($F > 2\sigma(F)$)	$R_1 = 0.0921, wR_2 = 0.2187$
$R_1 = \sum(F_o - F_c) / \sum F_o , wR_2 = (\sum w(F_o^2 - F_c^2)^2 / \sum w(F_o^2)^2)^{\frac{1}{2}}$	

Table A.10: Crystallographic data and structure-refinement parameters for complex $[\text{Co}_2(\text{HL}2^{\text{Busal}})_2] \cdot 4\text{DMF}$ (**10**).

empirical formula	$\text{C}_{114}\text{H}_{162}\text{Co}_2\text{N}_{10}\text{O}_{10}$
formula weight (g mol^{-1})	1950.40
crystal system	orthorhombic
space group	<i>Pbca</i>
a (pm)	1176.72(3)
b (pm)	2799.72(7)
c (pm)	3499.34(9)
α ($^\circ$)	90.00
β ($^\circ$)	90.00
γ ($^\circ$)	90.00
V (nm^3)	11.5285(5)
Z	4
crystal size (mm)	0.4 x 0.4 x 0.4
D_{calcd} (Mg m^{-3})	1.124
μ (mm^{-1})	0.345
θ range of data collection ($^\circ$)	2.54, 20.83
measured reflections	37748
unique reflections/ R_{int}	6020/0.1138
goodness-of-fit on F^2	1.056
R indices (all data)	$R_1 = 0.1307, wR_2 = 0.2596$
final R indices ($F > 2\sigma(F)$)	$R_1 = 0.0888, wR_2 = 0.2297$
$R_1 = \sum(F_o - F_c) / \sum F_o , wR_2 = (\sum w(F_o^2 - F_c^2)^2 / \sum w(F_o^2)^2)^{\frac{1}{2}}$	

Table A.11: Crystallographic data and structure-refinement parameters for complex $[\text{Cu}_4(\text{L2}^{\text{Busal}})_2(\text{hfac})_2(\text{MeOH})_2] \cdot 5\text{CHCl}_3 \cdot 3\text{MeOH}$ (**11**).

empirical formula	$\text{C}_{122}\text{H}_{157}\text{Cl}_{15}\text{Cu}_4\text{F}_{12}\text{N}_6\text{O}_{15}$
formula weight (g mol^{-1})	2961.45
crystal system	triclinic
space group	$P\bar{1}$
a (pm)	1365.65(4)
b (pm)	1599.10(4)
c (pm)	1902.10(6)
α ($^\circ$)	111.467(1)
β ($^\circ$)	98.007(1)
γ ($^\circ$)	101.384(1)
V (nm^3)	3.68634(18)
Z	1
crystal size (mm)	0.5 x 0.5 x 0.4
D_{calcd} (Mg m^{-3})	1.334
μ (mm^{-1})	0.912
θ range of data collection ($^\circ$)	2.77, 27.48
measured reflections	25535
unique reflections/ R_{int}	16698/0.0318
goodness-of-fit on F^2	1.011
R indices (all data)	$R_1 = 0.1246, wR_2 = 0.2549$
final R indices ($F > 2\sigma(F)$)	$R_1 = 0.0828, wR_2 = 0.2201$
$R_1 = \sum(F_o - F_c) / \sum F_o , wR_2 = (\sum w(F_o^2 - F_c^2)^2 / \sum w(F_o^2)^2)^{\frac{1}{2}}$	

Table A.12: Crystallographic data and structure-refinement parameters for complex $[\text{Fe}_3(\text{L3}^{\text{Brsal}})(\text{py})_6\text{Cl}_3]\text{ClO}_4 \cdot 3\text{H}_2\text{O}$ (**12**).

empirical formula	$\text{C}_{52}\text{H}_{48}\text{Br}_3\text{Cl}_4\text{Fe}_3\text{N}_{12}\text{O}_{10}$
formula weight (g mol^{-1})	1550.10
crystal system	hexagonal
space group	$P\bar{3}$
a (pm)	1533.80(4)
b (pm)	1533.80(4)
c (pm)	1635.24(6)
α ($^\circ$)	90.00
β ($^\circ$)	90.00
γ ($^\circ$)	120.00
V (nm^3)	3.33157(17)
Z	2
crystal size (mm)	0.7 x 0.7 x 0.7
D_{calcd} (Mg m^{-3})	1.545
μ (mm^{-1})	2.664
θ range of data collection ($^\circ$)	2.66, 27.48
measured reflections	22613
unique reflections/ R_{int}	5084/0.0750
goodness-of-fit on F^2	1.028
R indices (all data)	$R_1 = 0.0910, wR_2 = 0.1630$
final R indices ($F > 2\sigma(F)$)	$R_1 = 0.0618, wR_2 = 0.1471$
$R_1 = \sum(F_o - F_c) / \sum F_o , wR_2 = (\sum w(F_o^2 - F_c^2)^2 / \sum w(F_o^2)^2)^{\frac{1}{2}}$	

Table A.13: Crystallographic data and structure-refinement parameters for complex $[\text{Fe}_3(\text{L3}^{\text{Brsal}})(\text{q})_3(\text{py})_2\text{Cl}] \cdot 2\text{py} \cdot \text{MeOH}$ (**13**).

empirical formula	$\text{C}_{70}\text{H}_{54}\text{Br}_3\text{ClFe}_3\text{N}_{13}\text{O}_7$
formula weight (g mol^{-1})	1631.99
crystal system	monoclinic
space group	$C2/c$
a (pm)	2393.79(5)
b (pm)	1854.05(3)
c (pm)	3283.09(6)
α ($^\circ$)	90.00
β ($^\circ$)	110.7280(10)
γ ($^\circ$)	90.00
V (nm^3)	13.6279(4)
Z	8
crystal size (mm)	0.6 x 0.6 x 0.5
D_{calcd} (Mg m^{-3})	1.591
μ (mm^{-1})	2.493
θ range of data collection ($^\circ$)	2.33, 27.48
measured reflections	46998
unique reflections/ R_{int}	15430/0.0657
goodness-of-fit on F^2	1.011
R indices (all data)	$R_1 = 0.0998, wR_2 = 0.1326$
final R indices ($F > 2\sigma(F)$)	$R_1 = 0.0533, wR_2 = 0.1156$
$R_1 = \sum(F_o - F_c) / \sum F_o , wR_2 = (\sum w(F_o^2 - F_c^2)^2 / \sum w(F_o^2)^2)^{\frac{1}{2}}$	

Table A.14: Crystallographic data and structure-refinement parameters for complex $[\text{Fe}_6(\text{L}^{\text{Brsal}})_2(\mu\text{-OMe})_2(\text{py})_8\text{Cl}_6] \cdot \text{MeOH} \cdot \text{H}_2\text{O}$ (**14**).

empirical formula	$\text{C}_{87}\text{H}_{76}\text{Br}_6\text{Cl}_6\text{Fe}_6\text{N}_{20}\text{O}_{10}$
formula weight (g mol^{-1})	2588.94
crystal system	orthorhombic
space group	<i>Pbca</i>
a (pm)	1770.15(3)
b (pm)	2153.78(4)
c (pm)	2822.99(6)
α ($^\circ$)	90.00
β ($^\circ$)	90.00
γ ($^\circ$)	90.00
V (nm^3)	10.7627(4)
Z	4
crystal size (mm)	0.4 x 0.4 x 0.4
D_{calcd} (Mg m^{-3})	1.598
μ (mm^{-1})	3.225
θ range of data collection ($^\circ$)	2.33, 27.48
measured reflections	51549
unique reflections/ R_{int}	12281/0.0570
goodness-of-fit on F^2	1.020
R indices (all data)	$R_1 = 0.1018, wR_2 = 0.1849$
final R indices ($F > 2\sigma(F)$)	$R_1 = 0.0594, wR_2 = 0.1577$
$R_1 = \sum(F_o - F_c) / \sum F_o , wR_2 = (\sum w(F_o^2 - F_c^2)^2 / \sum w(F_o^2)^2)^{\frac{1}{2}}$	

Table A.15: Crystallographic data and structure-refinement parameters for complex $[\text{FeNi}_4(\text{L}3^{\text{Brsal}})_2(\text{tptz})_4](\text{ClO}_4)_{0.5}\text{Cl}_{0.5} \cdot 2.5\text{DMF} \cdot \text{MeOH} \cdot 9\text{H}_2\text{O}$ (**15**).

empirical formula	$\text{C}_{124.5}\text{H}_{111.5}\text{Br}_6\text{ClFeN}_{38.5}\text{Ni}_4\text{O}_{20.50}$
formula weight (g mol^{-1})	3280.62
crystal system	triclinic
space group	$P\bar{1}$
a (pm)	1633.06(4)
b (pm)	2162.13(8)
c (pm)	2170.90(7)
α ($^\circ$)	97.291(2)
β ($^\circ$)	96.961(2)
γ ($^\circ$)	94.706(2)
V (nm^3)	7.5101(4)
Z	2
crystal size (mm)	0.05 x 0.05 x 0.05
D_{calcd} (Mg m^{-3})	1.451
μ (mm^{-1})	2.273
θ range of data collection ($^\circ$)	1.91, 27.50
measured reflections	33337
unique reflections/ R_{int}	15750/0.0531
goodness-of-fit on F^2	1.008
R indices (all data)	$R_1 = 0.0847, wR_2 = 0.2088$
Final R indices ($F > 2\sigma(F)$)	$R_1 = 0.1896, wR_2 = 0.2678$
$R_1 = \sum(F_o - F_c) / \sum F_o , wR_2 = (\sum w(F_o^2 - F_c^2)^2 / \sum w(F_o^2)^2)^{\frac{1}{2}}$	

Table A.16: Crystallographic data and structure-refinement parameters for complex $[\text{Cu}_3(\text{L}3^{\text{py}})(\text{py})_2\text{Cl}_4] \cdot 0.5\text{py}$ (**18**).

empirical formula	$\text{C}_{31.50}\text{H}_{28}\text{Cl}_4\text{Cu}_3\text{N}_{11.50}$
formula weight (g mol^{-1})	900.07
crystal system	triclinic
space group	$P\bar{1}$
a (pm)	1181.02(5)
b (pm)	1259.73(5)
c (pm)	1342.84(5)
α ($^\circ$)	70.187(2)
β ($^\circ$)	75.531(3)
γ ($^\circ$)	66.894(2)
V (nm^3)	1.71296(12)
Z	2
crystal size (mm)	0.4 x 0.4 x 0.4
D_{calcd} (Mg m^{-3})	1.745
μ (mm^{-1})	2.202
θ range of data collection ($^\circ$)	2.66, 27.46
measured reflections	12177
unique reflections/ R_{int}	7813/0.0286
goodness-of-fit on F^2	1.005
R indices (all data)	$R_1 = 0.0561, wR_2 = 0.0800$
final R indices ($F > 2\sigma(F)$)	$R_1 = 0.0364, wR_2 = 0.0720$
$R_1 = \sum(F_o - F_c) / \sum F_o , wR_2 = (\sum w(F_o^2 - F_c^2)^2 / \sum w(F_o^2)^2)^{\frac{1}{2}}$	

Table A.17: Crystallographic data and structure-refinement parameters for complex $[\text{Ni}_3(\text{L3}^{\text{py}})(\text{py})_6\text{Cl}_3]\text{Cl} \cdot \text{py} \cdot 0.5\text{MeOH} \cdot 3.5\text{H}_2\text{O}$ (**19**).

empirical formula	$\text{C}_{54.50}\text{H}_{59}\text{Cl}_4\text{N}_{16}\text{Ni}_3\text{O}_4$
formula weight (g mol^{-1})	1320.11
crystal system	monoclinic
space group	$P2_1/c$
a (pm)	2310.13(4)
b (pm)	1205.74(2)
c (pm)	2215.94(4)
α ($^\circ$)	90.00
β ($^\circ$)	91.8840(10)
γ ($^\circ$)	90.00
V (nm^3)	6.16898(19)
Z	4
crystal size (mm)	0.5 x 0.4 x 0.4
D_{calcd} (Mg m^{-3})	1.421
μ (mm^{-1})	1.137
θ range of data collection ($^\circ$)	2.07, 27.47
measured reflections	43254
unique reflections/ R_{int}	14107/0.0615
goodness-of-fit on F^2	1.007
R indices (all data)	$R_1 = 0.0933, wR_2 = 0.1746$
final R indices ($F > 2\sigma(F)$)	$R_1 = 0.0560, wR_2 = 0.1530$
$R_1 = \sum(F_o - F_c) / \sum F_o , wR_2 = (\sum w(F_o^2 - F_c^2)^2 / \sum w(F_o^2)^2)^{\frac{1}{2}}$	

Table A.18: Crystallographic data and structure-refinement parameters for complex $[\text{Ni}_3(\text{L}3^{\text{py}})(\text{py})_6(\text{N}_3)_3]\text{ClO}_4 \cdot \text{MeOH}$ (**20**).

empirical formula	$\text{C}_{50}\text{H}_{49}\text{ClN}_{24}\text{Ni}_3\text{O}_5$
formula weight (g mol^{-1})	1277.71
crystal system	cubic
space group	$P\bar{a}3$
a (pm)	2295.95(2)
b (pm)	2295.95(2)
c (pm)	2295.95(2)
α ($^\circ$)	90.00
β ($^\circ$)	90.00
γ ($^\circ$)	90.00
V (nm^3)	12.10284(18)
Z	8
crystal size (mm)	0.6 x 0.6 x 0.5
D_{calcd} (Mg m^{-3})	1.402
μ (mm^{-1})	1.033
θ range of data collection ($^\circ$)	1.77, 27.48
measured reflections	85704
unique reflections/ R_{int}	4633/0.0546
goodness-of-fit on F^2	1.052
R indices (all data)	$R_1 = 0.0809, wR_2 = 0.2063$
final R indices ($F > 2\sigma(F)$)	$R_1 = 0.0613, wR_2 = 0.1764$
$R_1 = \sum(F_o - F_c) / \sum F_o , wR_2 = (\sum w(F_o^2 - F_c^2)^2 / \sum w(F_o^2)^2)^{\frac{1}{2}}$	

Table A.19: Crystallographic data and structure-refinement parameters for complex $[\text{Ni}_3(\text{L3}^{\text{py}})(\text{bpca})_3]\text{PF}_6 \cdot 2.5\text{MeOH}$ (**21**).

empirical formula	$\text{C}_{57.50}\text{H}_{49}\text{F}_6\text{N}_{18}\text{Ni}_3\text{O}_{8.50}\text{P}$
formula weight (g mol^{-1})	1449.25
crystal system	triclinic
space group	$P\bar{1}$
a (pm)	1264.69(2)
b (pm)	1291.83(3)
c (pm)	2008.78(4)
α ($^\circ$)	80.062(1)
β ($^\circ$)	75.892(1)
γ ($^\circ$)	82.854(1)
V (nm^3)	3.1235(1)
Z	2
crystal size (mm)	0.6 x 0.6 x 0.4
D_{calcd} (Mg m^{-3})	1.541
μ (mm^{-1})	1.008
θ range of data collection ($^\circ$)	2.17, 27.45
measured reflections	22512
unique reflections/ R_{int}	14154/0.0266
goodness-of-fit on F^2	1.023
R indices (all data)	$R_1 = 0.0623, wR_2 = 0.1247$
final R indices ($F > 2\sigma(F)$)	$R_1 = 0.0432, wR_2 = 0.1150$
$R_1 = \sum(F_o - F_c) / \sum F_o , wR_2 = (\sum w(F_o^2 - F_c^2)^2 / \sum w(F_o^2)^2)^{\frac{1}{2}}$	

Table A.20: Crystallographic data and structure-refinement parameters for complex $[\text{Co}_3(\text{L3}^{\text{py}})(\text{py})_6\text{Cl}_3]\text{ClO}_4 \cdot 3.5\text{py}$ (**22**).

empirical formula	$\text{C}_{66.50}\text{H}_{62.50}\text{Cl}_4\text{Co}_3\text{N}_{18.50}\text{O}_4$
formula weight (g mol^{-1})	1503.44
crystal system	monoclinic
space group	C2
a (pm)	2403.90(5)
b (pm)	2338.24(8)
c (pm)	1541.55(6)
α ($^\circ$)	90.00
β ($^\circ$)	128.260(2)
γ ($^\circ$)	90.00
V (nm^3)	6.8037(4)
Z	4
crystal size (mm)	0.8 x 0.8 x 0.5
D_{calcd} (Mg m^{-3})	1.468
μ (mm^{-1})	0.943
θ range of data collection ($^\circ$)	2.42 , 27.48
measured reflections	24124
unique reflections/ R_{int}	13871/0.0451
goodness-of-fit on F^2	1.000
R indices (all data)	$R_1 = 0.0736, wR_2 = 0.1028$
final R indices ($F > 2\sigma(F)$)	$R_1 = 0.0466, wR_2 = 0.0928$
flack parameter	-0.025(11)

$$R_1 = \sum(|F_o| - |F_c|) / \sum |F_o|, wR_2 = (\sum w(F_o^2 - F_c^2)^2 / \sum w(F_o^2)^2)^{\frac{1}{2}}$$

Table A.21: Crystallographic data and structure-refinement parameters for complex $[\text{Mn}_3(\text{L}3^{\text{py}})(\text{py})_6\text{Cl}_3]\text{ClO}_4 \cdot 3\text{py}$ (**23**).

empirical formula	$\text{C}_{64}\text{H}_{60}\text{Cl}_4\text{Mn}_3\text{N}_{18}\text{O}_4$
formula weight (g mol^{-1})	1451.92
crystal system	monoclinic
space group	$P2_1$
a (pm)	1243.42(2)
b (pm)	1735.70(4)
c (pm)	1627.31(3)
α ($^\circ$)	90.00
β ($^\circ$)	105.123(1)
γ ($^\circ$)	90.00
V (nm^3)	3.39044(11)
Z	2
crystal size (mm)	0.5 x 0.5 x 0.5
D_{calcd} (Mg m^{-3})	1.422
μ (mm^{-1})	0.769
θ range of data collection ($^\circ$)	2.06, 27.47
measured reflections	24228
unique reflections/ R_{int}	14863/0.0285
goodness-of-fit on F^2	1.004
R indices (all data)	$R_1 = 0.0483$, $wR_2 = 0.0838$
final R indices ($F > 2\sigma(F)$)	$R_1 = 0.0371$, $wR_2 = 0.0783$
flack parameter	-0.003(10)

$$R_1 = \sum(|F_o| - |F_c|) / \sum |F_o|, \quad wR_2 = (\sum w(F_o^2 - F_c^2)^2 / \sum w(F_o^2)^2)^{\frac{1}{2}}$$

Table A.22: Crystallographic data and structure-refinement parameters for complex $[\text{Cu}_3(\text{L3}^{\text{py}})(\mu\text{-ox})_2(\text{H}_2\text{O})_2]_n \cdot 0.25n\text{EtOH} \cdot 3.5n\text{H}_2\text{O}$ (**24**).

empirical formula	$\text{C}_{47}\text{H}_{55}\text{Cu}_6\text{N}_{18}\text{O}_{27.50}$
formula weight (g mol^{-1})	1693.33
crystal system	triclinic
space group	$P\bar{1}$
a (pm)	1420.19(6)
b (pm)	1466.51(5)
c (pm)	1782.93(9)
α ($^\circ$)	93.821(3)
β ($^\circ$)	112.736(2)
γ ($^\circ$)	111.342(2)
V (nm^3)	3.0957(2)
Z	2
crystal size (mm)	0.4 x 0.4 x 0.4
D_{calcd} (Mg m^{-3})	1.817
μ (mm^{-1})	2.126
θ range of data collection ($^\circ$)	1.74, 27.46
measured reflections	21573
unique reflections/ R_{int}	14037/0.0478
goodness-of-fit on F^2	1.008
R indices (all data)	$R_1 = 0.1124, wR_2 = 0.1665$
final R indices ($F > 2\sigma(F)$)	$R_1 = 0.0621, wR_2 = 0.1402$
$R_1 = \sum(F_o - F_c) / \sum F_o , wR_2 = (\sum w(F_o^2 - F_c^2)^2 / \sum w(F_o^2)^2)^{\frac{1}{2}}$	

Table A.23: Crystallographic data and structure-refinement parameters for complex $\{[\text{Ni}_3(\text{L}3^{py})(\text{bpca})_3]\text{Na}(\text{ClO}_4)_2(\text{H}_2\text{O})_2\}_n$ (25).

empirical formula	$\text{C}_{55}\text{H}_{43}\text{Cl}_2\text{N}_{18}\text{NaNi}_3\text{O}_{16}$
formula weight (g mol^{-1})	1482.09
crystal system	monoclinic
space group	$P2_1/c$
a (pm)	2521.50(2)
b (pm)	2485.61(2)
c (pm)	2185.70(2)
α ($^\circ$)	90.00
β ($^\circ$)	113.486(1)
γ ($^\circ$)	90.00
V (nm^3)	12.56395(18)
Z	8
crystal size (mm)	0.6 x 0.6 x 0.5
D_{calcd} (Mg m^{-3})	1.567
μ (mm^{-1})	1.064
θ range of data collection ($^\circ$)	1.33, 27.46
measured reflections	84535
unique reflections/ R_{int}	28514/0.0398
goodness-of-fit on F^2	1.043
R indices (all data)	$R_1 = 0.0993, wR_2 = 0.2081$
final R indices ($F > 2\sigma(F)$)	$R_1 = 0.0649, wR_2 = 0.1779$
$R_1 = \sum(F_o - F_c) / \sum F_o , wR_2 = (\sum w(F_o^2 - F_c^2)^2 / \sum w(F_o^2)^2)^{\frac{1}{2}}$	

Bibliography

- [1] W. Plass, *Chem. unserer Zeit* **1998**, 32, 323–333.
- [2] K. Maekawa, D. Shiomi, T. Ise, K. Sato, T. Takui, *Org. Biomol. Chem.* **2007**, 5, 1641–1645.
- [3] M. Deumal, F. Mota, M. J. Bearpark, M. A. Robb, J. J. Novoa, *Mol. Phys.* **2006**, 104, 857–873.
- [4] Y. Hosokoshi, Y. Nakazawa, K. Inoue, K. Takizawa, H. Nakano, M. Takahashi, T. Goto, *Phys. Rev. B* **1999**, 60, 12924–12932.
- [5] M. Mito, T. Kawae, M. Takumi, K. Nagata, M. Tamura, M. Kinoshita, K. Takeda, *Phys. Rev. B* **1997**, 56, R14255–R14258.
- [6] Y. Nakazawa, M. Tamura, N. Shirakawa, D. Shiomi, M. Takahashi, M. Kinoshita, M. Ishikawa, *Phys. Rev. B* **1992**, 46, 8906–8914.
- [7] J. M. Rawson, A. Alberola, A. Whalley, *J. Mater. Chem.* **2006**, 16, 2560–2575.
- [8] J. M. Rawson, G. D. McManus, *Coord. Chem. Rev.* **1999**, 189, 135–168.
- [9] S. J. Blundell, F. L. Pratt, *J. Phys.: Condens. Matter* **2004**, 16, R771–R828.
- [10] A. Caneschi, D. Gatteschi, R. Sessoli, *Mol. Cryst. Liq. Cryst.* **1996**, 279, 177–194.
- [11] A. J. Banister, N. Bricklebank, I. Lavender, J. M. Rawson, C. I. Gregory, B. K. Tanner, W. Clegg, M. R. J. Elsegood, F. Palacio, *Angew. Chem., Int. Ed.* **1996**, 35, 2533–2535.
- [12] A. J. Banister, N. Bricklebank, W. Clegg, M. R. J. Elsegood, C. I. Gregory, I. Lavender, J. M. Rawson, B. K. Tanner, *J. Chem. Soc., Chem. Commun.* **1995**, 679–680.
- [13] A. Caneschi, D. Gatteschi, N. Lalioti, R. Sessoli, L. Sorace, V. Tangoulis, A. Vindigni, *Chem. Eur. J.* **2002**, 8, 286–292.
- [14] A. Caneschi, D. Gatteschi, N. Lalioti, C. Sangregorio, R. Sessoli, G. Venturi, A. Vindigni, A. Rettori, M. G. Pini, M. A. Novak, *Angew. Chem., Int. Ed.* **2001**, 40, 1760–1763.
- [15] K. Bernot, J. Luzon, A. Caneschi, D. Gatteschi, R. Sessoli, L. Bogani, A. Vindigni, A. Rettori, M. G. Pini, *arXiv:0901.4409v1 [cond-mat.mtrl-sci]* **2009**.
- [16] K. Bernot, J. Luzon, L. Bogani, M. Etienne, C. Sangregorio, M. Shanmugam, A. Caneschi, R. Sessoli, D. Gatteschi, *J. Am. Chem. Soc.* **2009**, 131, 5573–5579.

Bibliography

- [17] K. Bernot, L. Bogani, R. Sessoli, D. Gatteschi, *Inorg. Chim. Acta* **2007**, *360*, 3807–3812.
- [18] K. Bernot, L. Bogani, A. Caneschi, D. Gatteschi, R. Sessoli, *J. Am. Chem. Soc.* **2006**, *128*, 7947–7956.
- [19] L. Bogani, C. Sangregorio, R. Sessoli, D. Gatteschi, *Angew. Chem., Int. Ed.* **2005**, *44*, 5817–5821.
- [20] G. A. Candela, L. J. Swartzendruber, J. S. Miller, M. J. Rice, *J. Am. Chem. Soc.* **1979**, *101*, 2755–2756.
- [21] J. S. Miller, *Polyhedron* **2009**, *28*, 1596–1605.
- [22] J. S. Miller, *Inorg. Chem.* **2000**, *39*, 4392–4408.
- [23] J. M. Manriquez, G. T. Yee, R. S. McLean, A. J. Epstein, J. S. Miller, *Science* **1991**, *252*, 1415–1417.
- [24] R. Sessoli, H. L. Tsai, A. R. Schake, S. Wang, J. B. Vincent, K. Folting, D. Gatteschi, G. Christou, D. N. Hendrickson, *J. Am. Chem. Soc.* **1993**, *115*, 1804–1816.
- [25] R. Sessoli, D. Gatteschi, A. Caneschi, M. A. Novak, *Nature* **1993**, *365*, 141–143.
- [26] T. Lis, *Acta Cryst.* **1980**, *B36*, 2042–2046.
- [27] D. Gatteschi, R. Sessoli, *Angew. Chem., Int. Ed.* **2003**, *42*, 268–297.
- [28] O. Roubeau, R. Clérac, *Eur. J. Inorg. Chem.* **2008**, 4325–4342.
- [29] L. Lecren, W. Wernsdorfer, Y.-G. Li, A. Vindigni, H. Miyasaka, R. Clerac, *J. Am. Chem. Soc.* **2007**, *129*, 5045–5051.
- [30] C.-I. Yang, W. Wernsdorfer, G.-H. Lee, H.-L. Tsai, *J. Am. Chem. Soc.* **2007**, *129*, 456–457.
- [31] E. Brechin, *Chem. Commun.* **2005**, 5141–5153.
- [32] H. Oshio, M. Nihei, A. Yoshida, H. Nojiri, M. Nakano, A. Yamaguchi, Y. Karaki, H. Ishimoto, *Chem. Eur. J.* **2005**, *11*, 843–848.
- [33] M. Murugesu, M. Habrych, W. Wernsdorfer, K. A. Abboud, G. Christou, *J. Am. Chem. Soc.* **2004**, *126*, 4766–4767.
- [34] A. J. Tasiopoulos, W. Wernsdorfer, B. Moulton, M. J. Zaworotko, G. Christou, *J. Am. Chem. Soc.* **2003**, *125*, 15274–15275.
- [35] S. Hill, R. S. Edwards, N. Aliaga-Alcalde, G. Christou, *Science* **2003**, *302*, 1015–1018.
- [36] C. J. Milios, R. Inglis, A. Vinslava, R. Bagai, W. Wernsdorfer, S. Parsons, S. P. Perlepes, G. Christou, E. K. Brechin, *J. Am. Chem. Soc.* **2007**, *129*, 12505–12511.
- [37] C. J. Milios, A. Vinslava, W. Wernsdorfer, S. Moggach, S. Parsons, S. P. Perlepes, G. Christou, E. K. Brechin, *J. Am. Chem. Soc.* **2007**, *129*, 2754–2755.

- [38] L. Lecren, O. Roubeau, C. Coulon, Y.-G. Li, X. F. Le Goff, W. Wernsdorfer, H. Miyasaka, R. Clerac, *J. Am. Chem. Soc.* **2005**, *127*, 17353–17363.
- [39] L. Lecren, W. Wernsdorfer, Y.-G. Li, O. Roubeau, H. Miyasaka, R. Clerac, *J. Am. Chem. Soc.* **2005**, *127*, 11311–11317.
- [40] B. Hussain, D. Savard, T. J. Burchell, W. Wernsdorfer, M. Murugesu, *Chem. Commun.* **2009**, 1100–1102.
- [41] J. Luzon, K. Bernot, I. J. Hewitt, C. E. Anson, A. K. Powell, R. Sessoli, *Phys. Rev. Lett.* **2008**, *100*, 247205.
- [42] J. Tang, I. Hewitt, N. T. Madhu, G. Chastanet, W. Wernsdorfer, C. E. Anson, C. Benelli, R. Sessoli, A. K. Powell, *Angew. Chem., Int. Ed.* **2006**, *45*, 1729–1733.
- [43] J.-D. Compain, P. Mialane, A. Dolbecq, I. M. Mbomekallé, J. Marrot, F. Sécheresse, E. Rivière, G. Rogez, W. Wernsdorfer, *Angew. Chem., Int. Ed.* **2009**, *48*, 3077–3081.
- [44] J. Martinez-Lillo, D. Armentano, G. De Munno, W. Wernsdorfer, J. M. Clemente-Juan, J. Krzystek, F. Lloret, M. Julve, J. Faus, *Inorg. Chem.* **2009**, *48*, 3027–3038.
- [45] G. Novitchi, W. Wernsdorfer, L. Chibotaru, J.-P. Costes, C. Anson, A. Powell, *Angew. Chem., Int. Ed.* **2009**, *48*, 1614–1619.
- [46] D. Gatteschi, R. Sessoli, A. Cornia, *Chem. Commun.* **2000**, 725–732.
- [47] A. Mishra, W. Wernsdorfer, K. A. Abboud, G. Christou, *J. Am. Chem. Soc.* **2004**, *126*, 15648–15649.
- [48] D. Li, S. Parkin, G. Wang, G. T. Yee, R. Clerac, W. Wernsdorfer, S. M. Holmes, *J. Am. Chem. Soc.* **2006**, *128*, 4214–4215.
- [49] M. Ferbinteanu, H. Miyasaka, W. Wernsdorfer, K. Nakata, K.-i. Sugiura, M. Yamashita, C. Coulon, R. Clerac, *J. Am. Chem. Soc.* **2005**, *127*, 3090–3099.
- [50] V. M. Mereacre, A. M. Ako, R. Clerac, W. Wernsdorfer, G. Filoti, J. Bartolome, C. E. Anson, A. K. Powell, *J. Am. Chem. Soc.* **2007**, *129*, 9248–9249.
- [51] L. F. Chibotaru, L. Ungur, C. Aronica, H. Elmol, G. Pilet, D. Luneau, *J. Am. Chem. Soc.* **2008**, *130*, 12445–12455.
- [52] S. Accorsi, A.-L. Barra, A. Caneschi, G. Chastanet, A. Cornia, A. C. Fabretti, D. Gatteschi, C. Mortalo, E. Olivieri, F. Parenti, P. Rosa, R. Sessoli, L. Sorace, W. Wernsdorfer, L. Zobbi, *J. Am. Chem. Soc.* **2006**, *128*, 4742–4755.
- [53] D. Gatteschi, A. Caneschi, L. Pardi, R. Sessoli, *Science* **1994**, *265*, 1054–1058.
- [54] S. T. Ochsenein, M. Murrie, E. Rusanov, H. Stoeckli-Evans, C. Sekine, H. U. Güdel, *Inorg. Chem.* **2002**, *41*, 5133–5140.

Bibliography

- [55] K. W. Galloway, A. M. Whyte, W. Wernsdorfer, J. Sanchez-Benitez, K. V. Kamenev, A. Parkin, R. D. Peacock, M. Murrie, *Inorg. Chem.* **2008**, *47*, 7438–7442.
- [56] V. Mereacre, A. Ako, R. Clrac, W. Wernsdorfer, I. Hewitt, C. Anson, A. Powell, *Chem. Eur. J.* **2008**, *14*, 3577–3584.
- [57] F. Branzoli, P. Carretta, M. Filibian, G. Zoppellaro, M. J. Graf, J. R. Galan-Mascaros, O. Fuhr, S. Brink, M. Ruben, *J. Am. Chem. Soc.* **2009**, *131*, 4387–4396.
- [58] N. Ishikawa, M. Sugita, W. Wernsdorfer, *J. Am. Chem. Soc.* **2005**, *127*, 3650–3651.
- [59] N. Ishikawa, M. Sugita, T. Ishikawa, S.-y. Koshihara, Y. Kaizu, *J. Phys. Chem. B* **2004**, *108*, 11265–11271.
- [60] N. Ishikawa, M. Sugita, T. Ishikawa, S.-y. Koshihara, Y. Kaizu, *J. Am. Chem. Soc.* **2003**, *125*, 8694–8695.
- [61] M. Pascu, F. Lloret, N. Avarvari, M. Julve, M. Andruh, *Inorg. Chem.* **2004**, *43*, 5189–5191.
- [62] T. Glaser, M. Heidemeier, S. Grimme, E. Bill, *Inorg. Chem.* **2004**, *43*, 5192–5194.
- [63] M.-C. Dul, X. Ottenwaelder, E. Pardo, R. Lescouëzec, Y. Journaux, L.-M. Chamoreau, R. Ruiz-Garcia, J. Cano, M. Julve, F. Lloret, *Inorg. Chem.* **2009**, *48*, 5244–5249.
- [64] A. Rajca, *Chem. Eur. J.* **2002**, *8*, 4834–4841.
- [65] H. Iwamura, N. Koga, *Acc. Chem. Res.* **1993**, *26*, 346–351.
- [66] D. A. Dougherty, *Acc. Chem. Res.* **1991**, *24*, 88–94.
- [67] T. Ishida, T. Kawakami, S.-i. Mitsubori, T. Nogami, K. Yamaguchi, H. Iwamura, *J. Chem. Soc., Dalton Trans.* **2002**, 3177–3186.
- [68] Y. Takano, T. Onishi, Y. Kitagawa, T. Soda, Y. Yoshioka, K. Yamaguchi, *Int. J. Quantum Chem.* **2000**, *80*, 681–691.
- [69] J. Cano, E. Ruiz, S. Alvarez, M. Verdaguer, *Comments Inorg. Chem.* **1998**, *20*, 27–56.
- [70] A. Bencini, D. Gatteschi, F. Totti, D. N. Sanz, M. D. Ward, *J. Phys. Chem. A* **1998**, *102*, 10545–10551.
- [71] O. Kahn, *Chem. Phys. Lett.* **1997**, *265*, 109–114.
- [72] L. Rigamonti, A. Cinti, A. Forni, A. Pasini, O. Piovesana, *Eur. J. Inorg. Chem.* **2008**, 3633–3647.
- [73] M. S. Ray, S. Chattopadhyay, M. G. B. Drew, A. Figuerola, J. Ribas, C. Diaz, A. Ghosh, *Eur. J. Inorg. Chem.* **2005**, 4562–4571.
- [74] J.-H. Zhou, R.-M. Cheng, Y. Song, Y.-Z. Li, Z. Yu, X.-T. Chen, Z.-L. Xue, X.-Z. You, *Inorg. Chem.* **2005**, *44*, 8011–8022.
- [75] J. Yoon, L. M. Mirica, T. D. P. Stack, E. I. Solomon, *J. Am. Chem. Soc.* **2004**, *126*, 12586–12595.

- [76] X. Liu, M. P. de Miranda, E. J. L. McInnes, C. A. Kilner, M. A. Halcrow, *Dalton Trans* **2004**, 59–64.
- [77] B. Cage, F. A. Cotton, N. S. Dalal, E. A. Hillard, B. Rakvin, C. M. Ramsey, *J. Am. Chem. Soc.* **2003**, *125*, 5270–5271.
- [78] B. Cage, F. A. Cotton, N. S. Dalal, E. A. Hillard, B. Rakvin, C. M. Ramsey, *C. R. Chim.* **2003**, *6*, 39–46.
- [79] S. Ferrer, F. Lloret, I. Bertomeu, G. Alzuet, J. Borrás, S. Garcia-Granda, M. Liu-Gonzalez, J. G. Haasnoot, *Inorg. Chem.* **2002**, *41*, 5821–5830.
- [80] H. López-Sandoval, R. Contreras, A. Escuer, R. Vicente, S. Bernès, H. Nöth, G. J. Leigh, N. Barba-Behrens, *J. Chem. Soc., Dalton Trans.* **2002**, 2648–2653.
- [81] S. Ferrer, J. G. Haasnoot, J. Reedijk, E. Müller, M. Biagini Cingi, M. Lanfranchi, A. M. Manotti Lanfredi, J. Ribas, *Inorg. Chem.* **2000**, *39*, 1859–1867.
- [82] J. Padilla, D. Gatteschi, P. Chaudhuri, *Inorg. Chim. Acta* **1997**, *260*, 217–220.
- [83] J. Yoon, E. I. Solomon, *Coord. Chem. Rev.* **2007**, *251*, 379–400.
- [84] D. Stepanenko, M. Trif, D. Loss, *Inorg. Chim. Acta* **2008**, *361*, 3740–3745.
- [85] S. Carretta, P. Santini, G. Amoretti, F. Troiani, M. Affronte, *Phys. Rev. B* **2007**, *76*, 024408.
- [86] M. N. Leuenberger, D. Loss, *Nature* **2001**, *410*, 789–793.
- [87] T. Glaser, M. Heidemeier, R. Fröhlich, P. Hildebrandt, E. Bothe, E. Bill, *Inorg. Chem.* **2005**, *44*, 5467–5482.
- [88] T. Glaser, M. Heidemeier, T. Lügger, *Dalton Trans.* **2003**, 2381–2383.
- [89] T. Glaser, M. Gerenkamp, R. Fröhlich, *Angew. Chem., Int. Ed.* **2002**, *41*, 3823–3825.
- [90] X. Ottenwaelder, J. Cano, Y. Journaux, E. Rivière, C. Brennan, M. Nierlich, R. Ruiz-Garcia, *Angew. Chem., Int. Ed.* **2004**, *43*, 850–852.
- [91] I. Müller, D. Möller, *Eur. J. Inorg. Chem.* **2005**, 257–263.
- [92] I. M. Müller, R. Robson, *Angew. Chem., Int. Ed.* **2000**, *39*, 4357–4359.
- [93] S. R. Marshall, A. L. Rheingold, L. N. Dawe, W. W. Shum, C. Kitamura, J. S. Miller, *Inorg. Chem.* **2002**, *41*, 3599–3601.
- [94] J. Mroziński, A. Bieńko, P. Kopel, V. Langer, *Inorg. Chim. Acta* **2008**, *361*, 3723–3729.
- [95] S. Kitagawa, S. Masaoka, *Coord. Chem. Rev.* **2003**, *246*, 73–88.
- [96] H. Grove, J. Sletten, M. Julve, F. Lloret, L. Lezama, J. Carranza, S. Parsons, P. Rillema, *J. Mol. Struct.* **2002**, *606*, 253–265.
- [97] H. Grove, J. Sletten, M. Julve, F. Lloret, *J. Chem. Soc., Dalton Trans.* **2001**, 1029–1034.

Bibliography

- [98] G.-X. Liu, K. Zhu, H. Chen, R.-Y. Huang, H. Xu, X.-M. Ren, *Inorg. Chim. Acta* **2009**, *362*, 1605–1610.
- [99] Y. Qi, Y.-X. Che, J.-M. Zheng, *Cryst. Growth Des.* **2008**, *8*, 3602–3608.
- [100] L. Xu, E.-Y. Choi, Y.-U. Kwon, *J. Solid State Chem.* **2008**, *181*, 3185–3188.
- [101] S. Zhu, H. Zhang, Y. Zhao, M. Shao, Z. Wang, M. Li, *J. Mol. Struct.* **2008**, *892*, 420–426.
- [102] W. Li, M.-X. Li, M. Shao, Z.-X. Wang, H.-J. Liu, *Inorg. Chem. Commun.* **2008**, *11*, 954–957.
- [103] W. Zhang, S. Bruda, C. P. Landee, J. L. Parent, M. M. Turnbull, *Inorg. Chim. Acta* **2003**, *342*, 193–201.
- [104] O. M. Yaghi, M. O’Keeffe, N. W. Ockwig, H. K. Chae, M. Eddaoudi, J. Kim, *Nature* **2003**, *423*, 705–714.
- [105] J. W. Ko, K. S. Min, M. P. Suh, *Inorg. Chem.* **2002**, *41*, 2151–2157.
- [106] M. Eddaoudi, D. B. Moler, H. Li, B. Chen, T. M. Reineke, M. O’Keeffe, O. M. Yaghi, *Acc. Chem. Res.* **2001**, *34*, 319–330.
- [107] O. M. Yaghi, H. Li, C. Davis, D. Richardson, T. L. Groy, *Acc. Chem. Res.* **1998**, *31*, 474–484.
- [108] O. M. Yaghi, C. E. Davis, G. Li, H. Li, *J. Am. Chem. Soc.* **1997**, *119*, 2861–2868.
- [109] M. J. Plater, M. R. S. J. Foreman, R. A. Howie, J. M. S. Skakle, E. Coronado, C. J. Gmez-Garca, T. Gelbrich, M. B. Hursthouse, *Inorg. Chim. Acta* **2001**, *319*, 159–175.
- [110] M. J. Plater, M. R. S. J. Foreman, E. Coronado, C. J. Gómez-García, A. M. Z. Slawin, *J. Chem. Soc., Dalton Trans.* **1999**, 4209–4216.
- [111] T. Glaser, H. Theil, M. Heidemeier, *C. R. Chim.* **2008**, *11*, 1121–1136.
- [112] V. A. Ung, A. M. W. Cargill Thompson, D. A. Bardwell, D. Gatteschi, J. C. Jeffery, J. A. McCleverty, F. Totti, M. D. Ward, *Inorg. Chem.* **1997**, *36*, 3447–3454.
- [113] T. Glaser, M. Heidemeier, J. Strautmann, H. Bögge, A. Stammler, E. Krickemeyer, R. Huenerbein, S. Grimme, E. Bothe, E. Bill, *Chem. Eur. J.* **2007**, *13*, 9191–9206.
- [114] T. Glaser, M. Heidemeier, R. Fröhlich, *C. R. Chim.* **2007**, *10*, 71–78.
- [115] H. Theil, C. G. F. von Richthofen, A. Stammler, H. Bogge, T. Glaser, *Inorg. Chim. Acta* **2008**, *361*, 916–924.
- [116] T. Glaser, M. Heidemeier, E. Krickemeyer, H. Bögge, A. Stammler, R. Fröhlich, E. Bill, J. Schnack, *Inorg. Chem.* **2009**, *48*, 607–620.
- [117] T. Glaser, M. Heidemeier, T. Weyhermüller, R.-D. Hoffmann, H. Rupp, P. Müller, *Angew. Chem., Int. Ed.* **2006**, *45*, 6033–6037.
- [118] E. Pardo, R. Ruiz-Garcia, J. Cano, X. Ottenwaelder, R. Lescouëzec, Y. Journaux, F. Lloret, M. Julve, *Dalton Trans.* **2008**, 2780–2805.

- [119] D. Y. Jeter, W. E. Hatfield, *Inorg. Chim. Acta* **1972**, *6*, 440–442.
- [120] E. F. Hasty, L. J. Wilson, D. N. Hendrickson, *Inorg. Chem.* **1978**, *17*, 1834–1841.
- [121] I. Fernández, R. Ruiz, J. Faus, M. Julve, F. Lloret, J. Cano, X. Ottenwaelder, Y. Journaux, M. C. Muñoz, *Angew. Chem., Int. Ed.* **2001**, *40*, 3039–3042.
- [122] R. H. Laye, E. C. Sañudo, *Inorg. Chim. Acta* **2009**, *362*, 2205–2212.
- [123] A. R. Paital, T. Mitra, D. Ray, W. T. Wong, J. Ribas-Ariño, J. J. Novoa, J. Ribas, G. Aromi, *Chem. Commun.* **2005**, 5172–5174.
- [124] C. T. Zeyrek, A. Elmali, Y. Elerman, I. Svoboda, *Z. Naturforsch.* **2005**, *60b*, 143–148.
- [125] R. Hernández-Molina, A. Mederos, P. Gili, S. Dominguez, F. Lloret, J. Cano, M. Julve, C. Ruiz-Pérez, X. Solans, *J. Chem. Soc., Dalton Trans.* **1997**, *22*, 4327–4334.
- [126] B. Biswas, S. Salunke-Gawali, T. Weyhermüller, V. Bachler, E. Bill, P. Chaudhuri, *Eur. J. Inorg. Chem.* **2008**, 2391–2395.
- [127] P. J. Bailey, K. J. Grant, L. A. Mitchell, S. Pace, A. Parkin, S. Parsons, *J. Chem. Soc., Dalton Trans.* **2000**, 1887–1891.
- [128] G. R. Giesbrecht, A. Shafir, J. Arnold, *J. Chem. Soc., Dalton Trans.* **1999**, 3601–3604.
- [129] N. Thirupathi, G. P. A. Yap, D. S. Richeson, *Chem. Commun.* **1999**, 2483–2484.
- [130] P. J. Bailey, R. O. Gould, C. N. Harmer, S. Pace, D. S. Wright, *Chem. Commun.* **1997**, 1161–1162.
- [131] P. J. Bailey, A. J. Blake, M. Kryszczuk, S. Parsons, D. Reed, *J. Chem. Soc., Chem. Commun.* **1995**, 1647–1648.
- [132] I. M. Müller, D. Möller, K. Föcker, *Chem. Eur. J.* **2005**, *11*, 3318–3324.
- [133] I. M. Müller, D. Möller, *Angew. Chem., Int. Ed.* **2005**, *44*, 2969–2973.
- [134] I. M. Müller, D. Möller, C. A. Schalley, *Angew. Chem., Int. Ed.* **2005**, *44*, 480–484.
- [135] I. M. Müller, R. Robson, F. Separovic, *Angew. Chem., Int. Ed.* **2001**, *40*, 4385–4386.
- [136] I. M. Müller, S. Spillmann, H. Franck, R. Pietschnig, *Chem. Eur. J.* **2004**, *10*, 2207–2213.
- [137] I. M. Oppel, K. Föcker, *Angew. Chem., Int. Ed.* **2008**, *47*, 402–405.
- [138] W. Plass, *Coord. Chem. Rev.* **2009**, *253*, 2286–2295.
- [139] A. Zharkouskaya, *Mehrkernige Übergangsmetallkomplexe als Basis für neue Klassen magnetischer Materialien*, Ph.D. thesis, Friedrich Schiller University Jena **2006**.

Bibliography

- [140] A. E. Ion, *Magneto-structural characterization of polynuclear complexes with supramolecular architectures*, Ph.D. thesis, Friedrich Schiller University Jena **2006**.
- [141] A. E. Ion, E. T. Spielberg, H. Görls, W. Plass, *Inorg. Chim. Acta* **2007**, *360*, 3925–3931.
- [142] A. Zharkouskaya, H. Görls, G. Vaughan, W. Plass, *Inorg. Chem. Commun.* **2005**, *8*, 1145–1148.
- [143] A. Zharkouskaya, A. Buchholz, W. Plass, *Eur. J. Inorg. Chem.* **2005**, 4875–4879.
- [144] J. Kempe, D. Bacon, D. A. Lidar, K. B. Whaley, *Phys. Rev. A* **2001**, *63*, 042307.
- [145] V. Cerletti, W. A. Coish, O. Gywat, D. Loss, *Nanotechnology* **2005**, *16*, R27–R49.
- [146] A. Fert, *Angew. Chem., Int. Ed.* **2008**, *47*, 5956–5967.
- [147] F. Meier, J. Levy, D. Loss, *Phys. Rev. B* **2003**, *68*, 134417.
- [148] J. H. Chong, M. Sauer, B. O. Patrick, M. J. MacLachlan, *Org. Lett.* **2003**, *5*, 3823–3826.
- [149] H.-B. Li, *Acta Crystallogr., Sect. E: Struct. Rep. Online* **2008**, *64*, o465.
- [150] Y.-M. Wang, Z.-D. Zhao, Y.-X. Chen, L.-W. Bi, *Acta Crystallogr., Sect. E: Struct. Rep. Online* **2008**, *64*, o1009.
- [151] Q.-H. Jiang, Y.-H. Xu, L.-Y. Jian, L.-M. Zhao, *Acta Crystallogr., Sect. E: Struct. Rep. Online* **2008**, *64*, o338.
- [152] C.-B. Tang, *Acta Crystallogr., Sect. E: Struct. Rep. Online* **2008**, *64*, o767.
- [153] A. Roth, A. Buchholz, M. Gärtner, H. Görls, W. Plass, *Acta Crystallogr., Sect. E: Struct. Rep. Online* **2007**, *63*, o3073.
- [154] C. V. Yelamaggad, A. S. Achalkumar, D. S. S. Rao, S. K. Prasad, *J. Mater. Chem.* **2007**, 4521–4529.
- [155] P. Suresh, S. Srimurugan, B. Babu, H. N. Pati, *Tetrahedron: Asymmetry* **2007**, *18*, 2820–2827.
- [156] C. V. Yelamaggad, A. S. Achalkumar, D. S. S. Rao, S. K. Prasad, *J. Org. Chem.* **2007**, *72*, 8308–8318.
- [157] J. A. Riddle, S. P. Lathrop, J. C. Bollinger, D. Lee, *J. Am. Chem. Soc.* **2006**, *128*, 10986–10987.
- [158] J. A. Riddle, J. C. Bollinger, D. Lee, *Angew. Chem., Int. Ed.* **2005**, *44*, 6689–6693.
- [159] M. Sauer, C. Yeung, J. H. Chong, B. O. Patrick, M. J. MacLachlan, *J. Org. Chem.* **2006**, *71*, 775–788.
- [160] C. V. Yelamaggad, A. S. Achalkumar, D. S. Shankar Rao, S. K. Prasad, *J. Am. Chem. Soc.* **2004**, *126*, 6506–6507.
- [161] P. Suresh, B. Varghese, T. K. Varadarajan, B. Viswanathan, *Acta Crystallogr., Sect. E: Struct. Rep. Online* **2007**, *63*, o984–o986.
- [162] A. Roth, A. Buchholz, W. Plass, *Z. Anorg. Allg. Chem.* **2007**, *633*, 383–392.

- [163] S. Nica, A. Buchholz, M. Rudolph, A. Schweitzer, M. Wächtler, H. Breitzke, G. Buntkowsky, W. Plass, *Eur. J. Inorg. Chem.* **2008**, 2350–2359.
- [164] W. Plass, H.-P. Yozgatli, *Z. Anorg. Allg. Chem.* **2003**, 629, 65–70.
- [165] I. Lippold, H. Görls, W. Plass, *Eur. J. Inorg. Chem.* **2007**, 1487–1491.
- [166] B. J. Hathaway, A. E. Underhill, *J. Chem. Soc.* **1961**, 3091–3096.
- [167] D. Plaul, *Pyrimidin- und Resorcinolverbrückte dinukleare Übergangsmetallkomplexe*, Master's thesis, Friedrich Schiller University Jena **2005**.
- [168] A. Pohlmann, *Wasserstoffbrückenbindungen in Übergangsmetallkomplexen–Bedeutung für Enzym-Modelle und Magnetochemie*, Ph.D. thesis, University Siegen **2002**.
- [169] B. P. Hay, V. S. Bryantsev, *Chem. Commun.* **2008**, 2417–2428.
- [170] A. G. Orpen, L. Brammer, F. H. Allen, O. Kennard, D. G. Watson, R. Taylor, *J. Chem. Soc., Dalton Trans.* **1989**, S1–S83.
- [171] K. Delany, S. K. Arora, P. K. Mascharak, *Inorg. Chem.* **1988**, 27, 705–712.
- [172] J. D. Tan, S. E. Hudson, S. J. Brown, M. M. Olmstead, P. K. Mascharak, *J. Am. Chem. Soc.* **1992**, 114, 3841–3853.
- [173] M. Muetterties, P. K. Mascharak, M. B. Cox, S. K. Arora, *Inorg. Chim. Acta* **1989**, 160, 123–134.
- [174] D. Plaul, D. Geibig, H. Görls, W. Plass, *Polyhedron* **2009**, 28, 1982–1990.
- [175] V. V. Pavlishchuk, M. Prushan, A. Addison, *Theor. Exp. Chem.* **2005**, 41, 229–234.
- [176] M. J. Prushan, D. M. Tomezsko, S. Lofland, M. Zeller, A. D. Hunter, *Inorg. Chim. Acta* **2007**, 360, 2245–2254.
- [177] <http://www.ncnr.nist.gov/dave>.
- [178] O. Kahn, *Molecular Magnetism*, Wiley-VCH Inc., Weinheim **1993**.
- [179] M. Fondo, N. Ocampo, A. M. García-Deibe, J. Sanmartín, *Inorg. Chem.* **2009**, 48, 4971–4979.
- [180] A. Burkhardt, W. Plass, *Inorg. Chem. Commun.* **2008**, 11, 303–306.
- [181] R. Boca, *Coord. Chem. Rev.* **2004**, 248, 757–815.
- [182] R. Ivaníková, R. Boca, L. Dlhán, H. Fuess, A. Maslejová, V. Mrázová, I. Svoboda, J. Titis, *Polyhedron* **2006**, 25, 3261–3268.
- [183] E. Pardo, D. Cangussu, R. Lescouezec, Y. Journaux, J. Pasán, F. S. Delgado, C. Ruiz-Pérez, R. Ruiz-García, J. Cano, M. Julve, F. Lloret, *Inorg. Chem.* **2009**, 48, 4661–4673.

Bibliography

- [184] E. Pardo, R. Ruiz-Garcia, F. Lloret, M. Julve, J. Cano, J. Pasan, C. Ruiz-Pérez, Y. Filali, L.-M. Chamoreau, Y. Journaux, *Inorg. Chem.* **2007**, *46*, 4504–4514.
- [185] X. Ottenwaelder, R. Ruiz-Garcia, G. Blondin, R. Carasco, J. Cano, D. Lexa, Y. Journaux, A. Aukauloo, *Chem. Commun.* **2004**, 504–505.
- [186] E. Pardo, I. Morales-Osorio, M. Julve, F. Lloret, J. Cano, R. Ruiz-Garcia, J. Pasan, C. Ruiz-Perez, X. Ottenwaelder, Y. Journaux, *Inorg. Chem.* **2004**, *43*, 7594–7596.
- [187] I. Arai, Y. Sei, I. Muramatsu, *J. Org. Chem.* **1981**, *46*, 4597–4599.
- [188] J. C. Bottaro, R. Malhotra, A. Dodge, *Synthesis* **2004**, *4*, 499–500.
- [189] Y. V. Mitin, O. V. Glinskaya, *Tetrahedron Lett.* **1969**, *10*, 5267–5270.
- [190] D. J. Barnes, R. L. Chapman, R. S. Vagg, E. C. Watton, *J. Chem. Eng. Data* **1978**, *23*, 349–350.
- [191] P. M. Van Calcar, M. M. Olmstead, A. L. Balch, *Chem. Commun.* **1996**, 2597–2598.
- [192] R. D. Willett, *Magneto-Structural Correlations in Exchange Coupled Systems*, D. Reidel Publishing Company **1983**.
- [193] A. R. Paital, A.-Q. Wu, Guo, G. Aromi, J. Ribas-Ariño, D. Ray, *Inorg. Chem.* **2007**, *46*, 2947–2949.
- [194] Y. Pang, S. Cui, B. Li, J. Zhang, Y. Wang, H. Zhang, *Inorg. Chem.* **2008**, *47*, 10317–10324.
- [195] W. M. Davis, A. Zask, K. Nakanishi, S. J. Lippard, *Inorg. Chem.* **1985**, *24*, 3737–3743.
- [196] A. A. Ovchinnikov, *Theoret. Chim. Acta (Berl.)* **1978**, *47*, 297–304.
- [197] V. H. Crawford, H. W. Richardson, J. R. Wasson, D. J. Hodgson, W. E. Hatfield, *Inorg. Chem.* **1976**, *15*, 2107–2110.
- [198] M. Melník, *Coord. Chem. Rev.* **1982**, *42*, 259–293.
- [199] M. Kato, Y. Muto, *Coord. Chem. Rev.* **1988**, *92*, 45–83.
- [200] H. Merz, W. Haase, *J. Chem. Soc., Dalton Trans.* **1980**, 875–879.
- [201] F. Tuna, L. Patron, Y. Journaux, M. Andruh, W. Plass, J.-C. Trombe, *J. Chem. Soc., Dalton Trans.* **1999**, 539–545.
- [202] L. K. Thompson, S. K. Mandal, S. S. Tandon, J. N. Bridson, M. K. Park, *Inorg. Chem.* **1996**, *35*, 3117–3125.
- [203] P. L. Burk, J. A. Osborn, M. T. Youinou, Y. Agnus, R. Louis, R. Weiss, *J. Am. Chem. Soc.* **1981**, *103*, 1273–1274.
- [204] P. K. Coughlin, S. J. Lippard, *J. Am. Chem. Soc.* **1981**, *103*, 3228–3229.
- [205] V. McKee, J. V. Dagdigian, R. Bau, C. A. Reed, *J. Am. Chem. Soc.* **1981**, *103*, 7000–7001.

- [206] S. Foxon, G. Torres, O. Walter, J. Pedersen, H. Toftlund, M. Hüber, K. Falk, W. Haase, J. Cano, F. Lloret, M. Julve, S. Schindler, *Eur. J. Inorg. Chem.* **2004**, 335–343.
- [207] P. G. Lacroix, F. Averseng, I. Malfant, K. Nakatani, *Inorg. Chim. Acta* **2004**, 357, 3825–3835.
- [208] P. E. Kruger, N. Martin, M. Nieuwenhuyzen, *J. Chem. Soc., Dalton Trans.* **2001**, 1966–1970.
- [209] A. W. Addison, T. N. Rao, J. Reedijk, J. van Rijn, G. C. Verschoor, *J. Chem. Soc., Dalton Trans.* **1984**, 1349–1356.
- [210] B. Bleaney, K. D. Bowers, *Proc. Roy. Soc. (London) Ser. A* **1952**, 214, 451.
- [211] S. G. Baca, I. G. Filippova, O. A. Gherco, M. Gdaniec, Y. A. Simonov, N. V. Gerbeleu, P. Franz, R. Basler, S. Decurtins, *Inorg. Chim. Acta* **2004**, 357, 3419–3429.
- [212] J.-S. Sun, H. Zhao, X. Ouyang, R. Clerac, J. A. Smith, J. M. Clemente-Juan, C. Gomez-Garcia, E. Coronado, K. R. Dunbar, *Inorg. Chem.* **1999**, 38, 5841–5855.
- [213] E. T. Spielberg, *New Building Blocks for Molecular Spintronics*, Ph.D. thesis, Friedrich Schiller University Jena **2009**.
- [214] F. L. Scott, M. Cashman, J. Reilly, *J. Am. Chem. Soc.* **1952**, 74, 5802.
- [215] J. Tang, J. Sánchez Costa, S. Smulders, G. Molnár, A. Bousseksou, S. J. Teat, Y. Li, G. A. van Albada, P. Gamez, J. Reedijk, *Inorg. Chem.* **2009**, 48, 2128–2135.
- [216] M. S. Shongwe, B. A. Al-Rashdi, H. Adams, M. J. Morris, M. Mikuriya, G. R. Hearne, *Inorg. Chem.* **2007**, 46, 9558–9568.
- [217] S. Dorbes, L. Valade, J. A. Real, C. Faulmann, *Chem. Commun.* **2005**, 69–71.
- [218] J. M. Holland, J. A. McAllister, C. A. Kilner, M. Thornton-Pett, A. J. Bridgeman, M. A. Halcrow, *J. Chem. Soc., Dalton Trans.* **2002**, 548–554.
- [219] R. Viswanathan, M. Palaniandavar, T. Balasubramanian, P. T. Muthiah, *J. Chem. Soc., Dalton Trans.* **1996**, 2519–2525.
- [220] M. Lubben, A. Meetsma, F. van Bolhuis, B. L. Feringa, R. Hage, *Inorg. Chim. Acta* **1994**, 215, 123–129.
- [221] S. Lin, S.-X. Liu, Z. Chen, B.-Z. Lin, S. Gao, *Inorg. Chem.* **2004**, 43, 2222–2224.
- [222] S. Lin, S.-X. Liu, B.-Z. Lin, *Inorg. Chim. Acta* **2002**, 328, 69–73.
- [223] M. Gerloch, E. D. McKenzie, A. D. C. Towl, *J. Chem. Soc. (A)* **1969**, 2850–2858.
- [224] D. M. Kurtz, *Chem. Rev.* **1990**, 90, 585–606.
- [225] S. M. Gorun, S. J. Lippard, *Inorg. Chem.* **1991**, 30, 1625–1630.

Bibliography

- [226] F. Le Gall, F. F. de Biani, A. Caneschi, P. Cinelli, A. Cornia, A. C. Fabretti, D. Gatteschi, *Inorg. Chim. Acta* **1997**, *262*, 123–132.
- [227] O. Waldmann, R. Koch, S. Schromm, J. Schulein, P. Muller, I. Bernt, R. W. Saalfrank, F. Hampel, E. Balthes, *Inorg. Chem.* **2001**, *40*, 2986–2995.
- [228] H. Weihe, H. U. Güdel, *J. Am. Chem. Soc.* **1998**, *120*, 2870–2879.
- [229] C. Canada-Vilalta, T. A. O'Brien, E. K. Brechin, M. Pink, E. R. Davidson, G. Christou, *Inorg. Chem.* **2004**, *43*, 5505–5521.
- [230] A. Burkhardt, H. Görls, W. Plass, *Carbohydr. Res.* **2008**, *343*, 1266–1277.
- [231] S. Sharma, M. Chandra, D. Pandey, *Eur. J. Inorg. Chem.* **2004**, 3555–3563.
- [232] A. Das, G. M. Rosair, M. S. El Fallah, J. Ribas, S. Mitra, *Inorg. Chem.* **2006**, *45*, 3301–3306.
- [233] X.-P. Zhou, D. Li, S.-L. Zheng, X. Zhang, T. Wu, *Inorg. Chem.* **2006**, *45*, 7119–7125.
- [234] X.-P. Zhou, D. Li, T. Wu, X. Zhang, *Dalton Trans.* **2006**, 2435–2443.
- [235] T. Glaser, T. Lügger, R. Fröhlich, *Eur. J. Inorg. Chem.* **2004**, 394–400.
- [236] A. P. Summerton, A. A. Diamantis, M. R. Snow, *Inorg. Chim. Acta* **1978**, *27*, 123–128.
- [237] C. Janiak, *J. Chem. Soc., Dalton Trans.* **2000**, 3885–3896.
- [238] The program package julX was used for spin-Hamiltonian simulations and fittings of the magnetic susceptibility data by a full-matrix diagonalization approach (E. Bill, Max-Planck-Institut für Bioanorganische Chemie, Mühlheim, <http://ewww.mpi-muelheim.mpg.de/bac/logins/bill/julX.en.php>, Germany).
- [239] A. Kamiyama, T. Noguchi, T. Kajiwara, T. Ito, *Inorg. Chem.* **2002**, *41*, 507–512.
- [240] S. Triki, C. J. Gomez-Garcia, E. Ruiz, J. Sala-Pala, *Inorg. Chem.* **2005**, *44*, 5501–5508.
- [241] A. Kamiyama, T. Noguchi, T. Kajiwara, T. Ito, *CrystEngComm* **2003**, *5*, 231–237.
- [242] T. Zeegers-Huyskens, *J. Mol. Struct.* **2008**, *887*, 2–8.
- [243] D. Plaul, W. Plass, unpublished results.
- [244] T. Moriya, *Phys. Rev.* **1960**, *120*, 91–98.
- [245] I. Dzyaloshinsky, *J. Phys. Chem. Solids* **1958**, *4*, 241–255.
- [246] B. S. Tsukerblat, B. Y. Kuyavskaya, M. I. Belinskii, A. V. Ablov, V. M. Novotortsev, V. T. Kalinnikov, *Theoret. Chim. Acta (Berl.)* **1975**, *38*, 131–138.
- [247] Y. V. Rakitin, Y. V. Yablokov, V. V. Zelentsov, *J. Magn. Reson.* **1981**, *43*, 288–301.

- [248] J. F. Berry, F. A. Cotton, C. Y. Liu, T. Lu, C. A. Murillo, B. S. Tsukerblat, D. Villagran, X. Wang, *J. Am. Chem. Soc.* **2005**, *127*, 4895–4902.
- [249] T. Murao, *Phys. Lett. A* **1974**, *49*, 33–35.
- [250] A. B. Gaspar, M. C. Munoz, V. Niel, J. A. Real, *Inorg. Chem.* **2001**, *40*, 9–10.
- [251] L. L. Lohr, J. C. Miller, R. R. Sharp, *J. Chem. Phys.* **1999**, *111*, 10148–10158.
- [252] M. W. Makinen, L. C. Kuo, M. B. Yim, G. B. Wells, J. M. Fukuyama, J. E. Kim, *J. Am. Chem. Soc.* **1985**, *107*, 5245–5255.
- [253] D. J. Mackey, S. V. Evans, R. F. McMeeking, *J. Chem. Soc., Dalton Trans.* **1978**, 160–165.
- [254] J. L. Shaw, G. T. Yee, G. Wang, D. E. Benson, C. Gokdemir, C. J. Ziegler, *Inorg. Chem.* **2005**, *44*, 5060–5067.
- [255] O. Kahn, *Angew. Chem., Int. Ed.* **1985**, *24*, 834–850.
- [256] M. Julve, M. Verdaguer, A. Gleizes, M. Philoche-Levisalles, O. Kahn, *Inorg. Chem.* **1984**, *23*, 3808–3818.
- [257] W. Li, H.-P. Jia, Z.-F. Ju, J. Zhang, *Inorg. Chem. Commun.* **2008**, *11*, 591–594.
- [258] O. Castillo, A. Luque, S. Iglesias, C. Guzmán-Miralles, P. Román, *Inorg. Chem. Commun.* **2001**, *4*, 640–642.
- [259] H.-Y. Shen, W.-M. Bu, D.-Z. Liao, Z.-H. Jiang, S.-P. Yan, G.-L. Wang, *Inorg. Chem.* **2000**, *39*, 2239–2242.
- [260] S. Youngme, G. A. van Albada, N. Chaichit, P. Gunnasoot, P. Kongsaree, I. Mutikainen, O. Roubeau, J. Reedijk, U. Turpeinen, *Inorg. Chim. Acta* **2003**, *353*, 119–128.
- [261] H. Nuñez, J.-J. Timor, J. Server-Carrió, L. Soto, E. Escrivá, *Inorg. Chim. Acta* **2001**, *318*, 8–14.
- [262] H.-D. Bian, W. Gu, J.-Y. Xu, F. Bian, S.-P. Yan, D.-Z. Liao, Z.-H. Jiang, P. Cheng, *Inorg. Chem.* **2003**, *42*, 4265–4267.
- [263] R. Cao, S. Liu, L. Xie, Y. Pan, J. Cao, Y. Ren, L. Xu, *Inorg. Chem.* **2007**, *46*, 3541–3547.
- [264] O. Castillo, A. Luque, P. Román, F. Lloret, M. Julve, *Inorg. Chem.* **2001**, *40*, 5526–5535.
- [265] Z. Duan, Y. Zhang, B. Zhang, F. L. Pratt, *Inorg. Chem.* **2009**, *48*, 2140–2146.
- [266] U. Garcia-Couceiro, O. Castillo, A. Luque, J. P. Garcia-Terán, G. Beobide, P. Román, *Eur. J. Inorg. Chem.* **2005**, 4280–4290.
- [267] U. Garcia-Couceiro, D. Olea, O. Castillo, A. Luque, P. Román, P. J. de Pablo, J. Gomez-Herrero, F. Zamora, *Inorg. Chem.* **2005**, *44*, 8343–8348.
- [268] P. Román, C. Guzman-Miralles, A. Luque, J. I. Beitia, J. Cano, F. Lloret, M. Julve, S. Alvarez, *Inorg. Chem.* **1996**, *35*, 3741–3751.

Bibliography

- [269] H. Liu, W. Gu, G. Xu, Y. Feng, Y. Kou, L. Feng, S. Yan, D. Liao, P. Cheng, *Inorg. Chem. Commun.* **2007**, *10*, 1099–1101.
- [270] M. Juric, B. Peric, N. Brnicevic, P. Planinic, D. Pajic, K. Zadro, G. Giester, *Polyhedron* **2007**, *26*, 659–672.
- [271] S. Youngme, A. Cheansirisomboon, C. Danvirutai, N. Chaichit, C. Pakawatchai, G. A. van Albada, J. Reedijk, *Inorg. Chem. Commun.* **2006**, *9*, 973–977.
- [272] C. N. R. Rao, S. Natarajan, R. Vaidhyanathan, *Angew. Chem., Int. Ed.* **2004**, *43*, 1466–1496.
- [273] X.-D. Zhang, Z. Zhao, J.-Y. Sun, Y.-C. Ma, M.-L. Zhu, *Acta Crystallogr., Sect. E: Struct. Rep. Online* **2005**, *61*, m2643–m2645.
- [274] H.-D. Wang, Y.-L. Zhou, H.-Y. He, X.-H. Tu, L.-G. Zhu, *Acta Crystallogr., Sect. E: Struct. Rep. Online* **2006**, *62*, m1081–m1082.
- [275] M. J. Belousoff, B. Graham, B. Moubaraki, K. S. Murray, L. Spiccia, *Eur. J. Inorg. Chem.* **2006**, 4872–4878.
- [276] D. Marcos, J.-V. Folgado, D. Beltrán-Porter, M. T. do Prado-Gambardella, S. H. Pulcinelli, R. H. de Almeida-Santos, *Polyhedron* **1990**, *9*, 2699–2704.
- [277] S. Wocadlo, W. Massa, J.-V. Folgado, *Inorg. Chim. Acta* **1993**, *207*, 199–206.
- [278] D. Marcos, R. Martinez-Mañez, J. V. Folgado, A. Beltran-Porter, D. Beltran-Porter, A. Fuertes, *Inorg. Chim. Acta* **1989**, *159*, 11–18.
- [279] T. Kajiwara, T. Ito, *J. Chem. Soc., Dalton Trans.* **1998**, 3351–3352.
- [280] F. Pointillart, K. Bernot, R. Sessoli, D. Gatteschi, *Chem. Eur. J.* **2007**, *13*, 1602–1609.
- [281] A. M. Madalan, K. Bernot, F. Pointillart, M. Andruh, A. Caneschi, *Eur. J. Inorg. Chem.* **2007**, 5533–5540.
- [282] A. Kamiyama, T. Noguchi, T. Kajiwara, T. Ito, *Angew. Chem., Int. Ed.* **2000**, *39*, 3130–3132.
- [283] T. Kajiwara, R. Sensui, T. Noguchi, A. Kamiyama, T. Ito, *Inorg. Chim. Acta* **2002**, *337*, 299–307.
- [284] M. Ferbinteanu, T. Kajiwara, K.-Y. Choi, H. Nojiri, A. Nakamoto, N. Kojima, F. Cimpoesu, Y. Fujimura, S. Takaishi, M. Yamashita, *J. Am. Chem. Soc.* **2006**, *128*, 9008–9009.
- [285] T. Kajiwara, M. Nakano, Y. Kaneko, S. Takaishi, T. Ito, M. Yamashita, A. Igashira-Kamiyama, H. Nojiri, Y. Ono, N. Kojima, *J. Am. Chem. Soc.* **2005**, *127*, 10150–10151.
- [286] T. Kajiwara, I. Watanabe, Y. Kaneko, S. Takaishi, M. Enomoto, N. Kojima, M. Yamashita, *J. Am. Chem. Soc.* **2007**, *129*, 12360–12361.
- [287] S. I. Troyanov, O. Y. Gorbenko, A. A. Bosak, *Polyhedron* **1999**, *18*, 3505–3509.
- [288] M. J. Plater, M. R. S. J. Foreman, A. M. Z. Slawin, *Inorg. Chim. Acta* **2000**, *303*, 132–136.

- [289] J. H. Lee, Y. S. Jung, Y. S. Sohn, S.-J. Kang, *Bull. Korean Chem. Soc.* **1998**, *19*, 231–235.
- [290] S. Decurtins, H. W. Schmalke, R. Pellaux, P. Schneuwly, A. Hauser, *Inorg. Chem.* **1996**, *35*, 1451–1460.
- [291] A. Aukauloo, X. Ottenwaelder, R. Ruiz, Y. Journaux, Y. Pei, E. Rivière, B. Cervera, M. C. Muñoz, *Eur. J. Inorg. Chem.* **1999**, 209–212.
- [292] X. Qu, X. Song, W. Li, Y. Xu, L. Li, D. Liao, Z. Jiang, *Eur. J. Inorg. Chem.* **2008**, 1287–1292.
- [293] N. Gupta, N. Grover, G. A. Neyhart, P. Singh, H. H. Thorp, *Inorg. Chem.* **1993**, *32*, 310–316.
- [294] J. Halfpenny, R. W. H. Small, *Acta Crystallogr., Sect. B: Struct. Sci.* **1982**, *38*, 939–942.
- [295] E. I. Lerner, S. J. Lippard, *J. Am. Chem. Soc.* **1976**, *98*, 5397–5398.
- [296] E. I. Lerner, S. J. Lippard, *Inorg. Chem.* **1977**, *16*, 1537–1546.
- [297] M. Nihei, T. Shiga, Y. Maeda, H. Oshio, *Coord. Chem. Rev.* **2007**, *251*, 2606–2621.
- [298] I. Krivokapic, M. Zerara, M. L. Daku, A. Vargas, C. Enachescu, C. Ambrus, P. Tregenna-Piggott, N. Amstutz, E. Krausz, A. Hauser, *Coord. Chem. Rev.* **2007**, *251*, 364–378.
- [299] B. Djukic, P. A. Dube, F. Razavi, T. Seda, H. A. Jenkins, J. F. Britten, M. T. Lemaire, *Inorg. Chem.* **2009**, *48*, 699–707.
- [300] S. Hayami, Z.-z. Gu, H. Yoshiki, A. Fujishima, O. Sato, *J. Am. Chem. Soc.* **2001**, *123*, 11644–11650.
- [301] H. Oshio, K. Kitazaki, J. Mishiro, N. Kato, Y. Maeda, Y. Takashima, *J. Chem. Soc., Dalton Trans.* **1987**, 1341–1347.
- [302] G. Juhász, S. Hayami, O. Sato, Y. Maeda, *Chem. Phys. Lett.* **2002**, *364*, 164–170.
- [303] S. Hayami, Y. Maeda, *Inorg. Chim. Acta* **1997**, *255*, 181–184.
- [304] S. Hayami, Z.-z. Gu, M. Shiro, Y. Einaga, A. Fujishima, O. Sato, *J. Am. Chem. Soc.* **2000**, *122*, 7126–7127.
- [305] J. Stolze, D. Suter, *Quantum Computing*, Wiley-VCH Inc. **2004**.
- [306] D. P. DiVincenzo, *arXiv:quant-ph/0002077v3* **2000**.
- [307] J. van Slageren, C. Schlegel, M. Dressel, *Nachr. Chem.* **2009**, *57*, 124–128.
- [308] S. Bertaina, S. Gambarelli, A. Tkachuk, I. N. Kurkin, B. Malkin, A. Stepanov, B. Barbara, *Nat. Nanotech.* **2007**, *2*, 39–42.
- [309] SMART COLLECT, *Data Collection Software*, Nonius B. V., Netherlands **1998**.
- [310] SMART, *Software for the CCD Detektor System, version 5.05*: Bruker AXS: Madison, WI **1998**.

Bibliography

- [311] Z. Otwinowski, W. Minor, In C. W. Carter, R. M. Sweet (Editors) *Macromolecular Crystallography, Part A*, volume 276 of *Methods in Enzymology*, Academic Press, San Diego **1997** 307–326.
- [312] G. M. Sheldrick, *SHELXS97 and SHELXL97*, University of Göttingen, Germany **1997**.
- [313] H. J. Hoorn, P. deJoode, W. L. Driessen, J. Reedijk, *Recl. Trav. Chim. Pays-Bas* **1996**, 115, 191–198.
- [314] M. Schatz, M. Leibold, S. P. Foxon, M. Weitzer, F. Heinemann, F. Hampel, O. Walter, S. Schindler, *Dalton Trans.* **2003**, 1480–1487.
- [315] M. D. Coburn, G. A. Buntain, B. W. Harris, M. A. Hiskey, K.-Y. Lee, D. G. Ott, *J. Heterocyclic Chem.* **1991**, 28, 2049–2050.

Declaration of Originality

I certify that the work presented here is, to the best of my knowledge and belief, original and the result of my own investigations, except as acknowledged, and has not been submitted, either in part or whole, for a degree at this or any other university.

Ich erkläre, dass ich die vorliegende Arbeit selbstständig und nur unter Verwendung der angegebenen Hilfsmittel, persönlichen Mitteilungen und Quellen angefertigt habe und dass ich nicht die gleiche, eine in wesentlichen Teilen ähnliche oder eine andere Abhandlung bei einer anderen Hochschule als Dissertation eingereicht habe.

Jena, November 7, 2009

Daniel Plaul

Curriculum Vitae

Daniel Plaul

born on the 21st of October 1980 in Schmölln, Germany

Professional Experience

- | | |
|-------------------|---|
| since 10/2005 | Scientific coworker in the work group of Prof. Dr. W. Plass at the Friedrich Schiller University Jena |
| 10/2004 - 07/2005 | Diploma thesis in the work group of Prof. Dr. W. Plass at the Friedrich Schiller University Jena with the subject: "Pyrimidin- and Resorcinol-Bridged Dinuclear Transition Metal Complexes" |

Education and Studies

- | | |
|-------------------|--|
| 10/2000 - 09/2005 | Study of chemistry with focus on bioinorganic/bioorganic chemistry and metal assisted catalysis at the Friedrich Schiller University Jena, diploma (M.Sc.), grade: A (excellent) |
| 09/1991 - 06/1999 | Academic high school of Schmölln, graduation: A-Level |

Scholarships

- | | |
|-------------------|---|
| 04/2006 - 03/2008 | Scholarship of the "Freistaat Thüringen" |
| 10/2000 - 09/2002 | Anniversary scholarship of the "Stiftung Stipendien-Fonds des Verbandes der Chemischen Industrie (FCI)" |

Basic Military Service

- | | |
|-------------------|---|
| 11/1999 - 08/2000 | Panzergrenadierbataillon Mellrichstadt 4./352 |
|-------------------|---|

Jena, November 7, 2009

Daniel Plaul